Aus der Klinik für Hämatologie, Onkologie und Palliativmedizin
Medizinische Klinik III/Zentrum für Innere Medizin
der Universitätsmedizin Rostock

„Aktive Immuntherapie bei gastrointestinalen Tumoren – eine *in vitro* und *in vivo* Analyse“

Kumulative Habilitationsschrift
zur
Erlangung des akademischen Grades
doctor rerum naturalium habilitatus (Dr. rer. nat. habil.)
der Universitätsmedizin Rostock

Vorgelegt von
Dr. rer. nat. Claudia Maletzki
geb. am 21.02.1981 in Rostock
wohnhaft in Rostock, Schillingallee 29
Rostock, 12.07.2018

https://doi.org/10.18453/rosdok_id00002510

Gutachter:
1. Gutachter:
Prof. Dr. med. Christian Junghanß
Medizinische Klinik III, Klinik für Hämatologie, Onkologie und Palliativmedizin
Zentrum für Innere Medizin, Universität Rostock

2. Gutachter:
Professor Dr. med. Florian Lordick
Universitäres Krebszentrum Leipzig, Universitätsklinikum Leipzig

3. Gutachter:
Prof. Dr. med. Andreas Hochhaus
Abteilung für Hämatologie und Internistische Onkologie der KIM II
Universitätsklinikum Jena

Fachgebiet: experimentelle Hämatologie und Onkologie

Datum der Einreichung: 17. Juli 2018
Datum der Verteidigung: 25. März 2019
Datum der Probevorlesung: 06. Mai 2019

Inhaltsverzeichnis

Abkürzungsverzeichnis 4
1 Verwendete Originalarbeiten 5
2 Einleitung 6
  2.1 Epidemiologie und Ätiologie gastrointestinaler Tumoren 7
  2.2 Molekulare Pathogenesemechanismen 7
  2.3 Konventionelle Therapie des Kolorektalen Karzinoms 8
  2.4 Konventionelle Therapie des Pankreaskarzinoms 9
  2.5 Möglichkeiten der Immuntherapie 10
  2.6 *In vitro* und *in vivo* Modelle für präklinische Untersuchungen 13
  2.7 Die aktiv-spezifische Immuntherapie am Beispiel dMMR-assoziierter Neoplasien 17
3 Zusammenfassung und Ausblick 19
4 Literaturverzeichnis 21
5 Anlagen 27
  5.1 Originalarbeiten 27
  5.1.1 Anlage – Teil 1 27
  5.1.2 Anlage – Teil 2 43
  5.1.3 Anlage – Teil 3 54
  5.1.4 Anlage – Teil 4 67
  5.1.5 Anlage – Teil 5 82
  5.1.6 Anlage – Teil 6 96
  5.2 Wissenschaftlicher Lebenslauf 110
  5.3. Vollständiges Publikationsverzeichnis 112
6 Danksagung 119
7 Eidesstattliche Erklärung 120

Abkürzungsverzeichnis

CpG ODN – CpG-Oligodesoxyribonukleotid

CRC – kolorektales Karzinom *(colorectal cancer)*

FS – Folinsäure

5-FU – 5-Fluoruracil

HDP – Antimikrobielle Peptide (*Host defense Peptide)*

dMMR – Mismatch Reparatur Defizienz *(deficient DNA mismatch repair)*

MHC – Haupthistokompatibilitäts-Komplex *(major histocompatibility complex)*

PD-1 – programmierter Zelltod Protein 1 *(Programmed cell death protein 1)*

PD-L1 – programmierter Zelltod Protein 1 Ligand 1 (*Programmed cell death 1 ligand 1*)

PDX – Patienten-abgeleitetes Xenograft *(Patient-derived Xenograft)*

TLR – Toll-ähnlicher Rezeptor (*Toll-like receptor)*

1 Verwendete Originalarbeiten

1. Maletzki C, Klier U, Obst W, Kreikemeyer B, Linnebacher M. Reevaluating the concept of treating experimental tumors with a mixed bacterial vaccine: Coley's Toxin. *Clin Dev Immunol*. 2012;2012:230625.

2. Maletzki C, Linnebacher M, Savai R, Hobohm U. Mistletoe lectin has a shigatoxin-like structure and should be combined with other Toll-like receptor ligands in cancer therapy. *Cancer Immunol Immunother*. 2013;62(8):1283-92.

3. Maletzki C, Stier S, Gruenert U, Gock M, Ostwald C, Prall F, Linnebacher M. Establishment, characterization and chemosensitivity of three mismatch repair deficient cell lines from sporadic and inherited colorectal carcinomas. *PLoS One*. 2012;7(12):e52485.

4. Maletzki C, Huehns M, Knapp P, Waukosin N, Klar E, Prall F, Linnebacher M. Functional Characterization and Drug Response of Freshly Established Patient-Derived Tumor Models with CpG Island Methylator Phenotype. *PLoS One*. 2015 30;10(11):e0143194.

5. Maletzki C, Klier U, Marinkovic S, Klar E, Andrä J, Linnebacher M. Host defense peptides for treatment of colorectal carcinoma - a comparative *in vitro* and *in vivo* analysis. *Oncotarget*. 2014 30;5(12):4467-79.

6. Maletzki C, Gladbach YS, Hamed M, Fuellen G, Semmler ML, Stenzel J, Linnebacher M. Cellular vaccination of MLH1$^{-/-}$ mice - an immunotherapeutic proof of concept study. *Oncoimmunology*. 2017 14;7(3):e1408748.

2 Einleitung

Gastrointestinale Neoplasien zählen neben den geschlechtsspezifischen onkologischen Erkrankungen zu den häufigsten Karzinomen und umfassen u.a. Pankreaskarzinome und kolorektale Karzinome (*colorectal cancer*, CRC). Die Therapie stützt sich im Wesentlichen auf die drei klassischen Säulen bestehend aus Chirurgie, (multimodaler) Chemotherapie und Radiatio (Abb. 1). Wesentliche Fortschritte insbesondere in dem molekularen Verständnis haben in den letzten Dekaden dazu geführt, das die Immuntherapie – komplementär und in Kombination mit den klassischen Verfahren – zunehmend die vierte Säule der Behandlungsoptionen in der Onkologie darstellt (Abb. 1). Für die Gruppe der gastrointestinalen Neoplasien sind immunologische Therapieansätze eher gering etabliert verglichen mit anderen Tumorentitäten wie beispielsweise den Non-Hodgkin Lymphomen. Vor diesem Hintergrund wurden in der vorliegenden Arbeit verschiedene immuntherapeutische Strategien zur Behandlung des Pankreaskarzinoms und CRC experimentell *in vitro* und *in vivo* evaluiert.

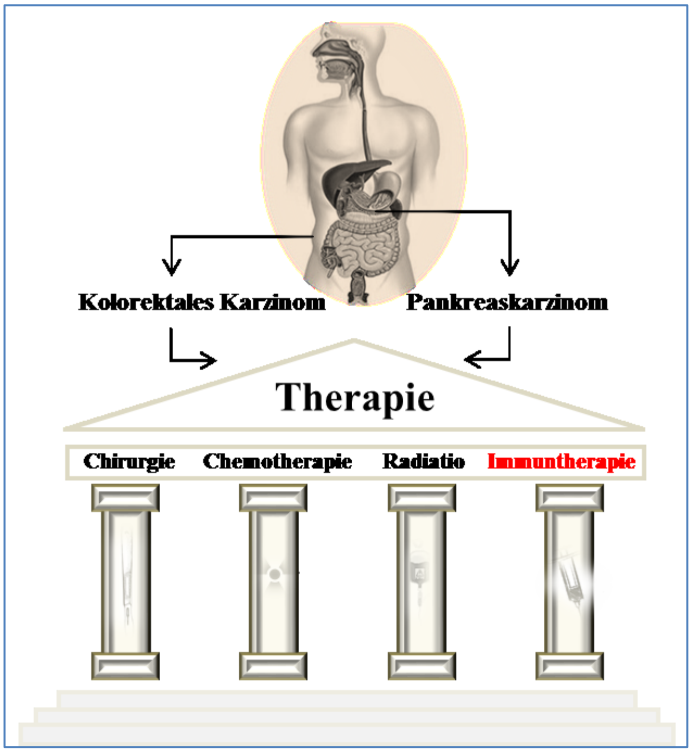

Abbildung 1: Überblick der drei klassischen Säulen der onkologischen Therapie, sowie der Immuntherapie als vierte Säule am Beispiel von Pankreaskarzinomen und kolorektalen Karzinomen.

2.1 Epidemiologie und Ätiologie gastrointestinaler Tumoren

Jährlich erkranken ca. 17.000 Menschen in Deutschland an einem Pankreaskarzinom, die Inzidenz für das CRC ist mit ca. 61.000 Neuerkrankungen/Jahr in Deutschland deutlich höher (Robert-Koch-Institut, 2014; Robert Koch-Institut, 2016). Beide Geschlechter sind in etwa gleich häufig betroffen. Aufgrund verbesserter Screening-Verfahren (Koloskopie-Screening) wird seit ca. 10 Jahren eine leichte Abnahme der CRC Inzidenzraten, sowie ein kontinuierlicher Rückgang der altersstandardisierten Sterberaten verzeichnet (Robert-Koch-Institut, 2014; Brenner, Stock and Hoffmeister, 2015). Ein vergleichbarer Trend ist für Pankreaskarzinome nicht zu beobachten. Epidemiologische Studien zeigen einen leichten, aber stetigen Anstieg hinsichtlich der Neuerkrankungen aufgrund des demographischen Wandels (Bertz *et al.*, 2010; Robert Koch-Institut, 2016). Angesichts der ungünstigen Prognose versterben fast genauso viele Patienten an diesem Tumor (Khadka *et al.*, 2018). Die relative 5-Jahres-Überlebensrate liegt, auch nach kurativer Intention durch chirurgische Resektion, bei max. 15 % (Kommalapati *et al.*, 2018; Roth and Berlin, 2018), damit ist das Pankreaskarzinom eine Erkrankung mit infauster Gesamtprognose. Es stellt die vierthäufigste Krebstodesursache in Deutschland dar (Bertz *et al.*, 2010; Robert Koch-Institut, 2016) .

Die Ätiologie beider Tumorerkrankungen ist multifaktoriell. Neben genetischen Prädispositionen, wie z.B. dem familiären atypischen multiplen Muttermal- und Melanom-Syndrom, sowie dem Lynch Syndrom, spielen nutritive und umwelt-assoziierte Faktoren eine wesentliche Rolle (Onkologie, 2013; Seufferlein *et al.*, 2013). Zu diesen zählen u.a. Essgewohnheiten, wie eine fett-, protein-, fleischreiche und ballaststoffarme Ernährung, mangelnde körperliche Aktivität, Adipositas und ein chronischer Nikotin- bzw. Alkoholabusus (Seufferlein *et al.*, 2013). Aufgrund der Prävalenz in den wirtschaftlich weiter entwickelten Regionen (Europa = USA > Asien/Afrika) stellen beide Krankheitsbilder typische Zivilisationskrankheiten dar.

2.2 Molekulare Pathogenesemechanismen

Das CRC ist ein sehr heterogenes Krankheitsbild. Ging man Anfang der 1990er Jahre mit der Entdeckung der *Adenom-Karzinom-Sequenz* durch Fearon und Vogelstein noch von einem einzigen Karzinogeneseweg aus (Fearon and Vogelstein, 1990), so ist heute bekannt, dass unterschiedliche molekulare Mechanismen zur Entstehung eines CRC beitragen (Abb.2) (Muller, Ibrahim and Arends, 2016).

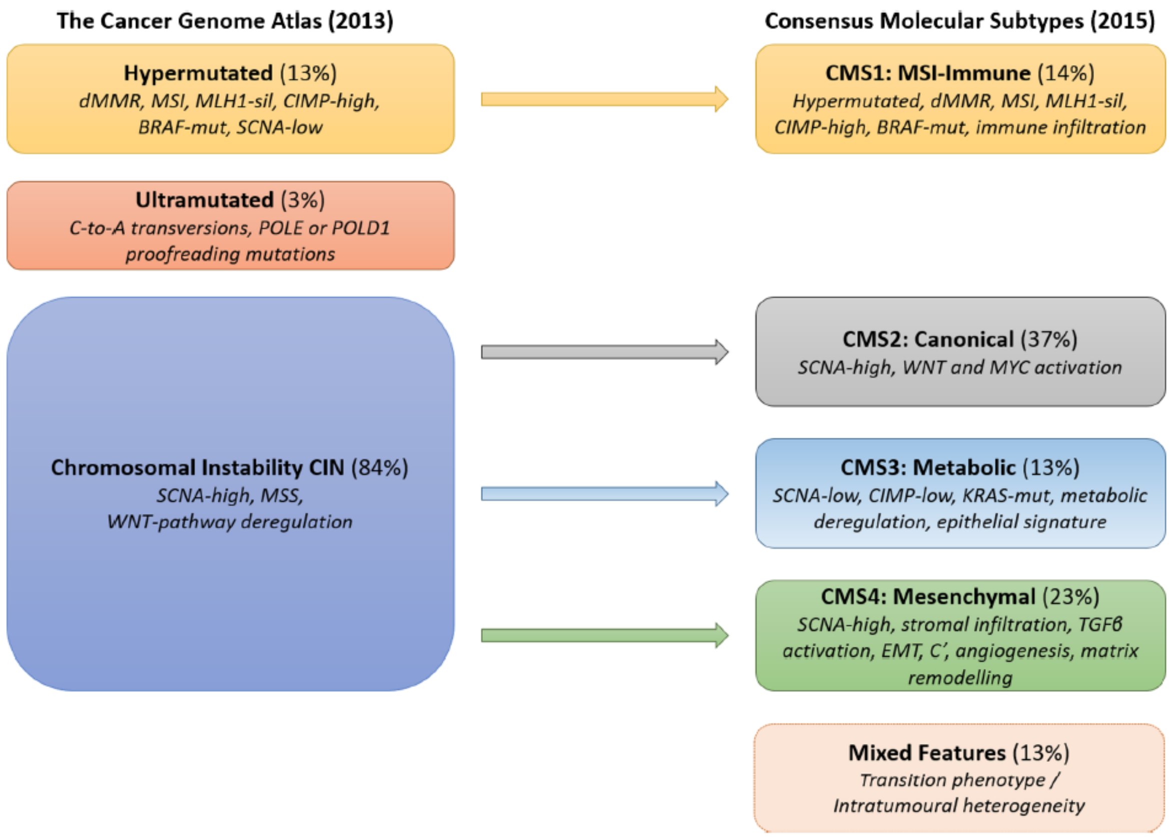
The Cancer Genome Atlas (2013)
Consensus Molecular Subtypes (2015)
Hypermutated (13%)
dMMR, MSI, MLH1-sil, CIMP-high, BRAF-mut, SCNA-low
Ultramutated (3%)
C-to-A transversions, POLE or POLD1 proofreading mutations
Chromosomal Instability CIN (84%)
SCNA-high, MSS, WNT-pathway deregulation
CMS1: MSI-Immune (14%)
Hypermutated, dMMR, MSI, MLH1-sil, CIMP-high, BRAF-mut, immune infiltration
CMS2: Canonical (37%)
SCNA-high, WNT and MYC activation
CMS3: Metabolic (13%)
SCNA-low, CIMP-low, KRAS-mut, metabolic deregulation, epithelial signature
CMS4: Mesenchymal (23%)
SCNA-high, stromal infiltration, TGFβ activation, EMT, C', angiogenesis, matrix remodelling
Mixed Features (13%)
Transition phenotype / Intratumoural heterogeneity

Abbildung 2: Molekulare Klassifikation von CRC (Muller, Ibrahim and Arends, 2016). CIMP – CpG Insel Methylierungsphänotyp; CMS – Consensus Molecular Subtype (Übereinstimmender molekularer Subtyp); dMMR - deficient DNA mismatch repair (Mismatch Reparatur Defizienz); EMT - Epithelial-mesenchymale Transition; MSI – Mikrosatelliteninstabilität; SCNA - Somatic Copy Number Alterations (somatische Chromosomenanomalien); POLE/D1 – DNA Polymerase E/D1; MSS – Mikrosatellitenstabil.

Pankreaskarzinome entstehen aus Vorläuferläsionen, den sogenannten *pankreatischen intraepithelialen Neoplasien*. Durch Akkumulation von Mutationen in Tumorsuppressor- und Protoonkogenen entwickeln sich diese Läsionen zum invasiven Karzinom - vergleichbar der *Adenom-Karzinom-Sequenz* im Kolorektum. Zu den häufigsten genetischen Veränderungen zählen aktivierende Mutationen im *KRAS* Gen, sowie die Inaktivierung von *TP53*, *DPC4*, *CDKN2* und *BRCA-2*. Eine detaillierte Übersicht der aktuell bekannten molekularen Mechanismen findet sich in (Oldfield, Connor and Gallinger, 2017).

2.3 Konventionelle Therapie des Kolorektalen Karzinoms

Das Standardtherapeutikum in der adjuvanten, aber auch palliativen Therapie des fortgeschrittenen CRC ist 5-Fluoruracil (5-FU), welches in Monotherapie und in Kombination mit anderen

Wirkstoffen (u.a. dem Platinderivat Oxaliplatin/Folinsäure (FS) (=FOLFOX) bzw. dem Topoisomerase I Inhibitor Irinotecan/FS (FOLFIRI)) eingesetzt wird (Leon *et al.*, 2011; Onkologie, 2013). Ergebnisse aus (prä-) klinischen Studien sind kontrovers, beschreiben jedoch häufig ein gutes Ansprechen von chromosomal instabilen Tumoren. Hingegen scheinen nur ca. 30 % aller Mismatch Reparatur-defizienten (dMMR)-Tumoren von einer 5-FU basierten Therapie zu profitieren (Juo *et al.*, 2014). Auf molekularer Ebene lässt sich dies wie folgt erklären: dMMR Tumoren mit trunkiertem *HSP110* Gen (Exon 9 Skipping Mutation (=HSP110ΔE9) sind sensitiv gegenüber einer 5-FU-basierten Chemotherapie, bei Vorliegen von wildtypischem *HSP110* kommt es zur Resistenz (Dorard *et al.*, 2011; Collura *et al.*, 2014). Die grundsätzliche prognostische Relevanz für ein Ansprechen auf 5-FU wird gegenwärtig in einer französischen Studie retro- und prospektiv (N~600 Patienten) erfasst (*ClinicalTrials.gov* Identifier: NCT02458664), wobei die Ergebnisse noch ausstehen. Es ist wahrscheinlich, dass die Erhebung des *HSP110* Mutationsstatus zukünftig Bestandteil der prädiktiven Diagnostik sein wird.

2.4 Konventionelle Therapie des Pankreaskarzinoms

Die zytostatische Therapie des Pankreaskarzinoms basiert auf der Applikation der Nukleosidanaloga Gemcitabin (2′,2′-Difluordesoxycytidin) bzw. 5-FU/FS (=Mayo-Protokoll) (Oettle *et al.*, 2007; Seufferlein *et al.*, 2013). Bei lokal fortgeschrittenen und/oder metastasierten und damit nicht-resektablen Pankreaskarzinomen wird in der Erstlinientherapie Gemcitabin bzw. eine Kombinationstherapie mit dem Epidermalen Wachstumsfaktor-Rezeptortyrosinkinase-Inhibitor Erlotinib eingesetzt, gegebenenfalls in Kombination mit Radiotherapie (Seufferlein *et al.*, 2013). Alternativ kann auch eine Kombination von 5-FU/FS, Irinotecan und Oxaliplatin nach dem sogenannten FOLFIRINOX-Protokoll eingesetzt werden. Eine weitere Option stellt die Kombination von Gemcitabin mit dem Taxan nab-Paclitaxel dar (Von Hoff *et al.*, 2013). Allerdings führen alle Therapiemodalitäten ausschließlich zur Verlängerung des Gesamtüberlebens (Wang *et al.*, 2015) – eine Heilung bzw. Krankheitsstabilisierung wird nicht erzielt. Andere systemisch-unspezifische sowie zielgerichtete Ansätze haben gegenwärtig keinen klinischen Stellenwert – dies reflektiert die infauste Prognose, sowie die Notwendigkeit alternative Therapieoptionen zu entwickeln.

2.5 Möglichkeiten der Immuntherapie

Heute gibt es eine Vielzahl aktiver (=direkte Immunstimulation) und passiver (=indirekte Immunstimulation) Strategien, um Tumoren immunologisch zu attackieren. Sie verfolgen das Ziel, maligne Zellen durch die Induktion einer spezifischen T-Zell-gerichteten Immunantwort zu eliminieren und eine protektive Immunität gegenüber residuellen Tumorzellen sowie potentiellen (Mikro-) Metastasen/Rezidiven zu vermitteln. Eine Übersicht der gegenwärtig zur Verfügung stehenden Konzepte ist in Abb. 3 dargestellt.

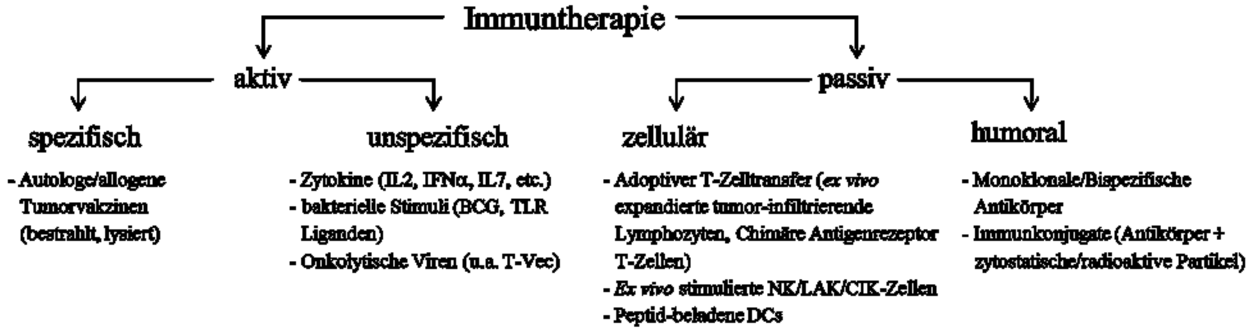
Immuntherapie
aktiv
passiv
spezifisch
- Autologe/allogene Tumorvakzinen (bestrahlt, lysiert)
unspezifisch
- Zytokine (IL2, IFNα, IL7, etc.)
- bakterielle Stimuli (BCG, TLR Liganden)
- Onkolytische Viren (u.a. T-Vec)
zellulär
- Adoptiver T-Zelltransfer (*ex vivo* expandierte tumor-infiltrierende Lymphozyten, Chimäre Antigenrezeptor T-Zellen)
- *Ex vivo* stimulierte NK/LAK/CIK-Zellen
- Peptid-beladene DCs
humoral
- Monoklonale/Bispezifische Antikörper
- Immunkonjugate (Antikörper + zytostatische/radioaktive Partikel)

Abbildung 3: Übersicht gegenwärtig zur Verfügung stehender immuntherapeutischer Konzepte. BCG – Bacille Calmette Guerin; TLR – Toll like Rezeptor.

Die breiteste klinische Anwendung finden Immuncheckpoint-Inhibitoren (z.B. anti-*Programmed cell death protein 1(*PD-1)/ *Programmed cell death 1 ligand 1*(PD-L1)), welche innerhalb kürzester Zeit die Immuntherapie revolutioniert haben (Carbone *et al.*, 2017; Giroux Leprieur *et al.*, 2017). Der Wirkmechanismus dieser monoklonalen Antikörper basiert auf der Hemmung der Rezeptor-Liganden-Bindung („Breaking the breaks“) zur Restoration der Immunantwort (Giroux Leprieur *et al.*, 2017; Marin-acevedo *et al.*, 2018).

Die erfolgreiche Anwendung dieser Strategie bei gastrointestinalen Tumoren wurde bislang jedoch fast ausschließlich bei dMMR-assoziierten CRCs (ca. 15 % aller CRCs) nachgewiesen, wohingegen alle anderen CRCs (ca. 85 % aller Fälle), sowie Pankreaskarzinome nicht von dieser Therapieform zu profitieren scheinen (Emambux *et al.*, 2018; Marginean and Melosky, 2018). Neuere Untersuchungen zeigen, dass, neben anderen Faktoren, das Antigenrepertoire resultierend aus der Mutationslast (hyper- vs. hypomutiert) prädiktiv für die Wirksamkeit ist (Cogdill, Andrews and Wargo, 2017; Chae *et al.*, 2018). Pankreaskarzinome, sowie mehrheitlich auch CRCs zählen nicht im klassischen Sinne zu den immunogenen Neoplasien (Sun, Suo and Yan, 2016; Emambux *et al.*, 2018), da sie eine geringe Anzahl tumor-spezifischer Neoantigene tragen bzw. nur solche, die keine starke Immunantwort auslösen (Zhang, Wolfgang and Zheng, 2018). CRCs mit dMMR hingegen tragen eine hohe Frequenz Haupthistokompatibilitäts-Komplex-I/II (*major histocompatibility complex*, MHC)-restringierter Neoantigene auf der Tumorzelloberfläche (Schwitalle *et al.*, 2008; Linnebacher *et al.*, 2010; Yuza *et al.*, 2017). Gleichzeitig zeichnen sich diese Tumoren aber auch durch eine sehr hohe Abundanz von Immuncheckpoint-Molekülen aus, welche einer effektiven Immunantwort entgegenwirken (Chabanon *et al.*, 2016; Sun, Suo and Yan, 2016). Damit stellen dMMR-assoziierte Tumoren als einziger molekularer Subtyp des CRC ideale Zielstrukturen für (Immuncheckpoint-Inhibitor-basierte) Ansätze dar.

Basierend auf diesen Daten erscheint es sinnvoll, weitere Strategien zu evaluieren, um auch Tumoren mit geringer/moderater Mutationslast einer Immuntherapie zugängig zu machen (Zhang, Wolfgang and Zheng, 2018).

Aktive immuntherapeutische Strategien zur Behandlung gastrointestinaler Tumore

Die aktive Immuntherapie in Form einer unspezifischen (z.B. mikrobieller Stimulus bzw. Toll-like Rezeptor (TLR) Agonist, proinflammatorische/immunstimulierende Agenzien) oder spezifischen Immunstimulation (z.B. Tumorlysate, Peptide, Tumor DNA/RNA) stellt einen vielversprechenden Ansatz zur Erhöhung der Immunogenität von Pankreaskarzinomen und CRCs dar. Sie verfolgt das Ziel, dass Immunsystem polyklonal zu stimulieren und geht ursächlich auf die Beobachtungen William B. Coleys und Rudolf Virchows zurück (Coley, 1910, 1991; Ichim, 2005). Das Prinzip der aktiv unspezifischen Immuntherapie wurde in einer vorangehenden Übersichtsarbeit dargelegt (Linnebacher *et al.*, 2012). Es basiert auf einer direkten Schädigung der Tumorzellen u.a. durch mikrobielle Toxine, welche sekundär zur Aktivierung des nicht-adaptiven Immunsystems (Makrophagen, Granulozyten, NK-Zellen, dendritische Zellen) und – im Idealfall – Generierung eines immunologischen Gedächtnisses (zellulär: Antigen-spezifische T-Zellen; humoral: Antigen-spezifische Antikörper) führt.

Die vorliegende Habilitationsarbeit adressiert verschiedene Aspekte im Bereich der immunologischen Therapieansätze. So wurde in einer Reihe von *in vivo* Studien die Wirksamkeit bakterieller Präparationen untersucht. Es konnte gezeigt werden, dass die einmalige systemische Gabe von *Clostridium novyi-NT* Sporen zur kompletten Remission muriner Pankreaskarzinome durch Stimulation des primär nicht-adaptiven Immunsystems führt (Maletzki *et al.*, 2010). Vergleichbare Befunde wurden in der nachfolgenden Arbeit erhoben, in der eine avitale bakterielle Präparation aus hitzeinaktivierten *S. pyogenes* and *S. marcescens* (= Coley's Toxins) *in vitro* und *in vivo* eingesetzt wurde ((Maletzki, Klier, *et al.*, 2012); s. Anlage 1). Im ektopen *in vivo* Modell wurde eine signifikante Beeinflussung des Tumorwachstums allerdings ausschließlich nach lokaler Therapie beobachtet, die systemische Applikation erzielte nur einen marginalen therapeutischen Effekt. Immunologische Veränderungen waren primär nach lokaler Gabe, durch Induktion von γ/δ T-Zellrezeptor-positiven Zellen nachweisbar.

Um die potentiell wirksamsten TLR Liganden für eine (prä-) klinische Anwendung zu identifizieren, wurde weiterhin die Wirksamkeit verschiedener, definierter TLR Agonisten (-kombinationen) im murinen Pankreaskarzinommodell untersucht ((Maletzki *et al.*, 2013); s. Anlage 2). Die Monoapplikation der TLR Liganden verzögerte das Tumorwachstum nach repetitiver Gabe. Jedoch zeigten sich Unterschiede hinsichtlich der Effizienz (LPS > Resiquimod > Flagellin > MDP). Die Kombination von drei TLR Liganden führte in 4/5 Fällen zur kompletten Remission bzw. zur signifikanten Hemmung des Tumorwachstums in dem verbleibenden Fall. Begleitende durchflusszytometrische Analysen zeigten eine bis zu 6-fache Reduktion des Anteils $CD11b^+Gr1^+$ myeloider Suppressorzellen sowohl nach Mono- (Resiquimod > LPS > MDP) als auch Kombinationstherapie. Myeloide Suppressorzellen stellen eine heterogene Gruppe dar, welche sowohl NK- als auch T-Zell-vermittelte Immunantworten supprimieren – ähnlich dem Wirkverhalten regulatorischer T-Zellen und tumor-assoziierter Makrophagen (Draghiciu *et al.*, 2015). Deren (selektive) Eliminierung zur Überwindung der tumor-induzierten Immuntoleranz ist Gegenstand aktueller Arbeiten (Draghiciu *et al.*, 2015; Adah *et al.*, 2016; Liu *et al.*, 2018) – die beobachteten Effekte nach TLR-vermittelter Immuntherapie erweitern das Spektrum vorhandener Substanzen.

In einer nachfolgenden Studie zum CRC wurden ähnliche, jedoch weniger stark ausgeprägte antitumorale, sowie immunmodulatorische Effekte nach Applikation verschiedener TLR Liganden beobachtet (Stier *et al.*, 2013). Es muss jedoch berücksichtigt werden, dass durch den Einsatz von Tumorzellen aus dem Kolorektum eine Entität gewählt worden, welche natürlicherweise ständig mit Bakterien bzw. bakteriellen Toxinen in Kontakt ist. Dieser schmale Grat zwischen Aufrechterhaltung der Gewebshomöostase unter physiologischen Bedingungen und Stimulation des Tumorwachstums nach chronischer Inflammation (Kluwe, Mencin and Schwabe, 2009; Khajeh Alizadeh Attar *et al.*, 2017) scheint entscheidend zur Wirksamkeit von TLR Liganden beizutragen. So wurde in einer anderen Studie gezeigt, dass ein TLR3 Ligand Apoptose in humanen Mammakarzinomzellen induziert, derselbe Ligand aber das Wachstum intestinaler Tumorzellen fördert (Kluwe, Mencin and Schwabe, 2009; Pavelic, 2014). Dies lässt den Schluss zu, dass primär Tumoren aus einer „sterilen" Umgebung – wie dem Pankreas – für die gewählte Therapieform geeignet sind, wohingegen die Anwendbarkeit beim CRC fraglich ist.

Eine weitere Limitation des gewählten Ansatzes stellt die Notwendigkeit zur lokalen Applikation, sowie die fehlende Induzierbarkeit tumor-spezifischer Immunantworten dar, welche die Voraussetzung für die Entwicklung eines immunologischen Gedächtnisses sind. Interessanterweise bestätigen die Befunde damit unsere vorangegangenen Untersuchungen zur Wirksamkeit avitaler bakterieller Präparationen (Klier *et al.*, 2011, 2012). Spezifische antitumorale Immunantworten können folglich primär nach Stimulation mit vitalen Bakterien bzw. Kombinationen mit spezifischen Stimulanzien erzielt werden (Maletzki *et al.*, 2008). Die Vor- und Nachteile dieser mikrobiellen Immuntherapie und deren potentielle Anwendbarkeit beim Pankreaskarzinom und dem CRC sind in unserer Übersichtsarbeit beschrieben (Linnebacher *et al.*, 2012).

Neben dieser Form der aktiv-unspezifischen Immuntherapie, stehen auch spezifische Ansätze durch Vakzinierung zur Verfügung. Auf diese wird im Kapitel 2.7 näher eingegangen.

2.6 *In vitro* und *in vivo* Modelle für präklinische Untersuchungen

Zur experimentellen Umsetzung wissenschaftlicher Fragestellungen stehen unterschiedliche Modellsysteme zur Verfügung, welche auch im Rahmen der Habilitationsarbeiten Anwendung fanden:

- *in vitro* 2D- und 3D-Zellkulturen: Langzeit-kultivierte Tumorzellen vs. Patienten-abgeleitete Tumorzellen in niedriger Passage
- *in vivo* Tumormodelle: ektopes, syn-/xenogenes Tumormodell sowie Patient-derived Xenograft (PDX) Modell vs. spontanes Tumorgenesemodell

Patienten-abgeleitete Tumorzellen bzw. PDX, idealerweise kurzzeitig passagiert („ultra-low-passage"), erlauben eine reale Abbildung des Originaltumors (Marangoni *et al.*, 2007; Byrne *et al.*, 2017). Idiosynkratische Charakteristika, wie inter- und intratumorale Heterogenität, molekulare Signatur, Oligoklonalität und Antigenität bleiben zumindest temporär erhalten (Maletzki, Gock, *et al.*, 2015; Lai *et al.*, 2017). Folglich ist die prädiktive Wertigkeit für nachfolgende *in vivo* Studien besonders hoch. Aufgrund der Limitierung von Tumorfrischgewebe werden häufig langzeit-kultivierte allogene Tumorzellen verwendet (u.a. NCI-60 Panel – eine Kollektion von Zelllinien unterschiedlichen Ursprungs, darunter 7x CRC (Reinhold *et al.*, 2014)). Solche Tumorzellen zeigen allerdings eine teilweise starke Adaptation an Kulturbedingungen. Diese korreliert mit der Kulturdauer und führt in der Konsequenz dazu, dass die Zelllinien andere biologische und molekulare Charakteristika aufweisen als Primärtumoren (Neri and Nicolson, 1981; Barnes, Moy and Dickson, 2006). Das ist insbesondere bei dMMR-assoziierten Tumoren relevant, welche aufgrund fehlender Reparaturmechanismen bei jeder Zellteilung neue Mutationen akkumulieren können. So wurde kürzlich in einer Studie an pädiatrischen Hirntumoren mit konstitutioneller (=biallelischer) dMMR nachgewiesen, dass Tumorzellen bis zu 600 neue Mutationen/Zellteilung akquirieren (Bouffet *et al.*, 2016). Die resultierenden Tumoren sind „ultramutiert" (i.d.R. nicht-synonyme Mutationen) und exprimieren ein komplexes Spektrum an Neoantigenen – eine ähnliche Zunahme der Mutationslast bei dMMR-assoziierten CRC Linien ist wahrscheinlich.

Um die entsprechenden Modelle von CRC Patienten für präklinische Therapiestudien zu erhalten, wurden analog zu einer vorherigen Arbeit (Dangles-Marie *et al.*, 2007) zwei Ansätze verfolgt (Abb. 4): (I) direkte *in vitro* Zellkultur primärer CRC durch Homogenisierung des erhaltenen Tumorstücks nach chirurgischer Resektion; (II) indirekt nach *in vivo* Transfer eines ca. 3x3x3 mm großen Tumorstücks in immunkompromitierte NMRI Foxn1^{nu} Mäuse und nachfolgender Resektion der resultierenden PDX.

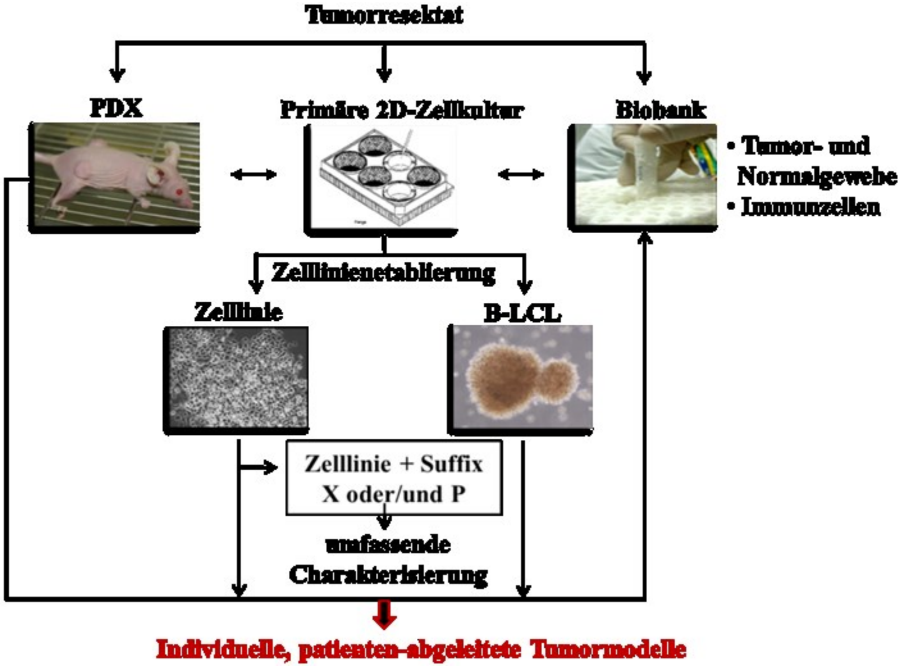
Tumorresektat
PDX
Primäre 2D-Zellkultur
Biobank
• Tumor- und Normalgewebe
• Immunzellen
Zelllinienetablierung
Zelllinie
B-LCL
Zelllinie + Suffix X oder/und P
umfassende Charakterisierung
Individuelle, patienten-abgeleitete Tumormodelle

Abbildung 4: Experimentelles Protokoll zur Etablierung Patienten-abgeleiteter Tumormodelle für funktionelle, molekulare und immunologische Untersuchungen. PDX – patient-derived Xenograft; X – Xenograft; P – Patient. Maletzki *et al.*, 2012.

Mit dieser Methode wurden individuelle Tumormodelle von allen CRC Subtypen, sowohl humanen, als auch murinen Ursprungs, generiert. Der Erfolg der Etablierung war relativ unabhängig vom molekularen Subtyp ((Maletzki, Stier, *et al.*, 2012; Maletzki, Huehns, *et al.*, 2015); s. Anlage Teil 3 und 4; sowie (Maletzki, Gock, *et al.*, 2015; Maletzki *et al.*, 2016).

Die Kulturen wurden als epitheliale (EpCAM$^+$ bzw. CD104$^+$) Zellen charakterisiert und zeigten ein heterogenes Oberflächenprofil. Interessanterweise wurde in einem Fall eine, im Vergleich zum Primarius, *de novo* Mutation im *KRAS* Gen (c.176C>G (A59G) nachgewiesen ((Maletzki, Huehns, *et al.*, 2015); s. Anlage Teil 4). Im Rahmen der Chemoresponsivitätsanalysen haben wir nicht nur zelllinienspezifische Unterschiede, sondern auch Differenzen zwischen dem *in vitro* und *in vivo* Ansatz detektiert. Es zeigte sich beispielsweise, dass der Topoisomerase-I-Inhibitor Irinotecan signifikant das Tumorwachstum *in vivo* hemmt (vs. moderates Ansprechen *in vitro*), wohingegen der TLR4 Ligand Paclitaxel nur bei einem von drei dMMR Tumormodellen therapeutisch wirksam war (vs. gutes Ansprechen *in vitro*) ((Maletzki, Stier, *et al.*, 2012); s. Anlage Teil 3). Des Weiteren konnten wir zeigen, dass die Kombination klassischer Zytostatika (5-FU und Gemcitabin) mit dem globalen demethylierenden Agenz 5-Azacytidin keine Verstärkung des antitumoralen Effektes bei hypermethylierten (= molekularer CRC Subtyp: CMS1 bzw. CMS3) Zelllinien bewirkt ((Maletzki, Huehns, *et al.*, 2015); s. Anlage Teil 4). Sowohl die simultane, als auch sequentielle Applikation hatte primär antagonistische Wirkung und bestätigt Befunde einer kürzlich durchgeführten klinischen Phase I/II Studie, in der 26 Patienten mit therapierefraktären CIMP CRC eine Kombination von 5-Azacytidin (75 mg/m^2/Tag, subkutan D1-5) und CAPOX (Capecitabin (=5-FU Vorstufe) und Oxaliplatin; alle drei Wochen) erhielten (Overman *et al.*, 2016). In dieser Studie wurde bei keinem der Patienten ein verbessertes klinisches Ansprechen durch die Kombination von 5-Azacytidin mit CAPOX erzielt (Overman *et al.*, 2016) – eine nahezu vollständige Translation der hier erhobenen *in vitro* Befunde. Folglich sollten Patienten-individuelle Tumormodelle im Fokus präklinischer Responseprädiktion stehen.

Neben diesen klassischen zytostatischen Substanzen gibt es Bestrebungen, neue und nebenwirkungsarme Substanzen in die klinische Anwendung zu überführen. Einen interessanten Ansatz bieten bestimmte antimikrobielle Strukturen, sogenannte *Host Defense Peptide* (HDP) (Deslouches and Di, 2017). HDPs sind Effektormoleküle des nicht-adaptiven Immunsystems, welche in einer Vielzahl von Organismen vorkommen (Schröder-Borm, Bakalova and Andrä, 2005; Mahlapuu *et al.*, 2016). Während einige Studien die direkte, physikalische Störung der

Zellmembranintegrität ohne spezifische Rezeptorinteraktion (Schröder-Borm, Bakalova and Andrä, 2005) bei langzeit-kultivierten Tumorzelllinien belegen, gibt es bislang keine Informationen zur Wirksamkeit gegenüber kurzzeitig passagierten, Patienten-individuellen Zelllinien. Um zu überprüfen, ob ein ähnliches Wirkverhalten vorliegt, wurde eine vergleichende Analyse durchgeführt ((Maletzki *et al.*, 2014); s. Anlage Teil 5). Zunächst konnte gezeigt werden, dass die Abundanz von oberflächenpräsentiertem Phospatidylserin, welches als Marker für ein Ansprechen auf HDPs diskutiert wird (Schröder-Borm, Bakalova and Andrä, 2005) bei langzeit-kultivierten Zellen höher ist, als bei kurzzeitig passagierten Zellen ((Maletzki *et al.*, 2014); s. Anlage Teil 5). Dies stellt vermutlich einen Adaptationsmechanismus an die *in vitro* Kultur dar. Sowohl langzeit-kultivierte, als auch Patienten-individuelle Zelllinien waren allerdings suszeptibel gegenüber einer HDP-vermittelten Onkolyse. Die Effekte waren primär auf Nekrose zurückzuführen. In einem murinen PDX Modell (dMMR Zelllinie HROC24, NMRI Foxn1^{nu} Maus) wurde schließlich die Wirksamkeit der HDPs (1 mg/kg KG, intratumoral) *in vivo* analysiert. Hierbei konnte erstmals die onkolytische Aktivität bestätigt werden. Gewonnene Tumorresektate zeigten eine erhöhte Anzahl an Tumorzellapoptosen und -nekrosen. Hämatotoxische Nebenwirkungen wurden nicht nachgewiesen. Dennoch konnte in diesem Ansatz keine selektive Wirksamkeit aufgezeigt werden, da ein irrelevantes Kontrollpeptid ebenfalls das Tumorwachstum beeinflusste. Folglich müsste zunächst die Tumorselektivität verbessert werden, bevor dieser Therapieansatz weiter evaluiert wird.

Eine andere Anwendung der vorgestellten Modelle ergibt sich für immunologische Therapieansätze. Zelllinien und PDX Modelle stellen eine theoretisch unlimitierte und einfach herzustellende Antigenquelle dar (Barnes, Moy and Dickson, 2006; Aurisicchio *et al.*, 2018; Williams, 2018). Bei der Verwendung von Gesamttumorlysaten wird ein breites Spektrum an (potentiell) immunologisch relevanten MHC-I/II-restringierten Antigenen zur Verfügung gestellt, um sowohl CD4^{+}, als auch CD8^{+}-vermittelte T-Zellantworten auszulösen bzw. präformierte, jedoch supprimierte Immunantworten zu verstärken ((Maletzki *et al.*, 2018); s. Anlage Teil 6). Dies erlaubt nicht nur eine repetitive Gabe in hoher Dosis, sondern bietet auch die Möglichkeit, Hochrisikopatienten, z.B. mit erblichen Tumorprädispositionssyndromen, wie dem Lynch Syndrom, prophylaktisch zu vakzinieren. Eine Möglichkeit zur Umsetzung im murinen Tumormodell wird in Kapitel 2.7 näher beschrieben.

2.7 Die aktiv-spezifische Immuntherapie am Beispiel dMMR-assoziierter Neoplasien

Die Erkenntnis, dass dMMR-assoziierte Neoplasien ideale Zielstrukturen für aktiv-spezifische Vakzinierungsansätze darstellen, geht auf verschiedene *in vitro* Analysen zurück, in denen wir und andere Arbeitsgruppen zeigen konnten, dass diese Tumoren Neoantigene exprimieren, die von zytotoxischen T-Zellen erkannt werden (Saeterdal *et al.*, 2001; Schwitalle *et al.*, 2004; Linnebacher *et al.*, 2010; Garbe, Maletzki and Linnebacher, 2011). Mit diesem Wissen wurde von der Radboud Universität in Nijmegen bereits eine klinische Phase I/II Studie initiiert, in der Lynch Syndrom Patienten sowohl prophylaktisch, als auch therapeutisch mit einem definierten Mix aus spezifischen Peptiden vakziniert werden (*ClinicalTrials.gov* Identifier: NCT01885702). Die Selektion der zur Vakzine eingesetzten Peptide erfolgte (I) aufgrund einer nachgewiesenen hohen Mutationsfrequenz in dMMR-assoziierten Tumoren (z.B. *TGFβRII, AIM-2*) und (II) der *in vitro* bestätigten starken Immunogenität (T-Zell-Stimulation) (Saeterdal *et al.*, 2001; Schwitalle *et al.*, 2004). Dies unterstreicht die klinische Relevanz dieses Ansatzes. Da mit Ausnahme dieser klinischen Studie bislang keine *in vivo* Untersuchungen vorlagen, wurde im Rahmen der vorliegenden Habilitationsschrift eine experimentelle Vakzinetherapie im spontanen MLH1$^{-/-}$ Tumorgenesemodell initiiert ((Maletzki *et al.*, 2018); s. Anlage Teil 6). Tiere mit ubiquitärem Knockout des *MLH1* Gens entwickeln innerhalb von neun Monaten Lynch Syndrom-ähnliche dMMR Adenome/Adenokarzinome, Non-Hodgkin-Lymphome sowie andere Tumoren (Edelmann *et al.*, 1999). Mutationen treten -in Analogie zu dem humanen Krankheitsbild- sowohl in kodierenden als auch nicht-kodierenden Bereichen von MLH1$^{-/-}$ Tumorgenese-assoziierten Zielgenen auf (Bacher *et al.*, 2005; Maletzki *et al.*, 2016). Folglich liegen ähnliche Pathogenesemechanismen zugrunde. Die repetitive prophylaktische Gabe des Vakzins (MLH1$^{-/-}$ Tumorlysat 10 mg/kg KG +/- Adjuvanz: CpG-Oligodesoxyribonukleotid (ODN) 1826 2,5 mg/kg KG, jeweils s.c.) führte zur Immunstimulation und verzögerte das Tumorwachstum gegenüber Kontrolltieren ((Maletzki *et al.*, 2018); s. Anlage Teil 6). Die therapeutische Applikation verlängerte das Gesamtüberleben signifikant (11,5 (Lysat) und 12 Wochen (Lysat + CpG ODN 1826) vs. 3 Wochen (Kontrolle)) durch Krankheitsstabilisierung und Reduktion der Tumorlast in einigen Fällen. Dies war relativ unabhängig von dem Adjuvanz CpG ODN 1826, welches als TLR9 Agonist antigen-spezifische Immunantworten verstärken soll (Lubaroff and Karan, 2009; Tian *et al.*, 2017). Im Rahmen unserer Studie konnte kein verstärkender Effekt durch CpG ODN 1826 nachgewiesen werden. Unabhängig vom Adjuvanz wurde in immunologischen Untersuchungen eine erhöhte Reaktivität und lytische Aktivität von Lymphozyten vakzinierter Tiere gegenüber autologen und allogenen MLH1$^{-/-}$ Tumorzellen beobachtet. Damit bestätigen die Untersuchungen die Induzierbarkeit polyklonaler T-Zell-vermittelter Immunantworten nach Vakzine und belegen die grundsätzliche Wirksamkeit von autologen Vakzinen (Sun, Suo and Yan, 2016). Gleichzeitig wurden in Tumorresektaten mehr infiltrierende T-Zellen (CD4^{+}/CD8^{+}) detektiert, jedoch auch vermehrt Immun-Checkpointmoleküle (PD1/PD-L1; Lymphozyten-Aktivierungsgen 3) nachgewiesen, welche sehr wahrscheinlich einen erworbenen Escape- bzw. Resistenzmechanismus darstellen (Abb. 5).

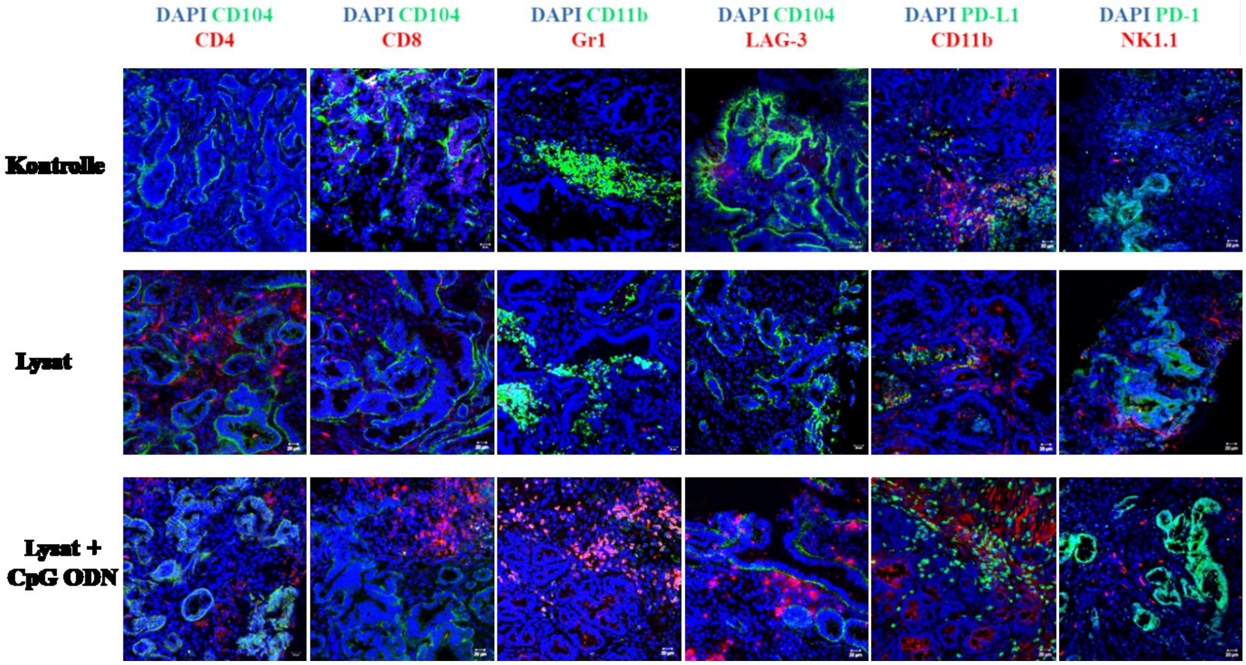

Abbildung 5: Immunzellinfiltration. Repräsentative immunfluoreszenzmikroskopische Darstellung von Tumorresektaten vakzinierter Tiere (Lysat, Lysat + CpG ODN) im Vergleich zu einem Kontrolltier (Kontrolle). Kernfärbung mit DAPI, Originalvergrößerung x200. LAG-3 - *Lymphozyten-Aktivierungsgen 3;* Maletzki *et al.,* 2018.

Folglich stellen Kombinationsansätze, bestehend aus tumor-spezifischer Vakzine und Immuncheckpoint-Inhibition, wie kürzlich u.a. für Glioblastome (dendritische Zellvakzine + anti-PD-1 Antikörper + Kolonie-stimulierender Faktor 1 Rezeptor Inhibition) und Prostatakarzinome (anti-zytotoxisches T-Zell-assoziiertes Protein 4 Antikörper + Granulozyten-Monozyten-Kolonie-stimulierende Faktor-sezernierende zelluläre Vakzine) propagiert (Wada *et al.*, 2013; Antonios *et al.*, 2017), eine aussichtsreiche Therapieoption dar, um diesen Ansatz langfristig in die klinische Anwendung zu überführen.

3 Zusammenfassung und Ausblick

In der vorliegenden Habilitationsschrift wurden verschiedene immunologische Fragestellungen und immuntherapeutische Konzepte bei gastrointestinalen Tumoren adressiert und umgesetzt.

Zunächst konnte festgestellt werden, dass gastrointestinale Tumoren grundsätzlich für immuntherapeutische Strategien geeignet sind. In Abhängigkeit der zugrunde liegenden Fragestellung können zur Untersuchung sowohl langzeit-kultivierte, als auch Patienten-abgeleitete und damit idealerweise kurzzeitig passagierte Zelllinien herangezogen werden. Dabei sollten potentielle biologische Veränderungen, wie Wachstum, Oberflächenprofil, (Chemo-) Responsivität, molekulare Signatur, und damit verbunden auch die Immunogenität vor der Therapieentscheidung berücksichtigt werden.

Der vorgestellte kombinierte Ansatz aus direkter (= aus Tumorfrischgewebe) und indirekter Zellkultur (= nach *in vivo* Transfer) erlaubt eine standardisierte und reproduzierbare Vorgehensweise, um Patienten-abgeleitete Tumormodelle zu etablieren. Die resultierenden *in vitro* Kulturen stellen eine gute Grundlage für Responsivitätstestungen dar. Die durchgeführten Untersuchungen zeigen aber auch, dass eine Kombination von *in vitro* und *in vivo* Analysen notwendig ist, um valide Aussagen bezüglich der Wirksamkeit neuartiger Substanzen machen zu können.

Die *in vivo* Umsetzung der Immuntherapie kann ausschließlich im immunkompetenten Wirt erfolgen. Hierbei wurde zunächst im ektopen Transplantationsmodell die Effizienz der aktiv-unspezifischen Immuntherapie nach Applikation von undefinierten bzw. definierten TLR-Mixen vergleichend analysiert. Es zeigte sich, dass das Tumorwachstum, in Abhängigkeit der untersuchten Tumorentität (CRC vs. Pankreaskarzinom) signifikant beeinflusst wird, die antitumorale Wirksamkeit jedoch nach lokaler Applikation deutlich stärker ausgeprägt ist, als nach systemischer Gabe. Ebenso ist ein definierter TLR-Mix effizienter, als die jeweilige Einzelsubstanz.

Aufgrund der Komplexität der immunologischen Mechanismen im Verlauf der Tumorgenese wurde zusätzlich ein spontanes Tumorgenesemodell herangezogen und die Wirksamkeit einer Vakzine hinsichtlich Tumorinzidenz, -wachstum und -mikromilieu erstmals präklinisch erfasst. Es konnte nachgewiesen werden, dass die repetitive Gabe des Vakzins sowohl die Entstehung, als auch Progression autochthoner dMMR-assoziierter Tumoren durch Stimulation des Immunsystems verzögert.

Insgesamt konnte in dieser Arbeit gezeigt werden, dass sowohl die unspezifische Immuntherapie in Form von mikrobiellen Stimuli, als auch die spezifische Form einer Tumorvakzine vielversprechende Ansätze zur Behandlung gastrointestinaler Tumoren darstellen.

Aus den gewonnenen Daten ergeben sich unterschiedliche Ansatzpunkte für weitere wissenschaftliche und translationale Arbeiten.

Zum einen sollte die prädiktive Wertigkeit der *in vitro* durchgeführten Responseanalysen an Patienten-abgeleiteten Tumormodellen *in vivo* unter Anwendung eines humanisierten murinen Modells verifiziert werden. Hierbei gibt es aktuell verschiedene Strategien, um die „nächste Generation humanisierter PDX Modelle“ für präklinische Immuntherapien zu etablieren (Williams, 2018). Im Idealfall werden hierbei autologe Immunzellen eingesetzt, um sowohl die MHC-Kompatibilität zwischen Tumor- und antigenspezifischen T-Zellen als auch die Aufrechterhaltung bzw. Wiederherstellung des Tumormikromilieus zu gewährleisten.

Hinsichtlich der Optimierung der Tumorvakzine gibt es viele Optionen. Diese umfassen neben dem Einsatz definierter Peptide, auch die Kombination mit niedrig-dosierter Chemotherapie, sowie Immun-Checkpoint-Inhibitoren, um einer potentiellen Resistenzentwicklung entgegenzuwirken.

4 Literaturverzeichnis

1 Adah, D. *et al.* (2016) ‘Implications of MDSCs-targeting in lung cancer chemo-immunotherapeutics’, *Pharmacological Research*. Elsevier Ltd, 110, pp. 25–34. doi: 10.1016/j.phrs.2016.05.007.

2 Antonios, J. P. *et al.* (2017) ‘Immunosuppressive tumor-infiltrating myeloid cells mediate adaptive immune resistance via a PD-1/PD-L1 mechanism in glioblastoma.’, *Neuro-oncology*. England, 19(6), pp. 796–807. doi: 10.1093/neuonc/now287.

3 Aurisicchio, L. *et al.* (2018) ‘The perfect personalized cancer therapy: cancer vaccines against neoantigens’, *Journal of Experimental & Clinical Cancer Research*. Journal of Experimental & Clinical Cancer Research, 37(1), p. 86. doi: 10.1186/s13046-018-0751-1.

4 Bacher, J. W. *et al.* (2005) ‘Use of Mononucleotide Repeat Markers for Detection of Microsatellite Instability in Mouse Tumors’, 292(July), pp. 285–292. doi: 10.1002/mc.20146.

5 Barnes, L. M., Moy, N. and Dickson, A. J. (2006) ‘Phenotypic variation during cloning procedures: analysis of the growth behavior of clonal cell lines.’, *Biotechnology and bioengineering*. United States, 94(3), pp. 530–537. doi: 10.1002/bit.20856.

6 Bertz, J. *et al.* (2010) *Verbreitung von Krebserkrankungen in Deutschland Gesundheitsberichterstattung des Bundes Beiträge zur Gesundheitsberichterstattung des Bundes Verbreitung von Krebserkrankungen in Deutschland*.

7 Bouffet, E. *et al.* (2016) ‘Immune checkpoint inhibition for hypermutant glioblastoma multiforme resulting from germline biallelic mismatch repair deficiency’, *Journal of Clinical Oncology*, 34(19), pp. 2206–2211. doi: 10.1200/JCO.2016.66.6552.

8 Brenner, H., Stock, C. and Hoffmeister, M. (2015) ‘Colorectal cancer screening: The time to act is now’, *BMC Medicine*. BMC Medicine, 13(1), pp. 1–5. doi: 10.1186/s12916-015-0498-x.

9 Byrne, A. T. *et al.* (2017) ‘Interrogating open issues in cancer precision medicine with patient-derived xenografts’, *Nature Reviews Cancer*. Nature Publishing Group, 17(4), pp. 254–268. doi: 10.1038/nrc.2016.140.

10 Carbone, D. P. *et al.* (2017) ‘First-Line Nivolumab in Stage IV or Recurrent Non–Small-Cell Lung Cancer’, *New England Journal of Medicine*, 376(25), pp. 2415–2426. doi: 10.1056/NEJMoa1613493.

11 Chabanon, R. M. *et al.* (2016) ‘Mutational landscape and sensitivity to immune checkpoint blockers’, *Clinical Cancer Research*, 22(17), pp. 4309–4321. doi: 10.1158/1078-0432.CCR-16-0903.

12 Chae, Y. K. *et al.* (2018) ‘Mutations in DNA repair genes are associated with increased neo-antigen load and activated T cell infiltration in lung adenocarcinoma’, 9(8), pp. 7949–7960.

13 Cogdill, A. P., Andrews, M. C. and Wargo, J. A. (2017) ‘Hallmarks of response to immune checkpoint blockade’, *British Journal of Cancer*. Nature Publishing Group, 117(1), pp. 1–7. doi: 10.1038/bjc.2017.136.

14 Coley, W. B. (1910) ‘The Treatment of Inoperable Sarcoma by Bacterial Toxins (the Mixed Toxins

of the Streptococcus erysipelas and the Bacillus prodigiosus).', *Proceedings of the Royal Society of Medicine*. England, 3(Surg Sect), pp. 1–48.

15 Coley, W. B. (1991) 'The treatment of malignant tumors by repeated inoculations of erysipelas. With a report of ten original cases. 1893.', *Clinical orthopaedics and related research*. United States, (262), pp. 3–11.

16 Collura, A. *et al.* (2014) 'Patients with colorectal tumors with microsatellite instability and large deletions in HSP110 T17 have improved response to 5-fluorouracil-based chemotherapy', *Gastroenterology*. Elsevier, Inc, 146(2), p. 401–411.e1. doi: 10.1053/j.gastro.2013.10.054.

17 Dangles-Marie, V. *et al.* (2007) 'Establishment of human colon cancer cell lines from fresh tumors versus xenografts: Comparison of success rate and cell line features', *Cancer Research*, 67(1), pp. 398–407. doi: 10.1158/0008-5472.CAN-06-0594.

18 Deslouches, B. and Di, Y. P. (2017) 'Antimicrobial peptides with selective antitumor mechanisms: prospect for anticancer applications.', *Oncotarget*. United States, 8(28), pp. 46635–46651. doi: 10.18632/oncotarget.16743.

19 Dorard, C. *et al.* (2011) 'Expression of a mutant HSP110 sensitizes colorectal cancer cells to chemotherapy and improves disease prognosis', *Nature Medicine*, 17(10), pp. 1283–1289. doi: 10.1038/nm.2457.

20 Draghiciu, O. *et al.* (2015) 'Myeloid derived suppressor cells — An overview of combat strategies to increase immunotherapy efficacy Myeloid derived suppressor cells — An overview of combat strategies to increase immunotherapy ef fi cacy', (October), pp. 1–10. doi: 10.4161/21624011.2014.954829.

21 Edelmann, W. *et al.* (1999) 'Tumorigenesis in Mlh1 and Mlh1 / Apc1638N Mutant Mice Tumorigenesis in Mlh1 and Mlh1 / Apc1638N Mutant Mice 1', pp. 1301–1307.

22 Emambux, S. *et al.* (2018) 'Results and challenges of immune checkpoint inhibitors in colorectal cancer', *Expert Opinion on Biological Therapy*. Taylor & Francis, pp. 1–13. doi: 10.1080/14712598.2018.1445222.

23 Fearon, E. R. and Vogelstein, B. (1990) 'A genetic model for colorectal tumorigenesis.', *Cell*. United States, 61(5), pp. 759–767.

24 Garbe, Y., Maletzki, C. and Linnebacher, M. (2011) 'An MSI Tumor Specific Frameshift Mutation in a Coding Microsatellite of MSH3 Encodes for HLA-A0201-Restricted CD8+ Cytotoxic T Cell Epitopes', *PLoS ONE*, 6(11). doi: 10.1371/journal.pone.0026517.

25 Giroux Leprieur, E. *et al.* (2017) 'Immunotherapy revolutionises non-small-cell lung cancer therapy: Results, perspectives and new challenges', *European Journal of Cancer*. Elsevier Ltd, 78, pp. 16–23. doi: 10.1016/j.ejca.2016.12.041.

26 Von Hoff, D. D. *et al.* (2013) 'Increased survival in pancreatic cancer with nab-paclitaxel plus

gemcitabine.', *The New England journal of medicine*. United States, 369(18), pp. 1691–1703. doi: 10.1056/NEJMoa1304369.

27 Ichim, C. V (2005) 'Revisiting immunosurveillance and immunostimulation: Implications for cancer immunotherapy', *Journal of Translational Medicine*. London, p. 8. doi: 10.1186/1479-5876-3-8.

28 Juo, Y. Y. *et al.* (2014) 'Prognostic value of CpG island methylator phenotype among colorectal cancer patients: A systematic review and meta-analysis', *Annals of Oncology*, 25(12), pp. 2314–2327. doi: 10.1093/annonc/mdu149.

29 Khadka, R. *et al.* (2018) 'Risk factor, early diagnosis and overall survival on outcome of association between pancreatic cancer and diabetes mellitus: Changes and advances, a review', *International Journal of Surgery*. IJS Publishing Group Ltd. doi: 10.1016/j.ijsu.2018.02.058.

30 Khajeh Alizadeh Attar, M. *et al.* (2017) 'Basic understanding and therapeutic approaches to target toll-like receptors in cancerous microenvironment and metastasis.', *Medicinal research reviews*. United States. doi: 10.1002/med.21480.

31 Klier, U. *et al.* (2011) 'Avitalized bacteria mediate tumor growth control via activation of innate immunity', *Cellular Immunology*, 269(2). doi: 10.1016/j.cellimm.2011.03.014.

32 Klier, U. *et al.* (2012) 'Combining bacterial-immunotherapy with therapeutic antibodies: A novel therapeutic concept', *Vaccine*, 30(17). doi: 10.1016/j.vaccine.2012.01.071.

33 Kluwe, J., Mencin, A. and Schwabe, R. F. (2009) 'Toll-like receptors, wound healing, and carcinogenesis', *Journal of Molecular Medicine*, 87(2), pp. 125–138. doi: 10.1007/s00109-008-0426-z.

34 Kommalapati, A. *et al.* (2018) 'Contemporary Management of Localized Resectable Pancreatic Cancer.', *Cancers*. Switzerland, 10(1). doi: 10.3390/cancers10010024.

35 Lai, Y. *et al.* (2017) 'Current status and perspectives of patient-derived xenograft models in cancer research', *Journal of Hematology & Oncology*. Journal of Hematology & Oncology, 10(1), p. 106. doi: 10.1186/s13045-017-0470-7.

36 Leon, L. G. *et al.* (2011) 'DNA Copy Number Profiles Correlate with Outcome in Colorectal Cancer Patients Treated with Fluoropyrimidine/Antifolate-based Regimens', *Current Drug Metabolism*, pp. 956–965. doi: http://dx.doi.org/10.2174/138920011798062337.

37 Linnebacher, M. *et al.* (2010) 'Identification of an MSI-H Tumor-Specific Cytotoxic T Cell Epitope Generated by the (− 1) Frame of U79260 (FTO)', 2010. doi: 10.1155/2010/841451.

38 Linnebacher, M. *et al.* (2012) 'Bacterial immunotherapy of gastrointestinal tumors', *Langenbeck's Archives of Surgery*, 397(4). doi: 10.1007/s00423-011-0892-6.

39 Liu, Y. *et al.* (2018) 'Targeting myeloid-derived suppressor cells for cancer immunotherapy.', *Cancer immunology, immunotherapy : CII*. Germany. doi: 10.1007/s00262-018-2175-3.

40 Lubaroff, D. M. and Karan, D. (2009) 'CpG oligonucleotide as an adjuvant for the treatment of

prostate cancer.', *Advanced drug delivery reviews*. Netherlands, 61(3), pp. 268–274. doi: 10.1016/j.addr.2008.12.005.

41 Mahlapuu, M. *et al.* (2016) 'Antimicrobial Peptides: An Emerging Category of Therapeutic Agents.', *Frontiers in cellular and infection microbiology*. Switzerland, 6, p. 194. doi: 10.3389/fcimb.2016.00194.

42 Maletzki, C. *et al.* (2008) 'Pancreatic cancer regression by intratumoural injection of live Streptococcus pyogenes in a syngeneic mouse model', *Gut*, 57(4), pp. 483–491. doi: 10.1136/gut.2007.125419.

43 Maletzki, C. *et al.* (2010) 'Bacteriolytic therapy of experimental pancreatic carcinoma', *World Journal of Gastroenterology*, 16(28). doi: 10.3748/wjg.v16.i28.3546.

44 Maletzki, C., Stier, S., *et al.* (2012) 'Establishment, Characterization and Chemosensitivity of Three Mismatch Repair Deficient Cell Lines from Sporadic and Inherited Colorectal Carcinomas', *PLoS ONE*, 7(12). doi: 10.1371/journal.pone.0052485.

45 Maletzki, C., Klier, U., *et al.* (2012) 'Reevaluating the concept of treating experimental tumors with a mixed bacterial vaccine: Coley's toxin', *Clinical and Developmental Immunology*, 2012. doi: 10.1155/2012/230625.

46 Maletzki, C. *et al.* (2013) 'Mistletoe lectin has a shiga toxin-like structure and should be combined with other Toll-like receptor ligands in cancer therapy', *Cancer Immunology, Immunotherapy*, 62(8). doi: 10.1007/s00262-013-1455-1.

47 Maletzki, C. *et al.* (2014) 'Host defense peptides for treatment of colorectal carcinoma-a comparative in vitro and in vivo analysis', *Oncotarget*, 5(12). doi: 10.18632/oncotarget.2039.

48 Maletzki, C., Gock, M., *et al.* (2015) 'Establishment and characterization of cell lines from chromosomal instable colorectal cancer', *World Journal of Gastroenterology*, 21(1). doi: 10.3748/wjg.v21.i1.164.

49 Maletzki, C., Huehns, M., *et al.* (2015) 'Functional characterization and drug response of freshly established patient-derived tumor models with cpg island methylator phenotype', *PLoS ONE*, 10(11). doi: 10.1371/journal.pone.0143194.

50 Maletzki, C. *et al.* (2016) 'The mutational profile and infiltration pattern of murine MLH1$^{-/-}$tumors - concurrences, disparities and cell line establishment for functional analysis', *Oncotarget*, 7(33). doi: 10.18632/oncotarget.10677.

51 Maletzki, C. *et al.* (2018) 'Cellular vaccination of MLH1$^{-/-}$mice–an immunotherapeutic proof of concept study', *OncoImmunology*, 7(3). doi: 10.1080/2162402X.2017.1408748.

52 Marangoni, E. *et al.* (2007) 'A new model of patient tumor-derived breast cancer xenografts for preclinical assays.', *Clinical cancer research : an official journal of the American Association for Cancer Research*. United States, 13(13), pp. 3989–3998. doi: 10.1158/1078-0432.CCR-07-0078.

53 Marginean, E. C. and Melosky, B. (2018) ‘Is There a Role for Programmed Death Ligand-1 Testing and Immunotherapy in Colorectal Cancer With Microsatellite Instability? Part II-The Challenge of Programmed Death Ligand-1 Testing and Its Role in Microsatellite Instability-High Colorectal Cancer.’, *Archives of pathology & laboratory medicine*. United States, 142(1), pp. 26–34. doi: 10.5858/arpa.2017-0041-RA.

54 Marin-acevedo, J. A. *et al.* (2018) ‘Next generation of immune checkpoint therapy in cancer : new developments and challenges’. Journal of Hematology & Oncology, pp. 1–20.

55 Muller, M. F., Ibrahim, A. E. K. and Arends, M. J. (2016) ‘Molecular pathological classification of colorectal cancer.’, *Virchows Archiv : an international journal of pathology*. Germany, 469(2), pp. 125–134. doi: 10.1007/s00428-016-1956-3.

56 Neri, A. and Nicolson, G. L. (1981) ‘Phenotypic drift of metastatic and cell-surface properties of mammary adenocarcinoma cell clones during growth in vitro.’, *International journal of cancer*. United States, 28(6), pp. 731–738.

57 Oettle, H. *et al.* (2007) ‘Adjuvant chemotherapy with gemcitabine vs observation in patients undergoing curative-intent resection of pancreatic cancer: a randomized controlled trial.’, *JAMA*. United States, 297(3), pp. 267–277. doi: 10.1001/jama.297.3.267.

58 Oldfield, L. E., Connor, A. A. and Gallinger, S. (2017) ‘Molecular Events in the Natural History of Pancreatic Cancer.’, *Trends in cancer*. United States, 3(5), pp. 336–346. doi: 10.1016/j.trecan.2017.04.005.

59 Onkologie, L. (2013) ‘S3-Leitlinie Kolorektales Leitlinie’, (August 2014), pp. 1–241. doi: Registrierungsnummer: 021-007OL, http://leitlinienprogramm-onkologie.de/Leitlinien.7.0.html.

60 Overman, M. J. *et al.* (2016) ‘Phase I/II study of azacitidine and capecitabine/oxaliplatin (CAPOX) in refractory CIMP-high metastatic colorectal cancer: evaluation of circulating methylated vimentin’, *Oncotarget*, 7(41), pp. 67495–67506. doi: 10.18632/oncotarget.11317.

61 Pavelic, T. M. G. and J. (2014) ‘The Exploitation of Toll-like Receptor 3 Signaling in Cancer Therapy’, *Current Pharmaceutical Design*, pp. 6555–6564. doi: http://dx.doi.org/10.2174/1381612820666140826153347.

62 Reinhold, W. C. *et al.* (2014) ‘NCI-60 Whole Exome Sequencing and Pharmacological CellMiner Analyses’, *PLoS ONE*. Edited by K. Wang. doi: 10.1371/journal.pone.0101670.

63 Robert-Koch-Institut (2014) ‘Krebs in Deutschland für 2013 / 2014’.

64 Robert Koch-Institut (2016) ‘Bericht zum Krebsgeschehen in Deutschland 2016’, *Bericht zum Krebsgeschehen in Deutschland 2016. Zentrum für Krebsregisterdaten im Robert Koch-Institut (Hrsg). Berlin, 2016*, pp. 16–77. doi: 10.17886/rkipubl-2016-014.

65 Roth, M. T. and Berlin, J. D. (2018) ‘Current Concepts in the Treatment of Resectable Pancreatic Cancer.’, *Current oncology reports*. United States, 20(5), p. 39. doi: 10.1007/s11912-018-0685-y.

66 Saeterdal, I. *et al.* (2001) ‘A TGF betaRII frameshift-mutation-derived CTL epitope recognised by HLA-A2-restricted CD8+ T cells.’, *Cancer immunology, immunotherapy : CII*. Germany, 50(9), pp. 469–476.

67 Schröder-Borm, H., Bakalova, R. and Andrä, J. (2005) ‘The NK-lysin derived peptide NK-2 preferentially kills cancer cells with increased surface levels of negatively charged phosphatidylserine’, *FEBS Letters*, 579(27), pp. 6128–6134. doi: 10.1016/j.febslet.2005.09.084.

68 Schwitalle, Y. *et al.* (2004) ‘Immunogenic peptides generated by frameshift mutations in DNA mismatch repair-deficient cancer cells.’, *Cancer immunity*. United States, 4, p. 14.

69 Schwitalle, Y. *et al.* (2008) ‘BASIC – ALIMENTARY TRACT Immune Response Against Frameshift-Induced Neopeptides in HNPCC Patients and Healthy HNPCC Mutation Carriers’, pp. 988–997. doi: 10.1053/j.gastro.2008.01.015.

70 Seufferlein, T. *et al.* (2013) ‘S3-Leitlinie zum exokrinen Pankreaskarzinom’, *Zeitschrift fur Gastroenterologie*, 51(12), pp. 1395–1440. doi: 10.1055/s-0033-1356220.

71 Stier, S. *et al.* (2013) ‘Combinations of TLR ligands: A promising approach in cancer immunotherapy’, *Clinical and Developmental Immunology*, 2013. doi: 10.1155/2013/271246.

72 Sun, X., Suo, J. and Yan, J. (2016) ‘Immunotherapy in human colorectal cancer: Challenges and prospective’, *World Journal of Gastroenterology*, 22(28), pp. 6362–6372. doi: 10.3748/wjg.v22.i28.6362.

73 Tian, Y. *et al.* (2017) ‘The novel complex combination of alum, CpG ODN and HH2 as adjuvant in cancer vaccine effectively suppresses tumor growth in vivo.’, *Oncotarget*. United States, 8(28), pp. 45951–45964. doi: 10.18632/oncotarget.17504.

74 Wada, S. *et al.* (2013) ‘Sequencing CTLA-4 blockade with cell-based immunotherapy for prostate cancer.’, *Journal of translational medicine*. England, 11, p. 89. doi: 10.1186/1479-5876-11-89.

75 Wang, J. P. *et al.* (2015) ‘Erlotinib is effective in pancreatic cancer with epidermal growth factor receptor mutations: a randomized, open-label, prospective trial’, *Oncotarget*, pp. 18162–18173.

76 Williams, J. (2018) ‘Using PDX for Preclinical Cancer Drug Discovery: The Evolving Field’, *Journal of Clinical Medicine*, 7(3), p. 41. doi: 10.3390/jcm7030041.

77 Yuza, K. *et al.* (2017) ‘Hypermutation and microsatellite instability in gastrointestinal cancers’, *Oncotarget*, 8(67), pp. 112103–112115. doi: 10.18632/oncotarget.22783.

78 Zhang, J., Wolfgang, C. L. and Zheng, L. (2018) ‘Precision immuno-oncology: Prospects of individualized immunotherapy for pancreatic cancer’, *Cancers*, 10(2), pp. 1–15. doi: 10.3390/cancers10020039.

5 Anlagen

5.1 Originalarbeiten

5.1.1 Anlage – Teil 1

Reevaluating the concept of treating experimental tumors with a mixed bacterial vaccine: Coley's Toxin

Hindawi Publishing Corporation
Clinical and Developmental Immunology
Volume 2012, Article ID 230625, 16 pages
doi:10.1155/2012/230625

Research Article

Reevaluating the Concept of Treating Experimental Tumors with a Mixed Bacterial Vaccine: Coley's Toxin

C. Maletzki,[1] U. Klier,[1] W. Obst,[2] B. Kreikemeyer,[3] and M. Linnebacher[1]

[1] *Section of Molecular Oncology and Immunotherapy, Department of General, Vascular, Thoracic and Transplantation Surgery, Schillingallee 69, 18055 Rostock, Germany*
[2] *Division of Gastroenterology, Department of Internal Medicine, University of Rostock, 18055 Rostock, Germany*
[3] *Department of Medical Microbiology and Hospital Hygiene, Institute of Medical Microbiology, Virology and Hygiene, University of Rostock, 18055 Rostock, Germany*

Correspondence should be addressed to C. Maletzki, claudia.maletzki@med.uni-rostock.de

Received 2 July 2012; Accepted 9 October 2012

Academic Editor: Y. Yoshikai

Copyright © 2012 C. Maletzki et al. This is an open access article distributed under the Creative Commons Attribution License, which permits unrestricted use, distribution, and reproduction in any medium, provided the original work is properly cited.

Several decades after Coley's initial work, we here systematically analyzed tumoricidal as well as immunostimulatory effects of the historical preparation Coley's Toxin (CT), a safe vaccine made of heat-inactivated *S. pyogenes* and *S. marcescens*. First, by performing *in vitro* analysis, established human pancreatic carcinoma cell lines responded with dose- and time-dependent growth inhibition. Effects were attributed to necrotic as well as apoptotic cell death as determined by increased Caspase 3/7 levels, raised numbers of cells with sub-G1-DNA, and induced p21$^{\text{waf}}$ expression, indicative for cell cycle arrest. Besides, CT effectively stimulated human peripheral blood leukocytes (huPBL) from healthy volunteers. Quantitative gene expression analysis revealed upregulated mRNA levels of selected Toll-like receptors. Flow cytometric phenotyping of CT-stimulated huPBLs identified raised numbers of CD25$^+$-activated leukocytes. *In vivo*, repetitive, local CT application was well tolerated by animals and induced considerable delay of Panc02 tumors. However, systemic treatment failed to affect tumor growth. Antitumoral effects following local therapy were primarily accompanied by stimulation of innate immune mechanisms. Data presented herein prove that the historical approach of using killed bacteria as active immunotherapeutic agents still holds promise, and further careful preclinical analyses may pave the way back into clinical applications.

1. Introduction

Chronic infection can lead to cancer. However, acute infection has beneficial effects and often contributes to complete eradication of even large tumor burden. In this regard, the use of microbial vaccines for immunotherapy is still being re-examined. This therapeutic concept is based on the early work of William Coley, an American surgeon in the nineteenth century, who reported infection-associated tumor regression over a century ago. Inspired by his findings, he injected his first patients with vital *Streptococcus pyogenes*, a gram-positive organism causing erysipelas. Coley observed tumor shrinkage, but also lethal systemic infections. Thus, he modified his treatment regimen and since 1893 he has used a mixture of heat inactivated *S. pyogenes* and *Serratia marcescens*. The inoculation of this bacterial vaccine, later known as "Coley's Toxin" (CT), marked the origin of modern immunotherapy and Coley is also referred to as "father of cancer immunotherapy" [1].

Discoveries of the last decades comprehensively deepened our functional understanding of the immune system. Coley himself believed that the effect of his bacterial mixture is based on release of toxins affecting tumor but sparing normal cells [2]. In fact, CT activates the innate as well as the adaptive immune system by binding Toll-like (TLR) and other pattern recognition receptors. With regard to the bacterial nature of CT, this mixture contains unmethylated CpG, lipoteichoic acid, and lipopolysaccharide (LPS), acting agonistic with several TLRs [3]. Engagement of TLRs induces an inflammatory cascade resulting in cytokine secretion and immune cell activation [4]. This proinflammatory milieu together with high fever breaks the tumor-induced immune tolerance and changes it to an antitumor immunity [5–7]. However, his original hypothesis resting on an immune reaction against a "toxin" present in the microbial material that cross-reacts with and destroys the tumor cells fells more and more into oblivion and up to now has only partly been re-examined [1].

In the 1960s and 1970s, commercial CT preparations were tested on small patient cohorts. In these experiments, results were variable—presumably because of relatively short treatment courses. Also, most of the patients were immunocompromised due to prior chemotherapy [8, 9]. Besides, plenty immune mediators relevant for the inflammatory process were used as single agents in cancer immunotherapy [10–12]. But most of them failed to prove clinical efficiency. Indeed, the benefit of CT treatment is supposed to base on the chronological sequence of single immune mediators to induce an optimal antitumor immune response. These facts strengthen the usefulness of a comprehensive analysis regarding the therapeutic potential of the toxin, generated from the original protocol. In 2005, a Canadian company (MBVax) started to produce CT and rekindle Coley's pioneer work. Since then, promising results for different tumor entities were obtained. These findings are an inducement for further investigations on the antitumoral efficiency of CT. Given the lack of experimental data for pancreatic carcinomas, we here picked up the idea of using CT for cancer immunotherapy. We comprehensively analyzed the potential of this toxin to affect tumor cell growth both *in vivo* and *in vitro*, taking advantage of its intrinsic immune stimulatory properties. We observed a direct impact on cell growth, proliferation, and viability. Of note, proapoptotic molecules in tumor target cells increased upon CT treatment. *In vivo*, repetitive local CT applications effectively controlled tumor growth by stimulating immune responses.

2. Material and Methods

2.1. Tumor Cell Lines, Human Peripheral Blood Lymphocytes (huPBL), and Culture Media. Human (AsPC-1, T3M4, MIA PaCa-2, and BxPc-3) and murine (Panc02) pancreatic carcinoma cell lines were maintained in DMEM/HamsF12 supplemented with 10% fetal calf serum (FCS), glutamine (2 mmol/L), and antibiotics (complete medium). Human peripheral blood leukocytes (huPBL) were isolated from blood of healthy donors with no known diseases. Purification of huPBLs was performed by Ficoll density-gradient centrifugation and subsequent cultivation in IMDM supplemented with 10% fetal calf serum (FCS), glutamine (2 mmol/L), and antibiotics. All media and supplements were from PAA unless stated otherwise (Cölbe, Germany).

2.2. Preparation of Coley's Toxin. Coley's Toxin (CT) was prepared following the original protocol. Briefly, A single group A streptococcal isolate, *S. pyogenes* serotype M49 (strain 591), was cultured in Todd-Hewitt (TH) broth (Oxoid Unipath, Wesel, Germany), supplemented with 10% glucose, and allowed to grow for ten days in an incubator (37°C, 5% CO_2). An aliquot was taken from the culture, plated on sheep blood agar, and incubated overnight to examine cell viability. Afterwards, the culture was seeded with 2 mL of live *S. marcescens* ($2 * 10^7$ cfu/mL) and further cultured at 25°C. Following a period of ten days, incubation was terminated by heat sterilization (65°C for two hours) and subsequent filtration. Bacterial inactivation was confirmed after plating on sheep blood agar and overnight incubation. Prior to cell treatment, CT was pelleted and diluted in sterile complete medium to a final concentration corresponding to $5 * 10^2$, $2.5 * 10^4$, and $2.5 * 10^6$ cfu/mL.

2.3. RNA Isolation, cDNA Synthesis, and Quantitative Real-Time PCR. Total RNA from treated and untreated tumor cells as well as from huPBLs was isolated with TRIzol reagent according to the manufacturer's instructions. RNA was reverse transcribed into cDNA from 0.5 μg RNA using the High Capacity cDNA Reverse Transcription Kit (Applied Biosystems, Foster City, CA, USA). Target cDNA levels were analyzed by quantitative real-time PCR using TaqManTM Universal PCR Master Mix and predesigned TaqMan gene expression assays (Hs00180269_m1 (Bax), Hs00355782_m1 ($p21^{waf}$), Hs01014511_m1 (TLR2), Hs00152939_m1 (TLR4), Hs00152825_m1 (TLR5), Hs00152973_m1 (TLR9), and Hs99999905_m1 (GAPDH, housekeeping gene control) in an ABI Prism 7000 sequence detection system (Applied Biosystems). PCR conditions were as follows: 95°C for 10 min, 40 cycles of 15 s at 95°C, 1 min at 60°C. Reactions were performed in triplicate wells and replicated three times. Expression levels of the gene of interest are given in relation to the housekeeping gene ($\Delta Ct = Ct_{target} - Ct_{GAPDH}$). Relative gene expression values are expressed as x-fold increase compared to untreated (i.e., tumor cells or huPBL) cells, whose expression was set to be 1.

2.4. Quantification of Cell Proliferation by BrdU Incorporation. Quantification of DNA synthesis was performed by measurement of 5-bromo-2′deoxyuridine (BrdU) incorporation using BrdU labeling and detection enzyme-linked immunosorbent assay (ELISA) kit (Roche). BrdU labeling was initiated after 24 and 48 hours of incubation with or without CT by addition of labeling solution at a final concentration of 10 μM. Following the incubation period of three hours, labeling was stopped and BrdU uptake was quantified on a plate reader at 450 nm according to the manufacturer's instructions. Percentage of proliferating cells was calculated compared to untreated control (=100%).

2.5. Cell Viability Staining. Cell viability was determined by fluorescent staining using Calcein AM (Sigma, final concentration: 2 μM). Analysis was performed on a fluorescence multiwell plate reader (Tecan Infinite M200, Crailsheim, Germany) at an excitation wavelength of 485 nm (emission 535 nm). For estimation of cell viability, the relative fluorescence intensities of Calcein AM-stained nontreated cells (=live control) were set to be 100%, and fluorescence intensities of the samples were calculated. Experiments were performed in duplicates and replicated at least three times.

2.6. Apoptosis Assays. Cells were grown to about 70% confluence in 24-well culture plates and then incubated in 2 mL complete medium with or without bacteria for 24 and 48 hours. At the end of treatment, the cells were harvested by trypisinzation, pelleted by centrifugation, washed twice with PBS and resuspended in 2 mL ice-cold 70% ethanol for at least 24 hours at −20°C. Afterwards, the cells were pelleted, washed with PBS, and incubated for one hour in 200 μL PBS containing 0.1% Tween 20 and 1 mg/mL RNase (Sigma Aldrich, Munich, Germany) at room temperature. Following the addition of 50 μg propidium iodide/10^6 cells (Sigma), the samples were subjected to flow cytometric analysis which was performed on a FACSCalibur Cytometer (Becton Dickinson) using the Cellquest program. Ten thousand events were measured for each sample.

Additionally, apoptosis induction was examined via caspase activity. Cells were cultured in 96-well half-area plates and treated with increasing CT doses for 24 and 48 hours. Caspase 3/7 activity was quantified using the Promega ApoTox-Glo Triplex Assay according to the manufacturer's instructions (Promega, Mannheim, Germany) and measurement on a luminometer (Promega). Background luminescence (cell culture medium without cells and Caspase-Glo 3/7 Reagent) was subtracted from all measurements. Luminescence values of nontreated cells (negative control) were set to be one and x-fold increases in caspase activity of samples were calculated. Experiments were performed in duplicates and replicated at least three times.

2.7. Flow Cytometric Phenotyping. HuPBLs were harvested for phenotyping following 24 hours of exposure towards increasing concentrations of CT. Therefore, huPBLs were stained with the following FITC- and PE-conjugated mouse antihuman monoclonal antibodies (mAbs): CD3, CD4, CD8, CD25, CD16, and CD56 (1 μg, Immunotools, Friesoythe, Germany). Negative controls were stained with the appropriate isotypes (Immunotools). Additionally, fractions of dead cells were quantified after 24 hours, 72 hours, and 7 days using propidium iodide (PI). Therefore, PI (1 mg/mL) was given to cells directly prior to measuring. Phenotyping of murine immune cells was conducted from blood samples and spleens, following lysis of erythrocytes in lysis buffer (0.17 M Tris, 0.16 M NH_4Cl) and labeling with the following FITC-conjugated rat antimouse mAbs: CD3, CD11b, CD19 (1 μg, Immunotools), hamster antimouse mAbs: CD11c (1 μg, Miltenyi Biotec, Bergisch-Gladbach, Germany) and PE-conjugated rat antimouse mAbs: CD4, CD8, Gr1 (Ly6G) (Miltenyi Biotec), and g/d TCR. Negative controls consisted of spleen and blood lymphocytes stained with the appropriate isotypes (BD Pharmingen). Samples were analyzed on a FACSCalibur Cytometer (BD Pharmingen). Data analysis was performed using CellQuest software (BD Pharmingen).

2.8. Co-Culture Experiments. Direct tumor cell killing in the presence of huPBLs was examined by co-culture experiments following 48 hours of incubation. Experiments were performed as described before [13]. Data are given as x-fold number of tumor cells compared to untreated controls.

2.9. Pancreatic Tumor Model and Treatment Regimen. Experiments were performed on female 8–10-week-old C57Bl/6N mice (Charles River, Fa. Wiga, Sulzfeld, Germany) weighing 18–20 g. All animals were fed standard laboratory chow and given free access to water. Experiments were performed in accordance with the German legislation on protection of animals and the Guide for the Care and Use of Laboratory Animals (Institute of Laboratory Animal Resources, National Research Council; NIH Guide, vol. 25, no. 28, 1996). Under brief ether anesthesia $1 * 10^6$ Panc02 cells were injected subcutaneously (s.c.) into the right hind leg. Tumor growth was routinely controlled at least twice a week and tumor volume was estimated according to the formula: $V = \text{width}^2 * \text{length} * 0.52$. After tumor establishment animals were subdivided into the following experimental groups: animals received twice weekly intratumoral CT injections (i.t., resuspended in 50 μL PBS), a total of six times ($n = 5$–7 per group). Another group was biweekly treated via tail vein injection (i.v., six injections in total, $n = 3$-4). As controls, one tumor-carrying group received PBS (vehicle) alone.

Tumor-carrying mice (treatment, control) were sacrificed at day 28 or when they became moribund before tumor volume reached 2000 mm^3. At the end of each experiment, blood samples, tumor, spleen, and mesenteric lymph nodes were removed from the animals of all groups for further analysis.

2.10. Statistical Analysis. Values are reported as the mean ± SEM for *in vitro* and *in vivo* data. After proving the assumption of normality, differences were determined by using the unpaired Student's t-test. If normality failed, the nonparametric Mann-Whitney U-Test was applied. The tests were performed by using Sigma-Stat 3.0 (Jandel Corp, San Rafael, CA). The criterion for significance was set to $P < 0.05$.

3. Results

3.1. Inhibition of Tumor Cell Proliferation and Viability. To evaluate the direct impact of CT on cell proliferation and vitality, tumor cells were first treated with increasing bacterial doses (corresponding to $5 * 10^2$, $2.5 * 10^4$, and $2.5 * 10^6$ cfu/mL). Electron microscopy following 24 hours of treatment demonstrated close adherence of CT to tumor cells via surface molecules, a characteristic common to *S. pyogenes* and *S. marcescens* (Figure 1(a), upper panel). Moreover, sustained structural integrity of bacteria was confirmed in these analyses (Figure 1(a), lower panel).

Functional proliferation experiments displayed a time and dose-dependent tumor cell growth inhibition (Figure 1(b)). As determined by BrdU incorporation, most pronounced effects were observed for AsPC-1 cells. Cell growth significantly decreased to 80% and 28% after 24 and 48 hours, respectively, (compared to untreated controls). T3M4, BxPc-3, and MIA PaCa-2 cells were less susceptible towards CT. Here, growth inhibition was rather transiently with a maximum of 28% observed after 24 hours in T3M4 cells (highest dose).

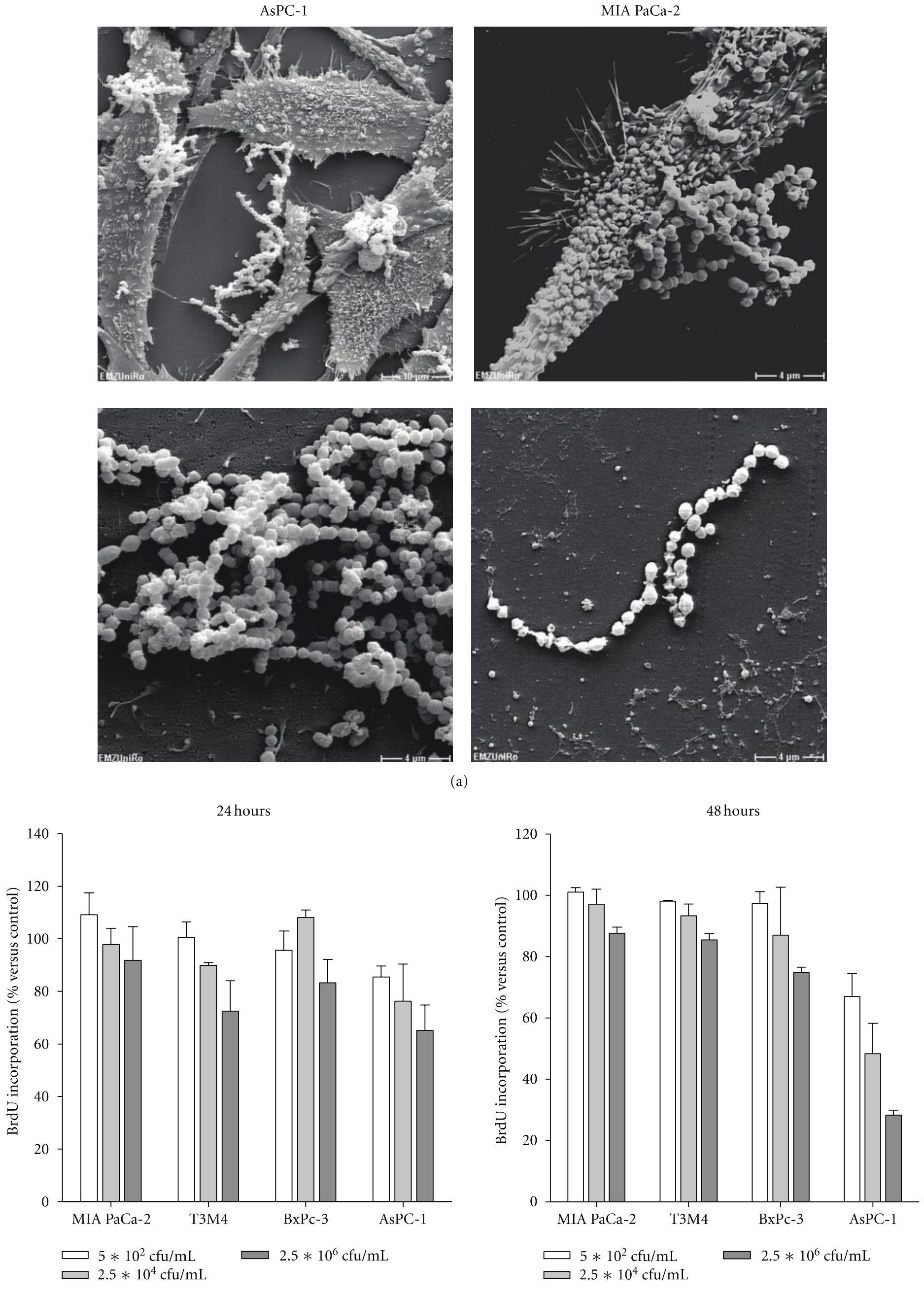

(a)

(b)

Figure 1: Continued.

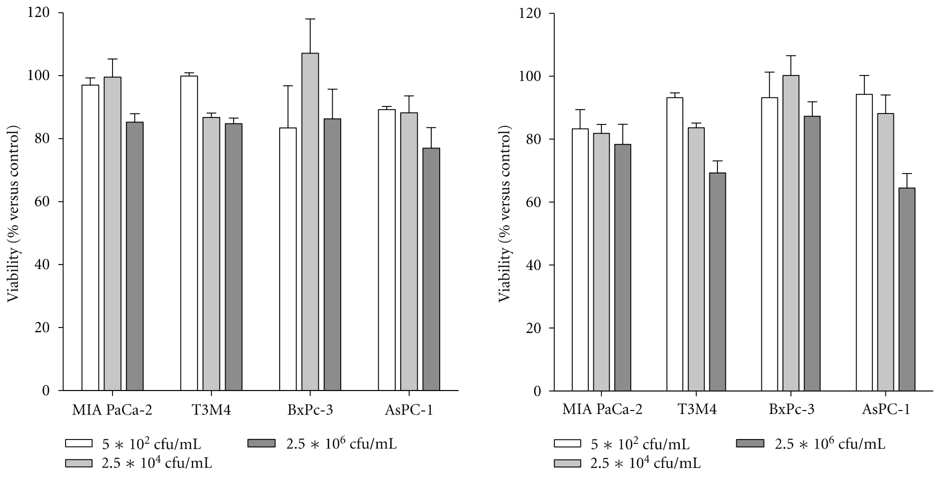

(c)

Figure 1: Electron microscopy. (a) Representative pictures showing CT binding to tumor cells via surface molecules (upper panel). Sustained cellular integrity despite heat inactivation was confirmed (lower panel). Cell proliferation and viability. (b) Tumor cells were seeded in 96-well plates and cultured with increasing CT concentrations (corresponding to $5 * 10^2$, $2.5 * 10^4$, and $2.5 * 10^6$ cfu/mL) for 24 and 48 hours. Thereafter, cell proliferation was estimated by BrdU uptake and quantification on a plate reader at 450 nm according to the manufacturer's instructions. Percentage of proliferating cells was calculated compared to untreated control (100%). (c) For estimating viability, tumor cells were seeded in 24-well plates and treated with CT as described above. Following the incubation period (24 and 48 hours), the cells were stained with Calcein AM and fluorescence intensity was measured on a plate reader (ex/em 485/535 nm). Cell viability was calculated by setting relative fluorescence intensities of Calcein AM-stained nontreated cells (live control) to 100%. Results show data of three separate experiments each performed in duplicates. Values are given as the mean ± SEM.

Antiproliferative effects could partly be attributed to cytotoxicity. Numbers of viable tumor cells were diminished, especially in the highest dose following a 48-hour incubation period (Figure 1(c)). Again, CT-mediated killing was most evident in AsPC-1 cells. Viability decreased time and dose dependently. Comparable, though less pronounced, effects were obtained for T3M4 and MIA PaCa-2 cells with a maximum of 20% dead cells (compared to untreated controls). Viability of BxPC-3 was only marginally affected by CT.

3.2. Induction of Cell Cycle Regulators.

As a first step towards functionally understanding the growth inhibitory and cytotoxic capacity of CT on tumor cells, gene expression of the cell cycle and DNA replication regulator $p21^{waf}$ as well as apoptotic activator Bax was examined. Due to technical limitations, gene expression could only be considered for three out of the four cell lines studied. Analysis revealed increased expression levels of both target genes (Figures 2(a) and 2(b)). In detail, $p21^{waf}$ expression was transiently induced in BxPC-3 target cells. T3M4 cells displayed a delayed response with highest expression levels after 48 hours. In those cells, expression correlated inversely with CT doses. AsPC-1 cells, whose viability was most affected by CT, reacted with sustained high $p21^{waf}$ expression. The effects of CT on Bax gene expression were comparably mild, with a fivefold upregulation in AsPC-1 as the most pronounced phenomenon. As can be depicted from Figure 2(b) (lower panel), expression was only slightly stimulated in the other cell lines.

3.3. Apoptosis Induction following CT Exposure.

Aforementioned analysis hinted towards potential contribution of CT-induced apoptosis induction in tumor target cells. Consequently, caspase activity as well as DNA fragmentation were investigated next. Caspase 3/7 levels dose and time dependently increased in all cell lines exposed to CT (Figure 3(a)). Levels showed up to sevenfold increases in BxPC-3 cells after 48 hours of treatment with intermediate and highest CT doses. Supplemental to the prior observation on highest susceptibility of AsPC-1 cells towards CT, maximal caspase activation was found in these cells after 48 hours. Likewise, DNA fragmentation, as determined by flow cytometric sub-G1-peak analysis, was most evident here (Figure 3(b)). In MIA PaCa-2, T3M4, and BxPC-3 cells, the fraction of apoptotic tumor cells also increased dose dependently (Figure 3(b)).

Further determinations on cell cycle analysis revealed rearrangement of cell phases. In line with increased $p21^{waf}$ expression, cell cycle arrest and accordingly loss of G2/M phase were apparent in CT exposed cells (Table 1). Therefore,

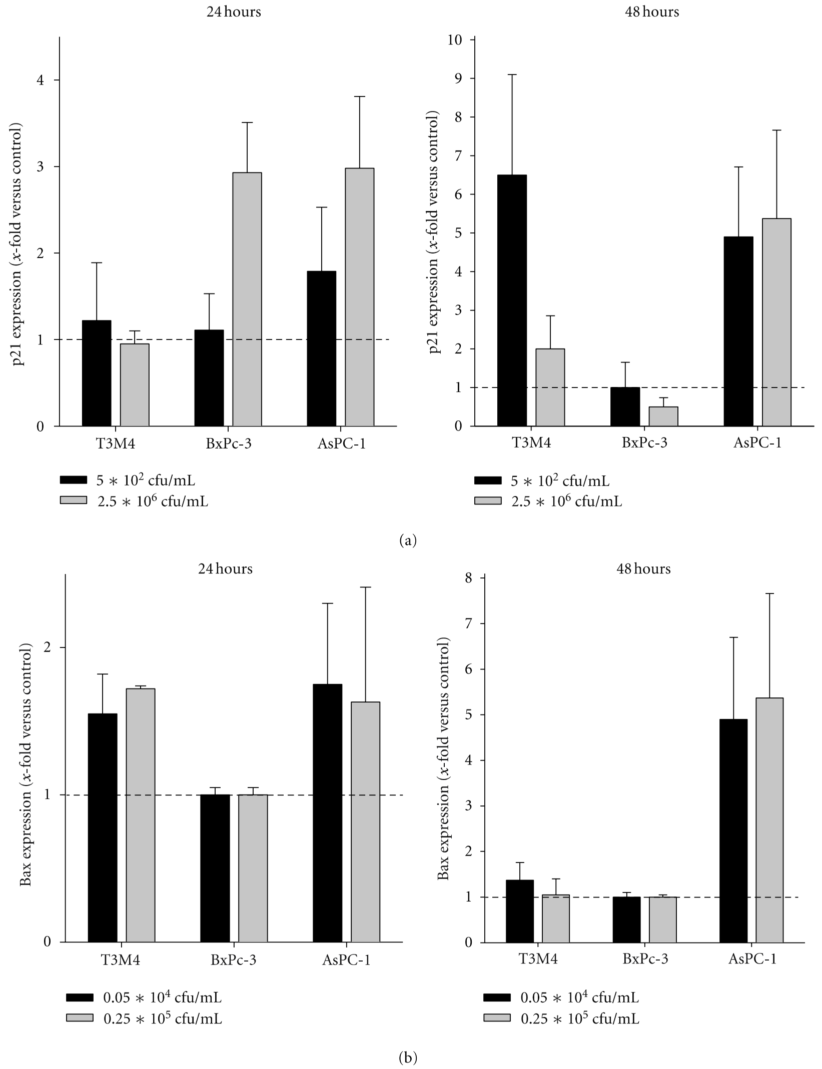

(a)

(b)

Figure 2: Gene expression analysis. mRNA expression of (a) $p21^{Waf}$ and (b) Bax in tumor target cells following 24 and 48 hours CT treatment. Quantitative real-time PCR was performed using predesigned TaqMan gene expression assays. Results show data of three separate experiments each performed in duplicates. Values are given as the mean ± SEM.

mechanisms independent from apoptosis are also likely to be involved in the exerted cytotoxic reactivity.

3.4. CT Activates Immune Cells in a Dose-Dependent Manner. Next, CTs' potential to stimulate huPBLs was examined. Given that CT is made of two bacterial species, that is, the gram-negative *S. marcescens* and the gram-positive *S. pyogenes*, we first determined mRNA levels of TLRs, known to be activated by microbial ligands.

These analyses showed a dose- and time-dependent increase in TLR expression (Figure 4(a)). TLR2 displayed

Table 1: Cell cycle distribution of tumor control cells and following CT treatment.

	MIA PaCa-2				T3M4				BxPc-3				AsPC-1			
Phase	0	$0.05 * 10^4$	$0.25 * 10^4$	$25 * 10^5$	0	$0.05 * 10^4$	$0.25 * 10^4$	$25 * 10^5$	0	$0.05 * 10^4$	$0.25 * 10^4$	$25 * 10^5$	0	$0.05 * 10^4$	$0.25 * 10^4$	$25 * 10^5$
	cfu/mL				cfu/mL				cfu/mL				cfu/mL			
G0/G1	48.7 ± 9.4	48.6 ± 13.9	43.1 ± 13.0	43.6 ± 0.7	77.5 ± 1.1	76.7 ± 3.5	67.4 ± 3.8	64.5 ± 2.2	44.7 ± 8.5	43.0 ± 1.0	31.8 ± 4.1	36.6 ± 9.9	48.1 ± 10.1	52.7 ± 6.8	37.5 ± 8.9	30.7 ± 3.6
S	33.4 ± 9.5	36.5 ± 10.4	43.1 ± 12.7	50.5 ± 6.2	18.0 ± 0.9	18.2 ± 4.5	28.7 ± 5.1	31.1 ± 1.5	24.1 ± 5.5	44.8 ± 7.1	$68.0 \pm 4.4^*$	$63.1 \pm 7.9^*$	39.5 ± 11.3	34.3 ± 11.5	58.9 ± 9.7	$67.9 \pm 3.1^\#$
G2/M	17.9 ± 3.9	15.6 ± 3.4	13.8 ± 0.9	8.5 ± 5.5	4.6 ± 0.3	5.1 ± 1.2	4.0 ± 1.3	4.4 ± 0.7	31.2 ± 3.2	$8.8 \pm 5.0^*$	$0.4 \pm 0.4^*$	$0.3 \pm 0.2^\#$	16.7 ± 5.9	13.0 ± 5.3	$0.4 \pm 0.4^\#$	$0.4 \pm 0.1^\#$

Data show percentage values of tumor cells (% positive cells) following 24 hours of treatment. Experiments were at least three times repeated. Values of are given as mean ± SEM; $^*P < 0.05$ versus control; t-test. $^\#P < 0.05$ versus control; U-test.

a maximal response after 72 hours stimulation with the highest CT concentration. Conversely, TLR5, the receptor for flagellin, and TLR9, recognizing unmethylated CpG islands of bacterial DNA, were transiently stimulated with up to threefold increases following 24 hours. The effects of CT on TLR4 could be neglected, since there was no stimulation at any time.

Further flow cytometric analysis revealed a dose-dependent rise in activated immune cells after 24 and 72 hours. Numbers of $CD25^+$ cells increased more than threefold (Table 2). Further analysis identified $CD3^+CD8^+$ cytotoxic T cells to be the main responding cell population. Fractions of $CD3^+CD4^+$ T cells as well as $CD16^+CD56^+$ NK cells were only marginally influenced by CT.

Moreover, CT mediated no significant cytotoxicity towards huPBLs. Numbers of PI^+ cells at 24 and 72 hours of culture were always below 10% and thus comparable to nonstimulated huPBLs (Figure 4(b)). Interestingly, there was an inverse correlation between toxicity and CT dose. Highest PI^+ levels were observed for lowest CT concentrations following 7 days of culture (Figure 4(b)). This might be best interpreted as a kind of missing stimuli at these low concentrations, resulting in leukocyte cell death.

3.5. Boosted Antitumoral Effect by Adding huPBLs to the Culture. Based on the observation that CT acts as immunostimulatory and antitumoral agent, a series of *in vitro* co-culture experiments was performed by adding immunocompetent cells and CT to tumor target cells (Figure 5).

Co-culture experiments demonstrated a boost of antitumoral effects. Viable tumor cell numbers notably decreased after a 48 hours incubation period especially at higher CT concentrations. Generally, antitumoral effects were rather cell specific, than donor dependent. Obvious tumor killing was found for T3M4 and BxPC-3 cells, while MIA PaCa-2 and AsPC-1 cells responded less.

3.6. Delayed Tumor Growth following Local Treatment. Finally, an *in vivo* experiment was carried out to test whether the observed *in vitro* findings on potent tumor growth inhibition and immune stimulation are reproducible in immunocompetent, tumor-carrying mice. Treatment of established Panc02 tumors was attempted by repetitive CT application. Two treatment protocols were employed, including local as well as systemic application routes.

Both regimens were well tolerated by all animals. No signs of tumor-associated clinical symptoms like anorexia or weight loss occurred, consequently resulting in a 100% survival rate (Figure 6(a)). Local CT application mediated substantial tumor growth alteration. This was evident from day 14 after treatment start until the end of experiments (day 28). Established Panc02 tumors macroscopically necrotized, tended to break up, and revealed significant growth delay. Specifically, at day 28, tumor volumes were about one-fifth of control tumors ($222.6 \pm 65.0\,\mathrm{mm}^3$ versus $1103.8 \pm 144.4\,\mathrm{mm}^3$, $P < 0.05$ versus control). By comparison, an increase in the number of injections did not further improve the therapeutic effect and thus resulted in equivalent tumor volumes (data not shown).

Quite the opposite results were obtained following systemic CT application. This regimen had no impact on Panc02 tumor growth. Tumors continuously grew and volumes were similar to controls until terminating the experiment (Figure 6(b)). Therefore, local application is more favorable than systemic.

3.7. Induction of Immune Cells following Local Therapy. Next, the composition of circulating as well as splenic immune cells was studied (Figures 5(c) and 5(d)). In these analyses, *in vivo* findings could clearly be correlated with immunological parameters. Mice locally treated with CT had significantly increased numbers of circulating $CD11c^+$ dendritic and γ/δ TCR^+ cells ($P < 0.05$ versus control). Moreover, levels of myeloid derived suppressor cells (MDSC, $CD11b^+Gr1^+$) decreased exclusively after local CT therapy (Figure 6(c)). Irrespective of the application route, T helper and cytotoxic T cells as well as $CD19^+$ pre B cells were only slightly altered.

In striking contrast, locally as well as systemically applied CT impacted splenic T and B cells (Figure 6(d)). Both treatment groups had decreased numbers of these cell populations. This dramatic decrease at day 28 possibly reflects migration of immunological effector cells more into lymphoid tissues than into the spleen. Numbers of γ/δ TCR^+ cells were significantly raised, especially in the local therapy group (local 42.6 ± 4.6% versus systemic; 17.4 ± 4.2% versus control 10.0 ± 2.4%). Expression levels of L-selectin (CD62L) on lymphocytes and transferrin-receptor-positive (CD71) cells remained comparable to controls (data not shown).

Taken together, these findings confirm our *in vitro* results on potent stimulation of immune responses by CT. However, they also prove dependency on the application route finally contributing to efficient tumor growth control *in vivo*.

4. Discussion

The main objective of this study was to ascertain whether a purely microbial-based approach, in the absence of additional (chemo- or targeted) therapies, can cure experimental non-immunogenic tumors. We therefore picked up the historical idea of using Coley's Toxin (CT), a complex mixture of gram-positive and gram-negative bacterial components, as an active antineoplastic agent. Our work focused on pancreatic carcinomas since this tumor entity is still one of the most malignant ones with high mortality and poor prognosis even with aggressive conventional and novel combinatorial therapies [14, 15]. Besides, successful eradication of experimental pancreatic carcinomas by local application of vital as well as avitalized gram-positive bacteria was demonstrated by our group before [16, 17].

For potential clinical application of microbial-based vaccines, several requirements need to be complied. These include (I) reducing unspecific toxicity to normal, non-neoplastic cells, (II) preserving antitumoral and tolerance-breaking immunostimulatory potential, and (III) applying a standardized treatment protocol. As for the latter, no

Table 2: Flow cytometric phenotyping of CT-stimulated huPBLs.

(a)

	Donor 1				Donor 2				Donor 3				Donor 4			
Antigen	0	$0.05 * 10^4$	$0.25 * 10^4$	$25 * 10^5$	0	$0.05 * 10^4$	$0.25 * 10^4$	$25 * 10^5$	0	$0.05 * 10^4$	$0.25 * 10^4$	$25 * 10^5$	0	$0.05 * 10^4$	$0.25 * 10^4$	$25 * 10^5$
	cfu/mL				cfu/mL				cfu/mL				cfu/mL			
$CD3^+CD4^+$	35.4	34.9	38.3	45.3	26.7	24.9	24.5	37.9	40.8	41.2	31.6	49.3	43.9	31.0	35.6	51.6
$CD3^+CD8^+$	17.8	18.9	19.5	22.3	13.7	15.9	14.7	16.8	20.8	21.6	18.5	24.2	9.5	10.8	9.9	12.2
$CD25^+$	22.2	23.4	39.2	46.6	12.3	18.7	29.2	41.1	12.4	12.9	20.1	29.6	10.0	11.5	22.8	33.8
$CD16^+CD56^+$	14.2	17.0	14.8	17.1	30.1	23.7	23.7	22.2	11.1	9.7	10.8	9.7	12.2	10.3	11.3	10.4

Data show percentage values of huPBLs (% positive cells) following 24 hours of stimulation.

(b)

	Donor 1				Donor 2				Donor 3				Donor 4			
Antigen	0	$0.05 * 10^4$	$0.25 * 10^4$	$25 * 10^5$	0	$0.05 * 10^4$	$0.25 * 10^4$	$25 * 10^5$	0	$0.05 * 10^4$	$0.25 * 10^4$	$25 * 10^5$	0	$0.05 * 10^4$	$0.25 * 10^4$	$25 * 10^5$
	cfu/mL				cfu/mL				cfu/mL				cfu/mL			
$CD3^+CD4^+$	33.4	38.2	42.6	52.5	16.0	16.2	22.0	33.2	31.0	33.6	31.7	53.7	35.5	35.0	33.5	61.0
$CD3^+CD8^+$	14.3	13.8	18.5	20.8	11.2	13.0	12.5	15.1	20.3	22.2	22.4	26.1	10.2	8.9	11.8	13.1
$CD25^+$	9.0	18.5	23.04	28.8	11.0	20.5	25.4	33.3	9.8	20.8	21.4	25.6	9.7	20.5	15.9	28.9
$CD16^+CD56^+$	8.9	8.1	8.0	8.0	16.5	27.6	14.2	14.5	5.8	8.4	6.4	6.2	7.8	2.5	6.5	7.8

Data show percentage values of huPBLs (% positive cells) following 72 hours of stimulation.

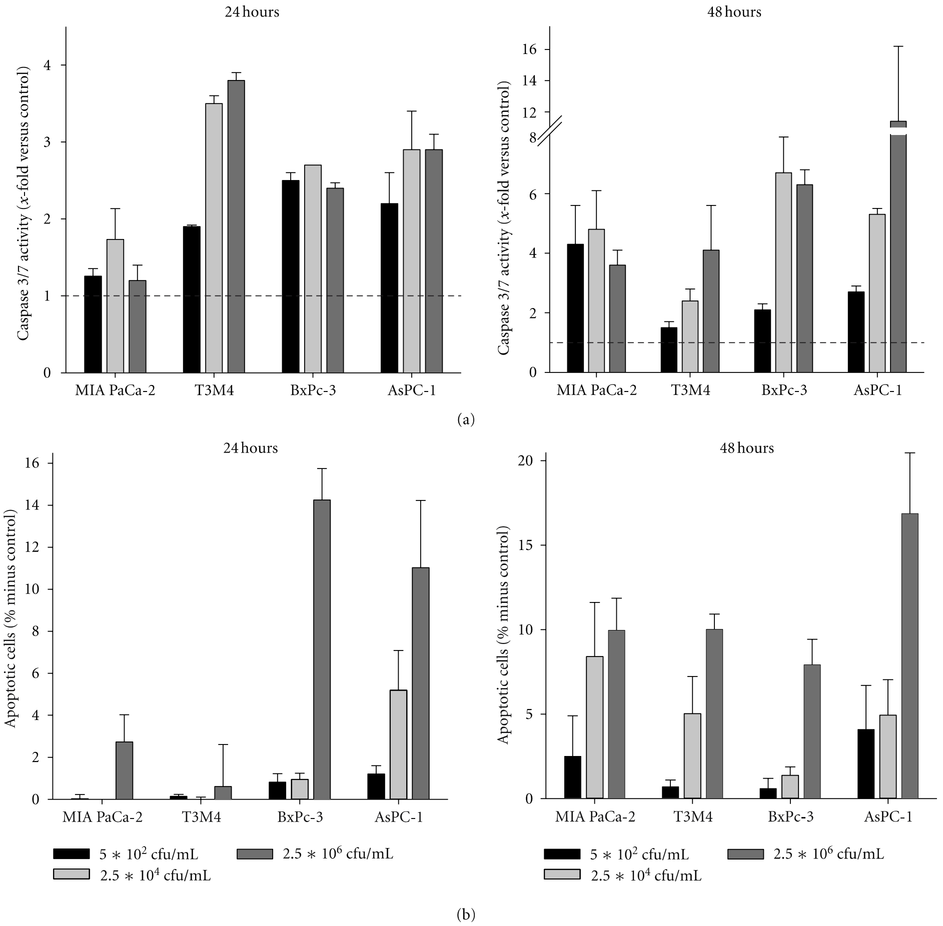

(a)

(b)

Figure 3: Apoptosis assay. (a) Increased Caspase 3/7 activity in tumor cells after CT treatment, as quantified using the Promega Caspase-Glo 3/7 Assay according to the manufacturer's instructions and measurement on a luminometer. (b) Flow cytometric sub-G1 Peak analysis following 24 and 48 hours of incubation with CT. Cells with DNA content lower than the G1 peak were considered to be apoptotic. Results show data of three separate experiments each performed in duplicates. Values are given as the mean ± SEM. (c) AsPC-1 cells show characteristic sub-G1 peaks at 24 hours after treatment (representative results out of three independent experiments).

such standardization was done in the past. Hence, despite Coley's high profile, his work came under criticism. At that time, 13 different preparations and various administration routes (i.v., i.m., and i.t.) existed and some of these were more effective than others [2, 18]. This may explain why Coley's results could not be reproduced by others. In order to overcome this obstacle, we designed CT under constant, standardized conditions according to the original protocol.

Results of our present study show that this preparation acts as a potent antitumoral and immune-activating agent. First, by performing a series of *in vitro* experiments, we were able to induce cell death in tumor target cells. Interestingly, a differential susceptibility towards CT was demonstrated. While AsPC-1 cells responded with substantial cell death, other cell lines were less affected. As central mechanisms of CT-induced growth alteration, we could identify an up-regulation of p21^{waf} gene expression and loss of G2/M phases, both indicative for cell cycle arrest. In line with the established capacity of bacteria to induce apoptosis as well as necrosis in target cells, we also observed both kinds of cell death. Proteins (i.e., LPS, Flagellin) delivered by *S. marcescens* may thus have preferentially induced necrosis, while factors

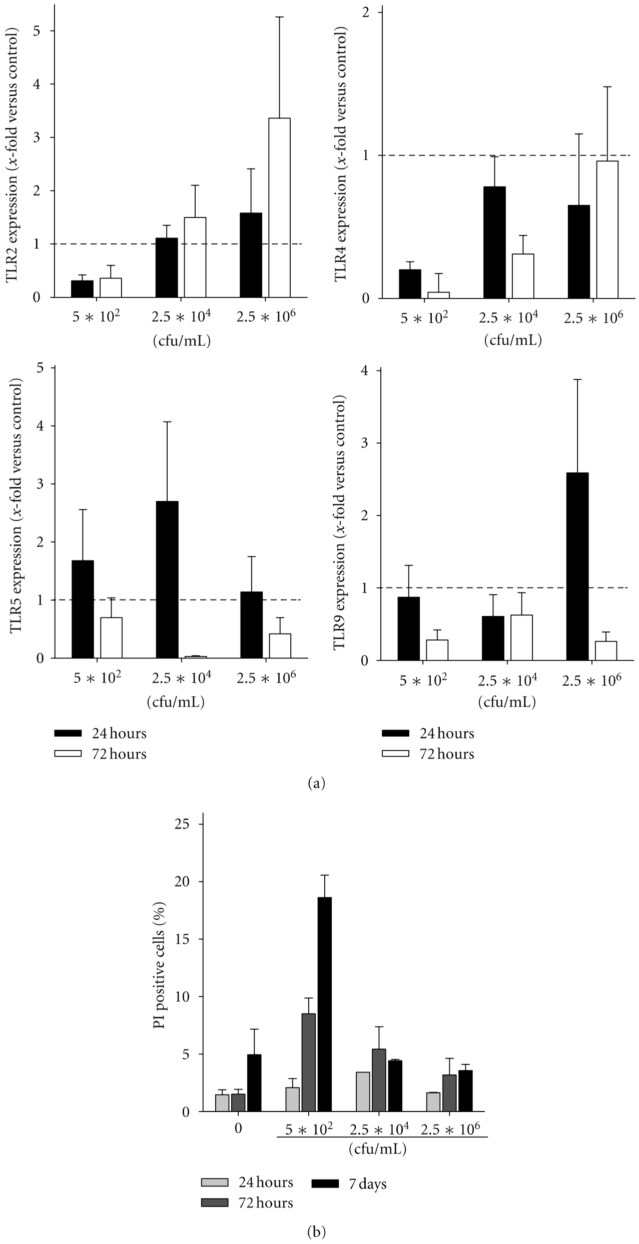

(a)

(b)

Figure 4: Gene expression analysis and viability of huPBLs. mRNA expression of (a) TLRs in huPBLs following 24 and 72 hours stimulation with CT. Quantitative real-time PCR was performed using predesigned TaqMan gene expression assays. Results show data of three separate experiments each performed in duplicates. (b) Viability of huPBLs as determined by flow cytometric PI staining. Prior to analysis, huPBLs were stimulated with increasing doses of CT and cultured for 24 hours, 72 hours, and 7 days. Results show data from four different healthy donors. Values are given as the mean ± SEM.

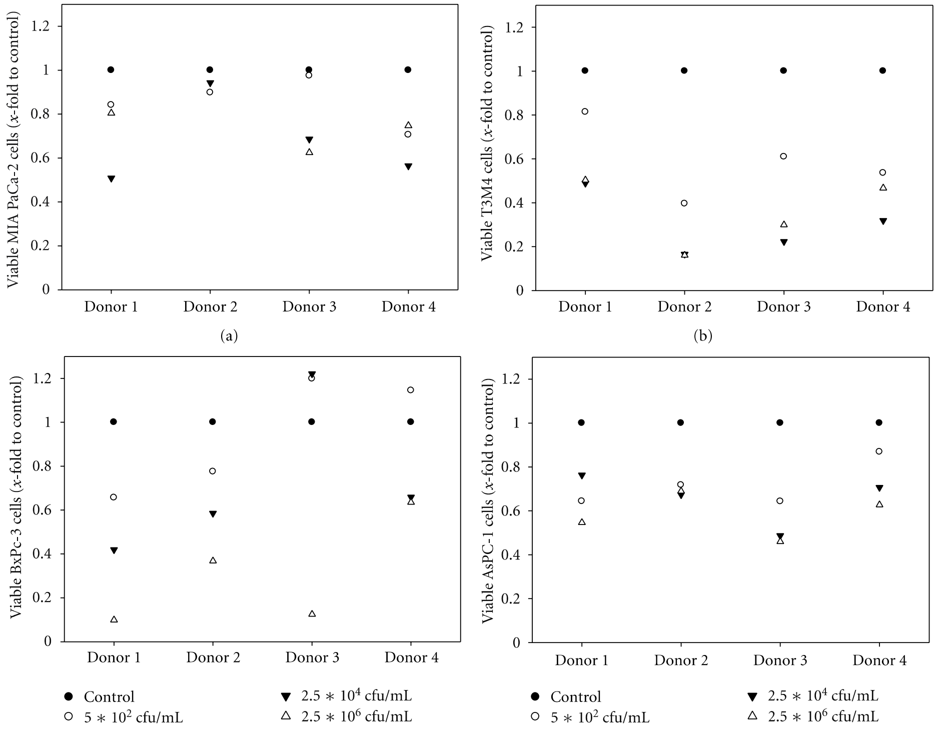

(a) (b) (c) (d)

Figure 5: Co-culture experiments. Tumor cells were Co-cultured with huPBLs of four different healthy donors in the presence of CT for 48 hours. Thereafter, numbers of viable tumor cells were quantified by flow cytometry using microsphere beads as calibrator. Untreated cells without CT were set as 1 and all other data were given as *x*-fold increase. Experiments were performed in duplicates.

provided by *S. pyogenes* (i.e., streptokinase, streptolysin, and lipoteichoic acid) led to apoptosis [1, 16, 19, 20]. Accordingly, caspase 3/7 activation and DNA fragmentation were detectable in CT-treated tumor cells.

In addition to the capacity of directly compromising tumor viability, CT was described as being a strong immune stimulator [2, 21–23]. The bacterial DNA (CpG ODN) present in this complex mixture may here be one of the best known immune-activating candidates. CpG ODNs has been found to improve antigen-presenting cell functions and boost humoral as well as cellular Th1-directed immune responses. They have shown promising results as adjuvants for vaccines and in combination with radio- or immunotherapy [3, 5, 24]. Several CpG ODN-based agents were already included into clinical trials for exploring their safety and efficacy in hematological and solid cancers [24–26] and [http://www.clinicaltrials.org/]. The underlying mechanism is due to activating TLRs, the most important innate immune receptors [5, 7]. TLR signaling in immune cells is crucial for regulating innate and adaptive immune responses, such as DC maturation and antigen presentation as well as CD8$^+$ T-cell toxicity [27, 28].

In our experimental setup, CT-stimulated leukocytes from healthy donors could be effectively activated and responded with up-regulation of TLR 2, 5, and 9. Likewise, CD25 expression was significantly and sustainably induced in these short-time-mixed leukocyte cultures. Though not analyzed in detail, stimulation of γ/δ T cells is very likely [29]. Besides, secretion of Th1 and other proinflammatory cytokines (e.g., IFN-γ, IL12, and TNF-α) by immune cells belonging to both the innate and adaptive arm can be anticipated, too. Hence, this mixture of TLR agonists likely stimulates a complex cascade, each of which plays a unique and vital role in orchestrating immune responses [30]. Quite in line, we observed a boost of antitumoral effects when leukocytes were added to tumor cells together with CT. This co-culture system mimics the *in vivo* situation. Here, tumor cell numbers massively decreased. Worth mentioning,

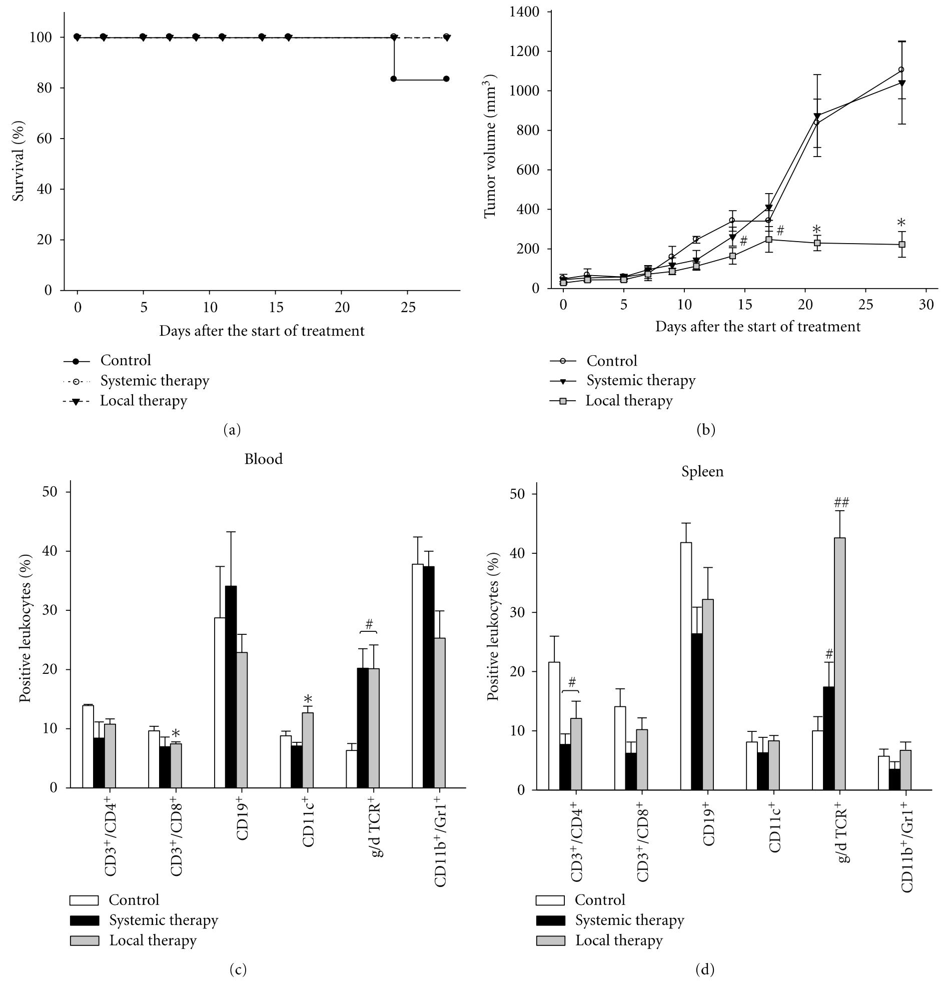

(a)

(b)

(c)

(d)

FIGURE 6: *In vivo* analysis. (a) Survival curve of Panc02 tumor-carrying C57Bl/6N mice and (b) tumor growth kinetic. After tumor establishment, mice received twice weekly i.t. or i.v. CT injections (six times in total (n = 3–7 mice per group). Control mice were given PBS. Mice were monitored for 28 days with adherence to ethical requirements. (c), (d) Flow cytometric phenotyping of circulating (blood) and splenic leukocyte subsets from tumor control and CT-treated animals. Values are given as mean ± SEM; $^*P < 0.05$ versus control; t-test. $^\#P < 0.05$ versus control; U-test.

however, is the fact that boosted antitumoral effects were rather tumor cell specific than dependent from the lymphocyte donor. T3M4 and BxPC-3 could be effectively killed by CT and leukocytes. However, comparable results were not obtained for AsPC-1 cells, which had been shown to be highly susceptible towards CT-mediated lysis alone. This can be attributed to a kind of tumor-escape mechanism. These cells probably secrete immunosuppressive factors (IL10, TGF-β), thereby preventing leukocyte stimulation and immune-mediated lysis.

In a subsequent syngeneic *in vivo* tumor model, CTs' potential to impact solid tumors was examined. Again, we focussed on a non-immunogenic tumor, although it is clearly established that low immunogenic tumors respond worse than their immunogenic counterpart [2]. Nonetheless, we observed strong oncopathic effects following local, repetitive administration in immune-competent mice bearing syngeneic Panc02 pancreatic carcinomas. This finally resulted in significantly delayed tumor growth. Of particular interest was the finding that maximal tumor growth control was obtained after six injections. Increasing the number of injections did not further boost therapeutic responses. Hence, CT may thus be best combined with other (antineoplastic) drugs rather than used as a single agent. In the case of pancreatic carcinomas, this would probably include gemcitabine, since this drug is still the most effective one [31, 32]. However, before further exploring such combinatorial approaches possible intolerable toxic side effects (e.g., cardiac, gastrointestinal, and hematological toxicity, anorexia, neuropathy, arthralgia, and myalgia) have to be excluded or at least minimized. Additional to identifying the optimal nontoxic dose, a proper application route (i.e., systemic versus local), an appropriate and feasible time schedule (simultaneous versus consecutive therapy), and potential synergistic or antagonistic effects of selected combinations have to be evaluated. In our experiments, we even observed differential responses using different application routes. Systemic applications failed to affect Panc02 tumors. This experimental observation fits to the historical fact of Coley himself primarily treating patients with soft tissue sarcomas. Those can be easily accessed and this might finally explain Coley's impressive clinical successes [2, 33].

In line with Coley's intuitions of stimulating the immune system to be effective in treating cancer, therapeutic effects following local CT application could be attributed to systemic immune activation primarily belonging to the innate arm. These included significantly increased numbers of circulating DCs and slightly reduced MDSC levels. MDSCs are by definition immature and contribute to tumor-related immunosuppression by inducing T- and NK-cell dysfunction [34]. Only recently, Zoglmeier and Coworkers described that several TLR-Ligands (e.g., CpG, Poly I:C) block the suppressive function of MDSCs by inducing maturation and differentiation, however, without affecting their total numbers [35]. These findings are in agreement with our observations on only marginal reductions in total circulating and splenic MDSCs levels, but efficient tumor growth control *in vivo*. We therefore hypothesize that local CT therapy was able to convert MDSC functions that allowed for immune-mediated tumor growth inhibition. Gaining deeper insights into the underlying mechanisms is of particular interest for subsequent follow-up studies.

Somewhat unexpected and yet partly unexplained remains the massive increase in γ/δ TCR$^+$ cells, especially in spleens of locally treated mice. These cells provide a link between innate and specific immune responses, capable of mediating non-MHC-restricted tumor lysis [36]. Additionally, they were found to act against invading pathogens by producing IFN-γ [37, 38]. In this regard, increased numbers of γ/δ TCR$^+$ cells may here be best interpreted as a mixture of both functions, that is, inducing Panc02 tumor lysis and acting against invading bacterial components in order to mediate host defense.

Taken together, we have shown that CT is still worth being employed for cancer immunotherapy due to its direct antitumoral as well as indirect immunostimulatory capacity. Accordingly, some standardized commercial bacterial extracts (MBVax, Vaccineurin, OK-432) comparable to the original CT exist nowadays. However, they mostly failed to prove effective in the clinics [9, 39]. Firstly, high fever, frequently occurring following infusion, was designated as being a stop criterion. Secondly, treatments were usually short lived, and thirdly, most of the patients were immunocompromised at time of treatment due to earlier or concurrent chemotherapy. Hence, before translating such microbial-based vaccines into clinical trials, carefully deliberating in- and exclusion criteria as well as treatment schedules is crucial.

5. Conclusions

In the era of increasing cancer incidence, the use of microbial vaccines for immunotherapy is still being re-examined. In this regard, the historical bacterial mixture of Coley's Toxin has here been shown of exhibiting antitumoral and immunostimulatory potential *in vitro* as well as *in vivo*. Data presented herein prove that this approach may provide a basis for local repetitive administration into tumor-carrying hosts, which would be best applied as combinatorial agent. Hence, Coley's Toxin still holds promise for further preclinical analyses that could finally contribute to a successful treatment regimen *in vivo*.

Abbreviations

LPS:	Lipoteichoic acid
CT:	Coley's Toxin
Cfu:	Colony forming unit
DC:	Dendritic cell
MDSC:	Myeloid derived suppressor cells
TLR:	Toll-like receptor
huPBL:	Human peripheral blood leukocytes
PI:	Propidium iodide.

Conflict of Interests

The authors declare that they have no conflict of interests.

Acknowledgment

The authors kindly thank Jana Normann for preparing the Coley's Toxin.

References

[1] L. R. Zacharski and V. P. Sukhatme, "Coley's toxin revisited: immunotherapy or plasminogen activator therapy of cancer?" *Journal of Thrombosis and Haemostasis*, vol. 3, no. 3, pp. 424–427, 2005.

[2] B. Wiemann and C. O. Starnes, "Coley's toxins, tumor necrosis factor and cancer research: a historical perspective," *Pharmacology and Therapeutics*, vol. 64, no. 3, pp. 529–564, 1994.

[3] H. Kumar, T. Kawai, and S. Akira, "Pathogen recognition by the innate immune system," *International Reviews of Immunology*, vol. 30, no. 1, pp. 16–34, 2011.

[4] M. Rossol, H. Heine, U. Meusch et al., "LPS-induced cytokine production in human monocytes and macrophages," *Critical Reviews in Immunology*, vol. 31, no. 5, pp. 379–446, 2011.

[5] U. Hobohm, J. L. Stanford, and J. M. Grange, "Pathogen-associated molecular pattern in cancer immunotherapy," *Critical Reviews in Immunology*, vol. 28, no. 2, pp. 95–107, 2008.

[6] J. J. Skitzki, E. A. Repasky, and S. S. Evans, "Hyperthermia as an immunotherapy strategy for cancer," *Current Opinion in Investigational Drugs*, vol. 10, no. 6, pp. 550–558, 2009.

[7] A. Oblak and R. Jerala, "Toll-like receptor 4 activation in cancer progression and therapy," *Clinical and Developmental Immunology*, vol. 2011, Article ID 609579, 12 pages, 2011.

[8] U. Hobohm, "Fever and cancer in perspective," *Cancer Immunology, Immunotherapy*, vol. 50, no. 8, pp. 391–396, 2001.

[9] H. C. Nauts and J. R. McLaren, "Coley toxins—the first century," *Advances in Experimental Medicine and Biology*, vol. 267, pp. 483–500, 1990.

[10] F. Belardelli, M. Ferrantini, E. Proietti, and J. M. Kirkwood, "Interferon-alpha in tumor immunity and immunotherapy," *Cytokine and Growth Factor Reviews*, vol. 13, no. 2, pp. 119–134, 2002.

[11] T. Petrella, I. Quirt, S. Verma et al., "Single-agent interleukin-2 in the treatment of metastatic melanoma," *Current Oncology*, vol. 14, no. 1, pp. 21–26, 2007.

[12] F. G. E. Perabo and S. C. Müller, "Current and new strategies in immunotherapy for superficial bladder cancer," *Urology*, vol. 64, no. 3, pp. 409–421, 2004.

[13] U. Klier, C. Maletzki, N. Göttmann, B. Kreikemeyer, and M. Linnebacher, "Avitalized bacteria mediate tumor growth control via activation of innate immunity," *Cellular Immunology*, vol. 269, no. 2, pp. 120–127, 2011.

[14] C. Neuzillet, A. Sauvanet, and P. Hammel, "Prognostic factors for resectable pancreatic adenocarcinoma," *Journal of visceral surgery*, vol. 148, no. 4, pp. e232–243, 2011.

[15] S. Heinrich, B. Pestalozzi, M. Lesurtel et al., "Adjuvant gemcitabine versus NEOadjuvant gemcitabine/oxaliplatin plus adjuvant gemcitabine in resectable pancreatic cancer: a randomized multicenter phase III study (NEOPAC study)," *BMC Cancer*, vol. 10, no. 11, p. 346, 2011.

[16] C. Maletzki, M. Linnebacher, B. Kreikemeyer, and J. Emmrich, "Pancreatic cancer regression by intratumoural injection of live *Streptococcus pyogenes* in a syngeneic mouse model," *Gut*, vol. 57, no. 4, pp. 483–491, 2008.

[17] M. Linnebacher, C. Maletzki, J. Emmrich, and B. Kreikemeyer, "Lysates of *S. pyogenes* serotype M49 induce pancreatic tumor growth delay by specific and unspecific antitumor immune responses," *Journal of Immunotherapy*, vol. 31, no. 8, pp. 704–713, 2008.

[18] U. Hobohm, "Fever therapy revisited," *British Journal of Cancer*, vol. 92, no. 3, pp. 421–425, 2005.

[19] M. Klenk, M. Nakata, A. Podbielski, B. Skupin, H. Schroten, and B. Kreikemeyer, "*Streptococcus pyogenes* serotype-dependent and independent changes in infected HEp-2 epithelial cells," *ISME Journal*, vol. 1, no. 8, pp. 678–692, 2007.

[20] K. Tsung and J. A. Norton, "Lessons from Coley's Toxin," *Surgical Oncology*, vol. 15, no. 1, pp. 25–28, 2006.

[21] H. Friedman, D. K. Blanchard, C. Newton et al., "Distinctive immunomodulatory effects of endotoxin and nontoxic lipopolysaccharide derivatives in lymphoid cell cultures," *Journal of Biological Response Modifiers*, vol. 6, no. 6, pp. 664–677, 1987.

[22] J. M. Park and D. E. Fisher, "Testimony from the Bedside: from Coley's Toxins to Targeted Immunotherapy," *Cancer Cell*, vol. 18, no. 1, pp. 9–10, 2010.

[23] J. A. Thomas and M. Badini, "The role of innate immunity in spontaneous regression of cancer," *Indian Journal of Cancer*, vol. 48, no. 2, pp. 246–251, 2011.

[24] K. A. Mason and N. R. Hunter, "CpG plus radiotherapy: a review of preclinical works leading to clinical trial," *Frontiers in Oncology*, vol. 2, no. 101, 2012.

[25] R. Ursu and A. F. Carpentier, "Immunotherapeutic approach with oligodeoxynucleotides containing CpG motifs (CpG-ODN) in malignant glioma," *Advances in Experimental Medicine and Biology*, vol. 746, pp. 95–108, 2012.

[26] C. S. Zent, B. J. Smith, Z. K. Ballas et al., "Phase I clinical trial of CpG oligonucleotide 7909 (PF-03512676) in patients with previously treated chronic lymphocytic leukemia," *Leukemia and Lymphoma*, vol. 53, no. 2, pp. 211–217, 2012.

[27] D. Xu, H. Liu, and M. Komai-Koma, "Direct and indirect role of Toll-like receptors in T cell mediated immunity," *Cellular & Molecular Immunology*, vol. 1, no. 4, pp. 239–246, 2004.

[28] J. Brown, H. Wang, G. N. Hajishengallis, and M. Martin, "TLR-signaling networks: an integration of adaptor molecules, kinases, and cross-talk," *Journal of Dental Research*, vol. 90, no. 4, pp. 417–427, 2011.

[29] T. Itoh, H. Satoh, N. Isono, H. Rikiishi, and K. Kumagai, "Mechanism of stimulation of T cells by *Streptococcus pyogenes*: isolation of a major mitogenic factor, cytoplasmic membrane-associated protein," *Infection and Immunity*, vol. 60, no. 8, pp. 3128–3135, 1992.

[30] W. K. Decker and A. Safdar, "Bioimmunoadjuvants for the treatment of neoplastic and infectious disease: coley's legacy revisited," *Cytokine and Growth Factor Reviews*, vol. 20, no. 4, pp. 271–281, 2009.

[31] N. Makrilia, K. N. Syrigos, and M. W. Saif, "Updates on treatment of gemcitabine-refractory pancreatic adenocarcinoma," *Journal of the Pancreas*, vol. 12, no. 4, pp. 351–354, 2011.

[32] M. Busch, R. Wilkowski, M. Schaffer, and E. Duhmke, "Combined chemotherapy, radiotherapy, and immunotherapy for pancreatic carcinoma—a case report," *Advances in Therapy*, vol. 17, no. 3, pp. 133–139, 2000.

[33] E. F. McCarthy, "The toxins of William B. Coley and the treatment of bone and soft-tissue sarcomas," *The Iowa Orthopaedic Journal*, vol. 26, pp. 154–158, 2006.

[34] C. A. Corzo, M. J. Cotter, P. Cheng et al., "Mechanism regulating reactive oxygen species in tumor-induced myeloid-derived suppressor cells," *Journal of Immunology*, vol. 182, no. 9, pp. 5693–5701, 2009.

[35] C. Zoglmeier, H. Bauer, D. Nörenberg et al., "CpG blocks immunosuppression by myeloid-derived suppressor cells in tumor-bearing mice," *Clinical Cancer Research*, vol. 17, no. 7, pp. 1765–1775, 2011.

[36] P. Fisch, M. Malkovsky, E. Braakman et al., "γ/δ T cell clones and natural killer cell clones mediate distinct patterns of non-major histocompatibility complex-restricted cytolysis," *Journal of Experimental Medicine*, vol. 171, no. 5, pp. 1567–1579, 1990.

[37] L. Mölne, A. Corthay, R. Holmdahl, and A. Tarkowski, "Role of gamma/delta T cell receptor-expressing lymphocytes in cutaneous infection caused by Staphylococcus aureus," *Clinical and Experimental Immunology*, vol. 132, no. 2, pp. 209–215, 2003.

5.1.2 Anlage – Teil 2

Mistletoe lectin has a shigatoxin-like structure and should be combined with other Toll-like receptor ligands in cancer therapy

Cancer Immunol Immunother (2013) 62:1283–1292
DOI 10.1007/s00262-013-1455-1

OPINION PAPER

Mistletoe lectin has a shiga toxin-like structure and should be combined with other Toll-like receptor ligands in cancer therapy

**Claudia Maletzki · Michael Linnebacher ·
Rajkumar Savai · Uwe Hobohm**

Received: 25 April 2013 / Accepted: 21 June 2013 / Published online: 6 July 2013
© Springer-Verlag Berlin Heidelberg 2013

Abstract Mistletoe extract (ME) is applied as an adjuvant treatment in cancer therapy in thousands of patients each year in Europe. The main immunostimulating component of mistletoe extract, mistletoe lectin, recently has been shown to be a pattern recognition receptor ligand and hence is binding to an important class of pathogen-sensing receptors. Pattern recognition receptor ligands are potent activators of dendritic cells. This activation is a prerequisite for a full-blown T-cell response against cancer cells. Pattern recognition receptor ligands are increasingly recognized as important players in cancer immunotherapy. We collect evidence from case studies on spontaneous regression, from epidemiology, from experiments in a mouse cancer model, and from protein structure comparisons to argue that a combination of mistletoe therapy with other pattern recognition receptor ligand substances leads to an increased immune stimulatory effect. We show that mistletoe lectin is a plant protein of bacterial origin with a 3D structure very similar to shiga toxin from *Shigella dysenteriae*, which explains the remarkable immunogenicity of mistletoe lectin. Secondly, we show that a combination of pattern recognition receptor ligands applied metronomically in a cancer mouse model leads to complete remission, while single pattern recognition receptor ligands slowed tumor growth. Taken together, we propose to combine mistletoe drugs with other pattern recognition receptor ligand drugs to increase its efficacy in adjuvant or even primary cancer therapy.

Keywords Mistletoe extract · Mistletoe lectin · Pattern recognition receptor ligands · Shiga toxin · Cancer immunotherapy

Introduction

Spontaneous regressions and remissions

Spontaneous regressions and remissions in cancer are still regarded as a conundrum. However, by exhaustive scanning of case studies, we could show that many, if not a majority of spontaneous remissions, were preceded by an acute feverish infection [1]. In a syngeneic pancreatic carcinoma mouse model, we could confirm that a single intra-tumoral injection of live *Streptococcus pyogenes* can result in complete tumor regression [2].

Spontaneous regressions in cancer are regarded as a rare phenomenon in case of larger tumors; yet, they occur in up to 20 % of small breast cancer nodules [3]. If the link in time between acute infect and regressions was not only coincidental but causal, it should also precipitate as protection, such that a personal history of infections should reduce the likelihood to develop cancer later. Subsequently, indeed, we found more than 30 studies which, as an ensemble, appear to confirm this prediction (Table 1).

It should be emphasized that these were acute, fully cleared infections, in contrast to chronic viral and bacterial infections, which are causally related with up to 20 % of all cancers [49].

C. Maletzki · M. Linnebacher
University of Rostock, Rostock, Germany

R. Savai
Max Planck Institute for Heart and Lung Research,
Bad Nauheim, Germany

U. Hobohm (✉)
University of Applied Sciences, Wiesenstrasse 14,
35390 Giessen, Germany
e-mail: uwe.hobohm@mni.thm.de

Table 1 Anti-correlation between acute, cured infections, and the likelihood to develop cancer

Observation	Effect	Year of publication	Pathogen	References
Lower risk of cancer in syphilitic prostitutes	Prophylactic	1725	*Treponema pallidum*	[4]
Collection of 302 cases of spontaneous regression (44 complete remissions), 27/302 cases accompanied by infection (9 %), 69 cases where "incomplete operation (was) often accompanied by postoperative fever" (28 %)	Therapeutic	1918	Diverse	[5]
Low risk of cancer in tuberculosis patients	Prophylactic	1929	*Mycobacterium tuberculosis*	[6]
Lower risk of cancer in malaria patients	Prophylactic	1929	Plasmodium falc., malariae, vivax	[7, 8]
Of 300 cancer patients, 113 had no febrile infectious childhood diseases (FICD), while in 300 controls, 16 lacked FICD	Prophylactic	1934	Diverse	[9]
Fewer childhood diseases, higher cancer risk in adults	Prophylactic	1936	Diverse	[10]
In a cohort of 300 cases of childhood leukemia, 26 spontaneous remissions were observed. 21/26 (80 %) were accompanied by infection	Therapeutic	1951	Diverse	[11]
Less benign ovary cysts in patients with childhood mumps	Prophylactic	1960	Paramyxovirus parotitis	[12]
"…according to the Cancer Centre in Sao Paulo (Brazil), among tens of thousands of cancer patients, only two gave a positive Machado reaction (indicating chronic or recovered trypanosoma infection), whereas among the remaining population, the number suffering from this infection varies from 10 to 20 percent.", anecdotal remark	Prophylactic	1963	*Trypanosoma cruzi*	[13]
Lower cancer mortality in 5,460 survivors of typhoid fever	Prophylactic	1970	*Salmonella typhi*	Ref. 58 in [14]
Fewer physician visits, secondary illnesses, and hospital referrals in 150 controls versus 150 cancer patients	Prophylactic	1970	Diverse	[15]
In 62/224 cases of spontaneous regression (28 %), either an infection or a persistent temperature elevation was observed prior to regression	Therapeutic	1971	Diverse	[16]
Occasional remissions in Hodgkin's lymphoma after measles attack	Therapeutic	1971	Morbillivirus	[17]
Patients developing empyema after lung cancer surgery have improved 5-year survival (50 % ($n = 18$) vs. 22 % ($n = 411$))	Therapeutic	1972	Diverse	[18]
Lower incidence of mumps, measles, rubella in 300 patients with cancer of the ovary compared to control group	Prophylactic	1977	MMR viruses	[19]
Lower incidence of mumps in patients with cancer of the ovary compared to control group	Prophylactic	1979	Paramyxovirus parotitis	[20, 21]
Increased cancer risk with an odds ratio of 2.6 for missing history of infectious organ diseases, 5.7 for missing history of common colds, and 15.1 for missing history of fever	Prophylactic	1983	Diverse	[22]
Out of 353 individuals with a negative history of measles, 21 developed cancer versus 1 case in 230 controls with a positive history of measles (p 0.001)	Prophylactic	1985	Diverse	[23]
Much lower cancer rate in wool and hemp factories; wool or hemp dust can carry bacterial endotoxins.	Prophylactic	1985	Diverse	[24]
Lower frequency of infections in the first year of life for children with leukemia	Prophylactic	1986	Diverse	[25]
Lower cancer incidence after Herpes infections	Prophylactic	1987	Herpes simplex	[26]
Posttransfusional hepatitis in patients with acute myelogenous leukemia doubles survival rate	Therapeutic	1982, 1992	Hepatitis viruses	[27, 28]
A history of common colds or gastroenteric influenza was found to be associated with a decreased cancer risk (odds ratio 0.18 and 0.23 vs. population and hospital controls, resp.)	Prophylactic	1991	Common cold viruses	[29]

Table 1 continued

Observation	Effect	Year of publication	Pathogen	References
Inverse correlation between number of infections and mortality from tumors in Italy in the period 1890–1960: each 2 % reduction in number of infectious diseases was followed by a 2 % increase in tumors about 10 years later	Prophylactic	1998	Diverse	[30]
Inverse association between number of carcinoma (but not breast cancer) and febrile infectious childhood diseases (FICD); association stronger for higher numbers of FICD and childhood in pre-antibiotic times; strongest protection by rubella (379 cancer cases vs. 379 office matched controls)	Prophylactic	1998	Diverse	[31]
Sixty-eight well-documented cases of spontaneous regression from melanoma, preceded in 21 (31 %) cases by a febrile infection	Therapeutic	1998	*Streptococcus pyogenes*	[32]
Statistically significant inverse association between a reported history of infections and glioma, meningioma (RR = 0.72, age- and gender-matched population control of 1,509 cases)	Prophylactic	1999	Diverse	[33]
Inverse correlation between melanoma risk and number of recorded infections on one hand and between melanoma risk and fever height on the other hand, leading to a combined reduction of melanoma risk of about 40 % for people with a history of three or more infections with high fever above 38.5 °C (age- and gender-matched population control)	Prophylactic	1999	Diverse	[34]
More than twofold higher incidence of cancer in Europe, GUS, and US compared to Africa and Asia of 381 versus 156 (ten most prominent cancer forms, age-standardized rate per 100,000 population; in Africa and Asia, a significant higher rate of infections is assumed here	Prophylactic	2003	Diverse	[35]
Prior immunization of melanoma patients with vaccinia or BCG is associated with better survival (age-matched controls)	Prophylactic	2005	Vaccinia, BCG vaccine	[36]
Dairy farmers, but not crop and orchard farmers, report one-third less cancers than the average population; protection diminishes over time after exposure is removed; dust in cattle houses can carry bacterial endotoxins which frequently lead to unspecific "day fever"	Prophylactic	2005	Diverse	[37]
The 10-year survival for patients with osteosarcoma with infection within 1 year after surgery (n = 41) was 84.5 % compared to 62.3 % in the non-infected group (n = 371)	Therapeutic	2007	Diverse	[38]
After allogeneic stem cell transplantation, patients who had a febrile infection (FI) before posttransplant day 21 (FI group) had a lower probability of leukemic relapse ($p < 0.001$) and a higher relapse-free survival rate ($p = 0.012$) than those patients who did not have a FI before posttransplant day 21 (non-FI group)		2008		[39]
Fourfold higher risk for Hodgkin lymphoma if tonsils are removed at age <15 years	Prophylactic	2010	Diverse	[40]
Reduced ALL (acute lymphoblastic leukemia) risk in kindergarten children (frequent mutual infectious contaminations presumed) (OR 0.8) or children with repeated common infections (OR 0.7)	Prophylactic	2010	Diverse	[41]
Reduced risk for ALL in children visiting kindergarten	Prophylactic	2010, 2011	Diverse	[42, 43]
Reduced HL risk (Hodgkin lymphoma, 128 cases aged 5–14) and NHL (non-Hodgkin lymphoma, 164 cases aged 2–15 years) versus 1,312 controls. HL + kindergarten: OR 0.5; HL + common infections + non-breast-feeding: OR 0.3; NHL + birth order 3: OR 0.7; NHL + prolonged breast-feeding: OR 0.5; NHL + frequent farm visits in early life: OR 0.5; NHL + asthma: OR 0.6	Prophylactic	2011	Diverse	[44]

Two publications were found, which could not confirm inverse association between infection and cancer [45, 46], one, in a low impact journal not listed in PubMed [47], reported an increased risk with mumps and whooping cough. All three publications are based on less than 200 cases. In one study, an inverse correlation between childhood mumps and ovary cancer could not be confirmed [48]

Coley's cancer treatment using bacterial extracts

On a related line of evidence, it should be remembered that Coley and contemporaries, between 1895 and 1936, by injecting fever-inducing bacterial extracts prepared from *S. pyogenes* and *Serratia marcescens* ("Coley's toxin"), "documented cases of the long-term survival of individuals with malignancies that remain a major challenge to treat now" [50] (see [51] for an impressive example reported 1928, to be downloaded from http://bioinfo.tg.fh-giessen.de/pamp-cancer/christian-1928-amjdsurg-coley.pdf). Coley used to increase the dosage of his extract on a per patient basis until a body temperature of 39 °C or above could be achieved [52]. He used a metronomic therapy regimen with 1–3 injections per week over month, thus stimulating the innate immune system again and again, with longer treatment resulting in better outcome.

As a biological mechanism underlying these three phenomena (spontaneous regression, epidemiological protection, and Coley's experiments), we suggested the unspecific activation of dendritic cells (DC) by pattern recognition receptor ligands (PRRL), for instance Toll-like receptor (TLR) ligands [53]. In this sense, "Coley's toxin" might be regarded as a PRRL mix.

PRRL drugs as potential substitutes for a proliferative infection

Pattern recognition receptor ligands act as mandatory co-stimulatory signals in DC activation and are the most potent activators of DC. DC activation, in turn, is needed for a full-blown T-cell response against cancer cells. Cancer tissues do not provide PRRL. DC activation by PRRL in infected cancer patients presumably extends to DC signalling both pathogen antigens and tumor antigens [53], leading to clonal expansion, maturation, and activation of both pathogen-specific and tumor cell-specific T-cell clones. We have outlined the immunological explanation in more detail in [54]. The repeated application of PRRL containing drugs, just like the repeated application of bacterial extracts, might serve as a substitute infection.

Immune-stimulating effects of mistletoe lectin and PRRL are similar

Mistletoe extract (ME) is manufactured from the European mistletoe *Viscum album* and available as pharmaceutical preparation under various brands including Helixor, Iscador, and Abnoba. ME therapy is an adjuvant treatment applied to thousands of cancer patients each year in Europe [55]. Immune-stimulating effects of ME depend largely on mistletoe lectin-1 (ML) [56]. Physicians often report better well-being and occasional remissions or disease stabilisations. Meta-analyses show small benefits of ME regarding survival [57] and clear benefits with respect to quality of life [58, 59]. Occasional cures have been reported after very long repeated application in otherwise therapy naive patients [60, 61].

Several immune-stimulating effects of ME or ML have been observed. In vitro effects include increased cytokine expression (IL-1b, IL-5, IL-6, TNF-alpha, and GM-CSF), higher phagocytic uptake by macrophages, increased NK-cell and cytotoxic T-lymphocyte (CTL) activity [62]. In vivo effects include increased counts of CD4 cells [63], of DC infiltrating the primary tumor [64], of tumor antigen-specific CD8+-T cells, of NK- and gamma-delta-T cells [65].

Recently, it has been shown that the Korean variant of mistletoe lectin (KMLC) is a TLR-4 ligand [66]. KMLC and European ML have a sequence identity of 84 % and thus the same 3D structures [67], so European ML presumably is a TLR-4 ligand as well.

The most prominent TLR-4-binding molecule is lipopolysaccharide (LPS). At first sight, it seems puzzling that KMLC shares binding to TLR-4 with LPS, which has a completely different molecular weight and 3D structure. However, LPS binds not directly to TLR-4 but its binding is mediated through scaffold proteins, including LPS-binding protein (LBP), CD14 and MD-2 [68]. Thus, mistletoe lectin binding to TLR-4 might as well be mediated by respective scaffold proteins. Several cytokines, including IL-1, IL-6, IL-12, TNF-alpha, and GM-CSF, show elevated levels both upon PRRL application [69] and ML application [68]; both KMLC [62] and LPS [70] increase the production of IL-1 and IL-6 in antigen-presenting cells.

In this study, we elucidated the remarkable immunogenicity of ML and set out to substantiate our hypothesis that the application of a combination of PRRL has unleveraged therapeutic potential.

Materials and methods

Bioinformatics

Sequence database searches were performed using Blast. Alignment, 3D overlay and rendering of mistletoe lectin-1 (PDB-ID 1SZ6-A) and shiga toxin (PDB-ID 1R4P-A) were done using PyMol.

Mouse experiments

Panc02 pancreatic tumor cells were injected s.c. (1×10^6) in C57BL/6J mice, leading to surface lesions of about 50 mm^2 after 7 days. PRRL ($n = 5$) or saline solution (control, $n = 8$) were injected s.c. (in 50 µl) 10 times over 21 days in regular intervals. Tumor size was measured at each injection day. PRRL applied were flagellin (Sigma, 25 µg/kg BW) targeting TLR-5, LPS (2 mg/kg BW) targeting TLR-4, MDP (100 µg/kg BW) targeting NOD-2, Resiquimod (60 µg/kg BW) targeting TLR-7/8 or a combination of LPS, Resiquimod and MDP. All chemicals were purchased from Enzo, Lörrach, Germany. Mice were killed at day 31 and residual tumor volume compared. Content of myeloid suppressor cells (MDSC) in spleen were analyzed by flow cytometry.

Body temperature was monitored wireless by subcutaneously implanted sensors (Respironics, PDT-4000 E-mitter).

Results

Mistletoe lectin chain A shares a striking structural similarity with shiga toxin chain A

The remarkable immunogenicity of ML, a protein produced by a plant, so far is unexplained. ML is classified as a protein with rRNA N-glycosylase activity, thus inhibiting ribosomes leading to mild ML cytotoxic activity in vitro. ML has two domains, the A-chain carrying the enzymatic site and the B-chain acting as cellular-binding domain. The closest related structure is ricin, with 49 % sequence identity, the same EAAR motif at the active site (catalytic residues E, R), similar length of both A- and B-chains, and a very similar 3D structure extending over both chains. Ricin is produced by the castor bean and exhibits a much stronger cytotoxicity than ML. While ricin does not bind to CD75s-ganglioside-linked cell surface receptors, a recombinant ML does [71]. Hence, the different toxicities might be attributed to different cell-type binding preferences or affinities of the B-chains.

Apart from the obvious relationship with ricin, we noticed that shiga toxin, a bacterial protein, has a sequence identity with ML at the borderline of significance (25 % sequence identity over 263 residues alignment length and Blast e value 0.00026). At this low sequence identity, indicating considerable evolutionary divergence, one would expect quite dissimilar functions and 3D structures.

To our surprise, both ML (PDB-Id 1SZ6 chain A) and ricin A-chains turned out to be structurally related to shiga toxin type-2 (PDB-Id 1R4P chain A). Shiga toxin is produced by *Shigella dysenteriae* and enterohemorrhagic *E. coli* (EHEC) and is, like ricin, a strong cytotoxin. Structural overlay of ML and shiga toxin showed that secondary structure elements are in striking spacial match (see Fig. 1): root mean square deviation (RSMD) is 2.1 over 240 residues. This almost perfect structural identity therefore implies a common evolutionary origin [72]. Both proteins share the same enzymatic activity and a conserved 4-amino acid active site motif (ML: EAAR, shiga toxin: EALR). Thus, ML might be considered in vaccination strategies against EHEC infections.

A lookup in the CATH database of related structures [73] revealed that structural motifs similar to parts of ML chain A (CATH IDs 3.40.420.10 and 4.10.470.10) can be found in some other bacteria including particular strains of *E. coli* and *Streptomyces*, but also in enterobacterial phages, and in a range of plants besides mistletoe.

Presumably, mistletoe, castor bean, and some other plants have captured bacterial ribosome inhibitors by horizontal gene transfer. The function of a toxin such as ML in plants might be the rebuff of herbivores. The evolutionary provenance of ML from bacteria can explain why human Toll-like receptors, otherwise preferentially binding pathogenic substances, could be targeted by ME. Mistletoe plant has strong immune stimulatory capacity because it produces a bacterial toxin.

PRRL should be applied in combination

To resemble a proliferative infection and according to the lessons to be learned from Coley's experiments, from case observations on spontaneous regressions [1] and epidemiological findings (Table 1), we have suggested to apply PRRL (1) in immuno-competent organisms, (2) in combination to address more than one PRR, (3) over a longer fixed period (metronomic treatment regimen), and (4) under appreciation of fever [53, 74]. To the best of our knowledge, this paradigm has not been tested before.

Hence, we challenged C57BL6J mice with Panc02 autologous pancreatic tumor cells and applied single and multiple PRRL 10 times over 3 weeks. While individual PRRL slowed tumor growth, only the combination induced complete remission in 4/5 mice. The tumor of the fifth mouse in the combi group, which was the largest in the mix group at treatment start, stopped tumor growth at day 14. The tumor size difference between control and mix at day 31 is significant at the 1 % level (t-Test, $p = 0.0068$) (see Fig. 2). The content of myeloid-derived suppressor cells (MDSC) in spleen, a heterogeneous population of cells expanding during cancer development with the ability to suppress T-cell responses [75], was reduced by all PRRL between twofold (MDP) to sixfold (Resiquimod, LPS), indicating counterbalanced immune suppression upon PRRL application.

Mice have limited capabilities to raise their body temperature. Still, a PRRL such as LPS can raise the body temperature of mice by about 1 °C (measured by subcutaneous wireless sensor, averaged over 24 h, data not shown).

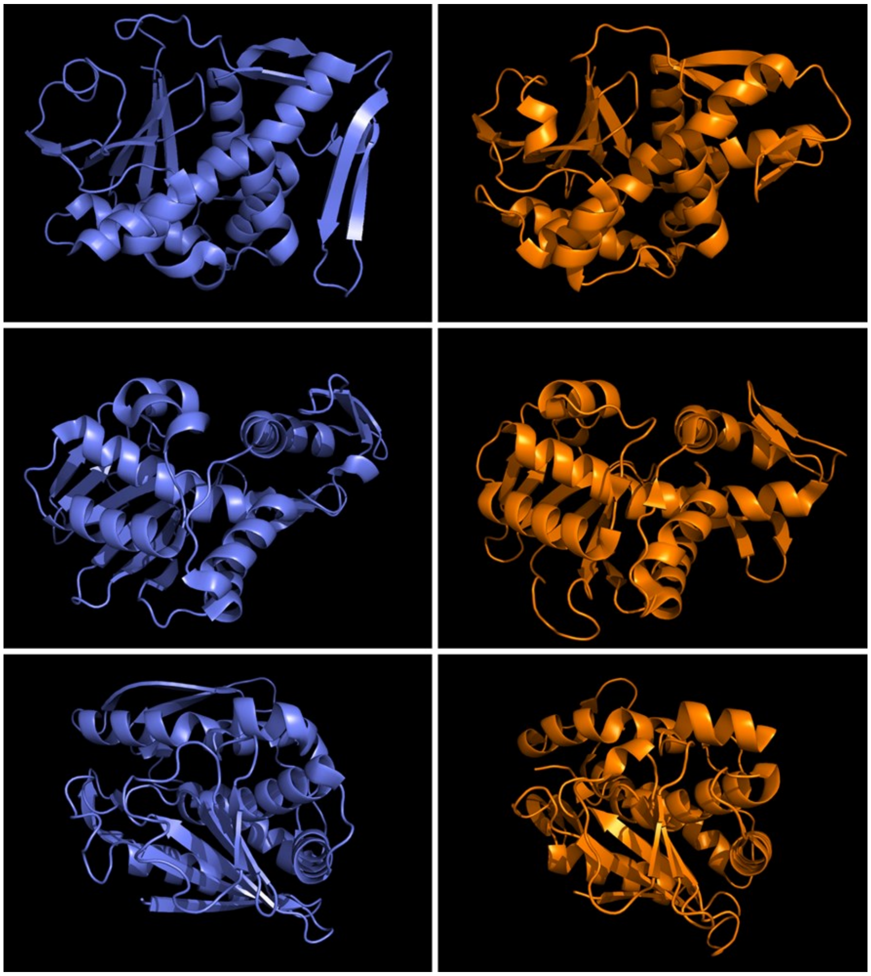

Fig. 1 Structural identity of mistletoe lectin-1 (*blue*) and shiga toxin (*orange*) shown in 3 orientations. RMSD = 2.1 along residues 1–240

Discussion

Mistletoe therapy might be augmented by PRRL

Besides Coley's seminal treatments for cancer patients with bacterial extracts of *S. pyogenes* and *S. marcescens* about a century ago, the application of pathogens in cancer therapy has a long history [76]. A clinical success is the administration of Bacillus Calmette–Guérin (BCG) immunotherapy as treatment standard for non-muscle invasive bladder cancer [77]. Repeated instillations with live BCG are necessary for a robust immune response. Some facultative anaerobic bacteria like *Bifidobacterium bifidum* [78], *Clostridium novyi,* and *Salmonella typhimurium* are known to home preferentially into solid tumors after systemic application, perhaps favouring hypoxic tumor environments. Hoffman et al. used a genetically modified strain of live *S. typhimurium* to treat prostate [79], breast [80], pancreatic [81], spinal chord [82], lung [83], and glioma [84] tumors in orthotopic or syngeneic mouse models and achieved some impressive remission rates. The authors suggest direct tumor killing effects; however,

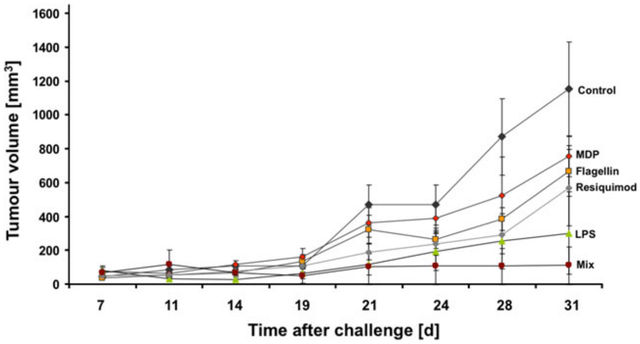

Fig. 2 C57BL/6J mice (n = 5) were challenged with autologous Panc02 tumor cells at day 0. PRRL treatment started at day 7 and was repeated 10× until day 28. PRR targeted were TLR-4 (LPS), TLR-5 (Flagellin), TLR-7/8 (Resiquimod), NOD2 (MDP). Mix contained LPS, Resiquimod, and MDP. *Error bars* are SEM. Tumor size difference between mix and control at day 31 is significant (*t*-Test, $p = 0.0068$)

metronomic treatment was more effective and better tolerated compared to bolus or few applications [84], and complete cure can be observed despite a residual well-oxygenated tumor rim after treatment [85]. So innate immune stimulation of an existing T-cell response as suggested here could be an alternative explanation at least in the immunocompetent mouse models.

The approval of live or even killed bacterial drugs nowadays faces severe obstacles due to batch-to-batch variability during production and the general lack of structure–function relationship data, which are usually requested by the authorities. Thus, drugs resembling a proliferative infection, where clear structure–function relationships can be established, are preferable compared to bacterial extracts. We suggest that PRRL combinations could serve as substitute infection. Different combinations of PRRL could be compared and optimized for effectivity.

Several PRRL were tested in clinical trials, mainly as adjuvants, to this end with uncertain benefits [86–88]. In these trials, PRRL are applied as single substances, in immunocompromised patients with a record of chemotherapy or radiation, a few times, with fever treated as toxic side effect. Previously, we have suggested to change PRRL therapy regimen and rather apply PRRL in immunocompetent cancer patients, in a metronomic fashion over several weeks, under the appreciation of periods of short (1-day) fever and in combination [53, 74].

Our preliminary results show (1) that single PRRL applied metronomically can slow tumor progression, (2) PRRL in combination and applied multiple times over 3 weeks can induce complete remissions, and (3) the count of MDSC was reduced 2- to 6-fold after PRRL application.

While it is known that chronic CpG application in tumor-free hosts can lead to expansion of MDSC and T-cell suppression, the therapeutic application of CpG in tumor-bearing mice decreased MDSC and blocked suppressive activity on T-cell proliferation [89]. We confirmed a similar decrease on MDSC count after PRRL application, likely leading to a similar lift of T-cell suppression.

Protein PRRL like flagellin or ML are expected to induce neutralizing antibodies after repeated application. Yet, immune stimulatory effects of ME can be found in patients after repeated application despite ML serum antibody titers. Innate immune responses can occur within minutes, so innate responses are likely triggered before any neutralization takes place, in particular upon s.c. or intratumoral or peri-tumoral application. For i.v. application, nonprotein PRRL might be preferable.

Mistletoe extract, in particular at higher dosages and at the beginning of treatment, often leads to fever. Clinicians with long experience in mistletoe therapy try to adjust a fever-inducing dosage on a per patient basis. ME-induced fever usually rises and declines within 1 day and lacks potential severe side effects of fever induced by a proliferative infection. Mistletoe therapy often is applied over longer periods. Thus, our suggestions to apply PRRL in a metronomic fashion and not suppressing fever are already implemented by present-day ME therapy regimen, since the main actor in ME, mistletoe lectin, is a PRRL of bacterial origin. To improve the outcome of mistletoe therapy, we suggest to combine ML with other PRRL to extend the range of PRR addressed.

Conflict of interest All authors declare that neither of us has a significant financial arrangement or affiliation with any product or services used or discussed in our paper, nor any potential bias against another product or service.

Animal experiment declaration Animal experiments were performed in accordance with the German legislation on the protection of animals and the Guide for the Care and Use of Laboratory Animals (Institute of Laboratory Animal Resources, National Research Council; NIH Guide, vol. 25, No. 28, 1996). All animal experiments were approved by the local agency for animal welfare (Landesamt für Landwirtschaft, Lebensmittelsicherheit und Fischerei, Mecklenburg-Vorpommern).

References

1. Hobohm U (2001) Fever and cancer in perspective. Cancer Immunol Immunother 50:391–396
2. Maletzki C, Linnebacher M, Kreikemeyer B, Emmrich J (2008) Pancreatic cancer regression by intratumoural injection of live *Streptococcus pyogenes* in a syngeneic mouse model. Gut 57:483–491. doi:10.1136/gut.2007.125419
3. Zahl PH, Maehlen J, Welch HG (2008) The natural history of invasive breast cancers detected by screening mammography. Arch Intern Med 168:2311–2316. doi:10.1001/archinte.168.21.2311
4. Deidier A (1725) Dissertation Medecinal et Chirurgical sur les Tumeurs, Paris
5. Rohdenburg G (1918) Fluctuations in the growth energy of malignant tumors in man, with especial reference to spontaneous recession. J Cancer Res 3:193–225
6. Pearl R (1929) Cancer and tuberculosis. Am J Hyg 9:97–162
7. Braunstein A (1929) Krebs und malaria. Z Krebsforsch 29:330–333
8. Braunstein A (1929) Experimentelle und klinische Grundlagen fuer Malariabehandlung des Krebses. Z Krebsforsch 29:468–490
9. Engel P (1934) Ueber den Infektionsindex der Krebskranken. Wien Klin Wochenschr 47:1118–1119
10. Sinek F (1936) Versuch einer statistischen Erfassung endogener Faktoren bei Carcinomerkrankungen. Z Krebsforsch 44:492–527
11. Diamond LK, Luhby LA (1951) Pattern of 'spontaneous' remissions in leukemia of the childhood, observed in 26 of 300 cases. Am J Med 10:238ff
12. West RO (1966) Epidemiologic study of malignancies of the ovaries. Cancer 19(7):1001–1007
13. Klyuyeva NG, Roskin GI (1963) Biotherapy of malignant tumours. Pergamon Press, Oxford
14. Kienle GS (2012) Fever in cancer treatment: Coley's therapy and epidemiological observations. Glob Adv Health Med 1(1):90–98
15. Witzel L (1970) History and other diseases in patients with malignant neoplasms. Med Klin 65(18):876–879
16. Stephenson HE Jr et al (1971) Host immunity and spontaneous regression of cancer evaluated by computerized data reduction study. Surg Gynecol Obstet 133(4):649–655
17. Zygiert Z (1971) Hodgkin's disease: remissions after measles. Lancet 1(7699):593
18. Ruckdeschel JC et al (1972) Postoperative empyema improves survival in lung cancer. documentation and analysis of a natural experiment. N Engl J Med 287(20):1013–1017
19. Newhouse ML et al (1977) A case control study of carcinoma of the ovary. Br J Prev Soc Med 31(3):148–153
20. Menczer J et al (1979) Possible role of mumps virus in the etiology of ovarian cancer. Cancer 43(4):1375–1379
21. Cramer DW et al (1983) Mumps, menarche, menopause, and ovarian cancer. Am J Obstet Gynecol 147(1):1–6
22. Remy W et al (1983) Tumorträger haben selten Infekte in der Anamnese. Med Klin 78:95–98
23. Ronne T (1985) Measles virus infection without rash in childhood is related to disease in adult life. Lancet 1(8419):1–5
24. Enterline PE et al (1985) Endotoxins, cotton dust, and cancer. Lancet 2(8461):934–935
25. van Steensel-Moll HA, Valkenburg HA, van Zanen GE (1986) Childhood leukemia and infectious diseases in the first year of life: a register-based case–control study. Am J Epidemiol 124(4):590–594
26. Grossarth-Maticek R et al (1987) Reported herpes-virus-infection, fever and cancer incidence in a prospective study. J Chronic Dis 40(10):967–976
27. Rotoli B et al (1982) Long-term survival in acute myelogenous leukemia complicated by chronic active hepatitis. N Engl J Med 307(27):1712–1713
28. Treon SP, Broitman SA (1992) Beneficial effects of post-transfusional hepatitis in acute myelogenous leukemia may be mediated by lipopolysaccharides, tumor necrosis factor alpha and interferon gamma. Leukemia 6(10):1036–1042
29. Abel U et al (1991) Common infections in the history of cancer patients and controls. J Cancer Res Clin Oncol 117(4):339–344
30. Mastrangelo G, Fadda E, Milan G (1998) Cancer increased after a reduction of infections in the first half of this century in Italy: etiologic and preventive implications. Eur J Epidemiol 14(8):749–754
31. Albonico HU, Braker HU, Husler J (1998) Febrile infectious childhood diseases in the history of cancer patients and matched controls. Med Hypotheses 51(4):315–320
32. Maurer S, Koelmel KF (1998) Spontaneous regression of advanced malignant melanoma. Onkologie 21:14–18
33. Schlehofer B et al (1999) Role of medical history in brain tumour development. Results from the international adult brain tumour study. Int J Cancer 82(2):155–160
34. Koelmel KF et al (1999) Infections and melanoma risk: results of a multicenter EORTC case study. Melanoma Res 9:511–519
35. Stewart BW, Kleihues P (2003) World Cancer report. World Health Organization, IARC Press, Lyon
36. Koelmel KF et al (2005) Prior immunisation of patients with malignant melanoma with vaccinia or BCG is associated with better survival. An European Organization for Research and Treatment of Cancer cohort study on 542 patients. Eur J Cancer 41(1):118–125
37. Mastrangelo G et al (2005) Lung cancer risk: effect of dairy farming and the consequence of removing that occupational exposure. Am J Epidemiol 161(11):1037–1046
38. Jeys LM et al (2007) Post operative infection and increased survival in osteosarcoma patients: are they associated? Ann Surg Oncol 14(10):2887–2895
39. Kim SY et al (2008) The influence of infection early after allogeneic stem cell transplantation on the risk of leukemic relapse and graft-versus-host disease. Am J Hematol 83(10):784–788
40. Vestergaard H et al (2010) Tonsillitis, tonsillectomy and Hodgkin's lymphoma. Int J Cancer 127(3):633–637
41. Rudant J et al (2010) Childhood acute leukemia, early common infections, and allergy: the ESCALE Study. Am J Epidemiol 172(9):1015–1027
42. Urayama KY et al (2010) A meta-analysis of the association between day-care attendance and childhood acute lymphoblastic leukaemia. Int J Epidemiol 39(3):718–732
43. Urayama KY et al (2011) Early life exposure to infections and risk of childhood acute lymphoblastic leukemia. Int J Cancer 128(7):1632–1643
44. Rudant J et al (2011) Childhood Hodgkin's lymphoma, non-Hodgkin's lymphoma and factors related to the immune system: the Escale Study (SFCE). Int J Cancer 129(9):2236–2247
45. Chilvers C et al (1986) The common cold, allergy, and cancer. Br J Cancer 54(1):123–126
46. Cardwell CR et al (2008) Infections in early life and childhood leukaemia risk: a UK case–control study of general practitioner records. Br J Cancer 99(9):1529–1533
47. Hoffmann C et al (2002) Childhood diseases, infectious diseases, and fever as potential risk factors for cancer? Forsch Komplementarmed Klass Naturheilkd 9:324–330
48. Chen Y et al (1992) Risk factors for epithelial ovarian cancer in Beijing, China. Int J Epidemiol 21(1):23–29
49. Mantovani A, Pierotti MA (2008) Cancer and inflammation: a complex relationship. Cancer Lett 267:180–181
50. Mantovani A, Allavena P, Sica A, Balkwill F (2008) Cancer-related inflammation. Nature 454:436–444. doi:10.1038/nature07205

51. Christian S, Palmer L (1928) An apparent recovery from multiple sarcoma with involvement of both bone and soft parts treated by toxin of erysipelas and bacillus prodigiosus. Am J Surg 43:188–197
52. Coley-Nauts HC, Fowler GAA, Bogatko FH (1953) A review of the influence of bacterial infection and of bacterial products (Coley's toxins) on malignant tumors in man. Acta Med Scand 145:5–102
53. Hobohm U, Stanford JL, Grange JM (2008) Pathogen-associated molecular pattern in cancer immunotherapy. Crit Rev Immunol 28:95–107
54. Hobohm U (2009) Toward general prophylactic cancer vaccination. BioEssays 31:1071–1079. doi:10.1002/bies.200900025
55. Molassiotis A, Fernadez-Ortega P, Pud D et al (2005) Use of complementary and alternative medicine in cancer patients: a European survey. Ann Oncol 16:655–663. doi:10.1093/annonc/mdi110
56. Kirsch A, Hajto T (2011) Case reports of sarcoma patients with optimized lectin-oriented mistletoe extract therapy. J Altern Complement Med 17:973–979. doi:10.1089/acm.2010.0596
57. Ostermann T, Bussing A (2012) Retrolective studies on the survival of cancer patients treated with mistletoe extracts: a meta-analysis. Explore (NY) 8:277–281. doi:10.1016/j.explore.2012.06.005
58. Bussing A, Raak C, Ostermann T (2012) Quality of life and related dimensions in cancer patients treated with mistletoe extract (iscador): a meta-analysis. Evid Based Complement Alternat Med. 2012:219402. doi:10.1155/2012/219402
59. Kienle GS, Kiene H (2010) Review article: influence of *Viscum album* L. (European mistletoe) extracts on quality of life in cancer patients: a systematic review of controlled clinical studies. Integr Cancer Ther 9:142–157. doi:10.1177/1534735410369673
60. Orange M, Fonseca M, Lace A, Laue HB, Geider S (2010) Durable tumour responses following primary high dose induction with mistletoe extracts: two case reports. Eur J Integr Med 2:63–69
61. Orange M, Lace A, Fonseca MP, Laue BH, Geider S, Kienle GS (2012) Durable regression of primary cutaneous B-cell lymphoma following fever-inducing mistletoe treatment: two case reports. Global Adv Health Med 1:18–25
62. Lee CH, Kim JK, Kim HY, Park SM, Lee SM (2009) Immunomodulating effects of Korean mistletoe lectin in vitro and in vivo. Int Immunopharmacol 9:1555–1561. doi:10.1016/j.intimp.2009.09.011
63. Huber R, Ludtke H, Wieber J, Beckmann C (2011) Safety and effects of two mistletoe preparations on production of Interleukin-6 and other immune parameters: a placebo controlled clinical trial in healthy subjects. BMC Complement Altern Med 11:116. doi:10.1186/1472-6882-11-116
64. Thies A, Dautel P, Meyer A, Pfuller U, Schumacher U (2008) Low-dose mistletoe lectin-I reduces melanoma growth and spread in a scid mouse xenograft model. Br J Cancer 98:106–112. doi:10.1038/sj.bjc.6604106
65. Ma YH, Cheng WZ, Gong F, Ma AL, Yu QW, Zhang JY, Hu CY, Chen XH, Zhang DQ (2008) Active Chinese mistletoe lectin-55 enhances colon cancer surveillance through regulating innate and adaptive immune responses. World J Gastroenterol 14:5274–5281
66. Park HJ, Hong JH, Kwon HJ, Kim Y, Lee KH, Kim JB, Song SK (2010) TLR4-mediated activation of mouse macrophages by Korean mistletoe lectin-C (KML-C). Biochem Biophys Res Commun 396:721–725. doi:10.1016/j.bbrc.2010.04.169
67. Abagyan RA, Batalov S (1997) Do aligned sequences share the same fold? J Mol Biol 273:355–368
68. Peri F, Piazza M (2012) Therapeutic targeting of innate immunity with Toll-like receptor 4 (TLR4) antagonists. Biotechnol Adv 30:251–260. doi:10.1016/j.biotechadv.2011.05.014
69. Biswas SK, Lopez-Collazo E (2009) Endotoxin tolerance: new mechanisms, molecules and clinical significance. Trends Immunol 30:475–487. doi:10.1016/j.it.2009.07.009
70. Benwell RK, Lee DR (2010) Essential and synergistic roles of IL1 and IL6 in human Th17 differentiation directed by TLR ligand-activated dendritic cells. Clin Immunol 134:178–187. doi:10.1016/j.clim.2009.09.013
71. Muthing J, Meisen I, Kniep B et al (2005) Tumor-associated CD75s gangliosides and CD75s-bearing glycoproteins with Neu5Acalpha2-6Galbeta1-4GlcNAc-residues are receptors for the anticancer drug rViscumin. FASEB J 19:103–105. doi:10.1096/fj.04-2494fje
72. Branden C, Tooze J (1999) Introduction to protein structure. Garland Science, New York
73. Greene LH, Lewis TE, Addou S et al (2007) The CATH domain structure database: new protocols and classification levels give a more comprehensive resource for exploring evolution. Nucleic Acids Res 35:D291–D297. doi:10.1093/nar/gkl959
74. Hobohm U (2005) Fever therapy revisited. Br J Cancer 92:421–425. doi:10.1038/sj.bjc.6602386
75. Gabrilovich DI, Nagaraj S (2009) Myeloid-derived suppressor cells as regulators of the immune system. Nat Rev Immunol 9:162–174. doi:10.1038/nri2506
76. Pawelek JM, Low KB, Bermudes D (2003) Bacteria as tumour-targeting vectors. Lancet Oncol 4:548–556
77. Gandhi NM, Morales A, Lamm DL (2013) Bacillus Calmette–Guerin immunotherapy for genitourinary cancer. BJU Int. doi:10.1111/j.1464-410X.2012.11754.x
78. Kimura NT, Taniguchi S, Aoki K, Baba T (1980) Selective localization and growth of *Bifidobacterium bifidum* in mouse tumors following intravenous administration. Cancer Res 40:2061–2068
79. Zhao M, Yang M, Li XM, Jiang P, Baranov E, Li S, Xu M, Penman S, Hoffman RM (2005) Tumor-targeting bacterial therapy with amino acid auxotrophs of GFP-expressing *Salmonella typhimurium*. Proc Natl Acad Sci USA 102:755–760. doi:10.1073/pnas.0408422102
80. Zhao M, Yang M, Ma H, Li X, Tan X, Li S, Yang Z, Hoffman RM (2006) Targeted therapy with a *Salmonella typhimurium* leucine-arginine auxotroph cures orthotopic human breast tumors in nude mice. Cancer Res 66:7647–7652. doi:10.1158/0008-5472.CAN-06-0716
81. Hayashi K, Zhao M, Yamauchi K, Yamamoto N, Tsuchiya H, Tomita K, Hoffman RM (2009) Cancer metastasis directly eradicated by targeted therapy with a modified *Salmonella typhimurium*. J Cell Biochem 106:992–998. doi:10.1002/jcb.22078
82. Kimura H, Zhang L, Zhao M, Hayashi K, Tsuchiya H, Tomita K, Bouvet M, Wessels J, Hoffman RM (2010) Targeted therapy of spinal cord glioma with a genetically modified *Salmonella typhimurium*. Cell Prolif 43:41–48. doi:10.1111/j.1365-2184.2009.00652.x
83. Liu F, Zhang L, Hoffman RM, Zhao M (2010) Vessel destruction by tumor-targeting *Salmonella typhimurium* A1-R is enhanced by high tumor vascularity. Cell Cycle 9:4518–4524
84. Momiyama M, Zhao M, Kimura H, Tran B, Chishima T, Bouvet M, Endo I, Hoffman RM (2012) Inhibition and eradication of human glioma with tumor-targeting *Salmonella typhimurium* in an orthotopic nude-mouse model. Cell Cycle 11:628–632. doi:10.4161/cc.11.3.19116
85. Agrawal N, Bettegowda C, Cheong I et al (2004) Bacteriolytic therapy can generate a potent immune response against experimental tumors. Proc Natl Acad Sci USA 101:15172–15177. doi:10.1073/pnas.0406242101
86. Kanzler H, Barrat FJ, Hessel EM, Coffman RL (2007) Therapeutic targeting of innate immunity with Toll-like receptor agonists and antagonists. Nat Med 13:552–559. doi:10.1038/nm1589

87. Krishnan J, Lee G, Choi S (2009) Drugs targeting Toll-like receptors. Arch Pharm Res 32:1485–1502. doi:10.1007/s12272-009-2100-6
88. Goutagny N, Estornes Y, Hasan U, Lebecque S, Caux C (2012) Targeting pattern recognition receptors in cancer immunotherapy. Target Oncol 7:29–54. doi:10.1007/s11523-012-0213-1
89. Zoglmeier C, Bauer H, Norenberg D et al (2011) CpG blocks immunosuppression by myeloid-derived suppressor cells in tumor-bearing mice. Clin Cancer Res 17:1765–1775. doi:10.1158/1078-0432.CCR-10-2672

5.1.3 Anlage – Teil 3

Establishment, characterization and chemosensitivity of three mismatch repair deficient cell lines from sporadic and inherited colorectal carcinomas

OPEN ACCESS Freely available online PLOS ONE

Establishment, Characterization and Chemosensitivity of Three Mismatch Repair Deficient Cell Lines from Sporadic and Inherited Colorectal Carcinomas

Claudia Maletzki[1], Saskia Stier[1], Ulrike Gruenert[1], Michael Gock[2], Christiane Ostwald[3], Friedrich Prall[3], Michael Linnebacher[1]*

1 Division of Molecular Oncology and Immunotherapy, University of Rostock, Rostock, Germany, **2** Department of General, Thoracic, Vascular and Transplantation Surgery, University of Rostock, Rostock, Germany, **3** Institute of Pathology, University of Rostock, Rostock, Germany

Abstract

Background: Colorectal cancer (CRC) represents a morphologic and molecular heterogenic disease. This heterogeneity substantially impairs drug effectiveness and prognosis. The subtype of mismatch repair deficient (MMR-D) CRCs, accounting for about 15% of all cases, shows particular differential responses up to resistance towards currently approved cytostatic drugs. Pre-clinical *in vitro* models representing molecular features of MMR-D tumors are thus mandatory for identifying biomarkers that finally help to predict responses towards new cytostatic drugs. Here, we describe the successful establishment and characterization of three patient-derived MMR-D cell lines (HROC24, HROC87, and HROC113) along with their corresponding xenografts.

Methodology: MMR-D cell lines (HROC24, HROC87, and HROC113) were established from a total of ten clinicopathological well-defined MMR-D cases (120 CRC cases in total). Cells were comprehensively characterized by phenotype, morphology, growth kinetics, invasiveness, and molecular profile. Additionally, response to clinically relevant chemotherapeutics was examined *in vitro* and *in vivo*.

Principal Findings: Two MMR-D lines showing CIMP-H derived from sporadic CRC (HROC24: K-ras^{wt}, B-raf^{mut}, HROC87: K-ras^{wt}, B-raf^{mut}), whereas the HROC113 cell line (K-ras^{mut}, B-raf^{wt}) was HNPCC-associated. A diploid DNA-status could be verified by flow cytometry and SNP Array analysis. All cell lines were characterized as epithelial (EpCAM^{+}) tumor cells, showing surface tumor marker expression (CEACAM^{+}). MHC-class II was inducible by Interferon-γ stimulation. Growth kinetics as well as invasive potential was quite heterogeneous between individual lines. Besides, MMR-D cell lines exhibited distinct responsiveness towards chemotherapeutics, even when comparing *in vitro* and *in vivo* sensitivity.

Conclusions: These newly established and well-characterized, low-passage MMR-D cell lines provide a useful tool for future investigations on the biological characteristics of MMR-D CRCs, both of sporadic and hereditary origin. Additionally, matched patient-derived immune cells allow for comparative genetic studies.

Citation: Maletzki C, Stier S, Gruenert U, Gock M, Ostwald C, et al. (2012) Establishment, Characterization and Chemosensitivity of Three Mismatch Repair Deficient Cell Lines from Sporadic and Inherited Colorectal Carcinomas. PLoS ONE 7(12): e52485. doi:10.1371/journal.pone.0052485

Editor: Devanand Sarkar, Virginia Commonwealth University, United States of America

Received August 30, 2012; **Accepted** November 14, 2012; **Published** December 31, 2012

Copyright: © 2012 Maletzki et al. This is an open-access article distributed under the terms of the Creative Commons Attribution License, which permits unrestricted use, distribution, and reproduction in any medium, provided the original author and source are credited.

Funding: This work was substantially supported by grant number 2006/A29 from the Else-Kröner Fresenius Stiftung to ML and by grant number 108919 from the Deutsche Krebshilfe (http://www.northgermantumorbank-crc.de). The funders had no role in study design, data collection and analysis, decision to publish, or preparation of the manuscript.

Competing Interests: The authors have declared that no competing interests exist.

* E-mail: michael.linnebacher@med.uni-rostock.de

Introduction

Developing preclinical cancer models has substantially contributed to a more detailed understanding of colon carcinoma (CRC) initiation and progression [1,2]. Pivotal to these studies has been the growing appreciation of the histological and genetical heterogeneity that exists within CRC. At present, at least three major molecular mechanisms, i.e. chromosomal instability, the CpG island methylator phenotype (CIMP) as well as high-degree of microsatellite instability (MSI or MMR-D for mismatch repair deficiency), have been identified as promoters of CRC carcinogenesis [3–6].

MMR-D accounts for 15% of all CRCs [5]; with 3% being associated with hereditary non-polyposis colorectal carcinoma (HNPCC), and the remaining 12% arise sporadically. MMR-D results from functional inactivation of DNA mismatch repair (MMR) genes; to the most part MLH1 and MSH2. Irrespective of some genetic and epigenetic differences that exist between these two types, there are several features common to both sporadic and inherited MMR-D tumors. They typically possess strong lymphocytic infiltration, an enhanced tumor cell apoptosis, and a distinct response to adjuvant chemotherapy (i.e. 5-fluoruracil- (5-FU) and cisplatin-based therapies) [7]. Correct prediction of cytotoxic agents' efficacy is a crucial step to improve the outcome of patients suffering from a MMR-D CRC. To date, the mutational status of

K-ras is the most recognized predictive molecular marker in CRC. Additional novel markers have been found to be helpful in identifying patients likely to benefit from (e.g. EGFR-) targeted therapies [8]. These include B-raf^{V600E} mutations and loss of PTEN expression.

Mandatory for identifying accurate novel molecular markers and for testing innovative treatment regimen is the availability of suitable *in vitro* and *in vivo* models. Cell line establishment has been described to be successful either directly from fresh tumor tissue or from so-called xenopatients by engrafting tumor fragments in immunocompromised mice before the *in vitro* culture step. For both cases, maintenance of the original tumor's cell differentiation, morphology and molecular signature is initially warranted [9]. Although some of the resulting MMR-D CRC cell lines were biologically examined and made commercially available [10], they usually are of high passage and thus do not longer reflect the biology of the original tumor, like growth behaviour, morphology and mutational profile [11,12]. Therefore, the ongoing development of novel low-passage MMR-D CRC lines is imperative. Ideally, a complete set of cell lines, together with matched xenopatients and autologous immune cells, should be at hand for development of novel therapeutic approaches.

In this study, we describe a feasible and straightforward method for establishing new MMR-D cell lines, along with their corresponding xenopatients. Subsequent detailed analysis of tumor biology, genetic, as well as *in vitro* and *in vivo* chemosensitivity towards selected antineoplastic drugs provides a ready basis for preclinical evaluation of innovative treatment regimens. Such patient-derived cell line sets are especially ideal tools to optimize development of individualized therapeutic strategies in the near future.

Materials and Methods

Tumor Preparation, Xenografting & Cell Line Establishment

Primary CRC resection specimens were received fresh from surgery, with informed written patient consent ($n = 10$). All procedures were approved by the Ethics Committee of the Medical faculty, University of Rostock (Ethikkommission an der Medizinischen Fakultät der Universität Rostock, St.-Georg-Str. 108, 18055 Rostock, Germany; reference number II HV 43/2004) in accordance with generally accepted guidelines for the use of human material. Tumor samples were cut into small pieces. For cryopreservation and subsequent xenografting, pieces (3×3×3 mm) were frozen (FCS, 10% DMSO) at −80°C. Other pieces were stored in liquid nitrogen for molecular analysis. Cell culture was started from single cell suspensions, seeded on collagen-coated plates in Quantum tumor medium (+10% FCS, 2 mM L-glutamine, antibiotics and antimycotics) and incubated at 37°C in a humidified atmosphere of 5% $C0_2$. All cell culture reagents were obtained from PAA (Cölbe, Germany), antibiotics and antifungal agents were provided by the university hospital's pharmacy.

Medium was changed regularly. Initial passage into a 25 cm^2 culture flask was performed when tumor cell growth was observed. Continually growing cell cultures were further passaged and regularly stocked in low passages.

For *in vivo* engraftment, six-week-old female NMRI nu/nu mice were used as recipients. Mice were bred in the university's animal facility and maintained in specified pathogen-free conditions. All experimental procedures were carried out in strict accordance with the recommendations in the Guide for the Care and Use of Laboratory Animals of the National Institutes of Health. The protocol was approved by the Committee on the Ethics of Animal Experiments of the University of Rostock (Landesamt für Landwirtschaft, Lebensmittelsicherheit und Fischerei Mecklenburg-Vorpommern; Thierfelder Str. 18, 18059 Rostock, Germany; permit number: LALLF M-V/TSD/7221.3-1.1-071-10). All surgery was performed under Ketamin/Xylazin anesthesia (dose: 90/25 mg/kg bw), and all efforts were made to minimize suffering. Subcutaneous (s.c.) tumor implantation was performed as described [13]. Established xenografts (≥ 1500 mm^3) were removed and underwent *in vitro* culture protocols as described above.

Histology and Immunohistochemistry of Original Tumors

Histopathological examination of primary tumors was done according to standard protocols for clinicopathological CRC staging [14] and additional staging information was compiled from patients' clinical charts. H & E sections; β-catenin, MLH1, and MSH2 immunostainings were obtained from paraffin-embedded tumors.

Molecular Analysis

Molecular classification was done according to [3]. These data as well as staging information compiled from the clinical charts are summarized in Tables 1–3. MMR-D was examined using the Bethesda panel and additionally the mononucleotide marker Cat25 [15]. Mutational analyses of the APC, p53, K-Ras and B-Raf^{V600E} genes were done as described. Finally, DNA-methylation in CIMP-sensitive promoters was traced by the MethyLight technology with a modified marker panel originally published by [16]. Chromosomal instability (CIN) was assessed using SNP Array 6.0 from Affymetrix (Cleveland, OH) according to manufacturer's instructions.

Generation of Peripheral B Cell Cultures from Primary Tumors

B-lymphoid cell lines (B-LCLs) were generated from purified peripheral blood leukocytes by Epstein-Barr virus (EBV)-transformation as described [17]. Outgrowing B-LCL cultures were harvested, expanded, characterized, and frozen.

In vitro Growth Kinetics, Ploidy and Cell Cycle Analysis

Population doubling times were determined by viable cells seeded into replicate 25 cm^2 flasks and daily counted for seven days. Ploidy and cell cycle analysis was conducted by flow cytometry (FACSCalibur; BD Biosciences, Heidelberg, Germany) as described [18]. Human blood leukocytes were used as diploid controls.

Flow Cytometry and Cytokine Secretion Pattern of Primary Cell Lines

Cell surface marker expression on established tumor cell lines was traced by flow cytometry with and without IFN-γ pretreatment using a panel of Abs (for details please see Table 4). Samples were analysed using CellQuest software (BD Biosciences). Cytokine release was determined from cell free supernatants, harvested at different time points and quantified by ELISA according to the manufacturer's instructions.

Matrigel Invasion Assay

Tumor cells invasiveness was examined using a matrigel-based assay according to [19] with minor modifications. Cells on the lower surface were quantified after 72 hours of incubation by MTT assay (Promega, Mannheim, Germany) and absorbance

Table 1. Clinical and pathological characteristics of patients as well as cell line establishment protocol.

Tumor-ID	Age/ Gender	Tumor location	TNM-Stage	Tumor type	Molecular type	β-Catenin translocation	MLH1 IHC	Corresponding xenograft	Direct cell line establishment	Cell line from xenograft	Paired B-LCL
HROC24	98/m	colon ascendens	G2T2N0M0	primary adenocarcinoma	spMMR-D	negative	−	+	+	+	yes
HROC29	59/m	colon ascendens	G3T3N2M1	primary adenocarcinoma	HNPCC	negative	−	+	−	−	yes
HROC48	68/m	colon transversum	G3T2N1M0	primary adenocarcinoma	spMMR-D	negative	−	+	−	−	n.d.
HROC50	67/f	colon ascendens	G2T4N0M0	primary adenocarcinoma	spMMR-D	negative	−	+	−	+/−	yes
HROC53	72/f	colon ascendens	G3T3N0M0	primary adenocarcinoma	spMMR-D	positive	−	+	−	−	yes
HROC71	52/m	caecum	G2T3N0M0	primary adenocarcinoma	HNPCC	positive	−	+	−	+/−	yes
HROC87	76/f	colon ascendens	G3T3N0M0	primary adenocarcinoma	spMMR-D	negative	−	+	−	+	yes
HROC108	81/f	colon ascendens	G3T3N0M0	primary adenocarcinoma	spMMR-D	positive	−	+	−	−	n.d.
HROC109	75/m	colon transversum	G3T4N2M0	primary adenocarcinoma	spMMR-D	negative	−	+	−	−	n.d.
HROC113	41/f	colon ascendens	G3T4N2Mx	primary adenocarcinoma	HNPCC	negative	−	+	+	−	yes

m – male, f – female, spMMR-D – sporadic mismatch repair deficient, HNPCC – hereditary non-polyposis colorectal carcinoma, B-LCL – B lymphoid cell line,+– positive, − – negative; IHC – immunohistochemistry; n.d. – not done.
doi:10.1371/journal.pone.0052485.t001

Table 2. Molecular characterization of MMR-D CRC cell lines.

Cell line (HROC.)	Mutation								MMR-D status					
	p53				APC	K-Ras		B-Raf	BAT25	BAT26	CAT26	D5S346	D17S250	D2S123
	ex 5	ex 6	ex 7	ex 8	ex 15	cd 12	cd13	V600E						
24P	wt	wt	wt	wt	mut	wt	wt	mut	−5	−5	−8	+18	−6/wt	−6/−4
87X	wt	mut	mut	wt	wt	wt	wt	mut	−6	−10/−6	−12	−2/+4	+2/wt	0
113P	wt	wt	wt	wt	wt	mut	wt	wt	0	−8	−8/−5	0	−6/wt	0

wt – wildtype, mut – mutated, ex – exon, cd – codon.

doi:10.1371/journal.pone.0052485.t002

measurement at 490 nm (reference 620 nm). Data are expressed as percentage invasion versus the highly invasive CRC line HCT116 (unpublished own observation) set to 100%.

Mycoplasma and Viral Infection

Mycoplasma contamination was tested by the 16S-rRNA-gene-based polymerase chain reaction (PCR) amplification method from cell lysates. Amplification was carried out in a total volume of 25 µl (2 mM $MgCl_2$, 0.5 mM each primer (Metabion, Martinsried, Germany). Primers were: forward: 5′-GGC GAA TGG GTG AGT AAC ACG-3′; reverse: 5′-CGG ATA ACG CTT GCG ACC TAT G-3′ yielding an approximately 500 bp product (conditions: 94°C, 5 min, 94°C, 1 min; 60°C, 1 min; 72°C, 90 s; 40 cycles). Potential polyomavirus infection was tested from gDNA according to [20]. PCR for detecting HBV, HCV, or HIV in tumor cells was kindly performed by the Institute of Medical Microbiology, Virology and Hygiene (University of Rostock).

In vitro and *in vivo* Chemosensitivity

Cells were seeded into 96-well microtiter plates (5×10^3 or 1×10^4 cells/well). Two days after plating, triplicate wells were treated with increasing drug concentrations (pharmacy of the university hospital Rostock). This procedure was repeated after three days of treatment (= two cycles). Cellular metabolic activity in treated versus control wells was estimated by MTT assay as described above. Drug effects were determined at the level of 50% inhibition (IC_{50}) compared to controls.

Thereafter, response to selected therapeutics was tested *in vivo*. 5×10^6 cells were injected s. c. into nude mice. Additionally, tumor fragments of HNPCC-derived xenografts (HROC29, HROC71) were implanted s.c. into nude mice under anaesthesia (Ketamin/Xylazin 90/25 mg/kg bw) and allowed to grow until tumor establishment. Mice with established tumors received therapeutic applications of selected drugs (i.p.; 20 mg/kg bw each, n = 6–7 mice per group, twice weekly, six times in total). Tumor-carrying mice receiving PBS (n = 7 per group) served as controls. Tumor growth was controlled regularly and volume was estimated according to the formula: $V = \text{width}^2 * \text{length} * 0.52$. All mice (treatment, control) were sacrificed at day 21 or when they became moribund before the tumor volume reached 2000 mm^3. Tumors were removed for further histological examinations.

Statistics

Values are reported as the mean ± SD for *in vitro* data and

Table 3. DNA-methylation profile of MMR-D CRC cell lines.

Cell line	DNA-methylation					
	MLH1	CDKN2A	NEUROG1	CRABP1	CACNA1G	MGMT
HROC24P	+	+	+	+	+	+
HROC87X	+	+	+	+	+	−
HROC113P	−	−	−	−	−	+

+ – methylated; − – not methylated.

doi:10.1371/journal.pone.0052485.t003

Table 4. Flow cytometric phenotyping of primary MMR-D CRC cell lines & MHC expression with and without IFN-γ pre-treatment (% positive cells).

Antigen		HROC24P	HROC87X	HROC113P
CD11b		0.0	0.0	0.0
CD15		80.8	53.2	40.7
CD20		0.0	0.0	0.0
CD24		0.0	0.0	0.0
CD28		0.0	0.0	0.0
CD34		0.0	0.0	0.0
CD43		0.0	0.0	0.0
CD44		60.4	49.1	42.9
CD45		0.0	0.0	0.0
CD45ra		0.0	0.0	0.0
CD45rb		7.8	8.3	5.8
CD45ro		0.0	0.0	0.0
CD50		0.0	0.0	0.0
CD55		11.5	15.6	21.2
CD56		0.0	0.0	0.0
CD58		79.8	11.3	10.8
CD62L		0.0	0.0	0.0
CEACAM		53.9	12.7	63.4
CD71		77.1	67.9	75.0
CD80		11.2	56.9	75.3
EpCAM		99.5	98.9	99.3
HLA A2		0.0	0.0	89.2
MHC I	**− IFN-γ**	0.0	1.0	6.8
	+ IFN-γ	0.0	1.0	93.8
MHC II	**− IFN-γ**	0.0	0.0	0.0
	+ IFN-γ	94.2	73.3	95.0

Data are given from one representative experiment out of four replicates.

doi:10.1371/journal.pone.0052485.t004

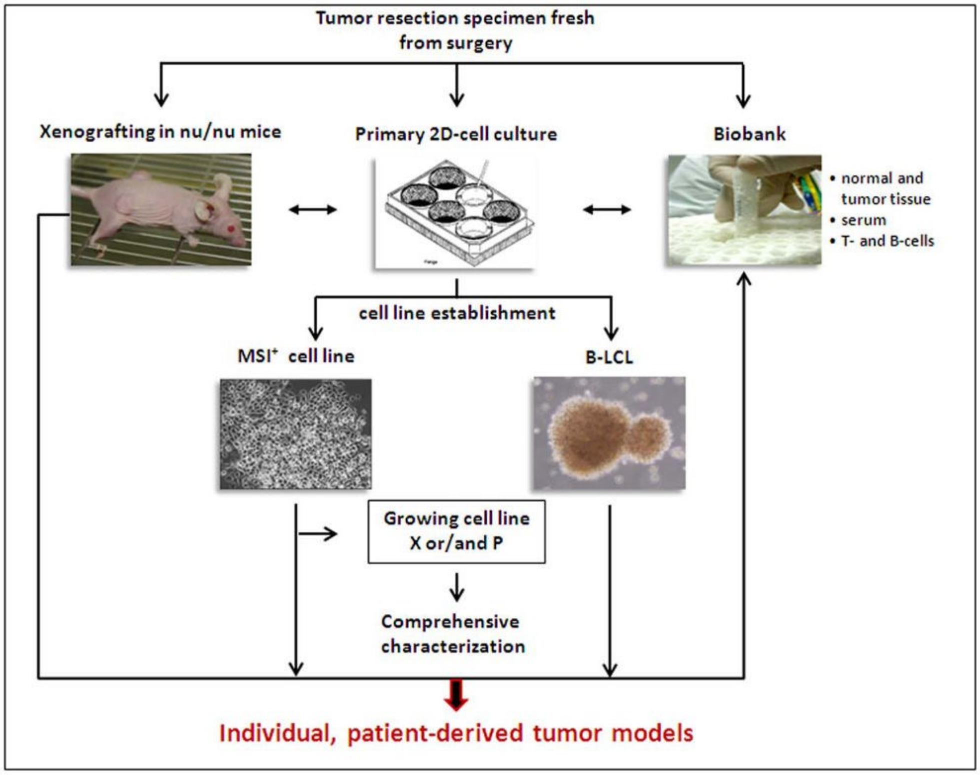
Tumor resection specimen fresh from surgery
Xenografting in nu/nu mice
Primary 2D-cell culture
Biobank
• normal and tumor tissue
• serum
• T- and B-cells
cell line establishment
MSI⁺ cell line
B-LCL
Growing cell line X or/and P
Comprehensive characterization
Individual, patient-derived tumor models

Figure 1. Scheme of the experimental protocol for cell line establishment either fresh from surgery specimens (=patient-derived cell line) of following xenografting in nu/nu mice (=xenopatient-derived cell line). Established cell lines were comprehensively characterized and routinely cyropreserved together with xenograft-tissue, immune cells, serum, and normal as well as primary tumor tissue in a biobank. This procedure leads to generation of individualized, patient-derived tumor models available for functional analyses.
doi:10.1371/journal.pone.0052485.g001

mean ± SEM for *in vivo* data. Statistics were done on *in vivo* experiments. After proving the assumption of normality, differences between saline and treated animals were determined by using the unpaired Student's *t*-test. If normality failed, the nonparametric Mann–Whitney *U*-Test was applied. The tests were performed by using Sigma-Stat 3.0 (Jandel Corp, San Rafael, CA). The criterion for significance was set to $p<0.05$.

Results

Clinicopathological Patients' Characteristics

In this study, ten cases of clinicopathological well-defined MMR-D tumors were collected from a series of 120 CRC cases. Samples were obtained from resection specimens without prior therapy. Clinicopathological patient's characteristics are summarized in Table 1. Seven samples were classified as sporadic MMR-D tumors and three cases as HNPCC. Except for the two of the latter cases (HROC29, HROC113), no distant metastases were present in any of the MMR-D tumor patients.

Cell Line Establishment

To increase the success rate of tumor cell line establishment, *in vitro* and *in vivo* approaches were combined: parts of surgical tumor specimens were either directly processed for *in vitro* cell line establishment or frozen native for subsequent xenopatient generation (Figure 1) [21].

With this method, direct cell line establishment was successful for 2/8 cases. The cell line HROC24P (P = direct cell line establishment from patient) originated from a sporadic CRC patient and HROC113P was derived from a HNPCC patient with a germline MLH1 mutation.

In a parallel series of experiments, xenografting was performed on 8/10 tumors by subcutaneous implantation into immunocompromised recipients. Preservation of morphology was confirmed by comparing histology of xenografts with the original tumor (Figure 2).

Tumor growth was obtained in 62% and thus to a significantly higher efficiency than the direct *in vitro* approach (Table 1). However, subsequent cell line establishment was so far only successful in two cases, namely HROC24X and HROC87X

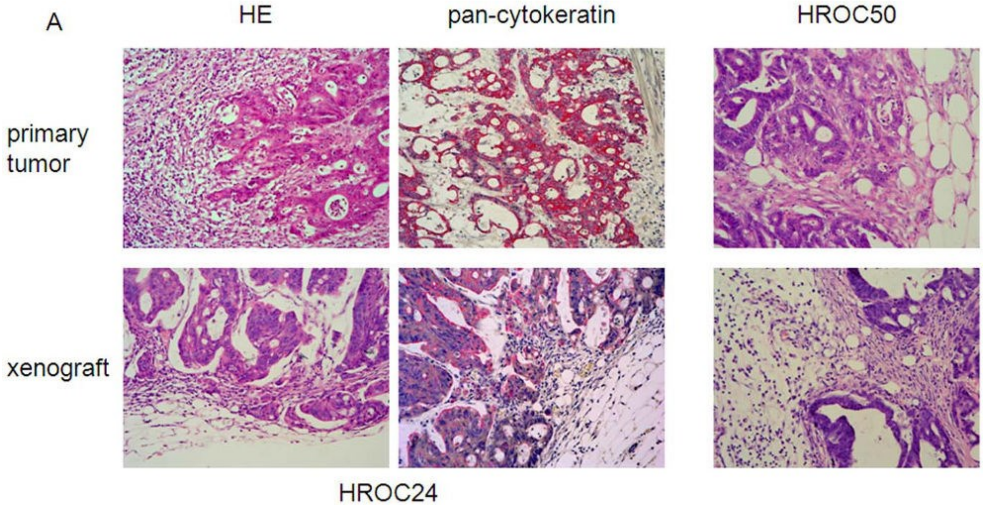

Figure 2. Morphology of primary MMR-D tumors and their corresponding xenografts. HE-histology representing maintenance of HROC24 tumor morphology following xenografting. The pan-cytokeratin staining is strongly positive, consistent with the tumors' epithelial origin (left upper and lower panel). HE-histology of HROC50 tumors (right upper and lower panel).
doi:10.1371/journal.pone.0052485.g002

(X = xenopatient-derived). For these two lines, continuous *in vitro* growth was observed immediately after starting cultures.

Finally, detailed characterization was performed on the patient-derived cell lines, HROC24P and HROC113P, as well as the xenopatient-derived line HROC87X. As determined by PCR, all MMR-D lines were found free of contaminating mycoplasma or human pathogenic viruses (SV40, JC/BK, HBV, HCV, and HIV; data not shown).

Molecular Characterization

Comprehensive molecular classification on freshly established MMR-D cell lines was paralleled by examinations on original tumor material as well as on corresponding xenografts (HROC24 and HROC87). This analysis revealed no difference in any of the samples and hence data presented in Table 2 and 3 refer to the cell lines only.

The MMR-D status was evidenced by using the advanced Bethesda panel. All three cell lines exhibited instability in the six markers analyzed. Mutations in tumor-associated genes varied among cell lines. HROC24P and HROC87X displayed high-degree of CIMP (methylation in 6/6 markers), including MLH1 promoter methylation. The HROC113P cell line showed characteristic molecular features associated with the HNPCC syndrome like mutations in codon 12 of the K-ras gene, but wildtype B-raf. Moreover, methylation –except for MGMT– was absent. MMR-D tumors are by definition devoid of or have very low levels of CIN [3]. However, for this detailed characterization, we performed a genomic analysis with very high resolution taking advantage of the SNP Array 6.0. Even in this analysis, very low if any instability on the chromosomal level could be detected with the exception of HROC87X cells, which had an amplification of 13q and 15q (Figure 3A). HROC24P and HROC113P were close to normal (Figure 3B, C).

Cell Morphology & Phenotyping

Determining morphology revealed tight adherence to the bottom of the cell culture flasks. All cell lines were characterized as epithelial-like cells without contaminating fibroblasts. Initially, HROC24P cells proliferated as tightly packed multi-cellular islands (Figure 4 upper panel). Following serial passages, they changed their morphology and appeared as rather undifferentiated small, polygonal and round cells not strictly growing in monolayer (Figure 4 upper panel). Morphology at later passages was identical to HROC24X, which had been generated from a xenopatient (Figure 4, upper panel). HROC87X cells displayed comparable growth behaviour, forming small floating aggregates or grape-like cell clusters (Figure 4 lower panel) with no change in phenotype during long-term culture (≥40 passages).

HROC113P cells strictly grew as monolayers. In the initial cell culture (<4 passages), two different cellular clones were observed. After serial passages, numbers of large cells gradually decreased and were entirely replaced by the dominant smaller cell clone (Figure 4 lower panel). Unlike the other cell lines, they did not grow to complete confluence.

The epithelial phenotype was confirmed by positive immunoreactivity for the epithelial cell adhesion molecule (EpCAM; each >98%; Table 4) as well as expression of the tumor marker CEACAM (Table 3). Further characterisation revealed comparable expression levels for the cellular adhesion and migration marker CD44 and the transferrin receptor CD71, whereas heterogeneous expression of adhesion markers was observed (CD15, CD58). High MHC class I expression was only observed in HROC113P cells, which were additionally found to be HLA-A2 positive (Table 4). MHC class II expression was absent on all cells, but could –to varying degrees– be induced by IFN-γ pretreatment (Table 4).

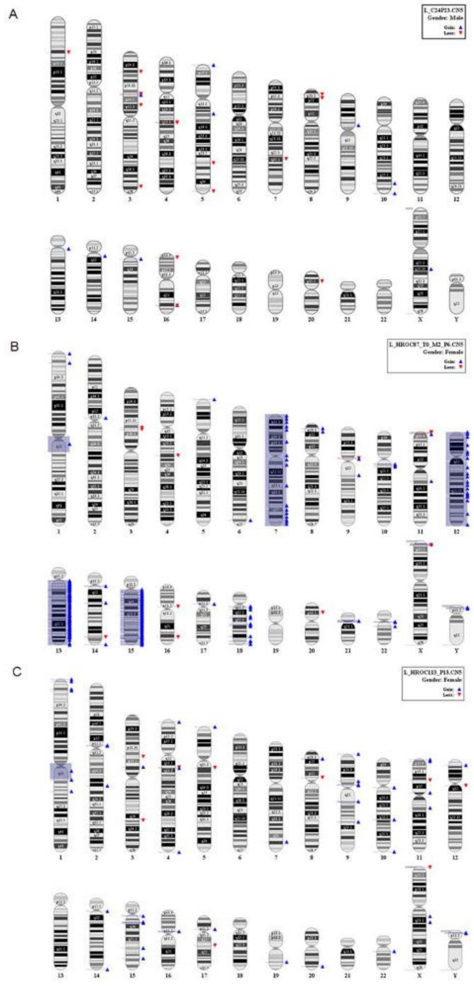

Figure 3. SNP Array 6.0 for assessment of CIN in MMR-D cell lines. Analysis was performed according to manufacturer's instructions. (A) HROC24P cells, (B) HROC87X cells, and (C) HROC113P cells.
doi:10.1371/journal.pone.0052485.g003

Growth Kinetics, Ploidy & Cellular Invasiveness

To get an idea on the *in vivo* growth behavior of the original tumor, we examined growth kinetic and invasive potential of the cell lines.

As anticipated, growth kinetics were quite different between cells, with HROC24P growing more rapidly than HROC87X and HROC113P cells (33 vs. 50 and 41 hours; Figure 5A). In subsequent cell cycle analysis, no statistical differences between the three cell lines were found in terms of cell numbers in the G0/G1, S, and G2/M phases. In line with the SNP Array 6.0 data, a diploid DNA-status could be verified, too (Figure 5B).

Apart from these findings, we observed considerable differences with regard to the invasive potential (Figure 5C). Highest invasiveness was found for HROC87X cells, which was above the control cell line HCT116. Contrary, the cell lines HROC24P and HROC113P were markedly less invasive.

Cytokine Secretion Pattern of MMR-D Tumor Cell Lines

Examining Th1 and Th2 cytokine secretion for several days revealed a comparable pattern between cell lines (data not shown). Highest levels were observed for the neutrophil-attracting chemokine IL8. Values of the Th2 cytokine IL4 were identical between all three lines, ranging from 110 to 230 pg/ml (HROC24P vs. HROC113P cells, 4d culture). A similar pattern was seen for IL10. IL6 production was quite low in the MMR-D lines and none of them secreted detectable levels of the immunostimulatory IFN-γ.

In vitro Drug Response

As a first step towards establishing test systems that may predict MMR-D chemosensitivity, an *in vitro* system was used. Exponentially growing cells were treated for a total of six days. In order to mimic the *in vivo* situation, cells received two chemotherapeutic cycles and IC_{50} levels were calculated (Table 5).

These experiments revealed heterogeneous drug responses. In detail, the two sporadic MMR-D cell lines (HROC24P, HROC87X) were sensitive towards irinotecan-mediated growth inhibition; with doses comparable to or even lower than plasma concentrations in patients (Table 5). Interestingly, HROC113P cells did not response to this compound. Comparable results were obtained for 5-FU, with HROC24P being the most sensitive cell line. Again, HROC113P cells showed relative resistance towards 5-FU. All cell lines were susceptible to cisplatin-induced growth arrest.

Thereafter, sensitivity towards several additional cytostatic drugs was tested. The microtubule-stabilizing compound paclitaxel showed effectiveness comparable to the standard drugs. Again, highest efficacy was observed against HROC24P and HROC87X cells, while it was less potent towards HROC113P cells. A somewhat unexpected finding was the high responsiveness towards gemcitabine. All three cell lines showed substantial response, even at very low doses. Inhibition of cell proliferation was achieved at concentrations well below plasma levels under standard therapy.

In summary, *in vitro* chemosensitivity patterns to cytotoxic drugs were very individual with the HNPCC-derived HROC113 tending to be more resistant than their sporadic counterparts.

In vivo Tumorigeneicity & Drug Response

All three cell lines engrafted well and gave rise to growth *in vivo*. Similar to the *in vitro* growth behavior, HROC24P tumors displayed fastest growth, HROC87X tumors grew slowest and HROC113P tumors showed an intermediate growth rate. No distant metastases were detected neither at necropsy, nor following histologic examination of the inner organs (data not shown).

Subsequently, the effectiveness of chemotherapeutics was studied *in vivo* (Figure 6). The topoisomerase-1 inhibitor irinotecan mediated substantial tumor growth control. Unexpected from the *in vitro* results, most pronounced effects were obtained for HROC113P with more than 90% growth inhibition compared to untreated mice. Tumors immediately stopped growing after the first therapy cycle. This was evident until the end of experiments at day 21 (Figure 6C). HROC24P and HROC87X tumors showed a weaker, though still significant response to irinotecan. Tumors

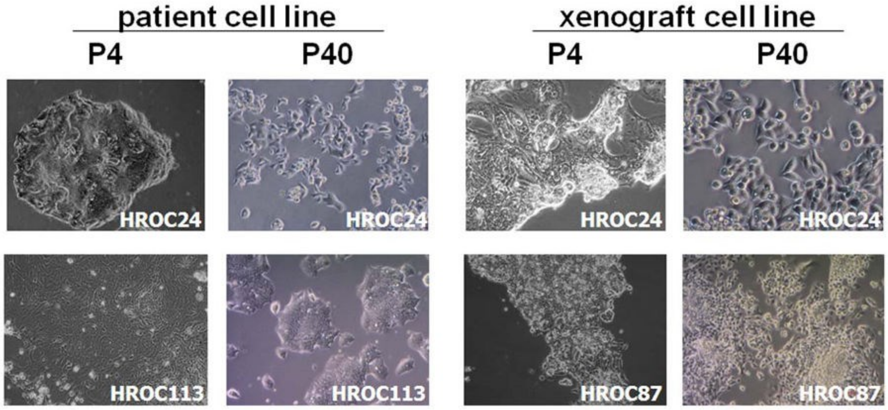

Figure 4. Light microscopy of MMR-D CRC cell lines both directly after establishment (P4) and following long-term *in vitro* culture (P40). (A) Morphology of patient-derived cell lines HROC24P and HROC113P. (B) Morphology of HROC24X and HROC87X. Both cell lines were established from xenopatients as described in material & methods. Original magnification x100.
doi:10.1371/journal.pone.0052485.g004

tended to keep growing very slowly, finally resulting in sizes less than half of untreated tumors (Figure 6A, B).

Quite the opposite results were obtained for paclitaxel. Despite effective inhibition *in vitro*, this drug affected tumor growth only in the HNPCC-associated HROC113P tumors (Figure 6C) while it

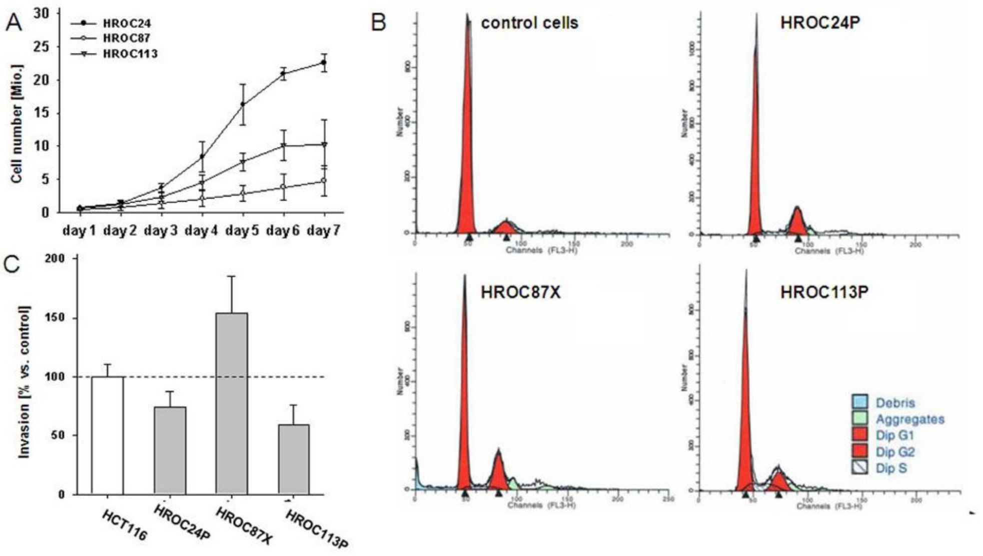

Figure 5. *In vitro* growth kinetic, ploidy analysis & invasiveness of MMR-D tumor cells. (A) Growth curve of HROC24P, HROC87X and HROC113P cells in culture. The results shown are the mean population doubling times ± standard deviation. Results were calculated from three independent assays each performed in duplicates. (B) Exemplary DNA histograms of MMR-D tumor cells compared to normal cells (PBMC). All cells were classified as diploid. (C) Tumor invasiveness was analysed using a matrigel-based assay. Quantification of cellular invasiveness was estimated by MTT assay. Data are expressed as percentage invasion versus HCT116 cells (= internal positive control). All experiments were repeated at least three times.
doi:10.1371/journal.pone.0052485.g005

Table 5. IC$_{50}$ values of antitumor drugs evaluated for MMR-D cell lines.

Cell line	**IC$_{50}$ value**				
	irinotecan [μM]	**cisplatin [μg/ml]**	**5-FU [μg/ml]**	**paclitaxel [μM]**	**gemcitabine [μg/ml]**
HROC24P	2.2	2.0	0.2	<0.01	0.00015
HROC87X	0.9	1.7	0.8	<0.01	0.002
HROC113P	12.8	1.3	1.0	2.8	0.00018
plasma levels (pharmacokinetic)	10.0	2.0	20.0	50.0–70.0	6.0

Values are given as mean, resulting from at least three independent experiments each performed in triplicates.

doi:10.1371/journal.pone.0052485.t005

had no or only marginal effect on HROC87X and HROC24P tumor growth, respectively (Figure 6A, B).

Due to the high sensitivity of all MMR-D cell lines towards gemcitabine *in vitro*, this drug was consequently applied therapeutically *in vivo*. Most prominent antitumoral effects were observed for HROC113P-tumors, finally leading to complete remission of 4/7 tumors (Figure 6C). HROC24P-tumor growth was also effectively controlled (Figure 6A). HROC87X-tumors behaved completely different (Figure 6B). Here, the tumor growth rate was slightly enhanced by gemcitabine. These results let us hypothesize that HNPCC tumors might probably better respond to this regimen. Consequently, we included two further HNPCC-associated cases, i.e. HROC29 and HROC71. Gemcitabine effectively controlled HROC71 xenograft growth, but failed to affect HROC29 tumors (Figure 6D, E).

Discussion

Advancement in molecular understanding of CRC biology has emerged important for preclinical and early clinical studies. With regard to MMR-D tumors, differential response up to chemoresistance was observed, yet these findings have so far not ended in personalized treatment regimen [22]. This is, at least in part, attributable to the paucity of well-characterized preclinical models. Establishing novel low-passage MMR-D CRC lines and xenopatients, which provide a virtually unlimited source of tumor material [23,24,25], may thus help to improve preclinical optimization of personalized therapy.

In this study, we picked up the idea of establishing and characterizing patient-derived individual MMR-D tumor models for testing treatment modalities. Firstly, to ameliorate the success rate for CRC cell line establishment, an experimental strategy – based on the combination of *in vitro* and *in vivo* approaches– was elaborated. From ten MMR-D tumors included in this study, cell line establishment was successful in three cases: Two cell lines (HROC24 and HROC113) were directly established from surgical resection specimens, whereas one cell line (HROC87) was obtained subsequent to xenografting. In addition, a paired xenograft cell line from the HROC24 tumor was obtained, too. By combining xenografting and direct *in vitro* cell culture, even more individual patient-derived cell lines, reflecting the original tumors' molecular signature, will probably become available in the future. Moreover, preselection based on criteria like node infiltration, advanced stage, and elevated CEA in serum may increase the rate of successful tumor engraftment rate into immunocompromised mice [25].

The three newly established MMR-D cell lines exhibited variations in terms of morphology and growth kinetic. Confirming their origin, they were recognized as epithelial tumor cells (EpCAM$^+$, CEACAM$^+$) with heterogeneous adhesion (CD15, CD44, CD58) and co-stimulatory marker (CD80) expression as well as different cytokine secretion patterns. MHC class I was only expressed by HROC113 cells. Whereas MHC-class II expression was normally absent but inducible by Interferon-γ stimulation. These findings are of interest for development of immune-based therapeutic concepts. Of note, paired immune cells, i.e. antigen-presenting B-LCL and (effector) T cells, offer the chance to work in complete autologous settings. For the MMR-D models described here, limited amounts of immune cells are available to us.

Comparing molecular profiles of MMR-D cell lines with original tumor material as well as matched xenopatients revealed virtually no differences. Somehow unexpected, tumor-associated mutations, MMR-D-status, DNA-methylation in CIMP-specific promoters and LOH profiles remained identical between these samples. It is noteworthy that cells were exclusively studied at early *in vitro* passages (<50), thereby reflecting the original tumors' biology and not a genotypic and phenotypic heterogeneity that could arise following long-term culture [26]. The molecular signatures found in the MMR-D cell lines corresponded well with the pathways of carcinogenesis ascribed to them. These include B-raf^{V600E} mutations and high-degree promoter methylations in CpG islands of sporadic tumors (HROC24P, HROC87X); and a K-ras mutation but CIMP^{neg} in the HNPCC-associated HROC113P. Which molecular markers predict patients' clinicopathological outcome best is currently a matter of debate. Bae and colleagues recently claimed that CIMP status might be crucial for MMR-D CRCs response to cytotoxic chemotherapeutics [27]. They correlated clinicopathological features with CIMP status and observed that patients with high level of methylation had worse clinical outcome than their CIMP^{neg} counterparts. Also, BRAF^{V600E} mutations, which have never been found in CIMP^{neg} tumors, seem to be another independent prognosticator of poor outcome and thus an important confounder to the prognostic role of CIMP [28,29]. These findings further endorse the importance of developing subtype-specific therapeutic strategies.

Additionally, it led us to hypothesize that even molecular closely matched cancer cell lines may respond different towards certain chemotherapeutics. Indeed, chemosensitivity varied between our cell lines.MMR-D. Of particular interest was the difference in terms of *in vitro* and *in vivo* response, especially of the HNPCC-associated HROC113P cells. MMR-DD tumors were described to be more sensitive towards microtubule-stabilizing agents than their CIN counterparts [22,29,30]. MMR-DMMR-DIn our study, paclitaxel proved effective *in vitro*, but failed *in vivo*.

Of particular interest was the sensitivity towards gemcitabine, the standard drug for treatment of pancreatic carcinoma – but not of CRC [31]. 4/7 HROC113 xenopatients were cured with this drug. Clinical studies showed controversial effects of gemcitabine either alone or in combination with other anti-neoplastic agents on

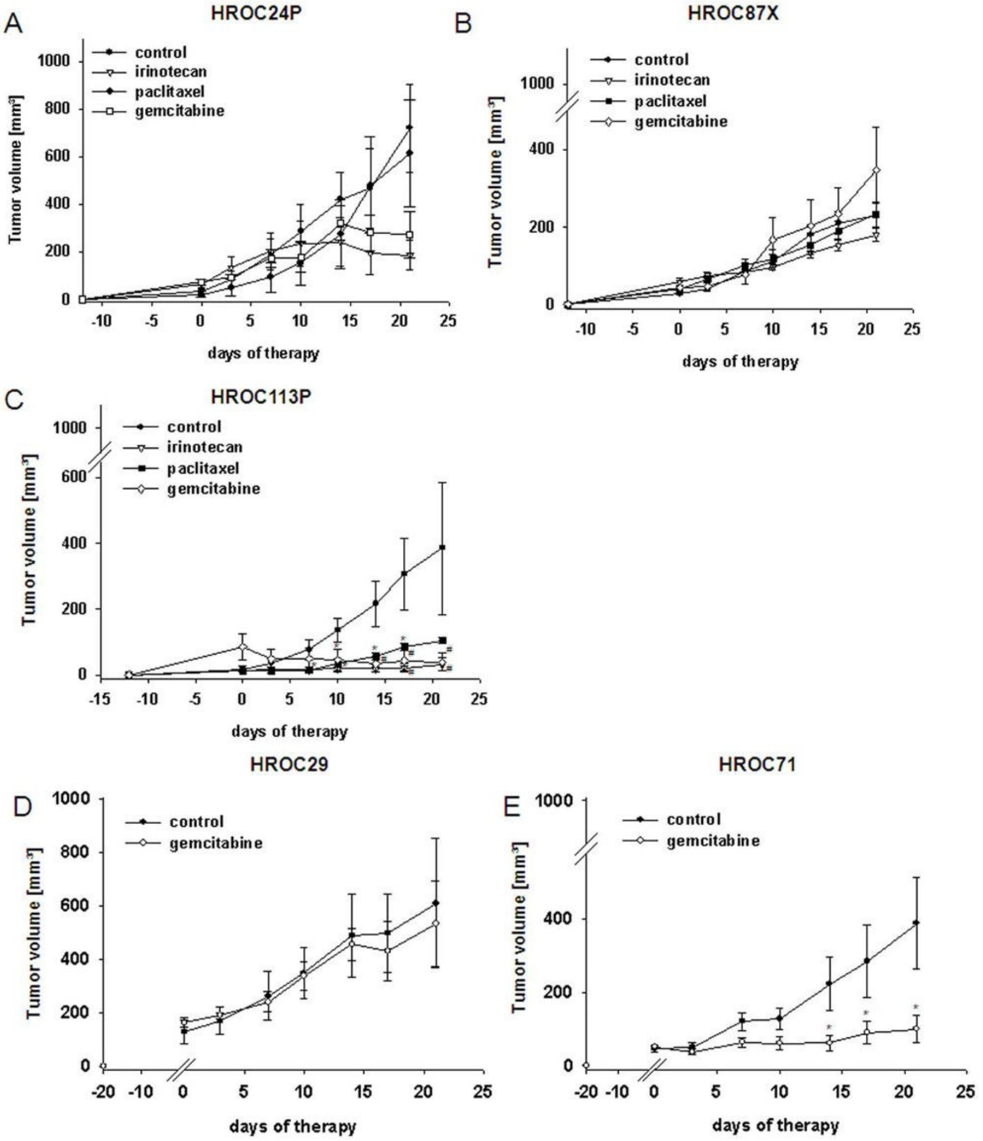

Figure 6. ***In vivo*** **tumorigeneicity & response to selected chemotherapeutics.** NMRI nu/nu mice either received s.c. injections of established MMR-D cell lines (5 Mio. cells/mouse; A–C) or were s.c grafted with HROC29 and HROC71 tumor fragments (D, E). For analyzing *in vivo* drug response, mice with established (A) HROC24, (B) HROC87 or (C) HROC113 tumors were treated with irinotecan, paclitaxel or gemcitabine (i.p.; 20 mg/kg bw each, n = 6−7 mice per group). HROC71 and HROC29 xenografts were given gemcitabine (i.p.; 20 mg/kg bw, n = 5−6 mice per group). Therapeutic regimens consisted of six injections in total, applied twice a week. Control animals received equivalent volumes of saline (n = 6−7). Values of are given as mean ± SEM. *$p<0.05$ vs. control, *U*-Test; $^{\#}p<0.05$ vs. control, *t*-test.
doi:10.1371/journal.pone.0052485.g006

CRC patients [32–34]. These observations fit well with our results. Effective growth inhibition was observed in two cases (HROC24, HROC71) and ineffectiveness in two others (HROC29, HROC87). Response to gemcitabine seems thus quite individual. This should, however, be tested on larger patient cohorts in order to get more reliable information. Additionally, experiments may be performed in nude rats, which were found to resemble humans in terms of metabolism and drug pharmacokinetic profiles more accurately than mice [25,35]. Limitations of our experimental approach may be found in the comparably long time for obtaining tumor models before testing responsiveness and/or drug resistance. Particularly when facing metastases, drugs that proved to be effective against the primary tumor often fail to affect metastatic lesions. To expand the research in the future –especially for better preclinical testing of approved and new therapies– short-term primary cultures preserving to some extent the three-dimensional tumor organization may be used instead [37].

These experiments shall be combined with systems biology-based approaches for predicting patient outcome and responsiveness to conventional and novel, targeted treatment strategies [36]. Based on mathematically predicted system models, responses can be validated *in vitro* and subsequently verified in xenopatients. This will help to identify patients likely to benefit from optimal care, while sparing those unlikely to benefit. Thus, unnecessary toxicity and costs are avoided.

Our comprehensive biobanking strategy for CRC includes the collection of primary material (frozen and paraffin-embedded tumor and normal tissue as well as lymphocytes) together with established xenografts, patient as well as xenopatient-derived cell lines and matched B-LCLs. Recently, we broadened this approach by collecting tumor samples and correlating clinical data from multiple clinical centers in the context of a third-party funded biobanking initiative (http://www.northgermantumorbank-crc.de).

This strategy may thus be ideal to address the question of whether cell lines, xenopatients or both are suited models for predicting treatment and response. If so, this strategy will pave the way towards truly personalized therapy.

Author Contributions

Conceived and designed the experiments: CM ML. Performed the experiments: CM SS UG CO FP. Analyzed the data: CM SS UG CO FP MG. Contributed reagents/materials/analysis tools: CM ML. Wrote the paper: CM FP MG ML.

References

1. Hewitt RE, McMarlin A, Kleiner D, Wersto R, Martin P, et al. (2000) Validation of a model of colon cancer progression. J Pathol 192: 446–454.
2. Voskoglou-Nomikos T, Pater JL, Seymour L (2003) Clinical predictive value of the in vitro cell line, human xenograft, and mouse allograft preclinical cancer models. Clin Cancer Res 9: 4227–4239. Review.
3. Ostwald C, Linnebacher M, Weirich V, Prall F (2009) Chromosomally and microsatellite stable colorectal carcinomas without the CpG island methylator phenotype in a molecular classification. Int J Oncol 35: 321–327.
4. Harrison S, Benziger H (2011) The molecular biology of colorectal carcinoma and its implications: a review. Surgeon 9: 200–210. Review.
5. Pritchard CC, Grady WM (2011) Colorectal cancer molecular biology moves into clinical practice. Gut 60: 116–129. Review.
6. Kang GH (2011) Four molecular subtypes of colorectal cancer and their precursor lesions. Arch Pathol Lab Med 135: 698–703.
7. Kim ST, Lee J, Park SH, Park JO, Lim HY, et al. (2010) Clinical impact of microsatellite instability in colon cancer following adjuvant FOLFOX therapy. Cancer Chemother Pharmacol 66: 659–667.
8. Bass A (2011) Impact of KRAS and BRAF gene mutations on targeted therapies in colorectal cancer. J Clin Oncol 29: 2728–2729.
9. Marangoni E, Vincent-Salomon A, Auger N, Degeorges A, Assayag F, et al. (2007) A new model of patient tumor-derived breast cancer xenografts for preclinical assays. Clin Cancer Res 13: 3989–3998.
10. Ku JL, Shin YK, Kim DW, Kim KH, Choi JS, et al. (2010) Establishment and characterization of 13 human colorectal carcinoma cell lines: mutations of genes and expressions of drug-sensitivity genes and cancer stem cell markers. Carcinogenesis 31: 1003–1009.
11. Danes BS, Deangelis P, Traganos F, Melamed MR, Alm T (1988) Demonstration of altered cellular DNA content distribution in long-term colon epithelial cell lines with colon cancer genotypes. Scand J Gastroenterol 23: 840–846.
12. Bocsi J, Zalatnai A (1999) Establishment and long-term xenografting of human pancreatic carcinomas in immunosuppressed mice: changes and stability in morphology, DNA ploidy and proliferation activity. J Cancer Res Clin Oncol 125: 9–19.
13. Poupon MF, Arvelo F, Goguel AF, Bourgeois Y, Jacrot M, et al. (1993) Response of small-cell lung cancer xenografts to chemotherapy: multidrug resistance and direct clinical correlates. J Natl Cancer Inst 85: 2023–2029.
14. Fielding LP, Arsenault PA, Chapuis PH, Dent O, Gathright B, et al. (1991) Clinocpatholgoical staging for colorectal cancer: an International Documentation System (IDS) and an Interantional Comprehensive Anatomical Terminology (ICAT). J Gastroenterol Hepatol 6: 325–344.
15. Findeisen P, Kloor M, Merx S, Sutter C, Woerner SM, et al. (2005) T25 repeat in the 3′ untranslated region of the CASP2 gene: a sensitive and specific marker for microsatellite instability in colorectal cancer. Cancer Res 65: 8072–8078.
16. Ogino S, Nosho K, Kirkner GJ, Kawasaki T, Meyerhardt JA, et al. (2009) CpG island methylator phenotype, microsatellite instability, BRAF mutation and clinical outcome in colon cancer. Gut 58: 90–96.
17. Klier U, Maletzki C, Klar E, Linnebacher M (2010) Generation of highly pure fusions of colorectal carcinoma and antigen-presenting cells. Langenbecks Arch Surg 395: 365–371.
18. Jaster R, Lichte P, Fitzner B, Brock P, Glass A, et al. (2005) Peroxisome proliferator-activated receptor gamma overexpression inhibits pro-fibrogenic activities of immortalised rat pancreatic stellate cells. J Cell Mol Med 9: 670–682.
19. Ramer R, Hinz B (2008) Inhibition of cancer cell invasion by cannabinoids via increased expression of tissue inhibitor of matrix metalloproteinases-1. J Natl Cancer Inst 100: 59–69.
20. Tognon M, Casalone R, Martini F, De Mattei M, Granata P, et al. (1996) Large T antigen coding sequences of two DNA tumor viruses, BK and SV40, and nonrandom chromosome changes in two glioblastoma cell lines. Cancer Genet Cytogenet 90: 17–23.
21. Linnebacher M, Maletzki C, Ostwald C, Klier U, Krohn M, et al. (2010) Cryopreservation of human colorectal carcinomas prior to xenografting. BMC Cancer 10: 362.
22. Hewish M, Lord CJ, Martin SA, Cunningham D, Ashworth A (2010) Mismatch repair deficient colorectal cancer in the era of personalized treatment. Nat Rev Clin Oncol 7: 197–208.
23. Kirkland SC, Bailey IG (1986) Establishment and characterisation of six human colorectal adenocarcinoma cell lines. Br J Cancer 53: 79–85.
24. Dangles-Marie V, Pocard M, Richon S, Weiswald LB, Assayag F, et al. (2007) Establishment of human colon cancer cell lines from fresh tumors versus xenografts: comparison of success rate and cell line features. Cancer Res 67: 398–407.
25. Julien S, Merino-Trigo A, Lacroix L, Pocard M, Goere D, et al. (2012) Characterization of a large panel of patient-derived tumor xenografts representing the clinical heterogeneity of human colorectal cancer. Clin Cancer Res 18: 5314–28.
26. Gagos S, Iliopoulos D, Tseleni-Balafouta S, Agapitos M, Antachopoulos C, et al. (1996) Cell senescence and a mechanism of clonal evolution leading to continuous cell proliferation, loss of heterozygosity, and tumor heterogeneity: studies on two immortal colon cancer cell lines. Cancer Genet Cytogenet 90: 157–165.
27. Bae JM, Kim MJ, Kim JH, Koh JM, Cho NY, et al. (2011) Differential clinicopathological features in microsatellite instability-positive colorectal cancers depending on CIMP status. Virchows Arch 459: 55–63.
28. El-Osta H, Falchook G, Tsimberidou A, Hong D, Naing A, et al. (2011) BRAF Mutations in Advanced Cancers: Clinical Characteristics and Outcomes. PLoS One 6: 25806.
29. Ogino S, Shima K, Meyerhardt J, McCleary N, Ng K, et al. (2012) Predictive and Prognostic Roles of BRAF Mutation in Stage III Colon Cancer: Results from Intergroup Trial CALGB 89803. Clin Cancer Res 18: 890–900.
30. Swanton C, Caldas C (2009) Molecular classification of solid tumors: towards pathway-driven therapeutics. Br J Cancer 100: 1517–22.
31. Castellanos E, Berlin J, Cardin DB (2011) Current treatment options for pancreatic carcinoma. Curr Oncol Rep 13: 195–205. Review.
32. Madajewicz S, Waterhouse DM, Ritch PS, Khan MQ, Higby DJ, et al. (2012) Multicenter, randomized phase II trial of bevacizumab plus folinic acid, fluorouracil, gemcitabine (FFG) versus bevacizumab plus folinic acid, fluorouracil, oxaliplatin (FOLFOX4) as first-line therapy for patients with advanced colorectal cancer. Invest New Drugs 30: 772–778.

33. Correale P, Botta C, Cusi MG, Del Vecchio MT, De Santi MM, et al. (2012) Cetuximab +/− chemotherapy enhances dendritic cell-mediated phagocytosis of colon cancer cells and ignites a highly efficient colon cancer antigen-specific cytotoxic T-cell response in vitro. Int J Cancer 130: 1577–1589.
34. Saif MW, Kaley K, Penney R, Hotchkiss S, Syrigos KN, et al. (2011) The efficacy of gemcitabine as salvage treatment in patients with refractory advanced colorectal cancer (CRC): a single institution experience. Anticancer Res 31: 2971–2974.
35. O'Reilly T, McSheehy PM, Kawai R, Kretz O, McMahon L, et al. (2010) Comparative pharmacokinetics of RAD001 (everolimus) in normal and tumor-bearing rodents. Cancer Chemother Pharmacol 65: 625–39.
36. Hector S, Rehm M, Schmid J, Kehoe J, McCawley N, et al. (2012) Clinical application of a systems model of apoptosis execution for the prediction of colorectal cancer therapy responses and personalisation of therapy. Gut 61: 725–733.
37. Baguley BC, Marshall ES, Finlay GJ (1999) Short-term cultures of clinical tumor material: potential contributions to oncology research. Oncol Res 11: 115–124.

5.1.4 Anlage – Teil 4

Functional Characterization and Drug Response of Freshly Established Patient-Derived Tumor Models with CpG Island Methylator Phenotype

PLOS | ONE

RESEARCH ARTICLE

Functional Characterization and Drug Response of Freshly Established Patient-Derived Tumor Models with CpG Island Methylator Phenotype

Claudia Maletzki[1], Maja Huehns[2], Patrick Knapp[1], Nancy Waukosin[1], Ernst Klar[3], Friedrich Prall[2], Michael Linnebacher[1]*

1 Molecular Oncology and Immunotherapy, University of Rostock, Rostock, Germany, **2** Institute of Pathology, University of Rostock, Rostock, Germany, **3** Department of General Surgery, University of Rostock, Rostock, Germany

* michael.linnebacher@med.uni-rostock.de

CrossMark
click for updates

OPEN ACCESS

Citation: Maletzki C, Huehns M, Knapp P, Waukosin N, Klar E, Prall F, et al. (2015) Functional Characterization and Drug Response of Freshly Established Patient-Derived Tumor Models with CpG Island Methylator Phenotype. PLoS ONE 10(11): e0143194. doi:10.1371/journal.pone.0143194

Editor: Hiromu Suzuki, Sapporo Medical University, JAPAN

Received: August 14, 2015

Accepted: November 2, 2015

Published: November 30, 2015

Copyright: © 2015 Maletzki et al. This is an open access article distributed under the terms of the Creative Commons Attribution License, which permits unrestricted use, distribution, and reproduction in any medium, provided the original author and source are credited.

Data Availability Statement: All relevant data are within the paper.

Funding: The authors have no support or funding to report.

Competing Interests: The authors have declared that no competing interests exist.

Abbreviations: CIN, chromosomal instable; CIMP, CpG island and methylator phenotype; CRC, colorectal carcinoma; MSI, Microsatellite instable.

Abstract

Patient-individual tumor models constitute a powerful platform for basic and translational analyses both *in vitro* and *in vivo*. However, due to the labor-intensive and highly time-consuming process, only few well-characterized patient-derived cell lines and/or corresponding xenografts exist. In this study, we describe successful generation and functional analysis of novel tumor models from patients with sporadic primary colorectal carcinomas (CRC) showing CpG island methylator phenotype (CIMP). Initial DNA fingerprint analysis confirmed identity with the patient in all four cases. These freshly established cells showed characteristic features associated with the CIMP-phenotype (HROC40: APC^{wt}, $TP53^{mut}$, $KRAS^{mut}$; 3/8 marker methylated; HROC43: APC^{mut}, $TP53^{mut}$, $KRAS^{mut}$; 4/8 marker methylated; HROC60: APC^{wt}, $TP53^{mut}$, $KRAS^{wt}$; 4/8 marker methylated; HROC183: APC^{mut}, $TP53^{mut}$, $KRAS^{mut}$; 6/8 marker methylated). Cell lines were of epithelial origin ($EpCAM^{+}$) with distinct morphology and growth kinetics. Response to chemotherapeutics was quite individual between cells, with stage I-derived cell line HROC60 being most susceptible towards standard clinically approved chemotherapeutics (e.g. 5-FU, Irinotecan). Of note, most cell lines were sensitive towards "non-classical" CRC standard drugs (sensitivity: Gemcitabin > Rapamycin > Nilotinib). This comprehensive analysis of tumor biology, genetic alterations and assessment of chemosensitivity towards a broad range of (chemo-) therapeutics helps bringing forward the concept of personalized tumor therapy.

Introduction

Three main molecular pathways have been recognized in colorectal cancer (CRC). These include I) chromosomal instability (CIN); II) microsatellite instability (MSI), and III) CpG island methylator phenotype (CIMP). The latter subtype being first formulated by Toyota et al.

[1], is defined by aberrant DNA methylation, leading to concordant promoter hypermethylation of multiple genes. CpG island DNA methylation occurs early in malignant transformation [2] and consequently results in silencing of normal tumor-suppressor function and cancer formation, independent of (physiological) age-related methylation. The CIMP subtype exists with and without MSI, both showing distinct morphologic, molecular and most importantly, clinical characteristics [3]. MSI-high/CIMP$^+$ tumors, related to BRAF^{V600E} mutations and MLH1 promoter methylation, are usually associated with low cancer-specific mortality, mostly due to their natural immunogenicity [3]. By contrast, CIMP without MSI is independently related to significantly worse outcome [3–5]. The unique molecular signature includes a high frequency of KRAS mutations (>60%) and usually less extensive promoter methylation (designated as "CIMP-Low" vs. CIMP-High in MSI$^+$ tumors) [6–8].

Determining the precise genetic and/or epigenetic alterations of each cancer case is important to defining treatment strategies and predicting prognosis. To date, chemotherapy response of CIMP$^+$ tumors is still controversial. Preceding studies reported different results on 5-FU-based therapy, ranging from good response up to complete resistance [9, 10]. Very recently, methylation inhibitors have become increasingly recognized as another option for treatment of CIMP$^+$ tumors and hence, a clinical phase I/II trial has just been initiated (trial number: NCT01193517). In this study, metastatic colorectal cancer patients are being treated with Azacytidine (5-Aza-2-deoxycytidine) and CAPOX (Capecitabine + Oxaliplatin). First results will be published in 2016.

Additionally to attempts in improving treatment options, discovery of novel diagnostic and/or prognostic CRC-specific (DNA methylation) markers is ongoing [11]. To reflect the complexity and diversity of CIMP$^+$ tumors, both approaches may ideally be performed in patient-individual tumor models. Here, such models generated from four individual CIMP$^+$ tumors (CIMP-L and CIMP-H) are presented.

Material and Methods

Tumor preparation and cell line establishment protocol

Primary CRC cases were obtained upon resection, with informed written patient consent (n = 4). All procedures were approved by the institutional Ethics Committee (Ethikkommission an der Medizinischen Fakultät der Universität Rostock; St.-Georg-Str. 108, 18055 Rostock; reference number II HV 43/2004) in accordance with generally accepted guidelines for using human material. None of the patients' received prior tumor-related therapy. Upon surgical removal, tumor samples were processed further as described [12, 13]. Briefly, pieces of tumors (3 x 3 x 3 mm) were frozen viable (FCS, 10% DMSO) at -80°C for subsequent xenografting into NMRI Foxn1^{nu} mice. Other pieces were stored in liquid nitrogen for molecular analysis. Cell culture was started from single cell suspensions, seeded on collagen-coated plates in complete tumor medium and incubated at 37°C in a humidified atmosphere of 5% $C0_2$. All cell culture reagents were obtained from PAN Biotech (Aidenbach, Germany), antibiotics and antifungal agents were provided by the university hospital's pharmacy. Continually growing cell cultures were serially passaged and regularly stocked in low passages.

For *in vivo* engraftment, five to six-week-old female NMRI Foxn1^{nu} mice were used as recipients. Mice were bred in the university's animal facility and maintained in specified pathogen-free conditions in accordance with guidelines as put forth by the German Ethical Committee. All *in vivo* procedures were approved by the Committee on the Ethics of Animal Experiments of the University of Rostock (Landesamt für Landwirtschaft, Lebensmittelsicherheit und Fischerei Mecklenburg-Vorpommern; Thierfelder Str. 18, 18059 Rostock, Germany; approval number: LALLF M-V/TSD/7221.3–1.1-015-14). Subcutaneous (s.c.) tumor implantation into both flanks was performed under Ketamin/Xylazin anesthesia (dose: 90/6 mg/kg bw), and all efforts were made to minimize suffering. Established xenografts ($\geq$1500 mm^3) were removed and stored vitally for further analysis.

Tumor histology and immunohistochemistry

Histopathological examination of the primaries was done according to standard protocols for clinicopathological CRC staging [14], and additional staging information was compiled from patients' clinical charts. H & E sections and β-catenin immunostainings were obtained from paraffin-embedded tumors.

Molecular analysis

Molecular classification, MSI and mutational analysis of tumor-associated genes (APC, TP53, KRAS and B-Raf^{V600E}), as well as DNA methylation in CIMP-sensitive promoters was done as described [12, 13, 15]. All data including staging information compiled from the clinical charts are summarized in Table 1. To classify CIMP, a combined panel covering eight markers was applied. Analyzed markers resulted from those originally described by [16, 17]. On a basis of this panel, tumors with 1–5/8 methylated promoters are being classified as CIMP-L and with 6–8/8 methylated promoters as CIMP-H [18]. Chromosomal instability (CIN) was assessed using SNP Array 6.0 from Affymetrix (Cleveland, OH) according to manufacturer's instructions.

In vitro growth kinetics and Matrigel® invasion assay

Population doubling times were determined by viable cells seeded into replicate 25 cm^2 flasks (each 0.5 x 10^6 cells) and daily counted for five consecutive days. Cellular invasiveness was examined using a Matrigel®-based boyden chamber assay as described [12].

Flow cytometry and cytokine secretion pattern

Surface marker expression was done by flow cytometry with and without IFN-γ (200 IU/mL for 48 hours) pre-treatment using a panel of Abs (for details see Fig 1B). Samples were analyzed using CellQuest software (BD Biosciences). Additionally, multi-color flow cytometry was done on a FACSAria using following mAbs: anti-CD47-BV421, anti-CD36-PE, anti-CD73-BV510, anti-CD95-FITC, anti-Foxp3-Alexa Fluor 647, anti-CD284-BV421, anti-CD276-PE, anti-CD133-APC, anti-cFLIP-Alexa Fluor 488, anti-Indolamin-2.3-Dioxygenase-PE, anti-BIN1 (bridging integrator 1)-Alexa Fluor 488.

Table 1. Clinical and pathological characteristics of patients as well as cell line establishment protocol.

Tumor-ID	Age/ Gender	Tumor location	Grade and TNM-Stage	UICC Stage	β-Catenin translocation	Direct cell line establishment	Cell line from xenograft	Corresponding xenograft	Paired B-LCL
HROC40	69/m	descending colon	G3T3N1M0	IIIa	+	+	-	+	yes
HROC43	72/m	ascending colon	G3T3N2M0	IIIb	-	+	-	-	yes
HROC60	71/m	ascending colon	G2T2N0M0	I	+	+	-	+	yes
HROC183	59/f	ascending colon	G3T3N2M0	IIIb	-	+	+	+	yes

f–female, m–male, B-LCL–B lymphoid cell line, +–positive,—–negative

doi:10.1371/journal.pone.0143194.t001

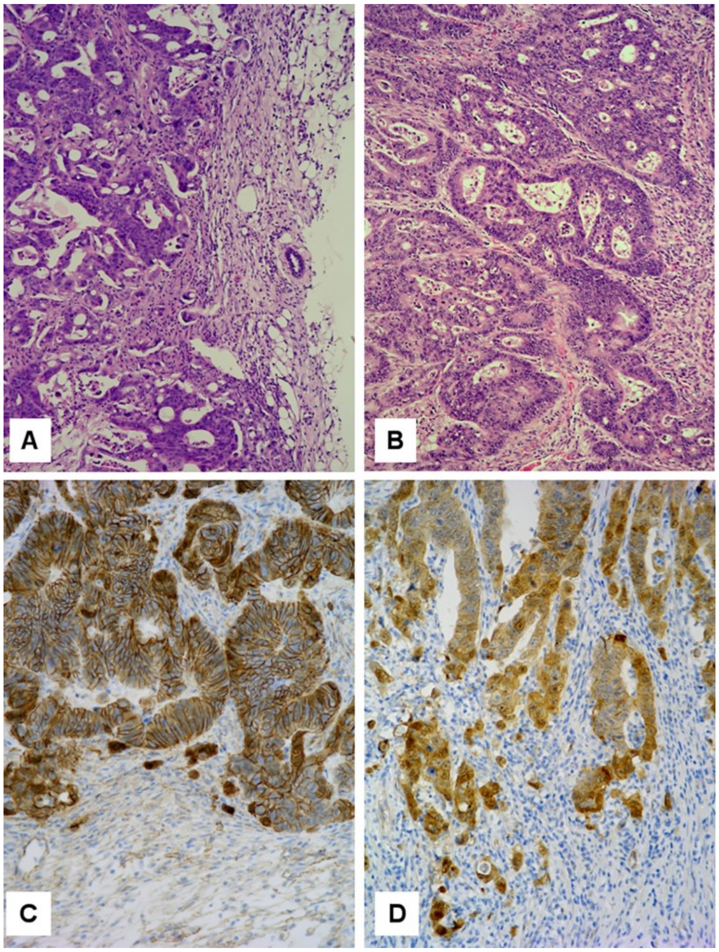

Fig 1. Tumor histology. H & E sections of (**A**) HROC40-PDX and (**B**) its primary. Note the invasive edge towards the right. Principal morphological features are retained in the PDX. β-catenin immunohistochemistry of (**C**) HROC60-PDX and (**D**) its primary. Note nuclear β-catenin translocation at the invasive edge of both tumors.

doi:10.1371/journal.pone.0143194.g001

Cytokine release was determined from cell free supernatants and quantified by ELISA according to the manufacturer's instructions.

Quality control

Quality controls included DNA Fingerprint (comparison of cell lines at different passages, matched tumor and normal tissue, as well as corresponding B cells) from genomic DNA according to [13]. Additionally, cell cultures were checked for contaminating mycoplasma and human viruses (SV40, JC/BK) [12].

In vitro chemosensitivity

Triplicate wells were exposed to increasing drug concentrations (pharmacy of the University hospital Rostock). IC_{50} values of selected drugs were determined. In selected experiments, drug combinations with Azacytidine (5-Aza-2'-deoxycytidine; 30μM) were used. Doses applied in this setting were below the IC_{50} value, as tested before. Cells received two or four treatment cycles, a total of 7 and 14 days, respectively. Drug response was calculated upon crystal violet staining and measurement at 570 nm (reference wavelength: 620 nm).

Statistics

Values are reported as the mean ± SD. IC_{50} values were calculated using Sigma Plot 12.5 software (Systat Software Inc., San Jose, CA) applying the four parameter logistic function standard curve analysis for dose response. Values are given as absolute numbers.

Results

Tumor histology

Primary tumors were moderately well differentiated (HROCs 40, 43, 60) or poorly differentiated (HROC183) tubular adenocarcinomas. Principal architectural and cytological features of the primaries were retained in the subcutaneous patient-derived xenografts (PDX; see Fig 1A and 1B for an example). Nuclear β-catenin translocation, if present in the primary, was also observed in the PDX (Fig 1C and 1D) and *vice versa*.

Patient characteristics and primary cell line establishment

Cell lines were established from primary resection specimens upon surgery (clinicopathological patients' data in Table 1). With the exception of HROC60, all tumors were resected at an advanced tumor stage (T3) showing regional lymph node infiltration, but no distant metastases. However, two out of four patients developed liver (HROC40) and brain (HROC43) metastasis, respectively, within one year after initial removal of the primary.

All cell lines were established from patients' tumor material. Additionally, a PDX-derived cell line from HROC183 was obtained. Tumor cell cultures started to proliferative immediately upon initial culture.

Of note, *in vivo* tumorigenicity was absent in three out of four cases (positive case: HROC43, data not shown). Injecting cells at later passage (>40) and/or together with matrigel did not increase tumorigenic potential.

As determined by PCR, no contaminating mycoplasma or human pathogenic viruses (SV40, and JC/BK, data not shown) were detected within the $CIMP^+$ cell lines.

Cell morphology and phenotyping

Light microscopy revealed tight adherence to the bottom of the flasks (Fig 2A). In the early cell culture (< 3 passages), several different epithelial-like cellular clones were observed. At later passage, one cell clone dominated the culture in all cases. Morphologically, all cultures appeared as multi-cellular islands forming aggregates or polygonal cell clusters. All but one of the cell cultures were dominated by a phenotypically small cell clone. The exception is HROC60. In this cell line, flat-shaped adhesive cells with large nuclei, having an irregular size

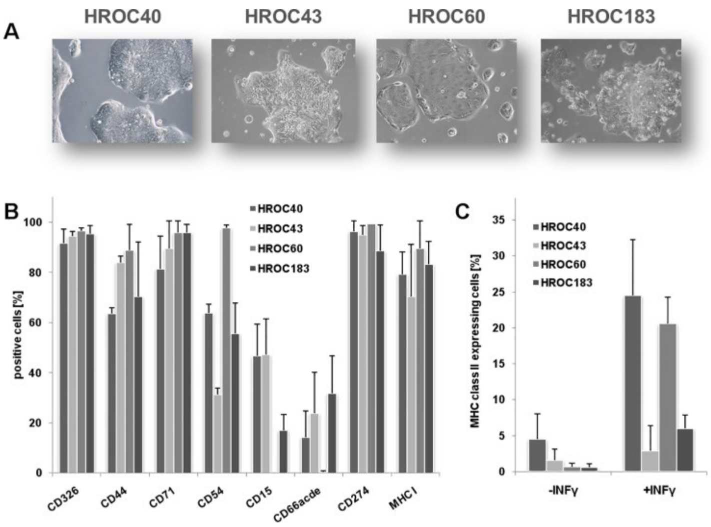

Fig 2. Morphology and phenotype of individual CIMP$^+$ cell lines. (**A**) Light microscopy of freshly established tumor cell lines (all Passage 15). Cell lines were directly established from patients' tumor material as described in material and methods. Original magnification ×100. (**B**) Phenotyping was conducted by flow cytometry using fluorochrome-labeled mAbs as given on the x-axis. (**C**) MHC class II expression as assessed by flow cytometry with and without IFN-γ (200 IU/mL for 48 hours) pre-treatment. Results are given as the mean % of positive cells + standard deviation of three independent experiments.

doi:10.1371/journal.pone.0143194.g002

and silhouette were present. HROC60 cells were the only one that grew to complete confluence.

Additional flow cytometric phenotyping confirmed their epithelial origin (>90% EpCAM$^+$). Detailed information on cellular phenotype is given in Fig 2B and 2C. In line with their immunosuppressive phenotype, several molecules, known to be linked to cancer progression and immune evasion, were highly expressed (>80%: CD47, CD274, CD276, and Indoleamine 2,3 dioxygenase-1). By contrast, an individual profile was seen for cFLIP (cellular FLICE (FADD-like IL-1β-converting enzyme)-inhibitory protein), CD73, CD95 and CD133 (Fig 3).

Molecular features

The identity with the patient was verified by DNA fingerprint. Additional comprehensive molecular classification of cell lines was paralleled by analyses on original tumor material. Analyses identified differences in the KRAS gene mutational status between HROC60 tumor and the corresponding cell line. In line with the dynamic molecular changes, these cells acquired a c.176C>G (A59G) mutation in codon 13 of exon 2 during *in vitro* culture. However, no further differences between original tumors and corresponding cell lines were evident. Data presented in Tables 2 and 3 therefore refer to the cell lines only.

A consensus panel for determining cytosine methylation at promoter CpG islands of tumor suppressor genes is only starting to take shape. We decided to use a combined panel covering eight tumor-specific methylation markers [16–18]. Hence, three cell lines (HROC40 (3/8 methylated promoters), HROC43 and HROC60 (each 4/8 methylated promoters)) were defined as

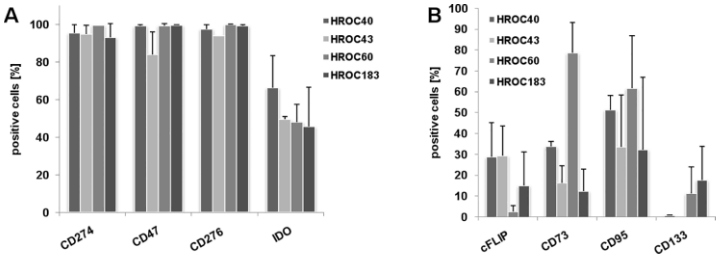

Fig 3. Immunosuppressive phenotype of CIMP$^+$ cell lines. Assessment of immune evasion markers was conducted by multi-color flow cytometry using fluorochrom-labeled mAbs as given on the x-axis. Results are given as the mean % of positive cells + standard deviation of three independent experiments.

doi:10.1371/journal.pone.0143194.g003

CIMP-L and the remaining cell line HROC183 (6/8 methylated promoters) exhibited a CIMP-H phenotype. MSI was excluded by using the advanced Bethesda panel (0/6 marker). Additionally, instability on the chromosomal level was analyzed by SNP 6.0 arrays (Fig 4). Cell lines exhibited complex chromosomal aberrations, present as both deletions and insertions. Besides, typical molecular characteristics associated with the CIMP phenotype were present, i.e. KRAS mutations (codon 12 or 13 of exon 2 [19]), and BRAF^{V600} wildtype. By contrast, conflicting results have been reported for the TP53 gene [8, 20]. Here, mutations were evident in all four cases.

Cytokine secretion profile

All cell lines secreted high amounts of CEA in a time-dependent manner (Fig 5A). A comparable pattern was observed for CA19-9. However, this tumor marker was only detectable in supernatants of HROC40 and HROC43 cells (Fig 5A). By contrast, IL-8, an autocrine growth factor, was secreted by all four CIMP$^+$ lines (Fig 5A). None of the cell lines secreted detectable amounts of IL-6, IL-10, TGF-β, or TNF-α.

Growth kinetics and invasive potential

As anticipated, growth kinetics were quite different between cells, with HROC40 and HROC60 growing more rapidly than HROC43 and HROC183 cells (Fig 5B). Apart from these findings, we observed marginal differences with regard to their invasive potential (Fig 5C). All cell lines

Table 2. Mutational profile of CIMP$^+$ cell lines.

Cell line	Mutation										
	TP53				APC		KRAS		BRAF	PIK3CA	
(HROC...)	ex5	ex6	ex7	ex8	cd1	cd2	cd12	cd13	V600E	ex9	ex20
40	wt	wt	wt	mut	wt	wt	wt	mut	wt	wt	wt
43	wt	wt	mut	wt	wt	mut	mut	wt	wt	wt	wt
60	wt	wt	wt	mut	mut	wt	wt	mut	wt	wt	wt
183	wt	wt	wt	mut	mut	wt	mut	wt	wt	wt	wt

wt–wildtype, mut–mutated, ex–exon, cd–codon.

doi:10.1371/journal.pone.0143194.t002

Table 3. Methylation marker and molecular classification of CIMP⁺ cell lines.

	DNA Methylation									
HROC...	**MLH1**	**CDKN2A**	**NEUROG1**	**CRABP1**	**CACNA1G**	**MGMT**	**IGF2**	**SOCS2**	**RUNX3**	**Molecular type**
40	-	+	+	+	-	-	-	-	-	**CIMP-L**
43	-	+	+	+	-	-	-	-	+	**CIMP-L**
60	-	+	+	+	+	-	-	-	-	**CIMP-L**
183	-	+	+	+	+	-	+	-	+	**CIMP-H**

+—methylated;——not methylated.

doi:10.1371/journal.pone.0143194.t003

were less invasive than the control cell line HCT116. Highest invasion potential was seen for HROC43 cells, while the remaining three lines exhibited a comparable invasion pattern.

Response towards classical and novel drugs

To identify potential intrinsic resistance mechanisms, a panel of clinically approved and more experimental targeted agents was applied in a 2-D *in vitro* culture system (Table 4).

Drug response was individual between cells, with HROC40 being more resistant than the remaining three lines, especially towards Irinotecan (IC_{50} = 25.5 μM). All lines were susceptible towards 5-FU, although conflicting results have been reported in the literature for this substance [9, 10]. A good response was seen towards Gemcitabine, the tyrosine kinase inhibitor Nilotinib, and Rapamycin. Erlotinib did not prove to be effective against the cell lines tested here.

Additionally, Azacytidine alone and in combination with chemotherapeutic drugs was studied. Here, IC_{50} values for Azacytidine were above 30 μM, even in the CIMP-H cell line HROC183. Longer incubation time increased the antitumoral effect of Azacytidine (Fig 6, lower panel). Best effects were seen in HROC183 cells. Drug combinations, either given simultaneous or metronomic, slightly increased the antitumoral effect of Azacytidine (representative data are given in Fig 6). However, the different drug combinations were not better than single drug treatments and in virtually all cases; even antagonistic effects were observed (e.g. Azacytidine + 5-FU or Irinotecan; Fig 6).

Discussion

To realize the idea of personalized medicine, we here report establishment of novel patient-individual tumor models showing molecular features of CIMP. This subtype is associated with opposed clinical performance; a good prognosis in terms of positive MSI status, while poor response and short overall survival when patients tumors are MSI-negative. For the latter, an aggressive tumor phenotype with tendency to early spread to distant organs and frequent chemoresistance has been demonstrated [5].

Though no consensus regarding classification of CIMP exists yet, we decided to combine generally accepted gene panels and marker thresholds [16–18]. Hence, three cases were classified as CIMP-L (HROC40, HROC43, and HROC60) and the remaining cell line HROC183 was CIMP-H. The latter represents a very rare subtype, since this phenotype is usually associated with MSI. Here, MSI was not present in any case. Similar genes were affected by DNA hypermethylation (i.e. CDKN2A, NEUROG1, and CRABP1). The identified RUNX3 methylation in HROC43 und HROC183 confirms an advanced tumor stage. In line with the recent literature, MGMT promoter methylation was absent, while KRAS exon 2 and TP53 gene mutations were present [8]. The exclusively high number of KRAS mutations in

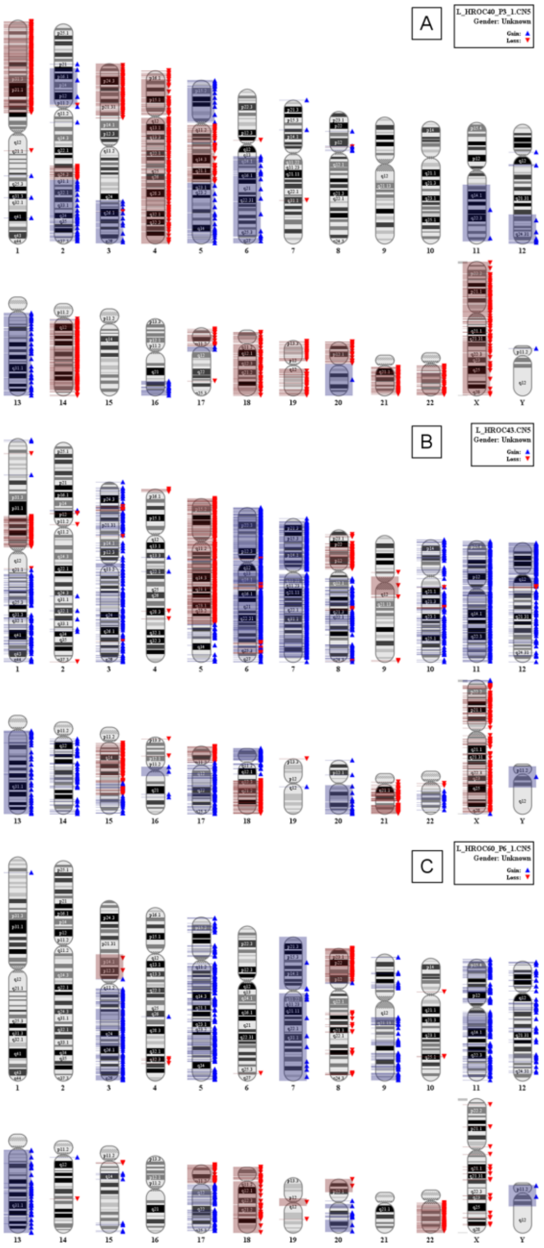
A
L_HROC40_P3_1.CN5
Gender: Unknown
Gain: ▲
Loss: ▼
1 2 3 4 5 6 7 8 9 10 11 12
13 14 15 16 17 18 19 20 21 22 X Y
B
L_HROC43.CN5
Gender: Unknown
Gain: ▲
Loss: ▼
1 2 3 4 5 6 7 8 9 10 11 12
13 14 15 16 17 18 19 20 21 22 X Y
C
L_HROC60_P6_1.CN5
Gender: Unknown
Gain: ▲
Loss: ▼
1 2 3 4 5 6 7 8 9 10 11 12
13 14 15 16 17 18 19 20 21 22 X Y

Fig 4. SNP Array 6.0 for assessment of CIN in CIMP$^+$ cell lines. Analysis was performed according to manufacturer's instructions. Data shown here result from three out of four CIMP$^+$ cell lines. (**A**) HROC40 cells, (**B**) HROC43 cells, and (**C**) HROC60 cells. SNP Array on HROC183 did not yield evaluable data due to quality control failure.

doi:10.1371/journal.pone.0143194.g004

CIMP-associated tumors has been explained as result of a favorable selection in the specific CIMP-created environment, rather than a driving event of CIMP tumorigenesis [8]. Indeed, abnormal DNA hypermethylation is already detectable in aberrant crypt foci, the earliest lesions in the colonic mucosa [3, 8].

Cell lines generated in this study were directly obtained from parental tumor material. Additionally, PDX could be established in three out of four cases (not for HROC43). These PDX models, showing high morphologic and molecular similarity with the corresponding patient tumor, can subsequently be applied in pharmacologic studies to predict clinical response [21]. Prior to applying cost and time consuming PDX models, research is usually being performed in cell culture systems. In the early 90s, the NCI panel, including 60 cell lines, has been formulated for such studies [22]. This panel includes only a limited number of lines for any given cancer and it does not consider patient-individual differences [23]. In case of CIMP, only few cell lines have been made commercially available [24]. The accumulation of further mutations and chromosomal aberrations are further drawbacks of cultured cells. Depending on the individual tumor case and stage at resection (early vs. advanced), molecular changes cells undergo during *in vitro* culture are already present after few passages. Here, HROC60 cells acquired a

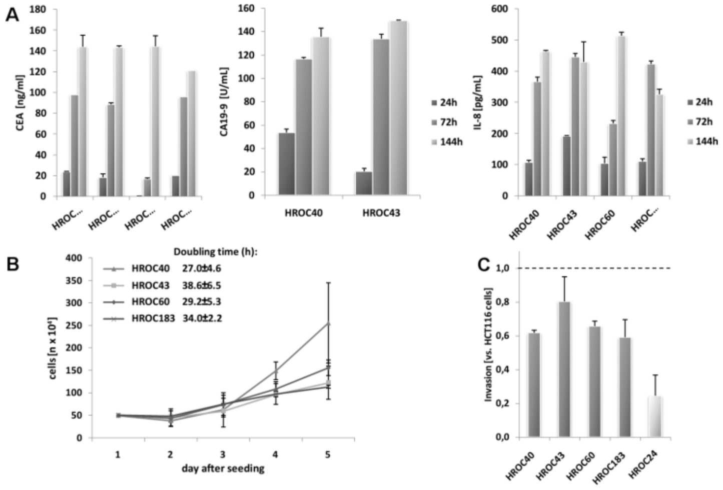

Fig 5. Secretion profile, growth kinetics and invasive potential of CIMP$^+$ cell lines. (**A**) Cytokine secretion pattern was quantified by ELISA. Cytokine concentrations were determined by comparison with a standard curve generated from serial dilutions of individual standards. Quantitative analysis of CEA, CA19-9 and IL8 secretion after one, three and six days of culture, respectively. (**B**) Growth kinetics of cells, counted every 24 hours for five consecutive days using a Neubauer chamber. (**C**) Cellular invasiveness was examined using a Matrigel®-based Boyden chamber assay. Quantification of cellular invasiveness was estimated by MTT assay. Data are expressed as percentage invasion versus HCT116 cells (= internal positive control). (**A-C**) Results show the mean + standard deviation of three independent experiments.

doi:10.1371/journal.pone.0143194.g005

Table 4. Drug response of CIMP$^+$ cell lines.

HROC…	IC_{50} 5-FU [μM]	Irinotecan [μM]	Cisplatin [μM]	Gemcitabine [nM]	Taxol [nM]	Erlotinib [μM]	Nilotinib [μM]	Rapamycin [μM]	Azycytidine [μM]
40	16	25.5	9.3	43	27.6	resistant	6.3	0.3	>30
43	1.5	4.5	2.7	9	45	62.5	6.9	0.2	>30
60	6.2	2.9	6.3	6.7	1.3	7.8	7.5	1.6	resistant
183	3.1	11.2	3.3	17.4	resistant	28	7	0.2	>30

doi:10.1371/journal.pone.0143194.t004

KRAS mutation that was not detectable in the parental tumor. This mutation most likely reflects the rapid dynamic molecular changes that occur in tumor cells following high numbers of cell divisions [25–27]. Alternatively, considering the genetic heterogeneity within tumors, these cells may represent a single mutated clone that had not been recognized in the resection specimen of parental tumor but gave rise to *in vitro* growth. However, the fact that this cell line

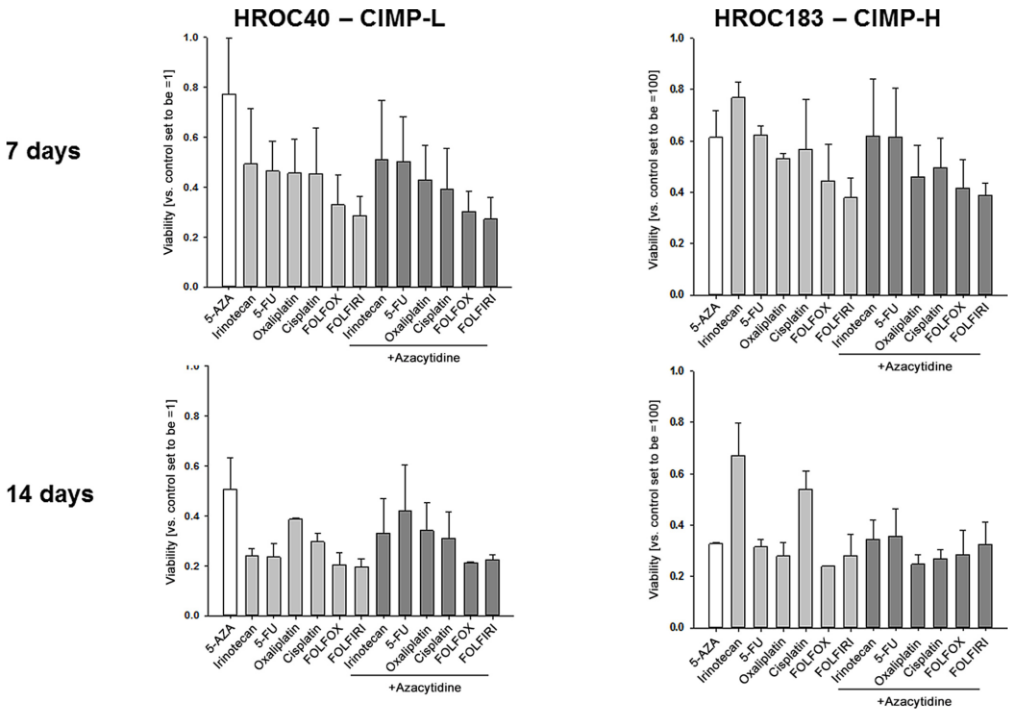

Fig 6. Response to Aza-based drug combinations. Representative quantitative analysis of HROC40 (left graph) and HROC183 cells (right graph) treated with Aza, standard drugs or combinations thereof. Cells received two (upper panel) or four (lower panel) treatment cycles in concentrations as indicated in the material and methods section. Cytotoxicity was quantified upon crystal violet staining and measurement at 570 nm (reference wavelength: 620 nm). Results show the mean + standard deviation of three independent experiments.

doi:10.1371/journal.pone.0143194.g006

had been established from a very early stage tumor (UICC stage I), rather supports the first hypothesis and underlines the necessity of using ultra-low passage cells, especially for preclinical drug screening and evaluation (in especially when targeting the Ras/Raf pathway).

These freshly established cell lines were of epithelial (EpCAM$^+$) origin, showing distinct morphology and growth kinetics. In line with their immunosuppressive phenotype, several molecules know to be related to immune evasion [28], apoptosis inhibition (cFLIP), tissue invasion (CD73), metastasis and consequently poor outcome (CD274) were found to be overexpressed. Moreover, all cell lines secreted high amounts of IL8 that has been linked to metastatic spread, as well [29, 30].

Patient-individual tumor models not only aid evaluating the efficacy of therapeutic strategies prior to therapy, but also help investigating resistance mechanisms of cancer cells–a major clinical problem. Here, intrinsic resistance of individual cases was detected against Erlotinib (HROC40) and Taxol (HROC183). Emphasizing the need for personalized medicine, an individual response was obtained for the commonly used antineoplastic drugs 5-FU, Irinotecan, Cisplatin, and Gemcitabine. Interestingly and in concert with our recent observation on CIN$^+$/non-CIMP-associated tumors, we here observed a good response towards the mTOR inhibitor Rapamycin [13, 31]. On a molecular level, PIK3CA and/or TP53 gene mutations seem to correlate with sensitivity [32] and in fact, all CIMP$^+$ cell lines described here carry a TP53 mutation. Cai and colleagues only recently reported activity against CRC stem-like cells, providing another rationale for mTOR-inhibitor tailored regimens [33].

All CIMP$^+$ cell lines were responsive to the tyrosine kinase inhibitor Nilotinib [34, 35]. In the only prior study on CRC lines, a comparable growth inhibiting potential of Nilotinib could be attributed to collagen receptor targeting [36].

In summary, our novel patient-individual tumor models (cell lines + PDX) of a rare and very aggressive CRC subtype represent ideal tools to realize personalized medicine shortly. Additionally to identifying (novel) molecular target structures, drug efficacy screening and resistance mechanism identification can be done.

Conclusion

Patient-derived tumor models provide ideal tools for identification of novel biomarkers and defining intrinsic resistance mechanisms. By combining *in vitro* and *in vivo* approaches, accurate prediction of drug responses can be realized.

Acknowledgments

The authors kindly thank Dr. Dirk Koczan for performing SNP Array 6.0 analysis.

Author Contributions

Conceived and designed the experiments: CM ML. Performed the experiments: CM PK NW MH FP. Analyzed the data: CM FP ML. Contributed reagents/materials/analysis tools: ML. Wrote the paper: CM ML. Revised the manuscript: EK.

References

1. Toyota M, Ahuja N, Ohe-Toyota M, Herman JG, Baylin SB, Issa JP. CpG island methylator phenotype in colorectal cancer. Proc Natl Acad Sci U S A. 1999; 96: 8681–8686. PMID: 10411935
2. Yamamoto E, Suzuki H, Yamano HO, Maruyama R, Nojima M, Kamimae S, et al. Molecular dissection of premalignant colorectal lesions reveals early onset of the CpG island methylator phenotype. Am J Pathol. 2012; 181: 1847–1861. doi: 10.1016/j.ajpath.2012.08.007 PMID: 22995252

3. Konda K, Konishi K, Yamochi T, Ito YM, Nozawa H, Tojo M, et al. Distinct molecular features of different macroscopic subtypes of colorectal neoplasms. PLoS One. 2014; 9: e103822. doi: 10.1371/journal.pone.0103822 PMID: 25093594
4. Curtin K, Slattery ML, Samowitz WS. CpG island methylation in colorectal cancer: past, present and future. Patholog Res Int. 2011; 2011: 902674. doi: 10.4061/2011/902674 PMID: 21559209
5. Juo YY, Johnston FM, Zhang DY, Juo HH, Wang H, Pappou EP, et al. Prognostic value of CpG island methylator phenotype among colorectal cancer patients: a systematic review and meta-analysis. Ann Oncol. 2014; 25: 2314–2327. doi: 10.1093/annonc/mdu149 PMID: 24718889
6. Toyota M, Ohe-Toyota M, Ahuja N, Issa JP. Distinct genetic profiles in colorectal tumors with or without the CpG island methylator phenotype. Proc Natl Acad Sci U S A. 2000; 97: 710–715. PMID: 10639144
7. Ogino S, Kawasaki T, Kirkner GJ, Loda M, Fuchs CS. CpG island methylator phenotype-low (CIMP-low) in colorectal cancer: possible associations with male sex and KRAS mutations. J Mol Diagn. 2006; 8: 582–588. PMID: 17065427
8. Hinoue T, Weisenberger DJ, Lange CP, Shen H, Byun HM, Van Den Berg D, et al. Genome-scale analysis of aberrant DNA methylation in colorectal cancer. Genome Res. 2012; 22: 271–282. doi: 10.1101/gr.117523.110 PMID: 21659424
9. Van Rijnsoever M, Elsaleh H, Joseph D, McCaul K, Iacopetta B. CpG island methylator phenotype is an independent predictor of survival benefit from 5-fluorouracil in stage III colorectal cancer. Clin Cancer Res. 2003; 9: 2898–2903. PMID: 12912934
10. Jover R, Nguyen TP, Pérez-Carbonell L, Zapater P, Payá A, Alenda C, et al. 5-Fluorouracil adjuvant chemotherapy does not increase survival in patients with CpG island methylator phenotype colorectal cancer. Gastroenterology. 2011; 140: 1174–1181. doi: 10.1053/j.gastro.2010.12.035 PMID: 21185836
11. Moon JW, Lee SK, Lee JO, Kim N, Lee YW, Kim SJ, et al. Identification of novel hypermethylated genes and demethylating effect of vincristine in colorectal cancer. J Exp Clin Cancer Res. 2014; 33: 4. doi: 10.1186/1756-9966-33-4 PMID: 24393480
12. Maletzki C, Stier S, Gruenert U, Gock M, Ostwald C, Prall F, et al. Establishment, characterization and chemosensitivity of three mismatch repair deficient cell lines from sporadic and inherited colorectal carcinomas. PLoS One. 2012; 7: e52485. doi: 10.1371/journal.pone.0052485 PMID: 23300683
13. Maletzki C, Gock M, Randow M, Klar E, Huehns M, Prall F, et al. Establishment and characterization of cell lines from chromosomal instable colorectal cancer. World J Gastroenterol. 2015; 21: 164–176. doi: 10.3748/wjg.v21.i1.164 PMID: 25574089
14. Fielding LP, Arsenault PA, Chapuis PH, Dent O, Gathright B, Hardcastle JD, et al. Clinicopathological staging for colorectal cancer: an International Documentation System (IDS) and an International Comprehensive Anatomical Terminology (ICAT). (ICAT). J Gastroenterol Hepatol. 1991; 6: 325–344. PMID: 1912440
15. Ostwald C, Linnebacher M, Weirich V, Prall F. Chromosomally and microsatellite stable colorectal carcinomas without the CpG island methylator phenotype in a molecular classification. Int J Oncol. 2009; 35: 321–327. PMID: 19578746
16. Ogino S, Nosho K, Kirkner GJ, Kawasaki T, Meyerhardt JA, Loda M, et al. CpG island methylator phenotype, microsatellite instability, BRAF mutation and clinical outcome in colon cancer. Gut 2009; 58: 90–96. doi: 10.1136/gut.2008.155473 PMID: 18832519
17. Weisenberger DJ, Siegmund KD, Campan M, Young J, Long TI, Faasse MA, et al. CpG island methylator phenotype underlies sporadic microsatellite instability and is tightly associated with BRAF mutation in colorectal cancer. Nat Genet. 2006; 38: 787–93. PMID: 16804544
18. Kaneda A, Yagi K. Two groups of DNA methylation markers to classify colorectal cancer into three epigenotypes. Cancer Sci. 2011; 102:18–24. doi: 10.1111/j.1349-7006.2010.01712.x PMID: 21159060
19. Imamura Y, Lochhead P, Yamauchi M, Kuchiba A, Qian ZR, Liao X, et al. Analyses of clinicopathological, molecular, and prognostic associations of KRAS codon 61 and codon 146 mutations in colorectal cancer: cohort study and literature review. Mol Cancer. 2014; 13: 135. doi: 10.1186/1476-4598-13-135 PMID: 24885062
20. Issa JP. CpG island methylator phenotype in cancer. Nat Rev Cancer. 2004; 4: 988–993. PMID: 15573120
21. Rosfjord E, Lucas J, Li G, Gerber HP. Advances in patient-derived tumor xenografts: from target identification to predicting clinical response rates in oncology. Biochem Pharmacol. 2014; 91: 135–143. doi: 10.1016/j.bcp.2014.06.008 PMID: 24950467
22. Monks A, Scudiero D, Skehan P, Shoemaker R, Paull K, Vistica D, et al. Feasibility of a high-flux anticancer drug screen using a diverse panel of cultured human tumor cell lines. J Natl Cancer Inst. 1991; 83: 757–766. PMID: 2041050

23. Wilding JL, Bodmer WF. Cancer cell lines for drug discovery and development. Cancer Res. 2014; 74: 2377–2384. doi: 10.1158/0008-5472.CAN-13-2971 PMID: 24717177

24. Ahmed D, Eide PW, Eilertsen IA, Danielsen SA, Eknæs M, Hektoen M, et al. Epigenetic and genetic features of 24 colon cancer cell lines. Oncogenesis. 2013 16; 2: e71. doi: 10.1038/oncsis.2013.35 PMID: 24042735

25. Hua VY, Wang WK, Duesberg PH. Dominant transformation by mutated human ras genes in vitro requires more than 100 times higher expression than is observed in cancers. Proc Natl Acad Sci U S A. 1997; 94: 9614–9619. PMID: 9275171

26. Jen J, Powell SM, Papadopoulos N, Smith KJ, Hamilton SR, Vogelstein B, et al. Molecular determinants of dysplasia in colorectal lesions. Cancer Res. 1994; 54: 5523–5526. PMID: 7923189

27. Tomasetti C, Marchionni L, Nowak MA, Parmigiani G, Vogelstein B. Only three driver gene mutations are required for the development of lung and colorectal cancers. Proc Natl Acad Sci U S A. 2015; 112: 118–123. doi: 10.1073/pnas.1421839112 PMID: 25535351

28. Sun J, Chen LJ, Zhang GB, Jiang JT, Zhu M, Tan Y, et al. Clinical significance and regulation of the costimulatory molecule B7-H3 in human colorectal carcinoma. Cancer Immunol Immunother. 2010; 59: 1163–1171. doi: 10.1007/s00262-010-0841-1 PMID: 20333377

29. Palena C, Hamilton DH, Fernando RI. Influence of IL-8 on the epithelial-mesenchymal transition and the tumor microenvironment. Future Oncol. 2012; 8: 713–722. doi: 10.2217/fon.12.59 PMID: 22764769

30. Xie K. Interleukin-8 and human cancer biology. Cytokine Growth Factor Rev. 2001; 12: 375–391. PMID: 11544106

31. Francipane MG, Lagasse E. mTOR pathway in colorectal cancer: an update. Oncotarget. 2014; 5: 49–66. PMID: 24393708

32. Atreya CE, Ducker GS, Feldman ME, Bergsland EK, Warren RS, Shokat KM. Combination of ATP-competitive mammalian target of rapamycin inhibitors with standard chemotherapy for colorectal cancer. Invest New Drugs. 2012; 30: 2219–2225. doi: 10.1007/s10637-012-9793-y PMID: 22270257

33. Cai Z, Ke J, He X, Yuan R, Chen Y, Wu X, et al. Significance of mTOR signaling and its inhibitor against cancer stem-like cells in colorectal cancer. Ann Surg Oncol. 2014; 21: 179–188. doi: 10.1245/s10434-013-3146-8 PMID: 23907312

34. Jabbour E, Kantarjian H. Chronic myeloid leukemia: 2014 update on diagnosis, monitoring, and management. Am J Hematol. 2014; 89: 547–556. doi: 10.1002/ajh.23691 PMID: 24729196

35. Pytel D, Sliwinski T, Poplawski T, Ferriola D, Majsterek I. Tyrosine kinase blockers: new hope for successful cancer therapy. Anticancer Agents Med Chem. 2009; 9: 66–76. PMID: 19149483

36. Leroy C, Robert B, Simon V, Roche S. The Abl tyrosine kinase inhibitor Nilotinib inhibits invasive properties of colon cancer cells by targeting the discoidin domain receptor 1. Abstract EJC supplements 8, no. 5 (2010).

5.1.5 Anlage – Teil 5

Host defense peptides for treatment of colorectal carcinoma - a comparative *in vitro* and *in vivo* analysis

www.impactjournals.com/oncotarget/ Oncotarget, Advance Publications 2014

Host defense peptides for treatment of colorectal carcinoma – a comparative *in vitro* and *in vivo* analysis

Claudia Maletzki[1], **Ulrike Klier**[1], **Samuel Marinkovic**[1], **Ernst Klar**[2], **Jörg Andrä**[3], **Michael Linnebacher**[1]

[1] Molecular Oncology and Immunotherapy, University of Rostock

[2] Department of General, Vascular, Thoracic and Transplantation Surgery, University of Rostock

[3] Department of Biotechnology, Hamburg University of Applied Sciences, Hamburg; Germany

***Correspondence to**: Michael Linnebacher, **email**: Michael.Linnebacher@med.uni-rostock.de*

Keywords: designer peptides, oncolytic therapy, individual tumor models

***Received**: April 15, 2014* ***Accepted**: May 27, 2014* ***Published**: May 29, 2014*

This is an open-access article distributed under the terms of the Creative Commons Attribution License, which permits unrestricted use, distribution, and reproduction in any medium, provided the original author and source are credited.

ABSTRACT

Host defense peptides (HDP) constitute effector molecules of the innate immune system. Besides acting against microbia and fungi, they exhibit broad and selective oncolytic activity. The underlying mechanism is at least partially attributable to elevated surface-exposed levels of phosphatidylserine (PS) on tumor targets. In this study, comprehensive analysis of NK-2-based derivatives (C7A, C7A-D21K, and C7A-Δ) was done on patient-derived ultra-low passage colorectal carcinoma (CRC) cell lines. Peptides were designed to improve antitumoral potential. Mellitin was used as positive control and a non-toxic peptide (NK11) served as negative control. Subsequently, effectiveness of local HDP application was determined in xenopatients.

Generally, CRC lines displayed a heterogeneous pattern of surface-exposed PS, which was usually below standard CRC cells. Of note, five out of seven cell lines were susceptible towards HDP-mediated lysis (lytic activity of peptides: C7A-D21K > C7A-Δ = C7A). Oncolytic activity correlated mostly with surface-exposed PS levels. Apoptosis as well as necrosis were involved in killing. In an *in vivo* experiment, substantial growth inhibition of HROC24 xenografts was observed after HDP therapy and, surprisingly, also after NK11 treatment.

These promising data underline the high potential of HDPs for oncolytic therapies and may provide a rationale for optimizing preclinical treatment schedules based on NK-2.

INTRODUCTION

Antimicrobial peptides, also referred to as Host defense peptides (HDP), have originally been identified as an alternative weapon against bacterial infections. This is particularly important, as clinical handling of multi-resistant bacterial variants is increasingly difficult. These peptides represent an ancient yet very effective part of the innate immune system as first line of defense against invading bacteria. They are ubiquitous in nature and were identified in a variety of multi-cellular organisms including insects, amphibians and mammals [1,2]. HDPs exhibit a unique mode of action. Due to their cationic amphipathic nature they preferentially bind to negatively charged membranes [3-5] – a common characteristic of bacterial membranes, thus making them a perfect HDP target. HDPs incorporate into the membrane bilayers and form pores in targeted membranes leading to unsustainable cell homeostasis [6,7]. Additionally, HDPs penetrate the cytoplasm and interact with essential intracellular molecules. Unlike commonly used antibiotics, these cationic peptides directly interact with the target cells' lipid matrix instead of a specific enzyme or receptor.

Drug resistance, either intrinsic or acquired, is a growing problem in cancer therapy, as well. Although recent years have seen major treatment advances, cancer is still the third leading cause of death worldwide [8]. Surgery, chemotherapy, and radiation are the methods of choice in oncological management. The major drawback

Table 1: Clinical characteristics of patients and molecular data of the corresponding tumor

Tumor-ID	Age/ Gender	Tumor location	TNM-Stage	Tumor type	Molecular type
HROC18	65/f	caecum	G2T2N0M0	primary adenocarcinoma	spStd
HROC24	98/m	colon ascendens	G2T2N0M0	primary adenocarcinoma	spMMR-D
HROC32	83/f	colon ascendens	G2T4N2M1	primary adenocarcinoma	spStd
HROC40	69/m	colon ascendens	G3T4N0M0	primary adenocarcinoma	CIMP-H
HROC60	71/m	colon ascendens	G2T2N0M0	primary adenocarcinoma	CIMP-H
HROC69	62/m	colon ascendens	G3T3NoMx	primary adenocarcinoma	spStd
HROC80	72/m	caecum	G2T3N2Mx	primary adenocarcinoma	spStd
HROC87	76/f	colon ascendens	G3T3N0M0	primary adenocarcinoma	spMMR-D
HROC107	81/f	colon ascendens	G3T3N0M0	primary adenocarcinoma	spMMR-D
HROC113	41/f	colon ascendens	G3T4N2Mx	primary adenocarcinoma	Lynch Syndrome

m – male, f – female, spStd – sporadic standard, spMMR-D – sporadic mismatch repair deficient, CIMP-H – CpG island methylator phenotype high, HNPCC – hereditary non-polyposis colorectal carcinoma

of the latter two is the missing selectivity between malignant and normal cells. Due to this unspecific toxicity most patients suffer from severe side effects. Additionally, there is growing evidence of multidrug resistant variants resulting for example from increased expression of multidrug resistance proteins. These proteins discharge antineoplastic drugs out of the cell and make them inefficient. This substantial problem emphasizes the necessity for developing new oncolytic agents.

It has become apparent that HDPs are not only effective against bacteria. Impressive results from pilot studies identified selective killing of malignant, but not normal cells by different HDPs [9-11]. Physiologically, the outer membranes of mammal cells consist of zwitterionic phosphatidylcholine and sphingomyelin without any net charges. The negatively charged phosphatidylserine (PS) is usually a component of the inner cell membranes' leaflet. Under certain conditions, like loss of membrane asymmetry or cellular apoptosis, PS can be shifted to the cell surface [12]. In this case, PS renders cells vulnerable to lysis by cationic peptides like HDPs. Quite a number of tumor cells exhibit increased levels of surface-exposed PS [13,14]. This feature clearly distinguishes malignant from normal cells and provides a rationale for HDP-based tumor therapy [15,16]. For that reason, this study aimed at testing the oncolytic potential of NK-2-based HDPs [17] against patient-derived colorectal cancer (CRC) cell lines in order to pave the way for further treatment optimizations based on these peptides.

RESULTS

Peptide design

Peptides (C7A, C7A-D21K, C7A-Δ and NK11) used in this study were based on NK-2 (Table 2 and [17]). The most basic modification entailed replacement of the non-functional sole Cys7 residue within the NK-2 sequence with an Ala residue (C7A). This substitution has been shown to improve anti-cancer cell activity of the lead structure NK-2 [17]. An enhancement of C7A´s positive net charge was achieved by substituting Asp21 by a Lys residue (C7A-D21K). Moreover, peptide C7A was shortened by deletion of a stretch of four amino acid residues (including Asp21), resulting in peptide C7A-Δ. In addition, we used melittin, the main lytic component of bee venom as a well-known reference compound, and NK11 as a non-toxic control peptide [21].

Membrane intercalation of peptides monitored by FRET spectroscopy

FRET spectroscopy served as a sensitive tool to detect lipid dependence of the membrane interaction of antimicrobial peptides. For this, all peptides were added to liposomes consisting of zwitterionic PC alone, of a mixture of PC and of negatively charged PS, as well as of pure PS (Figure 1). All lipid vesicles were doped with donor and acceptor dyes, peptides were added, and the emission intensities of both dyes were monitored over time. An increase of the fluorescence intensity of the donor (I_{Donor}) and a simultaneous decrease of the fluorescence intensity of the acceptor dye ($I_{Acceptor}$), i.e. a reduced FRET efficacy, indicated an increase in the overall mean distance between labeled phospholipids, and corresponded to an insertion of peptides into the lipid bilayer. For clarity, the $I_{Donor}/I_{Acceptor}$ ratio is shown (Figure 1).

Insertion kinetics are shown representatively for peptide C7A-D21K (Figure 1A-C) and the maximum increase of $I_{Donor}/I_{Acceptor}$ is depicted for all peptides in figure 1D-F. In general, negatively charged PS triggers membrane intercalation of all peptides. With the exception of melittin, no considerable intercalation was observed into pure PC liposomes. Upon addition of peptides to liposomes, we observed an immediate increase of the $I_{Donor}/I_{Acceptor}$ ratio, demonstrating a rapid interaction kinetic (Figure 1B, C). Intercalation of the NK-2 derivatives C7A, C7A-D21K, and C7A-Δ was pronounced into pure PS bilayers (Figure 1C, F) and slightly impaired into PC bilayers containing 10% PS (Fig. 1B, E). NK11 interaction was visible only with pure PS vesicles, but negligible with other liposomes.

PS expression on tumor cells

As a first step towards identifying HDP-susceptible cells, level of surface-exposed PS was determined using our panel of low-passage CRC cell lines. For better estimating PS levels, amounts of AnnexinV bound to normal lymphocytes (PBL) and standard CRC cell lines (HCT116, SW48, TC71 and HDC114) were determined

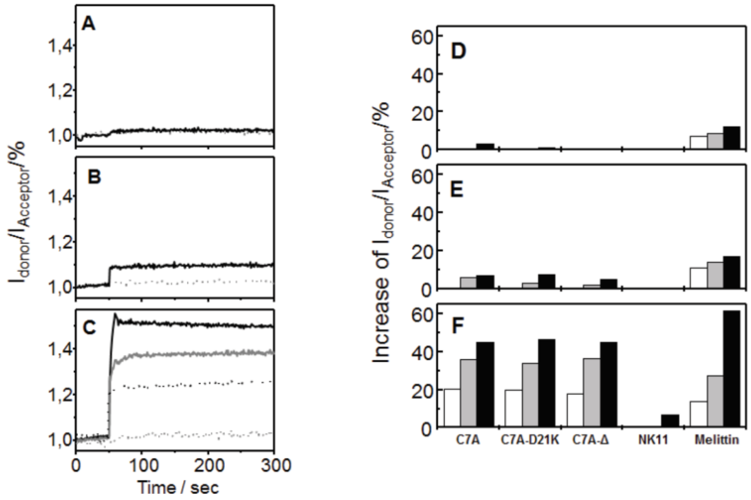

Figure 1: FRET spectroscopy. (A-C) Binding to and insertion of peptide C7A-D21K into phospholipid membranes. (A) C7A-D21K was added at time point 50 s to liposomes (10 µM) consisting of pure PC, (B) a 90:10 molar mixture of PC:PS, and (C) of pure PS, each doubly doped with the fluorescently labeled FRET pair NBD-PE (donor) and rhodamine-PE (acceptor). Intercalation was monitored by measuring donor and acceptor fluorescence emission intensities. For better visualization only the quotient ($I_{Donor}/I_{Acceptor}$) is shown. Addition of the peptide solvent alone had no effect (dotted grey line). Peptide concentrations used: 0.2 µM (dotted black line, only in C), 0.4 µM (solid grey line, only in C), and 0.8 µM (solid black line). (D-F) Binding to and insertion of peptides at different concentrations into phospholipid membranes. (A) Peptides were added to liposomes consisting of pure PC, (B) a 90:10 molar mixture of PC:PS, and (C) of pure PS, each doubly doped with the fluorescently labeled phospholipid FRET pair NBD-PE (donor) and rhodamine-PE (acceptor). Intercalation was monitored by measuring donor and acceptor fluorescence intensities. The relative increase of the $I_{Donor}/I_{Acceptor}$ ratio 250 s after peptide addition is shown (Increase of $I_{Donor}/I_{Acceptor}$ (%) = ($I_{Donor}/I_{Acceptor}$ (peptide) - $I_{Donor}/I_{Acceptor}$ (control))*100). Peptide concentrations used: 0.2 µM (open bars), 0.4 µM (grey bars), and 0.8 µM (black bars).

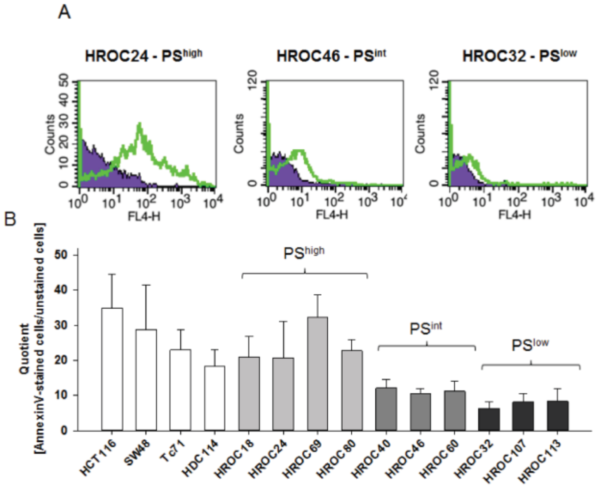

Figure 2: Flow cytometric analyses. Surface-bound PS was detected on CRC cell lines following staining with APC-labeled AnnexinV. (A) Representative histograms of AnnexinV-stained tumor cells (thick green line) and corresponding unstained controls (filled purple histogram). (B) Amounts of surface-bound PS were quantified by calculating the quotient of the mean fluorescence intensities (MFI) from unstained cells versus AnnexinV-stained cells. Results show data of three independent experiments (mean ± SD).

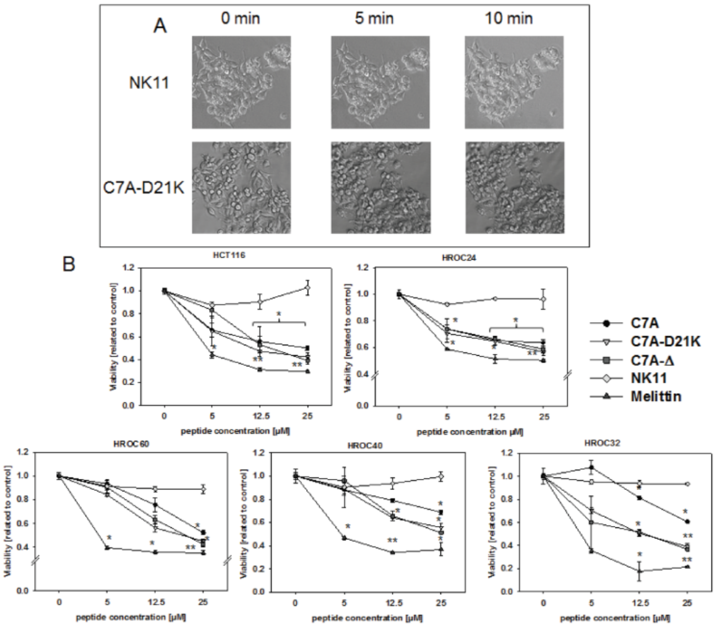

Figure 3: Short-term exposure of HDPs towards tumor cells. (A) Representative pictures showing morphological changes in HROC24 cells upon HDP C7A-D21K exposure (25 µM). As a control, HROC24 cells were treated with NK11 (25 µM). (B) Quantitative analysis of direct cytotoxicity towards tumor cells. Tumor cells were treated for 1h with increasing HDP concentrations. Thereafter, viability was assessed using Calcein-AM staining. Remaining viable tumor cells were quantified in comparison to untreated controls, which were set to be =1. Results show data of three separate experiments. Values are given as the mean x-fold increase ± SD, *p<0.05 vs. NK11; **p<0.01 vs. NK11.

Table 2: Amino acid sequences of synthetic peptides used in this study

Peptide		Sequence1	Net charge2
	NK-2	KILRGVCKKIMRTFLRRISKDILTGKK	+10
#1	C7A	KILRGVAKKIMRTFLRRISKDILTGKK	+10
#2	C7A-D21K	KILRGVAKKIMRTFLRRISKKILTGKK	+12
#3	C7A-Δ	KILRGVAKKIMRTFLRR ILTGKK	+10
#4	NK11	KISKRILTGKK	+6
#5	Melittin	GIGAVLKVLTTGLPALISWIKRKRQQ	+6

1all peptides were synthesized with an amidated C-terminus
2The net charge of the peptides was calculated by subtracting the number of Asp residues (the only negatively charged amino acid residues present in the peptides) from all the positive charges (Lys, Arg and the peptide´s N-terminus). Since the C-terminus of all peptides used was amidated, it did not bear a negative charge.

as well.

Analysis revealed striking differences between individual cell lines, ranging from high (e.g. HROC69 and HROC80) to low (e.g. HROC32 and HROC107) surface-exposed PS. When comparing with established standard CRC lines, PS levels tended to be lower (Figure 2). However, fluorescence intensity was always higher than on normal lymphocytes that displayed PS at extremely low level (quotient ≤3; data not shown). Starting from these findings, CRC lines were classified as high, intermediate

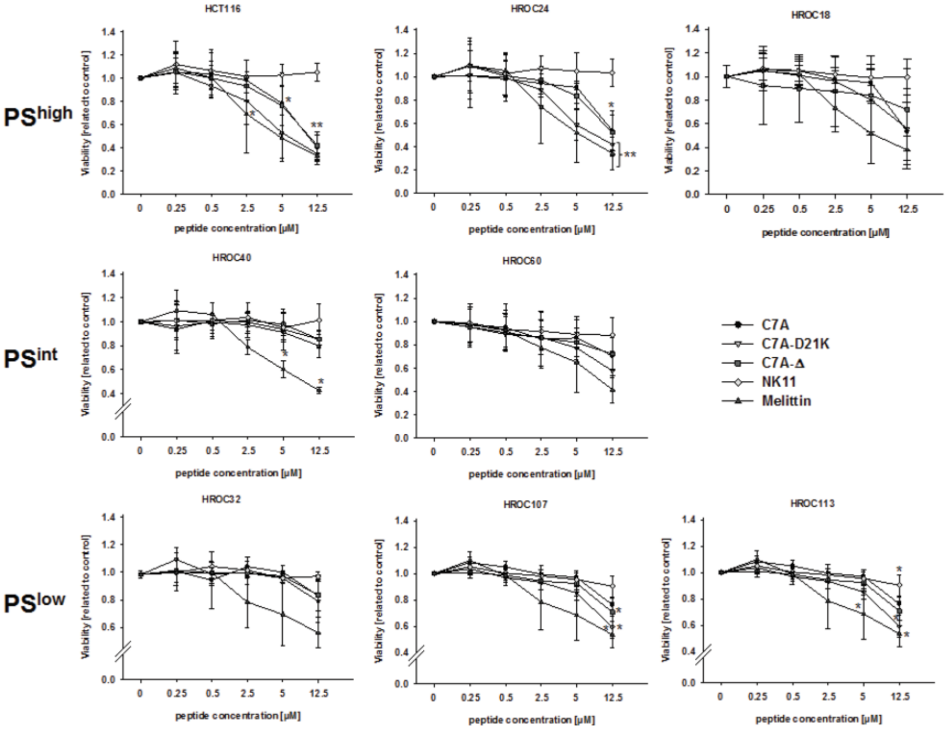

Figure 4: HDP-mediated cytotoxicity towards tumor cells. Quantitative analysis of direct cytotoxicity towards tumor cells following a 24h incubation period with increasing HDP concentrations. Viability was assessed using Calcein-AM staining. Remaining viable tumor cells were quantified in comparison to untreated controls, which were set to be =1. Results show data of three separate experiments. Values are given as the mean x-fold increase ± SD. *p<0.05 vs. NK11; **p<0.01 vs. NK11.

(int) or low PS-harboring cells (Figure 2).

Response to HDPs according to PS-expression status

To prove growth inhibiting and cytotoxic activity of newly designed NK-2 analogues, tumor cells were exposed to increasing peptide concentrations for 1h and 24h, respectively. According to our classification, we included three PS^{high} (HCT116, HROC18, and HROC24), three PS^{int} (HROC40, HROC60, and HROC113), and two PS^{low} (HROC32 and HROC107) surface-exposed cell lines.

Short-term exposure revealed strong response towards all peptides, with, however, cell line specific susceptibility (Figure 3). Morphological changes even appeared after a 10 min incubation period (representative pictures for HROC24 exposed to peptides C7A and NK11, respectively, are displayed in Figure 3A). Unspecific killing was excluded by lack of NK11-mediated tumor cell lysis (Figure 3).

Next, response after longer treatment schedules, i.e. 24h was examined. These analyses principally confirmed results from short-term exposure. HCT116 and HROC24 cells responded best; all tested HDPs exerted lytic activity towards these two cell lines (Figure 4). Of note, these peptides (C7A, C7A-D21K and C7A-Δ) were as effective as the reference compound Mellitin. HROC60 cells showed weaker though still noticeable vulnerability. In this cell line, obvious killing was obtained for C7A-D21K (>40% lysis vs. control). By contrast, HROC40 cells were relatively resistant towards HDP-induced lysis, even at high concentration (12.5 µM). When analyzing susceptibility of PS^{low} cell lines varying effects were obtained (Figure 4). Viability of HROC107 and HROC113

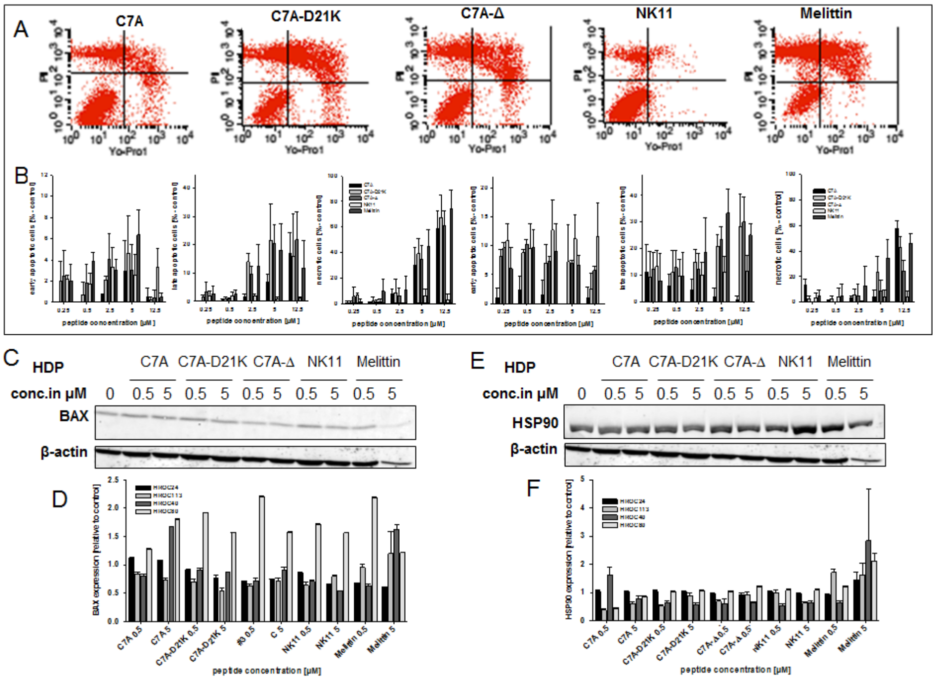

Figure 5: Apoptosis/necrosis assay and Western blot analysis. (A, B) HROC18 and HROC24 cells were exposed to increasing HDP concentrations for a period of 24 hours. Tumor cells were stained with YO-PRO-1 for detecting early and late apoptotic tumor cells. Prior to flow cytometric analysis, PI was added to detect necrotic cells, as well. (A) Representative dot plots showing HDP-treated HROC24 cells at a concentration of 5 µM. Lower right quadrant: early apoptotic cells; upper right quadrant: late apoptotic cells; upper left quadrant: necrotic cells. (B) For cell death quantification, values of background cell death (=untreated controls) were subtracted from values of HDP-treated cells. Upper panel: HROC24 cell; lower panel: HROC18 cells. (C, E) Representative western blot results showing HDP-treated HROC24 cells (20 µg of total protein per lane). (D, F) Quantitative analysis of BAX and HSP90 expression in HDP-treated cells was done as described in material & methods. Expression levels of untreated cells were set to be =1 and x-fold increases of HDP-exposed cells were calculated. Results show data of three separate experiments. Values are given as mean ± SD.

cells decreased dose-dependently. Of note, C7A-D21K proved to be most effective in killing these tumor cells. HROC32 cells did not respond well to HDPs. Overall, these observations are indicative for partial involvement of PS in the oncolytic action of HDPs.

Predominant necrosis induction by HDPs

To gain deeper inside into the type of cell death induced by HDPs, selected tumor cell lines (namely HROC24 and HROC18, both PS^{high}) were subjected to flow cytometric apoptosis/necrosis analysis. Using this test, we observed predominantly necrosis in both cell lines. Early apoptotic cells (YO-PRO-1^{+}/PI^{-}) were found at all concentrations (0.25 - 2.5 µM). However, levels were

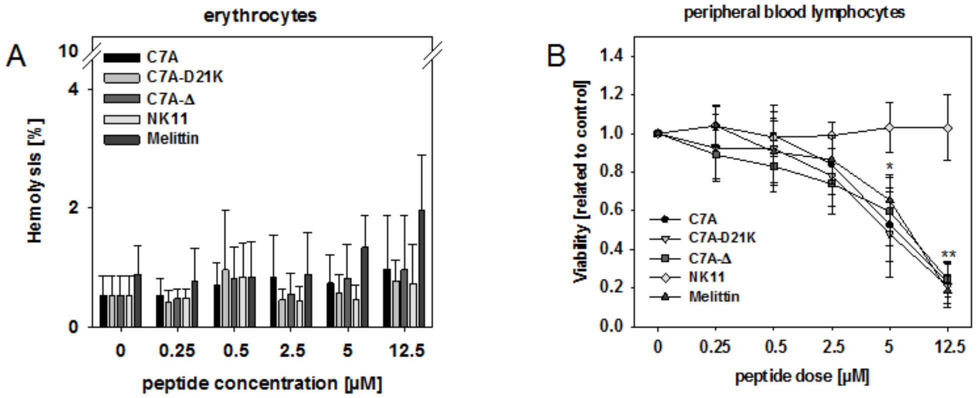

Figure 6: Hemolysis and lymphotoxicity assays. (A) Hemolytic activity of HDPs was determined by hemoglobin release from whole blood cells after 120 min incubation. Negative controls were left untreated whereas positive controls (=maximum lysis) were treated with 1% SDS. Hemolytic activity was quantified as described in the material and methods section. (B) PBLs were incubated in the presence of increasing HDP concentrations for a period of 24 hours. Viability was analyzed using Calcein-AM and quantified in comparison to untreated controls, which were set to be =1. Results show data of six different healthy donors. Experiments were performed in triplicates. Values are given as the mean x-fold increase ± SD.

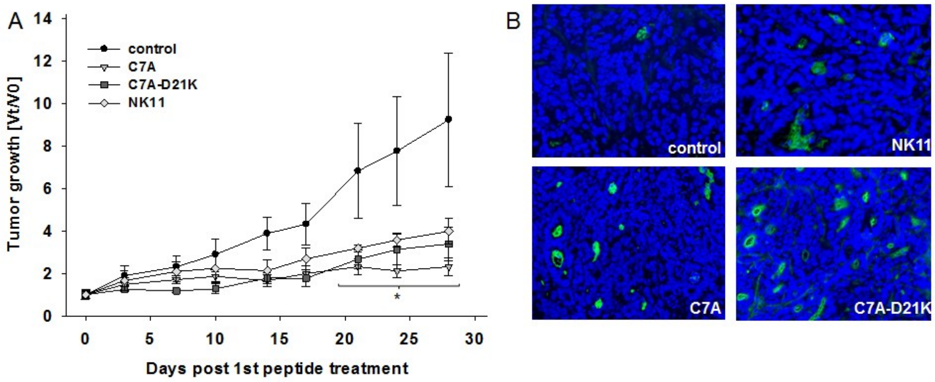

Figure 7: *In vivo* growth kinetics and tumor cell apoptosis of HROC24 tumors in NMRI Foxn1^{nu} mice with or without local treatment. (A) Therapy was performed by repetitive local application of HDPs C7A or C7A-D21K (1 mg/kg bw) every third day (a total of 9 injections) (n=5 per group). Tumor-carrying control animals received either equivalent volumes of peptide NK11 or saline (n=5 per group). Tumor volumes are given as x-fold increase vs. day 0 (V_t/V_0) (start of treatment) ± SD. *p<0.05 vs. PBS. (B) Representative immunofluorescence staining of apoptotic cells within HROC24 tumors. Cryopreserved tumor sections were stained with anti-M30 CytoDeath antibody, followed by anti-mouse IgG FITC antibody and nuclear DAPI as described in material and methods.

always below 20 % (Figure 5A, B). Higher concentrations increased the number of late apoptotic (YO-PRO-1$^+$/PI$^+$) and necrotic (YO-PRO-1$^-$/PI$^+$) cells, respectively. Levels of viable HROC24 cells fell to 17% (C7A-D21K and C7A-Δ) and 25 % (C7A). Here again, peptides C7A-D21K and C7A-Δ proved to be as effective in tumor killing as melittin. HROC18 cells presented with marginally lower lysis. In this cell line, C7A-D21K was the most effective one and even slightly better than melittin (74 vs. 71 % total killing; Figure 5B). Peptides C7A and C7A-Δ killed up to 60% of cells.

Subsequent western blot analysis principally confirmed that necrosis is the primary reason for HDP-mediated cell death. Protein expression levels of Bax and HSP90 remained largely unchanged in HDP-responsive cell lines (e.g. HROC24, HROC40, and HROC113; representative blots for HROC24 are given in Figure 5C). The sole exception was seen for melittin. Here, HSP90 expression was dose-dependently induced (Figure 5D). Cleaved PARP was not detectable at all.

HDPs exert no hemolytic, but lymphotoxic effects *in vitro*

To examine if the observed lytic effects were tumor-specific, whole blood was cultured in the presence of increasing peptide concentrations for 24h. Experiments revealed absent or minimal hemolysis, with values below 20% even at high concentration (i.e. melittin, dose: 12.5 µM, Figure 6A). In sharp contrast, all peptides reduced viability of lymphocytes in a dose-dependent manner (Figure 6B). Effects were most likely specific since NK11 did not affect lymphocyte viability. Lymphotoxicity was independent from donor and gender.

HDP-mediated tumor growth arrest *in vivo* is accompanied by increased tumor cell apoptosis

Finally, a proof of concept experiment was done *in vivo*. Female NMRI Foxn1^{nu} mice were inoculated with HROC24 cells, the cell line that showed highest vulnerability towards HDP-mediated killing *in vitro*. Mice with established xenografts received repetitive local injections of either peptide C7A or C7A-D21K. NK11 served as negative control. Melittin, which was applied as positive control *in vitro*, was excluded from this experiment due to its suspected high toxicity.

All treatment schedules were well tolerated by mice, with no adverse side effects, like weight loss, anemia, or ataxia. Application of peptide C7A demonstrated most effectiveness (Figure 7A). Tumors immediately reduced growing and macroscopically started to break up (in 4/5 cases). Of note, this arrest was evident until the end of experiments. A comparable initial delay was obtained following peptide C7A-D21K therapy (Figure 7B). HROC24 xenografts presented with strong growth retardation, though tumor growth was not completely impeded, especially at later time points (day 17). Opposed to C7A-treated tumors, no ulceration was observed. Finally, tumor sizes reached 3.4-fold increases (vs. PBS control: 10.3-fold). However, obtained effects were rather independent from specific NK-2 therapy, since control peptide NK11 induced tumor growth retardation as well. Though growth delay occurred to a lesser extent as compared to peptides C7A and C7A-D21K, there was still a significant effect (4-fold vs. PBS control: 10.3-fold, $p<0.05$). This finding was completely unforeseen since no antitumoral effects were found *in vitro*.

In line with the observed growth inhibition, all HDP-treated tumors showed marked increased levels of apoptotic tumor cells (Figure 7B). As given by positive M30 CytoDeath staining, apoptosis was most strongly induced in peptides C7A and C7A-D21K treated tumors, respectively. Tumors that had been exposed to peptide NK11 showed elevated cytokeratin 18 cleavage, as well. Besides, all HDP-treated tumors were considerably more necrotic than their untreated counterparts (data not shown).

DISCUSSION

HDPs have gained much attention as alternatives to conventional chemotherapeutics; they bypass multidrug-resistance mechanisms and exert additive oncolytic effects in certain combinations [22, 23]. Due to the limited number of experimental preclinical studies, we here analyzed HDP action on a series of ultra-low passage, patient-derived CRC cell lines. These cells provide ideal models for testing novel drugs, since they closely resemble the original tumors' molecular and biological signature [19, 24]. HDPs applied in this study were based on NK-2, a porcine immune cell-derived peptide, whose selective killing of different human cancer lines is well established [10]. NK-2 derivatives exhibit reduced sensitivity towards oxidation, show improved antibacterial and –most importantly– oncolytic activity [17].

NK-2 associated cytotoxicity was shown to be at least partially attributable to preferential binding towards surface-exposed PS. In this study, varying levels of surface-bound PS were detected on our freshly established CRC lines, ranging from high (e.g. HROC24) to very low (e.g. HROC32) levels, close to normal lymphocytes. Amounts of surface-exposed PS were independent from (I) molecular CRC subtype, i.e. chromosomal/microsatellite instability or CpG-island and methylator phenotype, that have been found to that impede drug response [25, 26]; (II) the corresponding mutational profile (i.e. K-ras, B-raf, p53, APC status); or (III) clinicopathological parameters (gender, age, TNM stage). Besides, there was no change over serial passages (at least from passage 10-50; data not shown), indicating that each tumor line harbors its own individual PS profile. Nonetheless, we occasionally observed differences between our patient-derived and "long-term" established standard cell lines, with tendency towards higher surface-exposed PS on the latter. On a basis of this initial finding, functional analyses were done for defining HDP-sensitivity and to test if the above mentioned mechanism also accounts for CRC lysis. Of note, all three newly designed NK-2 analogues (C7A, C7A-D2K1 C7A-Δ) exhibited antitumoral activities, even after short-term treatment schedules (1h). Although there was a trend towards higher susceptibility of cells displaying high PS surface-exposed levels (e.g. HROC24), vulnerability towards HDPs was more likely cell line and peptide specific. Two out of seven cell lines were completely resistant towards HDP-mediated lysis (i.e. HROC40^{int} and HROC32^{low}). Generally, derivative C7A-D21K proved to be most effective in killing CRC lines. Hence, substituting Asp^{21} by a Lys residue yielded higher antitumoral potential. Peptide C7A-Δ, which is a shortened form of C7A-D21K, presented with killing potential, as well. By deleting four amino acids (including anionic Asp^{21} and cationic Lys^{20}), the peptides' oncolytic activity was maintained. Moreover, these results provide evidence for the active domain to be within this region.

Overall, our findings indicate partial PS-dependent killing; yet, other mechanisms are likely to be involved as well. As a consequence of HDP-associated cell injury, apoptosis and necrosis play a role in cell death [10, 22, and 27]. Quite in line, we here also observed both modes with a prevalence of necrosis. The rapid killing kinetic (<1h) of NK-2 based derivatives further supports this finding. This strong membranolytic effect should even make it difficult for tumor cells to develop resistance. This is of particular meaning, since acquired resistance to (targeted) cancer therapies is increasingly observed in the clinics and represents a major problem [28].

A rather unexpected observation of the current study was the massive cytotoxicity against normal lymphocytes. Although erythrocytes were not affected by HDPs, viability of lymphocytes dramatically decreased upon HDP-exposure. This is in sharp contrast to previous studies in which lymphotoxicity for NK-2 was designated to be low or absent [10]. However, cytotoxicity towards the vascular system has been demonstrated for some HDPs [22]. Cathelicidin (=LL-37), an antimicrobial protein that is produced by leukocytes, epithelial, and mucosal cells is cytotoxic to human oral squamous carcinoma cells, but also to human PBLs [29]. Comparable results were reported for BMAP-27 & BMAP-28. These HDPs cause apoptosis of leukemic cells, but also hemolysis of red blood cells [30]. Though this finding may limit *in vivo* applicability, we still wanted to address the question whether NK-2 based analogues have the potential to control tumor disease *in vivo*. So far, only few studies described successful *in vivo* application of oncolytic HDPs in general [16, 27, 31] and neither applied NK-2 and/or derivatives thereof. Here, immunocompromised nude mice were engrafted with HROC24 cells. This cell line was chosen on the basis of *in vitro* responsiveness and reliable engraftment [19]. A total number of nine intratumoral injections of peptide C7A or C7A-D21K resulted in a notable tumor growth delay; tumors even stopped growing for several days and remained significantly smaller than PBS-treated control tumors. This growth inhibition was accompanied by increased induction of cellular apoptosis. Of note, no adverse side effects, like hemolysis or lymphotoxicity, were found. These peptides could thus be identified as potent and well tolerable antitumoral compounds. This is particularly important since doses applied here were lower than most of the published ones for HDPs [27, 31]. Hence, tumor growth control might be the result of: (I) suppressed tumor cell proliferation (i.e. reduced Ki-67 expression); (II) direct tumor cell killing (most likely via necrosis); and (III) angiogenesis inhibition.

Contrary to our expectations, NK11 application also affected HROC24 tumor growth *in vivo*. NK11 is an 11-residue derivative that was applied as an inactive and thus nontoxic control. Nonetheless, HROC24 xenograft growth was significantly impaired by this protein. Additionally to the fact that prior studies on HDPs excluded control peptides [16, 27, 31, and 32], several reasons might explain this observation: Firstly, the applied doses *in vitro* differed from those given *in vivo*. Secondly, NK11 was injected repetitively *in vivo*, while it was only once given to the cell culture. Thirdly, HDPs are known to be potent immune stimulators, especially of the innate immune system; hence unspecific immune activation is very likely.

We therefore propose the following model: local application of HDPs mediates rapid killing of tumor cells. However, the tumor microenvironment (including stromal cells) prevents parts of the tumor from lysis. Due to their natural behavior, HDPs enter the bloodstream and are recognized by the hosts' immune system, primary macrophages and NK cells. As a consequence, cells of the immune systems' innate arm infiltrate tumors. This proinflammatory local milieu helps controlling tumor growth transiently. Due to the lack of adaptive immune cells in nude mice, specific immune responses cannot be induced, preventing xenografted tumors from being completely eradicated. It is therefore conceivable that NK-2 and its derivatives exert substantially stronger antitumoral effects in immunocompetent hosts. Hence, oncolytic designer HDPs represent a very promising tool for inclusion into (chemotherapy-based) combinatorial treatment strategies. Due to the potentially rather unspecific mode of action, initial clinical studies should focus on intratumoral application.

MATERIAL AND METHODS

Tumor cell lines, lymphocyte preparation and culture media

CRC cell lines HROC18, HROC24, HROC32, HROC40, HROC57, HROC60, HROC69, HROC80, HROC87, HROC107, and HROC113 were established in our lab from patients subsequent to surgical resection. Molecular characterization was performed as described before 18,19]. Clinical characteristics of patients and molecular data of the corresponding tumor can be gathered from Table 1. The CRC cell line HCT116 (Kras^{mut}, Braf^{wt}) was originally obtained from the German collection of cell cultures (DSMZ; Braunschweig, Germany) and routinely cultured in our lab. For some experiments, established CRC lines SW48 (Kras^{mut}, Braf^{wt}), TC71, and HDC114 (both Kras^{wt}, Braf^{wt}) were included as well. Cells were maintained in full medium: DMEM/HamsF12 supplemented with 10% fetal calf serum (FCS), glutamine (2 mmol/L) and antibiotics (medium and supplements were purchased from PAA, Cölbe, Germany). Peripheral blood lymphocytes (PBL) were obtained from healthy volunteers following Ficoll density-gradient centrifugation (n=6).

Synthetic Peptides

All peptides were synthesized with an amidated C terminus by the Fmoc solid-phase peptide synthesis technique on an automatic peptide synthesizer (model 433 A, Applied Biosystems; Darmstadt, Germany) and purified by HPLC as described [20]. Peptide stock solutions (1 mM) were prepared by solubilization of the purified and lyophilized peptides in 0.01% trifluoroacetic acid and were stored at -20°C.

Lipids

Natural phospholipids L-α-phosphatidylcholine (PC) from hen egg and L-α-phosphatidylserine (PS) from porcine brain were purchased from Avanti Polar Lipids (Alabaster, AL, USA). Fluorescently labeled phospholipids N-(7-nitrobenz-2-oxa-1,3-diazol-4yl)-phosphatidylethanolamine (NBD-PE) and N-(lissamine rhodamine B sulfonyl)-phosphatidylethanolamine (rhodamine-PE) were from Molecular Probes (Eugene, OR, USA). Lipid stock solutions were prepared in chloroform.

Förster resonance energy transfer (FRET) spectroscopy

Intercalation of peptides into liposome membranes was determined FRET spectroscopy applied as a probe dilution assay. Liposomes were prepared by dissolving appropriate lipid mixtures (pure PC, a 90:10 molar mixture of PC:PS, as well as pure PS, each doped with 1% of the donor dye NBD-PE and 1% of the acceptor dye rhodamine-PE) in chloroform and drying them under a gentle stream of nitrogen. The resulting lipid film was dispersed in 20 mM HEPES, 150 mM NaCl, pH 7.4, sonicated for 30 min and subjected to 3-4 temperature cycles from 4 to 60°C with an incubation period of 30 min at each step. Lipid dispersions were stored at 4°C overnight before use. For the assay, donor fluorescence (NBD) was excited at 470 nm, and donor (NBD, ID at 531 nm) as well as acceptor (rhodamine, IA at 593 nm) emission intensities were monitored over time. An increase of the ratio of the donor fluorescence intensity to that of the acceptor fluorescence intensity ($I_{Donor}/I^{Acceptor}$) was interpreted as a membrane intercalation event. This ratio depends on the Förster efficiency, therefore a rising value means that the mean distance separation of donor and acceptor dyes is raising. The assay was performed at 37°C.

AnnexinV staining of tumor cells and lymphocytes

AnnexinV staining was applied for detection of surface-exposed phosphatidylserine (PS) on tumor cells. Controls included lymphocytes from healthy volunteers. Cells (2×10^5 cells/tube in PBS with Ca^{2+}/Mg^{2+}) were stained with APC (Allophycocyanin-) labeled AnnexinV (5 µl/tube, Immunotools, Friesoythe, Germany) for 20min at 4°C. Cells were washed, resuspended in 200 µl PBS and subjected to flow cytometric analysis, which was always performed on a FACSCalibur Flow Cytometer (BD Pharmingen, Heidelberg, Germany). Data analysis was performed from 20.000 events of each sample using CellQuest software (BD Pharmingen). Dying or dead cells were excluded by propidium iodide (PI). PI (1 mg/ml) was applied directly to cells prior to measuring. Amounts of surface-exposed PS were quantified by calculating the quotient of the mean fluorescence intensities (MFI) from unstained cells versus AnnexinV-stained cells.

Cell viability staining

This assay is based on Calcein-acetoxymethylester (Calcein-AM; Invitrogen, Darmstadt, Germany) staining to detect viable cells within a culture. Tumor and normal (PBL) cells ($1\text{-}2 \times 10^4$ cells/well in triplicates) were seeded in 96-well plates and incubated overnight. Thereafter, peptides were added in increasing concentrations (ranging from 0.25 µM – 12.5 µM). Untreated cells served as living cell control. Medium was removed after 1h or 24h, respectively. Calcein-AM (4 mM) was added and incubated for 30 min (37°C, 5% CO$_2$). Analysis was performed on a fluorescence multi-well plate reader (Tecan i Infinite® M200, Crailsheim, Germany) at an excitation wavelength of 485 nm (emission 535 nm). For estimation of cell viability, the relative fluorescence intensities of Calcein-AM-stained non-treated cells (=live control) were set to be 1, and fluorescence intensities of samples were calculated. Data of at least three independent experiments each performed in duplicates are given.

Apoptosis/necrosis assay

Cell death was quantified by YO-PRO-1 (Invitrogen) and PI double staining. Selected tumor cells (HROC24 and HROC18, 1 x 10^4 cells/well) were seeded in 24-well plates and incubated overnight. Thereafter, peptides were added in increasing concentrations (ranging from 0.25 µM – 12.5 µM). Untreated cells served as living control. Following a 24-hour incubation period, supernatants were collected; cells were trypsinized and washed in PBS. Cells were stained with YO-PRO-1 (final concentration: 0.2 µM) for 20 min at room temperature. Prior to flow cytometric analysis, PI was added at a final concentration of 100 µg/ml. For cell death quantification, values of background cell death (=untreated controls) were subtracted from values of HDP-treated cells.

Hemolysis assay

Hemolytic activity of HDPs was determined by hemoglobin release from whole blood cells after 120 min incubation. Briefly, whole blood of healthy donors (n=6) was seeded in 96-well plates and supplemented with HDPs at given concentrations (ranging from: 0.25 µM – 12.5 µM). Negative controls were left untreated and positive controls (=maximum lysis) were treated with 1% SDS. Following the incubation period, cell-free supernatants were transferred into a new 96-well plate and absorption was measured on a plate reader at 540 nm (reference wave length: 690 nm). Hemolytic activity was quantified according to the following formula:

$$\% \text{ hemolysis} = ((OD_{540nm\ sample} - OD_{540nm\ buffer})/OD_{540nm\ max} - OD_{540nm\ buffer}) * 100$$

Western Blot analysis

Cellular protein extracts were obtained from HDP-treated and control cells following incubation with lysis buffer (1 M Tris, pH 7.5, 5 M sodium chloride, 0.25 M ethylenediaminetetraacetic acid, 10% (v/v) triton-x 100, 4% (v:v) sodium azide, 0.1 M phenylmethanesulfonylfluoride, protease inhibitor cocktail (Roche, Mannheim, Germany)) on ice for 30 min. Cell lysates were centrifuged by 10.000×g for 10 min at 4°C. Protein concentration was determined using BCA Protein assay kit (Merck Calbiochem, Darmstadt, Germany) according to manufacturer's instructions. Proteins (20 µg) were separated on a 14% SDS-polyacrylamide gel and transferred to polyvinylidene fluoride membranes. Membranes were blocked for 1h with blocking buffer (Rockland, Gilbertsville, PA) prior to incubation with primary antibodies against Bax, cleaved PARP, HSP90, and β-actin (all New England Biolabs, Frankfurt am Main, Germany). IRDye® 800 CW- and IRDye® 680 CW-conjugated secondary antibodies (LI-COR-Biosciences, Bad Homburg, Germany) were applied for 30 min. Blots were scanned at a wavelength of 700 nm (for detecting IRDye® 680) and at a wavelength of 800 nm (for detecting IRDye® 800 CW) using an Odyssey® Infrared Imaging System (LI-COR-Biosciences). Signal integrated intensities were quantified applying the Odyssey® software version 3.16. Probes were normalized by calculating the ratio of the corresponding target protein to β-actin signal.

In vivo tumor models and treatment regimen

Experiments were performed on female 8–10-week old NMRI Foxn1^{nu} mice (Charles River, Sulzfeld, Germany) weighting 18-20 g. All animals were fed standard laboratory chow and given free access to water. Trials were performed in accordance with the German legislation on protection of animals and the Guide for the Care and Use of Laboratory Animals (Institute of Laboratory Animal Resources, National Research Council; NIH Guide, vol.25, no.28, 1996). NMRI Foxn1^{nu} mice were challenged with 5 x 10^6 HROC24 cells. Mice with established subcutaneous (s.c.) tumors received repetitive local injections of peptide C7A or C7A-D21K (1mg/kg bw, dissolved in 50 µl) every third day (a total of 9 injections) (n=5 per group). As control, tumor-carrying mice either received NK11 (1mg/kg bw, dissolved in 50 µl) or saline (50µl volume, n=5 per group). Tumor growth was controlled three times a week at time point of HDP injection and tumor volume was estimated according to the formula: V= width^2 * length * 0.52.

Tumor carrying mice were sacrificed at day 28 or when they became moribund before the tumor volume reached 2.000 mm^3. At the end of each experiment, tumors, blood and spleens were collected from the animals of all groups for further analysis.

Phenotyping of murine immune cells was conducted from blood samples and spleens, following lysis of erythrocytes in lysis buffer (0.17 M Tris, 0.16 M NH$_4$Cl) and labeling with the following FITC-conjugated rat anti-mouse mAbs: CD11b, γ/δ TCR, and CD69 (1µg, Immunotools), hamster anti-mouse mAbs: CD11c (1 µg, Miltenyi Biotec, Bergisch-Gladbach, Germany) and PE-conjugated rat anti-mouse mAbs: Gr1 (Ly6G), CD62L (Immunotools), and CD166 (ebioscience, Frankfurt, Germany). Negative controls consisted of spleen and blood lymphocytes stained with the appropriate isotypes (Immunotools).

Immunofluorescence

To study apoptotic cell death *in vivo*, 4 µm sections of HDP-treated and control tumors were mounted on poly-L-lysine-coated-slides. Following fixation in ice-cold methanol and blocking with 2% BSA (1h), cells were incubated with mouse anti-M30 CytoDeath antibody according to the manufacturer's instructions (Roche, Mannheim, Germany). A FITC-labeled anti-mouse IgG antibody was used as secondary antibody (Dako Envision Link, Hamburg, Germany). Cell nuclei were stained with DAPI and slides were embedded in mounting medium (Dako). Apoptotic cells were detected using a fluorescence microscope (Olympus, Münster, Germany).

Statistical analysis

All values are expressed as mean ± SD. After proving the assumption of normality, differences between controls and treated animals were determined by using the unpaired Student's *t*-test. If normality failed, the non-parametric Mann-Whitney *U*-Test was applied. The tests were performed by using Sigma-Stat 3.0 (Jandel Corp, San Rafael, CA). The criterion for significance was set to $p<0.05$.

ACKNOWLEDGEMENTS

Financial support of the Deutsche Forschungsgemeinschaft (AN301/5-1) is appreciated.

REFERENCES

1. Zasloff M. Antimicrobial peptides of multicellular organisms. Nature. 2002; 415: 389-399.
2. Steinstraesser L, Kraneburg UM, Hirsch T, Kesting M, Steinau HU, Jacobsen F, Al-Benna S. Host defense peptides as effector molecules of the innate immune response: a sledgehammer for drug resistance? Int J Mol Sci. 2009; 10: 3951-3970.
3. Shai Y. Mechanism of the binding, insertion and destabilization of phospholipid bilayer membranes by alpha-helical antimicrobial and cell non-selective membrane-lytic peptides. Biochim Biophys Acta. 1999; 1462: 55-70. Review.
4. Schröder-Borm H, Willumeit R, Brandenburg K, Andrä J. Molecular basis for membrane selectivity of NK-2, a potent peptide antibiotic derived from NK-lysin. Biochim Biophys Acta. 2003; 10: 164-171.
5. Iwasaki T, Ishibashi J, Tanaka H, Sato M, Asaoka A, Taylor D, Yamakawa M. Selective cancer cell cytotoxicity of enantiomeric 9-mer peptides derived from beetle defensins depends on negatively charged phosphatidylserine on the cell surface. Peptides. 2009; 30: 660-668.
6. Cruciani RA, Barker JL, Zasloff M, Chen HC, Colamonici O. Antibiotic magainins exert cytolytic activity against transformed cell lines through channel formation. Proc Natl Acad Sci U S A. 1991; 88: 3792-3796.
7. Bechinger B. Structure and functions of channel-forming peptides: magainins, cecropins, melittin and alamethicin. J Membr Biol. 1997; 156: 197-211.
8. Thun MJ, DeLancey JO, Center MM, Jemal A, Ward EM. The global burden of cancer: priorities for prevention. Carcinogenesis. 2010; 31: 100-110.
9. Chen YQ, Min C, Sang M, Han YY, Ma X, Xue XQ, Zhang SQ. A cationic amphiphilic peptide ABP-CM4 exhibits selective cytotoxicity against leukemia cells. Peptides. 2010; 31: 1504-1510.
10. Schröder-Borm H, Bakalova R, Andrä J. The NK-lysin derived peptide NK-2 preferentially kills cancer cells with increased surface levels of negatively charged phosphatidylserine. FEBS Lett. 2005; 7:6128-6134.
11. Drechlser S, Andrä J. Online monitoring of metabolism and morphology of peptide-treated neuroblastoma cancer cells and keratinocytes. J. Bioenerget. Biomem. 2011; 43: 275-285.
12. Zwaal RF, Schroit AJ. Pathophysiologic implications of membrane phospholipid asymmetry in blood cells. Blood. 1997; 89: 1121-32. Review
13. Utsugi T, Schroit AJ, Connor J, Bucana CD, Fidler IJ. Elevated expression of phosphatidylserine in the outer membrane leaflet of human tumor cells and recognition by activated human blood monocytes. Cancer Res. 1991; 51: 3062-3066.
14. Ran S, Downes A, Thorpe PE. Increased exposure of anionic phospholipids on the surface of tumor blood vessels. Cancer Res. 2002; 62: 6132-6140.
15. Eliassen LT, Berge G, Sveinbjørnsson B, Svendsen JS, Vorland LH, Rekdal Ø. Evidence for a direct antitumor mechanism of action of bovine lactoferricin. Anticancer Res. 2002; 22: 2703-2710.
16. Papo N, Seger D, Makovitzki A, Kalchenko V, Eshhar Z, Degani H, Shai Y. Inhibition of tumor growth and elimination of multiple metastases in human prostate and breast xenografts by systemic inoculation of a host defense-like lytic peptide. Cancer Res. 2006; 66: 5371-5378.
17. Gross S, Wilms D, Krause J, Brezesinski G, Andrä J. Design of NK-2-derived peptides with improved activity against equine sarcoid cells. J Pept Sci. 2013; 19: 619-628.
18. Linnebacher M, Maletzki C, Ostwald C, Klier U, Krohn

M, Klar E, Prall F. Cryopreservation of human colorectal carcinomas prior to xenografting. BMC Cancer. 2010; 10: 362.

19. Maletzki C, Stier S, Gruenert U, Gock M, Ostwald C, Prall F, Linnebacher M. Establishment, characterization and chemosensitivity of three mismatch repair deficient cell lines from sporadic and inherited colorectal carcinomas. PLoS One. 2012; 7: e52485.
20. Andrä J, Koch MHJ, Bartels R, Brandenburg K. Biophysical characterization of the endotoxin inactivation by NK-2, an antimicrobial peptide derived from mammalian NK-Lysin. Antimicrob. Agents Chemother. 2004; 48: 1593-1599.
21. Gross S, Andrä J. Anticancer peptide NK-2 targets cell surface sulphated glycans rather than sialic acids. Biol Chem. 2012; 393: 817-827.
22. Al-Benna S, Shai Y, Jacobsen F, Steinstraesser L. Oncolytic activities of host defense peptides. Int J Mol Sci. 2011; 12: 8027-8051.
23. Banković J, Andrä J, Todorović N, Ana P-R, Đorđe M, Jannike K, Ruždijić S, Tanić N, Pešić M. The elimination of P-glycoprotein over-expressing cancer cells by antimicrobial cationic peptide NK-2: the unique way of multi-drug resistance modulation. Exp. Cell Res. 2013; 319: 1013-1027.
24. Ray S, Langan RC, Mullinax JE, Koizumi T, Xin HW, Wiegand GW, Anderson AJ, Stojadinovic A, Thorgeirsson S, Rudloff U, Avital I. Establishment of human ultra-low passage colorectal cancer cell lines using spheroids from fresh surgical specimens suitable for in vitro and in vivo studies. J Cancer. 2012; 3: 196-206.
25. Jass JR. Molecular heterogeneity of colorectal cancer: Implications for cancer control. Surg Oncol. 2007; 16 Suppl 1: S7-9.
26. Ostwald C, Linnebacher M, Weirich V, Prall F. Chromosomally and microsatellite stable colorectal carcinomas without the CpG island methylator phenotype in a molecular classification. Int J Oncol. 2009; 35: 321-327.
27. Steinstraesser L, Schubert C, Hauk J, Becerikli M, Stricker I, Koeller M, Hatt H, von Duering M, Shai Y, Steinau HU, Jacobsen F.Oncolytic designer host defense peptide suppresses growth of human liposarcoma. Int J Cancer. 2011; 128: 2994-3004a.
28. Lackner MR, Wilson TR, Settleman J. Mechanisms of acquired resistance to targeted cancer therapies. Future Oncol. 2012; 8: 999-1014.
29. Oren Z, Lerman JC, Gudmundsson GH, Agerberth B, Shai Y. Structure and organization of the human antimicrobial peptide LL-37 in phospholipid membranes: relevance to the molecular basis for its non-cell-selective activity. Biochem J. 1999; 341: 501-513.
30. Risso A, Zanetti M, Gennaro R. Cytotoxicity and apoptosis mediated by two peptides of innate immunity. Cell Immunol. 1998; 189: 107-115.
31. Steinstraesser L, Hauk J, Schubert C, Al-Benna S, Stricker I, Hatt H, Shai Y, Steinau HU, Jacobsen F. Suppression of soft tissue sarcoma growth by a host defense-like lytic peptide. PLoS One. 2011; 6: e18321b.
32. Makovitzki A, Fink A, Shai Y. Suppression of human solid tumor growth in mice by intratumor and systemic inoculation of histidine-rich and pH-dependent host defense-like lytic peptides. Cancer Res. 2009; 69: 3458-63.

5.1.6 Anlage – Teil 6

Cellular vaccination of MLH1$^{-/-}$ mice - an immunotherapeutic proof of concept study

ONCOIMMUNOLOGY
2018, VOL. 7, NO. 3, e1408748 (13 pages)
https://doi.org/10.1080/2162402X.2017.1408748

ORIGINAL RESEARCH

Cellular vaccination of MLH1$^{-/-}$ mice – an immunotherapeutic proof of concept study

Claudia Maletzki[a], Yvonne Saara Gladbach[b], Mohamed Hamed[b], Georg Fuellen[b], Marie-Luise Semmler[a], Jan Stenzel[c], and Michael Linnebacher[a]

[a]Molecular Oncology and Immunotherapy, Department of General Surgery, Rostock University Medical Center, Rostock, Germany; [b]Institute for Biostatistics and Informatics in Medicine and Ageing Research – IBIMA Rostock University Medical Center, Rostock, Germany; [c]Core Facility Multimodal Small Animal Imaging, Rostock University Medical Center, Rostock, Germany

ABSTRACT

Mismatch-repair deficiency (MMR-D) is closely linked to hypermutation and accordingly, high immunogenicity. MMR-D-related tumors thus constitute ideal vaccination targets for both therapeutic and prophylactic approaches. Herein, the prophylactic and therapeutic impact of a cellular vaccine on tumor growth and tumor-immune microenvironment was studied in a murine MLH1$^{-/-}$ knockout mouse model. Prophylactic application of the lysate (+/− CpG ODN 1826) delayed tumor development, accompanied by increased levels of circulating T cell numbers. Therapeutic application of the vaccine prolonged overall survival (median time: 11.5 (lysate) and 12 weeks (lysate + CpG ODN) vs. 3 weeks (control group), respectively) along with reduced tumor burden, as confirmed by PET/CT imaging and immune stimulation (increased CD3$^+$CD8$^+$ T – and NK cell numbers, reduced levels of TIM-3$^+$ cells in both treatment groups). Coding microsatellite analysis of MMR-D-related target genes revealed increased mutational load upon vaccination (total mutation frequency within 28 genes: 28.6% vaccine groups vs. 14.9% control group, respectively). Reactive immune cells recognized autologous tumor cells, but also NK cells target YAC-1 in IFNγ ELISpot and, even more importantly, in functional kill assays. Assessment of tumor microenvironment revealed infiltration of CD8$^+$ T-cells and granulocytes, but also upregulation of immune checkpoint molecules (LAG-3, PD-L1).

The present study is the first reporting *in vivo* results on a therapeutic cellular MMR-D vaccine. Vaccination-induced prolonged survival was achieved in a clinically-relevant mouse model for MMR-D-related diseases by long-term impairment of tumor growth and this could be attributed to re-activated immune responses.

ARTICLE HISTORY
Received 26 September 2017
Revised 16 November 2017
Accepted 18 November 2017

KEYWORDS
cellular vaccine; MMR deficiency; *in vivo* imaging; tumor microenvironment; target gene identification

Introduction

Somatic hypermutation constitutes a molecular tumor make-up for which immunotherapy might be most effective.[1] This phenomenon is attributable to alterations in the DNA polymerases encoded by the *POLE/D1* genes, exposure to external (cigarette smoking, UV radiation) and endogenous mutagens.[1,2] Besides, individuals who are inherited deficient in DNA replication and repair processes develop tumors with high mutational load mainly consisting of insertions/deletions at repetitive DNA sequences (= microsatellites). MSI-induced neoantigens arise mostly from coding microsatellite frameshift mutations in specific target genes.[3,4] The high number of mutational events in coding microsatellites leads to the microsatellite instability (MSI) phenotype. Due to their high immunogenicity, these frameshift mutations are perfect targets for immunological approaches.

Germline mutations in one of the mismatch repair (MMR) genes (*MLH1, MSH2, MSH6, PMS1,* and *PMS2*) represent the underlying molecular mechanism causing malignancies in affected patients. Clinically, MMR-D related tumor syndromes include the autosomal dominant Lynch syndrome (LS) as well as their biallelic counterpart referred to as constitutional or compound MMR-D (CMMR-D).[5] LS-affected patients develop tumors upon inactivation of the second allele. Tumors predominantly manifest in the gastrointestinal system as well as in the endometrium and with an average age of 45 years.[6] By contrast, CMMR-D patients are prone to develop a more complex spectrum of ultra-mutated cancers during their (early childhood) life-time. CMMR-D-associated tumors include hematological, Lynch-like gastrointestinal tumors (GIT), and brain tumors.[7] Despite biological and clinico-pathological differences, many features are common to both diseases, based on the initial driving MMR-mutations.[5,8,9]

However, when comparing with LS patients, the prognosis for CMMR-D patients is extremely bad. CMMR-D-associated tumors show intrinsic resistance mechanisms against several known standard chemotherapeutic drugs, including O6-methylating agents.[7,10] This finding, together with the increasing

---

CONTACT Claudia Maletzki, PhD claudia.maletzki@med.uni-rostock.de Molecular Oncology and Immunotherapy/Department of General Surgery, University of Rostock, Schillingallee 69, D-18057 Rostock, Germany.

Supplemental data for this article can be accessed on the publisher's website.
This work was supported by a grant from the German research foundation to CM [grant number MA5799/2-1].

© 2018 Taylor & Francis Group, LLC

evidence of a good response to immunotherapeutic drugs inhibiting the PD-1/PD-L1 pathway even in the metastatic setting,[2,11,12] provides a rationale for investigation of immune-based strategies in general. Recent studies revealed that LS patients' own immune system is capable of recognizing a variety of neoantigens on the tumor cells' surface; thus contributing to a better prognosis.[13–15] Additionally to immune-checkpoint inhibition, more "classical" strategies like application of autologous tumor lysate, containing a large repertoire of (shared) MSI-specific tumor antigens, might be an effective treatment regimen for hypermutated tumors. Given the extremely high mutational load, these cancers are under selective pressure for obliterating antigen presentation.[16–18] Hence, simultaneous vaccination against a variety/multitude of tumor-specific antigens may prevent (or delay) the phenomenon of antigen-escape tumor cell variants.[19]

We here analyzed the impact of a cellular-based vaccine on tumor incidence, growth and immune response as a strategy to vaccinate mice with spontaneously developing MLH1$^{-/-}$ tumors, in both prophylactic and therapeutic settings. These mice combine characteristics of LS and CMMR-D, with the latter being represented by an early lymphomagenesis, while GIT development is seen at later age and thereby closely resembles LS-associated neoplasia.

Results

Whole exome sequencing analysis for the identification of vaccination antigens – a comparative analysis

Prior to vaccination, comparative whole exome sequencing was done on an MLH1$^{-/-}$-derived GIT allograft (namely MLH1$^{-/-}$ A7450, which was used for vaccination) and the corresponding parental tumor to analyze the mutanome of these tumors (Fig. 1). Firstly, marked increases in total mutational events in the allograft as compared to the primary were evident with regard to missense, nonsense and silent mutations as well as the number of mutations per type (Fig. 1A). As expected, the number of silent mutations is high whereas the nonsense mutation rate is small in both tumor samples. Focusing on the mutation type "nonsense", unexpectedly no SNP exclusive for the primary tumor and only one mutation of the *MSH3* gene, at position 93110760, has been reported.

In the genomic genetic fingerprint (Fig. 1B) the focus is on visualizing missense mutations in a pairwise fashion for the allograft and for their parental counterpart. The primary tumor shows three genes being mutated: *ERBB2, IDH2* and *ARID1A*, where *ARID1A* has eight mutations at different positions. These positions are exclusively mutated in the primary tumor

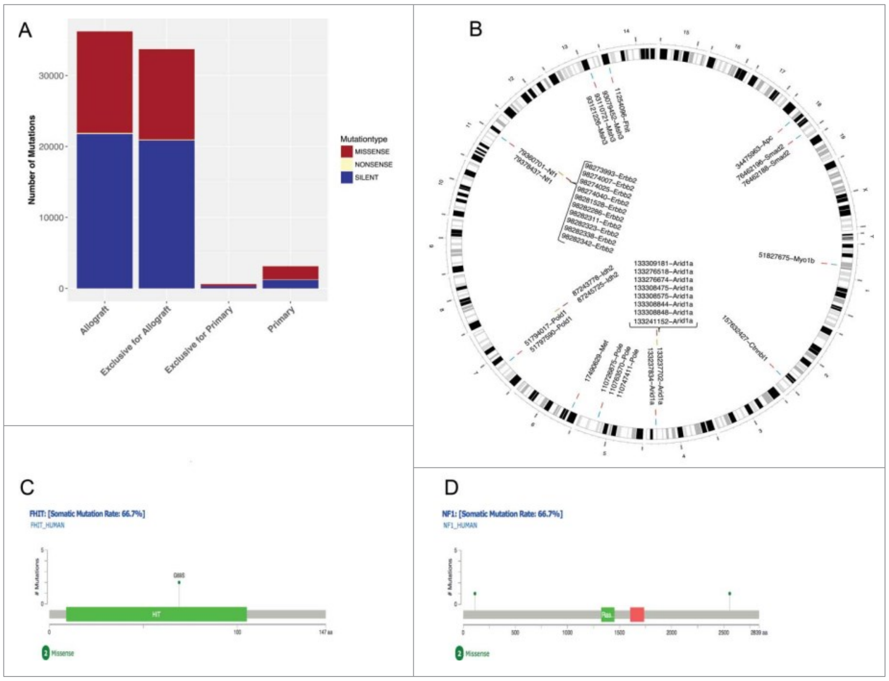

Figure 1. Comparative mutational analysis of MLH1$^{-/-}$ GIT and allograft. (A) The statistics of each mutation type (missense, nonsense and silent) are shown for the MLH1$^{-/-}$ GIT allograft and the primary tumor as well as the exclusive distribution for each. Silent mutations are dominating both samples and missense mutations are equally distributed. (B) Ideogram plots showing the genomic distributions of the missense mutations occurring in the annotated/known genes for both samples. All missense SNVs for MLH1$^{-/-}$ GIT allograft and the primary tumor are shown in blue and yellow respectively with their corresponding coordinate on the mouse reference genome mm9 cytoband. The exclusive missense SNVs for the MLH1$^{-/-}$ GIT allograft and the primary tumor are shown in red and annotated with a corresponding ID containing the SNV position and the affected gene name. (C) and (D) Missense mutations mapped on human protein sequences for the *FHIT* and the *NF1* genes, respectively. These two specific genes are frequently mutated in CMMR-D related diseases.

Table 1. Tumor development after prophylactic vaccination and tumor spectrum.

	median age of onset [weeks]		tumor type [%]			mice [%]	
Intervention	Lymphoma	GIT	Lymphoma	GIT	other	unexpected death	tumor free
CpG ODN 1826	26	32.5	60	20	20	0	0
ODN 1826 ctrl	26	38.5	60	20	10	10	0
Lysate	30	48	53.8	15.4	7.7	8.0	15.4
Lysate + CpG ODN 1826	32.5	46.5	41.2	23.5	11.8	5.8	17.7
Lysate + ODN 1826 ctrl	31.5	45	40.0	20.0	20.0	6.7	13.3

ctrl – control; GIT – gastrointestinal tumor; unexpected death – died under isoflurane anesthesia, found dead

(shown in red with the corresponding annotation containing the position and the gene, all SNPs are in yellow). For *ERBB2* only some positions are shown for better visualization. Interestingly, the allograft has *ARID1A* SNPs as well, but at different positions (for comparisons please see supplementary Tables 1 and 2 summarizing the exclusive SNPs). Besides *ARID1A*, the other mutated genes are: *CTNNBL1, FHIT, MET, MSH3, MYO1B, NF1, POLE, POLD1,* and *SMAD2. POLE* and *POLD1* frequently mutated in MMR-D related diseases[20,21] and [Fig. 1C and D] show two or three mutated positions, respectively. An additional analysis on insertions/deletions– known to be interesting target structures for peptide-based vaccination – identified 16 candidates with potential relevance (supplementary Table 3). The resulting proteins are involved in different biological processes (such as signaling and growth control).

Delayed tumorigenesis after prophylactic vaccination due to immune stimulation

Next, the impact of the cellular lysate prepared from the MLH1$^{-/-}$ GIT allograft was tested on tumor development in syngeneic animals. A vaccination schedule is provided as supplementary Fig. 1. Mice without any clinical signs of tumor development (i.e. normal behavior, no ruffling of fur, normal blood cell numbers) were included in this study and assigned to the different treatment arms (lysate, lysate + CpG ODN 1826, lysate + control ODN 1826) and control groups (CpG ODN 1826, control ODN 1826). Mice repeatedly received applications of the vaccine to boost immune responses. CpG was chosen based on a preliminary *in vitro* assay to study the immune stimulatory effect of different adjuvants (Complete Freund's Adjuvant, a bacterial lysate from *Streptococcus pyogenes*,[22] and CpG ODN 1826) (*data not shown*). In these experiments, lymphocytes from both heterozygous and homozygous mice (each n = 4) responded best towards CpG ODN 1826 in terms of activation (CD25$^+$, CD69$^+$) and viability.

Repeated application of the lysate was well-tolerated and without any signs of vaccination-induced side effects. To analyze the impact of the vaccine on the immune system, blood samples were taken routinely from mice of all groups. Mice of the vaccine groups (lysate +/− CpG ODN 1826 and control ODN 1826) had increased numbers of circulating T cells (Fig. 2A). Control mice did not show any altered immune response. As assessed on day 84, all vaccinated mice showed higher levels of cytotoxic T cells than control mice (lysate + CpG ODN 1826 up to 22% vs. control: 8 %). NK cell numbers were elevated as well (lysate up to 40 % vs. control: 23 %).

In addition to the observed immune stimulation, vaccinated mice lived longer than controls and developed tumors at later time points (Fig. 2B). Two and three mice of each of the two vaccination groups, respectively, even remained tumor free until the experimental end point (= 42 weeks), while all control mice displayed tumorigenesis within the expected time frame, i.e. lymphomas at around 26 weeks and GIT at around 32.5 (CpG ODN 1826) or 38.5 weeks (control ODN 1826), respectively (Table 1). Vaccination slightly delayed lymphoma formation and GI tumorigenesis, the latter being detectable around nine weeks later (lysate group) than in control mice (Table 1). Unexpectedly, adding the adjuvant to the lysate played a minor role and did not decelerate tumor development when compared to the lysate.

Tumor microenvironment and target cell recognition by lymphocytes of prophylactically vaccinated mice

To further investigate the observed immune stimulation, the tumor microenvironment was studied in detail. Immunofluorescence staining of GIT from vaccinated and control mice revealed increased numbers of infiltrating CD4$^+$ and CD8$^+$ T cells, both being located within the tumors (representative images are shown in Fig. 3A). Besides, the immune-checkpoint molecule PD-L1 was upregulated, mainly on macrophages, upon vaccination. Numbers of LAG-3- and NK1.1-positive cells remained largely unchanged (Fig. 3A and data not shown).

We next examined whether immune cells respond to stimulation from tumor cells. Therefore, the reaction of peripheral blood lymphocytes (= during vaccination) and splenocytes (= expe-rimental endpoint) co-incubated overnight with different target cell populations was measured in a classical IFNγ-ELISpot assay. The two tested MLH1$^{-/-}$ tumor target cell lines triggered IFNγ secretion of lymphocytes from vaccinated mice. Of note, there was a trend towards higher recognition at later time points, i.e. day 84. Strongest responses were seen in the lysate-treated group, followed by lymphocytes from lysate + adjuvant-treated mice (Fig. 3B). Control mice (CpG ODN 1826 and control ODN 1826) did not show any response towards the target cells (Fig. 3B).

Prolonged survival after therapeutic vaccination

Next, the impact of our vaccine was investigated in a therapeutic situation (supplementary Fig. 1). Mice with suspected GIT underwent *in vivo* PET/CT imaging, which was paralleled by weight monitoring and basic immune assays to determine the

Table 2. Analysis of coding microsatellite mutations in GIT from vaccinated and control tumors in comparing to the allograft, which was used for vaccination.

	cMS marker																		
Intervention	APC	Tmem60	Senp6	Phactr4	Casc3	SDCCAG1	Fasl	Kit	Rasal2	Tcf7l2	Casc5	Mbd6	Lig4	Bend5	NKtr1	Grb14	Kcnma1	Rfc3	ERCC5	Asnsd1
control	26.1	26.1	43.5	47.8	13.0	8.7	0.0	0.0	43.5	13.0	21.7	0.0	4.3	13.0	8.7	0.0	4.3	91.3	30.4	26.1
lysate	0.0	33.3	100.0	0.0	66.7	66.7	0.0	0.0	100.0	33.3	33.3	0.0	33.3	20.0	100.0	100.0	33.3	100.0	66.7	20.0
lysate + CpG ODN 1826	0.0	40.0	20.0	20.0	0.0	80.0	20.0	20.0	20.0	20.0	20.0	40.0	20.0	60.0	20.0	20.0	0.0	80.0	40.0	20.0
allograft*	wt/−1	wt	wt/−1	wt	wt	wt	wt	wt	wt/−1	wt	n.d.	wt	wt/−1	wt/−1/−2	wt	wt	wt	wt/−1	wt	wt

Cumulative mutation frequency in %; differences between individual tumors (control, vaccine, allograft) are highlighted in green, confirming vaccination-induced increased mutational load;
*used for vaccination; n.d. – not determined.

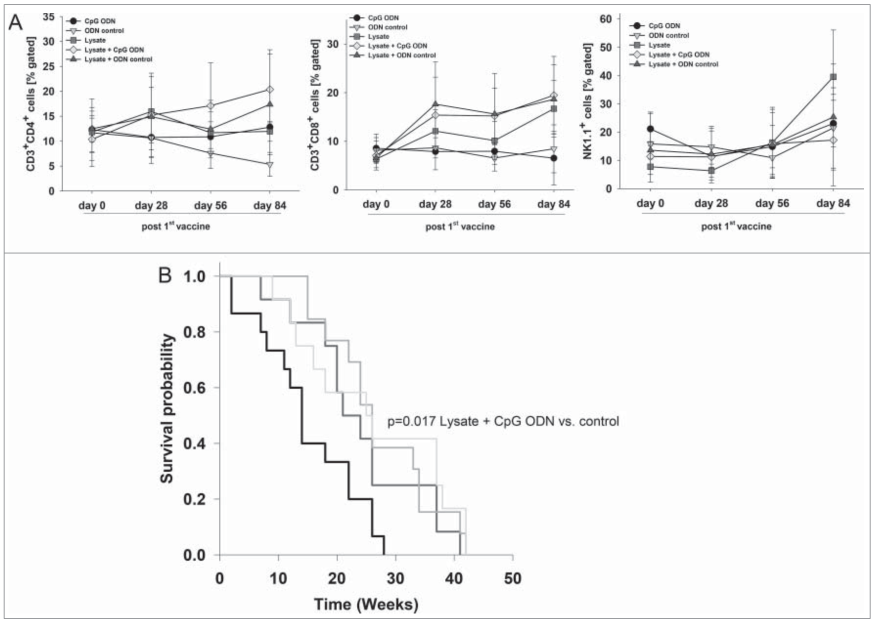

Figure 2. Prophylactic vaccination of MLH1$^{-/-}$ mice with a cellular lysate. (A) Flow cytometric phenotyping of peripheral blood leukocytes. Blood samples were taken at start of treatment (= day 0) and regularly during the experiment. Given are the percentage numbers of positively stained cells as determined by gating on viable cells from vaccinated (lysate (n = 12) +/− CpG ODN 1826 (n = 15) and ODN control (n = 12)) and control mice (CpG ODN 1826or control ODN 1826; n = 9 and n = 7 mice per group, respectively). Values are given as mean ± SD; $^{*}p < 0.05$ vs. control; t-test. (B) Kaplan Meier survival curve of vaccinated and control MLH1$^{-/-}$ mice. Log rank survival analysis, p = 0.017 Lysate + CpG ODN vs. control.

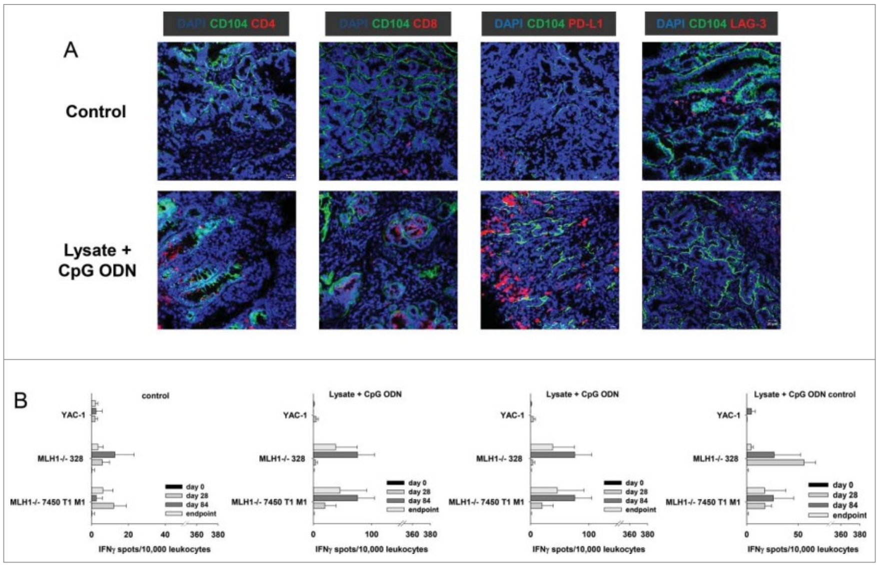
DAPI CD104 CD4
DAPI CD104 CD8
DAPI CD104 PD-L1
DAPI CD104 LAG-3
A
Control
Lysate + CpG ODN
B
control
Lysate + CpG ODN
Lysate + CpG ODN
Lysate + CpG ODN control
YAC-1
MLH1-/- 328
MLH1-/- 7450 T1 M1
day 0
day 28
day 84
endpoint
IFNγ spots/10,000 leukocytes
0
20
40
50
100
360
380

Figure 3. Immunofluorescence of MLH1$^{-/-}$ tumors and IFNγ–ELISpot after prophylactic vaccination. (A) Tumor microenvironment was studied from GIT cryostat sections of 4μm. Analyses were done on a laser scanning microscope (Zeiss) using 20x objectives. (B) Reactivity of PBL (during vaccination) or splenocytes (endpoint) against target cells (MLH1$^{-/-}$ 7450 T1 M1, MLH1$^{-/-}$ 328, and YAC-1) was examined after overnight co-incubation. Lymphocytes were isolated from vaccinated and control mice at different time points. Experiments revealed increased reactivity upon vaccination. Values are given as mean ± SD.

immune status before vaccination. When comparing with tumor-free young mice, T cell levels ($CD4^+$, $CD8^+$, γ/δ TCR^+) were slightly reduced in tumor-bearing hosts. *Vice versa*, immune-suppressive molecules (i.e. LAG-3 and IDO) as well as ALCAM (CD166) increased in numbers (Fig. 4A). Granulocyte and NK cell numbers were not altered. As assessed by PET/CT imaging, mice developed 3.2 ± 1.3 tumors on average with a mean volume of 74.1 ± 51.8 mm^3 (Fig. 4B, representative pictures showing PET/CT scan of a healthy mouse (left) in comparison to tumor-bearing mice (middle: GIT, right: lymphoma) are depicted in Fig. 4C). Tumorigenesis was accompanied by continuous weight loss (~ 5 % during the last three weeks of observation) and impairment of general behavior (ruffling of fur, reduced mobility, and socio-physiological segregation).

Upon vaccination, general state of health was improved. Additionally to stabilizing weight, mice showed improved mobility and parametric signs of disease vanished. Repeated PET/CT imaging on day 28 post vaccination revealed disease control, with tumor volumes being smaller than before vaccination (day 28: lysate: 60.2 ± 24.3mm^3 and lysate + CpG ODN: 46.0 ± 37.3mm^3). In some cases, single tumor nodules even disappeared (Fig. 4D). Disease control contributed to a better outcome and improved overall survival. Median survival time after vaccination was 11.5 ± 3.9 (lysate) and 12.0 ± 5.8 (lysate + CpG ODN 1826) weeks, compared to three weeks in the control group (median: 3.0 ± 0.6 weeks) (Fig. 4E). Therapeutic response was accompanied by immune stimulation in a way of reconstituting a "physiological" immune response. Of note, numbers of cytotoxic T and NK cells as well as granulocytes gradually increased during vaccination (Fig. 5). Amounts of TIM-3 positive T cells decreased, while CTLA-4, PD-1 and PD-L1 were only transiently down-regulated on immune cells (*data not shown*). Numbers of helper T cells did not significantly change during vaccination.

Considering treatment of highly aggressive lymphomas, median survival time upon vaccination with the GIT-derived lysate was 6.0 ± 2.5 weeks and thereby slightly prolonged compared to untreated control mice (2.0 ± 1.1 weeks). This finding suggests some overlapping but also different biological and immunological mechanisms among the two tumor types arising in $MLH1^{-/-}$ mice. Another interesting "single case" finding was successful eradication of a skin cancer by subcutaneous lysate application. The initial tumor (9 × 12 mm size) completely disappeared after three repetitive injections and the mouse remained tumor free for four months, before relapse. Re-administration of the vaccine mediated measurable tumor shrinkage, but not complete remission, and the mouse died from progressive disease four weeks later (supplementary Fig. 2).

Tumor microenvironment reveals increased T cell infiltration but also vaccine-induced up-regulation of immune-checkpoint molecules

The *in vivo* results obtained hint towards involvement of antitumoral immunological mechanisms. Consequently, tumor

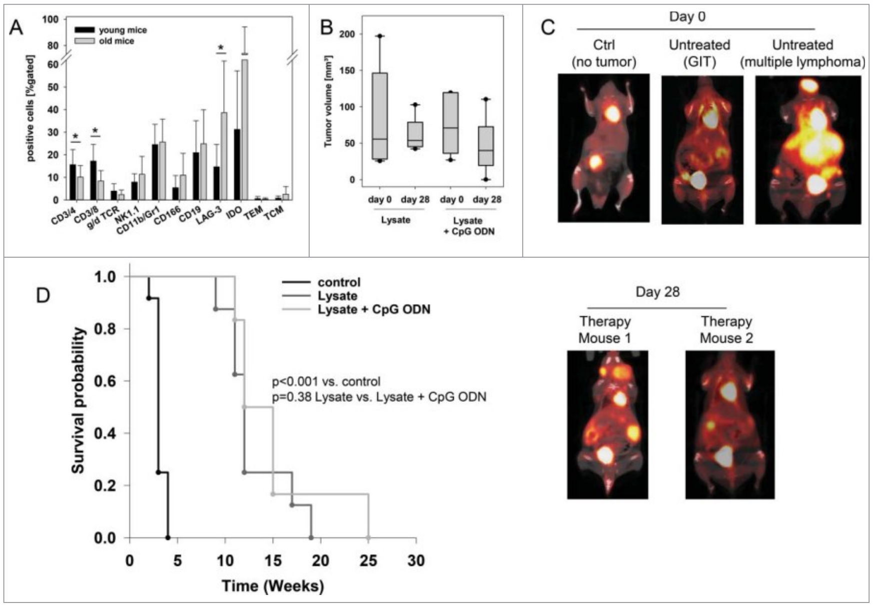

Figure 4. Therapeutic vaccination of $MLH1^{-/-}$ mice with a cellular lysate. (A) Comparative flow cytometric analyses from young and old mice for determining immune status prior to vaccination. * $p < 0.05$ vs. young mice; t-test. (B) Tumor volume as determined by PET/CT *in vivo* imaging using radiopharmacon ^{18}F-FDG. Values are given as mean ± SD. Whiskers (error bars) above and below the box indicate the 90th and 10th percentiles. (C) and (D) PET/CT *in vivo* imaging. Tumor nodules were visualized using radiopharmacom ^{18}F-FDG. Given are representative summed images in axial (left) and coronal view (right) (C) For comparison, exemplary images of a tumor-free mouse as well as mice with a GIT and lymphoma are shown. Arrows indicate detected tumors. The color scale indicates SUV. (D) Repeated imaging at day 28 after vaccine revealed disappearance of single tumor nodules. Images at day 28 were taken from the same mouse as on day 0. (E) Kaplan Meier survival curve of vaccinated and control $MLH1^{-/-}$ mice. Log rank survival analysis. $p < 0.001$ vs. control. $p = 0.38$ lysate vs. lysate + CpG ODN.

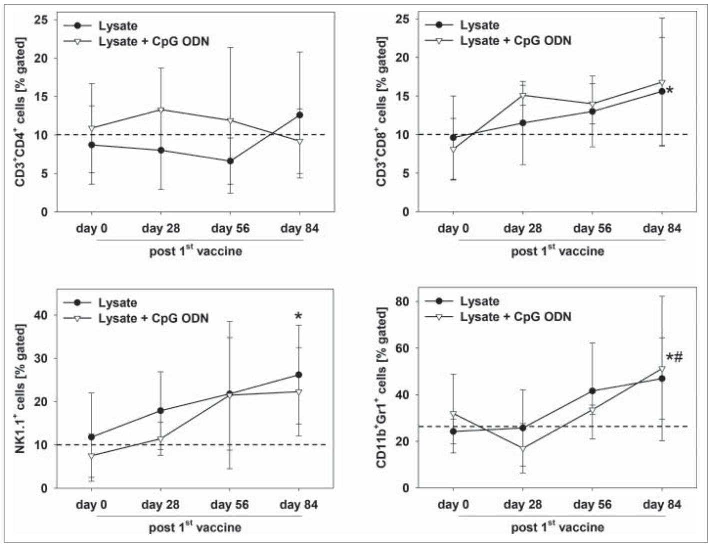

Figure 5. Immune status of therapeutically vaccinated mice. Flow cytometric phenotyping of peripheral blood leukocytes. Blood samples were taken at start of treatment (= day 0) and regularly during the experiment. Given are the percentage numbers of positively stained cells as determined by gating on viable cells from vaccinated (lysate (n = 9) +/− CpG ODN 1826 (n = 7). Values are given as mean ± SD; $^{*}p < 0.05$ lysate vs. day 0; t-test; # $p < 0.05$ vs. lysate + CpG ODN vs. day 0; t-test.

resection specimens were examined for infiltrating immune cells. Here, marked differences were seen between lysate and lysate + CpG ODN 1826 treated mice. In the latter group, infiltrating cytotoxic and helper T cell numbers markedly increased (Fig. 6). Although numbers of infiltrating granulocytes remained similar upon vaccination, their phenotype in lysate + CpG ODN 1826 treated tumors changed. Double positive CD11b^{+}Gr1^{+} myeloid-derived suppressor cells were exclusively seen in this group; possibly documenting a compensatory immune-escape mechanism. In support of these findings, PD-L1 and LAG-3 were highly upregulated on infiltrating cells in the MLH1$^{-/-}$ tumor microenvironment. However, there was no expression of PD-L1 on vaccine-induced infiltrating CD11b^{+} granulocytes, a mechanism reported to counteract CD8^{+} T cell mediated tumor cell lysis,[23] (Fig. 6). NK cell numbers were not altered at all (Fig. 6).

Increased mutational load in MSI-target genes upon vaccination

Prolonged survival of MLH1$^{-/-}$ mice was at least partially attributable to immune-stimulation. Since this might be associated with selective pressure and an accordingly increased mutational load, tumor resection specimens from control and vaccinated mice were subjected to molecular pathological analysis. Examination of coding microsatellites in selected MSI-target genes was based on our previous study to identify murine coding MSI target genes in MLH1$^{-/-}$ tumors.[9]

With this analysis, mutations were detectable in 31 % (lysate) and 25 % (lysate + CpG ODN 1826) of analyzed markers from vaccinated tumors, respectively (vs. 15 % controls; Table 2). Increased mutation frequencies were found in genes belonging to DNA repair (*Lig4*), signa-ling pathways that regulate growth and metabolism (*Grb14*), and transcriptional repression (*Bend5*). The latter gene shares functional and structural similarity with its human ortholog and is mutated in 10 % of cultured MSI-H cell lines [*Seltarbase.org*]. Besides, *NKtr1,* originally described to be present on the surface of natural killer cells to facilitate target cell binding, was more frequently mutated in vaccinated than in control tumors (100% (lysate) and 20% (lysate + CpG ODN 1826), respectively, vs. 9% in controls). In contrast, *APC* gene mutations, originally found in every fourth MLH1$^{-/-}$—associated GIT as well as in the allograft that was used for vaccination, were no longer detectable (Table 2).

Additional direct comparison of such MSI-specific alterations between vaccinated tumors and the allograft confirmed an increased vaccination-induced mutational load. Here again, some mutations were exclusively found upon vaccination, forced by MSI^{+} tumor cells to escape immune attack (Table 2).

Immune responses against MLH1$^{-/-}$ targets upon vaccination

Finally, lymphocytes from vaccinated mice were analyzed for their tumor-recognizing and killing ability in immunological standard assays. By determining the number of IFNγ secreting cells, recognition of MLH1$^{-/-}$ target cell lines 328 and 7450 T1 M1 was confirmed (Fig. 7A). Numbers of reactive lymphocytes increased during vaccination. How-ever, recognition was not confined to tumor cells, since YAC-1 cells gave also rise to IFNγ secretion, especially at later times of vaccination (day 56 and endpoint).

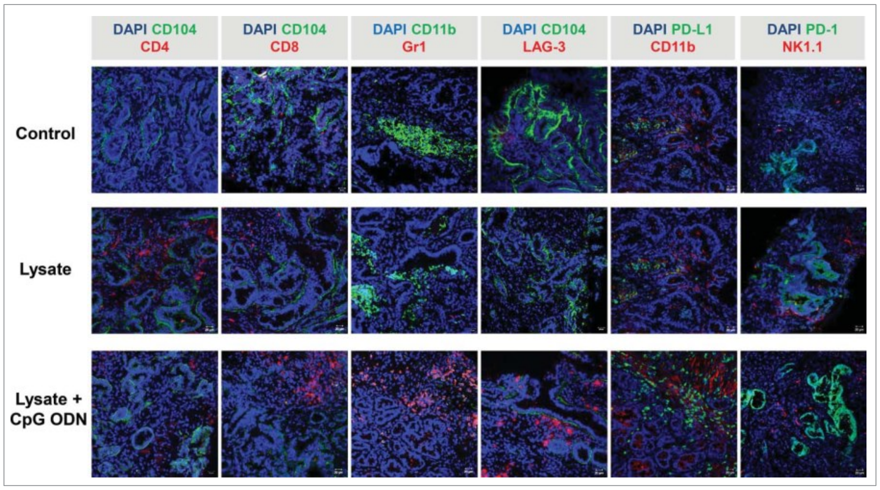

Figure 6. Immunofluorescence of MLH1$^{-/-}$ tumors after therapeutic vaccination. Tumor microenvironment was studied from GIT cryostat sections of 4μm. Pictures were done on a laser scanning microscope (Zeiss) using 20x objectives.

Results were confirmed on a functional level, in which splenocytes from vaccinated mice were capable of lysing MLH1$^{-/-}$ target cells. Of note, GIT and lymphoma target cells were both efficiently killed. Nonetheless, lytic activity was not exclusively antigen-restricted, since YAC-1 cells were again also recognized and killed (Fig. 7B). This is particularly interesting since T and NK cell proportions gradually increased upon vaccination. Hence, repeated application of the lysate seems to favor the induction of highly activated T as well as NK cells.

Discussion

In this study, we used a clinically relevant mouse model to answer the question whether a cellular vaccine, prepared from a

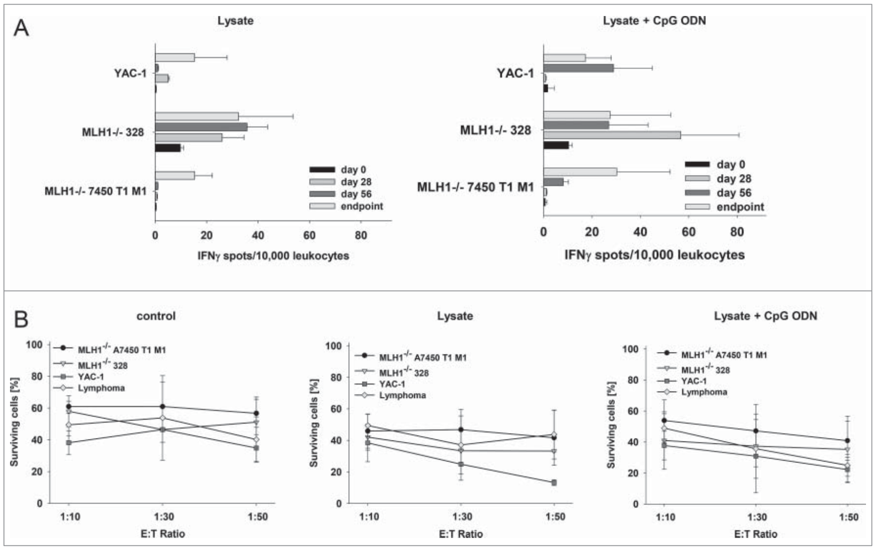

Figure 7. Functional immunological analysis. (A) IFNγ—ELISpot and (B) Flow cytometric cytotoxicity assay. (A) Reactivity of PBL (during vaccination) or splenocytes (endpoint) against target cells (MLH1$^{-/-}$ 7450 T1 M1, MLH1$^{-/-}$ 328, and YAC-1) was examined after overnight co-incubation. Lymphocytes were isolated from lysate-treated and control mice at different time points. These experiments identified increased reactivity post treatment. (B) Lytic activity of splenocytes against target cells (MLH1$^{-/-}$ 7450 T1 M1, MLH1$^{-/-}$ 328, and YAC-1) was examined after 12h co-incubation. Lymphocytes were isolated from spleens of lysate-treated and control mice. Again, an increased lytic activity upon vaccination was seen. Values are given as mean ± SD.

MSI-H GIT, constitutes a successful immunotherapeutic strategy for MMR-D related diseases. In addition, we analyzed if this vaccine protects mice from tumors with known biological and molecular pathological heterogeneity (GIT vs. lymphomas and skin tumors), since MMR-D tumors (especially CMMR-D associated cases[24]) arise in virtually all cancer-prone organs and may share immunogenic target structures.[25] We could show that: (I) repeated application of the vaccine stimulates both, the innate and the adaptive immune system, (II) it delays tumorigenesis of different origin in naïve mice, (III) it significantly prolongs survival of GI tumor-bearing mice by long-term impairment of tumor growth, but (IV) it has only marginal entity-overlapping antitumoral capacity in the therapeutic situation.

Application of tumor vaccines has a long-standing tradition in tumor immunology with proven efficacy in pre−(clinical) trials.[19,26] Whole tumor lysates constitute an undefined mixture of "altered self" antigens; hence, identifying vaccination antigens is crucial for subsequent development of poly-epitope vaccines – made of stably presented T cell epitopes for activating cytotoxic T and helper lymphocytes simultaneously. In this study, we first analyzed the cancer mutanome of a GIT MLH1$^{-/-}$ allograft which was subsequently used for vaccination (= lysate) and performed comparative analysis with the parental tumor counterpart. Firstly, by whole exome sequencing, an increased number of mutational events was confirmed in the allograft, a finding quite common to MMR-D-related tumors. These tumors acquire novel mutations after each cell cycle,[21] putting them into the subtype of "ultra-mutated" cancers. Secondly, mutations identified in the allograft were defined as true target antigens based on their physiological functional role, i.e. involvement in different biological processes (signaling, growth control; supplementary Table 1).

A high number of frameshift-derived neoantigens is described in the literature for human MSI^{+} cancers [*Seltarbase.org*] and some were even identified in the murine system.[3,9] Frameshift peptides (FSP) trigger T cell-mediated immune responses in LS patients as well as in healthy mutation carriers.[15] Consequently, clinical trials aiming to decelerate or even prevent tumorigenesis in affected patients after repetitive FSP-based vaccination have been initiated [trial numbers: NCT01461148 & NCT01885702]. Preliminary results from single cancer patients describe FSP-specific immune responses in a Phase I clinical trial.[27] By contrast, much less is known about the immunogenicity of CMMR-D associated cancers in terms of tumor microenvironment and antigenic profile. In the only prior published immunotherapeutic approach, two patients with recurrent multifocal brain tumor received complete remission after treatment with Nivolumab.[28] Besides, no experimental or clinical trials on CMMR-D immunotherapy have been reported so far.

The MMR-D-related MLH1$^{-/-}$ tumor model is ideally suited to develop and test immunotherapeutic strategies in order to not only substantially improve the clinical situation for patients suffering from MMR-D-related tumors but moreover also for the development of prophylactic strategies delaying or on the long run even preventing tumor occurrence in CMMR-D individuals.

To test the prophylactic capacity of the GIT allograft lysate, we vaccinated mice repetitively prior to tumor formation. Vaccination was accompanied by increased levels of circulating (cytotoxic and helper) T as well as NK cells. T cells were additionally found elevated *in situ* in tumor resection specimens. Noticeably, numbers of both helper and cytotoxic T cells increased upon vaccination, most likely explaining delayed tumorigenesis. This approach did, however, not completely inhibit tumor formation; with only 15 % of mice being tumor-free at the experimental end-point.

The functional *in vitro* analysis confirmed initial immune stimulation with immune cells from lysate (+/− CpG ODN 1826) treated mice recognizing to autologous tumor target cells, especially at early time points. However, development of immunological memory was obviously counteracted by developing tumor cells through immunoediting. Tumor cells are not characterized by a conserved set of immunogenic antigens. Accordingly, the tumor is sculpted with a preponderance of tumor cells to which the immune system appears to be tolerant. Mechanistically, this has additionally been attributed to (I) the production of immunosuppressive cytokines (e.g. TGF-β, IL-10) or soluble factors (e.g. ROS, NO)[23,26]; (II) involving inhibitory receptors (upregulation of CTLA-4 and IDO) and (III) preventing co-stimulation (low amount of antigen-presenting cells). Adding other adjuvants or applying tumor lysate-loaded dendritic cells to ensure appropriate migration to T lymphocyte areas in draining lymphoid tissues may provide a strategy to improve therapy. Finally, conquering the plethora of adaptations malignant cells develop along with restoration of an intact CD4/CD8 interplay ("cancer immune cycle") remains the main challenge to increase tumor rejection rates in the preclinical MLH1$^{-/-}$ model.

Therapeutic lysate application in GIT-bearing MLH1$^{-/-}$ mice significantly prolonged survival. PET/CT imaging with ^{18}F-FDG, a sensitive parameter to monitor treatment response,[29] confirmed vaccination-induced disease control with some tumor nodules even completely disappearing within four weeks. Immune responses, characterized by elevated numbers of cytotoxic T and NK cells as well as specific recognition of MLH1$^{-/-}$ GIT target cells by lymphocytes from vaccinated mice accompanied the therapeutic response. Marked immune cell infiltration was evident in residual tumors dominated by T cells and granulocytes; but also immunosuppressive checkpoint molecules expressed by the majority of cellular infiltrates.[30] In cytotoxicity assays, reactivity was further emphasized by the lymphocytes' ability to kill MLH1$^{-/-}$ tumor target cells. Interestingly, we also observed a cross-reactivity of lymphocytes isolated from lymphomas, hinting to the recognition of shared tumor antigens. This is particularly surprising since *in vivo* treatment of lymphomas did not significantly affect tumor growth and overall survival. In support of these findings, a distinct mutational susceptibility of target genes among human hematological and gastrointestinal (sporadic) MSI tumors was reported.[31] Besides, immune responses observed in our study were not exclusively antigen-restricted since NK cells target YAC-1 were also lysed. Confirmed by flow cytometric phenotyping, a mixture of highly activated, efficiently target cell killing NK cells and cytotoxic T cells attack MLH1$^{-/-}$ tumor targets; the latter in an MHC-I restricted manner.[32,33]

Another interesting finding of this study was the increased mutational load in selected MSI-target genes from vaccinated tumors, which likely constitutes some kind of escape mechanism by triggering antigenic drift. Together with the missing activation of T helper cells and upregulation of immune-checkpoint molecules this best explains final disease progression and treatment failure. Consequently, combining checkpoint-inhibition with vaccination represents a very promising strategy as has only recently been proposed for experimental glioblastomas (DC vaccine + anti-PD-1 antibody + colony stimulating factor 1 receptor inhibitor) and prostate cancer (anti-CTLA-4 antibody + GM-CSF-secreting cellular vaccine).[23,34]

Finally, we would like to bring forward the argument that the MLH1$^{-/-}$ mice that we used mirror – at least from an immunological point of view – many features of clinical CMMR-D. These include a biallelic MMR-D as the driver of tumorigenesis and the high incidence and early manifestation of lymphomas. Although not associated with clinically noticeable immune defects, impairment of Ig class switch recombination has been frequently found in CMMR-D patients.[24,35] Even though not analyzed in detail in this study, we observed a slightly impaired response towards antigenic stimuli of MLH1$^{-/-}$ lymphocytes when compared to lymphocytes from heterozygous and wildtype mice. This fact in mind, we want to emphasize that the overall success of the cellular lysate vaccination strategy used is unlikely to be over-estimating the underlying potential. Due to the hypermutative nature of (C)MMR-D-associated cancers, which allows such tumor cells to easily gain novel (escape) mutations rapidly, multifaceted treatment strategies will most likely be key to their successful long-term disease management.

Materials and methods

Whole exome sequencing (WES) analysis. Comparative WES analysis was done on MLH1$^{-/-}$ GIT allograft 7450 and their matched primary[9] using the Agilent SureSelectXT exome capture and sequencing via Genome Sequencer Illumina HiSeq in paired-end mode (GATC, Konstanz, Germany; coverage: 90x (primary) and 60x (allograft), respectively). Data preprocessing: For each sequence read the base quality is inspected for low quality calls and subsequently removed before proceeding with further processing using a sliding window approach. This means that bases with low quality are removed from the 3′ and 5′ ends. Additionally, bases are removed if the average quality is below 15. The whole exome reads were mapped to the published mouse genome build ENSEMBL mm9.64 reference using Burroughs Wheeler Aligner (BWA)[36] with the default parameters. PCR duplicate reads were removed by using Picard (http://picard.sourceforge.net) in order to prevent artificial coverage brought on by the PCR amplification step during library preparation. SNP and InDel calling was performed using the GATK Unified Genotyper[37,38] and the detected variants were annotated based on their gene context using snpEff.[39]

Data visualization

The summarized mutational profiles with the corresponding mutation type of the MLH1$^{-/-}$ GIT allograft and the primary tumor were generated as stacked bar plot with ggplot2.[40] To better compare the molecular profiles between the allograft and primary tumor, whole genome ideograms were generated using ggplot2 package[40] as well as circlize package[41] in R. The mutation data were filtered for the exclusive SNVs for each condition (allograft or primary). Additional mutation filters such as the mutation type (missense and nonsense) as well as those mutations occurring in known annotated genes, were applied. Next, the filtered mutations were presented as ideogram based on the mm9 mouse assembly provided by the circlize package.[41] The first track is the cytoband of the mm9 assembly. The following tracks include SNVs belonging to same condition (MLH1$^{-/-}$ GIT allograft or primary tumor). Further details about the overlaps in the mutation type profiles have been generated customized with the VennDiagram[42] package in R. The mutation mapper tool was utilized for mapping the mutations and its statistics on a linear gene product (proteins of interest).[43,44] For analysis, genes were chosen with high probability of mutation based on knowledge from the human MMR-D counterpart and general involvement in tumorigenesis.

MLH1$^{-/-}$ mouse model and vaccine preparation

Homozygous mice were generated by breeding heterozygous males and females of the ≥F5 generation. All animals received standard laboratory chow and free access to water. Mice breeding took place in the animal facilities (University of Rostock) under specified pathogen-free conditions. Trials were performed in accordance with the German legislation on protection of animals and the Guide for the Care and Use of Laboratory Animals (Institute of Laboratory Animal Resources, National Research Council; NIH Guide, vol.25, no.28, 1996; approval number: LALLF M-V/TSD/7221.3-1.1-053/12). Mlh1 genotyping was done according to.[45] In each generation, offspring of all three classes in the expected ratios were obtained (i.e. about 20–25% homozygous mice).

The vaccine originated from a molecularly and immunologically well-characterized MLH1$^{-/-}$ GIT,[9] grown as allograft in NMRI Foxn1^{nu} mice and serially passaged. The primary tumor grew in the small intestine of a female MLH1$^{-/-}$ mouse. Histopathologically, the tumor presented as well-differentiated adenocarcinoma with abundant extracellular mucin. Outgrowing allografts were resected, homogenized and washed. The vaccine was obtained after repetitive freeze/thaw cycles (n = 4), prior to heat-shock (42°C, 5 min). Protein lysates were gamma irradiated (60 Gy) and frozen immediately in aliquots at -80°C according to the procedure by.[46]

In vivo vaccination schedule

Mice were either vaccinated prophylactically or therapeutically. In case of prophylactic application, 8–10 week-old homozygous mice received four weekly subcutaneous injections of the vaccine (10 mg/kg bw, s.c., n = 12 mice) with or without CpG ODN 1826 (Invivogen, tlrl-1826) as adjuvant or its irrelevant control ODN 1826 (tlrl-1826c; 2.5 mg/kg bw, s.c., n = 15 and 12 mice per group, respectively). Control mice were given equivalent concentrations of CpG ODN or control ODN 1826 (n = 9 and n = 7 mice per group, respectively). Vaccination was continued until tumor development (monthly injections: 2.5mg/kg bw, without adjuvant). Therapeutic vaccinations started after *in vivo* confirmation of GI tumor growth, as determined by small animal PET/CT imaging.[29] Mice received four weekly injections of the vaccine (10 mg/kg bw, s.c.) again with or without CpG ODN 1826 (2.5 mg/kg bw, s.c., $n = 9$ and $n = 7$, respectively), followed by biweekly applications of the lysate only (2.5 mg/kg bw) until tumor progression. PET/CT imaging was repeated on day 28 of therapy. Control mice were given no treatment. Blood samples were taken at start of treatment (prophylactic and therapeutic) and regularly during the experiment. Mice were sacrificed followed by collecting blood samples, tumors and spleens from all animals for further analysis.

PET/CT imaging

Mice with suspected GIT or healthy control mice ($n = 30$ in total) were anaesthetized by isoflurane (1.5–2.5 %, Baxter) supplemented with oxygen. Mice received a mean dose of 16,91 ± 1,73 MBq Radiopharmacon ^{18}F-FDG intravenously via a microcatheter placed in a tail vein (1 h uptake). Afterwards, mice were imaged in prone position in the Inveon PET/CT scanner (Siemens Preclinical Solutions, Knoxville, TN, USA) for 15 min. During measurement animals were kept at constant temperature of 38 °C by an electrical heating pad and respiration was monitored.[29] CT images were reconstructed with a Feldkamp algorithm. PET data were first Fourier rebinned into a 2D dataset from which real-space images were reconstructed with an ordered subset expectation maximization (OSEM) algorithm with 16 subsets and four iterations. Attenuation correction was carried out using the CT data. Metabolic volumes and SUVs were determined using Inveon Research Workplace 4.2 software.

Flow cytometry on blood samples

Blood samples were taken routinely from the retrobulbar venous plexus of vaccinated and control MLH1$^{-/-}$ mice, as well as naïve young homozygous mice (<14 weeks, $n = 15$). Blood samples were stained with a panel of conjugated monoclonal antibodies (mAb, 1 μg each) followed by lysis of erythrocytes (155 mM NH_4Cl (MERCK Millipore, 101145), 10 mM $KHCO_3$ (MERCK Millipore, 104854), 0.1 mM EDTA (Applichem, A5097)). Negative controls consisted of lymphocytes stained with the appropriate isotypes (BD Pharmingen). Cells were washed, resuspended in PBS and analyzed by flow cytometry on a FACS Verse Cytometer (BD Pharmingen). Data analysis was performed using BD FACSuite software (BD Pharmingen).

Microsatellite and coding microsatellite (cMS) frameshift mutation analysis

The mutational profile of MLH1$^{-/-}$ tumors from vaccinated mice was compared with those of control mice analyzing a panel of $n = 26$ mononucleotide repeats in MSI target genes. Genes included in this study were described before.[9] PCR conditions were: 94 °C, 4 min (1 cycle); 94 °C, 30 s, 58 °C, 45 s and 72 °C, 30 s (35 cycles); and 72 °C, 6 min (1 cycle). Fluorescently labeled DNA fragments were analyzed on a 3500 Genetic Analyzer. In each reaction, normal tail DNA served as microsatellite stable (MSS) controls. Tumor samples were scored as instable if novel peaks were obtained compared to MSS controls or if the ratio of peak areas in MLH1$^{-/-}$ samples and stable controls revealed values ≤ 0.5or ≥ 2.

Immunofluorescence

Cryostat sections of 4 μm were air-dried and fixed in cold pure methanol for 8 min. Unspecific binding sites were 2 hours blocked in 2 % BSA (Roth, T844.4) followed by incubation with 1 μg of the following FITC- and PE-labeled mAbs: CD4, CD8α, CD11b, Gr1 (Immunotools), CD104, LAG-3, PD-1, NK1.1 and PD-L1 (Biolegend). Sections were washed and nuclei were stained with DAPI (0.5 μg/ml, Thermo Fisher Scientific, D1306). Target protein visualization was done on a laser scanning microscope (Zeiss, Jena, Germany) using 20x objectives.

IFNγ–ELISpot assay

2.5×10^3 target cells/well (MLH1$^{-/-}$ A7450, MLH1$^{-/-}$ 328, MLH1$^{-/-}$ lymphoma cells, YAC-1) were seeded in IFNγ–specific mAb (Mabtech, 3321–3)–coated, 96-well microtiter plates and incubated for 2 hours. Peripheral blood leukocytes or splenocytes (1×10^4/Well) were added to targets in triplicates and co-cultured overnight. Finally, bound antibody (Mabtech, 3321–6) was visualized by BCIP/NBT (KPL, Gaithersburg, Maryland, USA); spots were counted using an ELISpot reader. Presented are the numbers of IFNγ–secreting cells per 10,000 effector cells corrected for background levels counted in the absence of target cells, which was always ≤ 5 spots/well. Target cells without effector cells showed no background level.

Flow cytometric cytotoxicity assay

In a more functional cytotoxicity assay, lytic activity of effector cells against tumor target cells was determined by flow cytometry. Prior to co-culture, target cells (MLH1$^{-/-}$ A7450, MLH1$^{-/-}$ 328, MLH1$^{-/-}$ lymphoma cells, YAC-1) were labeled with CFDA-SE (carboxyfluorescein diacetate succinimidyl ester, Thermo Fisher Scientific, C1157; final concentration: 2 μmol/l). Target cells without effector cells were used as negative controls. Following co-incubation for twelve hours at an effector to target cell ratio of 10:1, 30:1, and 50:1, propidium iodide (PI, Sigma Aldrich, 11348639001; final concentration: 50μg/ml) was added to measure target cell death based on CFDA/PI double positive cells. Percentage (%) numbers of surviving cells were calculated from differences between normal and co-cultured cells in relation to the absolute number of measured events.

Statistics

All values are expressed as mean ± SD. After proving the assumption of normality (Kolmogorov-Smirnov test), differences between vaccinated and control mice were determined using the unpaired Student's *t*-test. Kaplan-Meier survival analysis was done by applying log rank test. The tests were performed by using Sigma-Stat 3.0 (Jandel Corp, San Rafael, CA). The criterion for significance was set to $p < 0.05$.

Abbreviations

CMMR-D	constitutional mismatch repair deficiency
CRC	colorectal cancer
FSM	frameshift mutation
GIT	gastrointestinal tumor
LS	Lynch Syndrome
MMR-D	mismatch repair deficiency
MSI	microsatellite instability

Disclosure of interest

The authors report no conflict of interest.

Acknowledgments

We gratefully thank Brigitte Vollmar and Bernd Krause for their continuous support in their efforts of chairing the Core Facility of Multimodal Small Animal Imaging. We also gratefully acknowledge the excellent technical assistance of Mrs. Anne Möller and Mrs. Joanna Förster. Furthermore, we thank Alexander Hohn, radiopharmacy team of the Department of Nuclear Medicine of the University Medical Centre Rostock, for providing ^{18}F-FDG for the small animal PET/CT experiments.

Funding

German research fundation (MA5799/2-1)

References

1. Dudley JC, Lin MT, Le DT, Eshleman JR. Microsatellite Instability as a Biomarker for PD-1 Blockade. Clin Cancer Res. 2016;22(4):813–20. doi:10.1158/1078-0432.CCR-15-1678. PMID:26880610.
2. Le DT, Durham JN, Smith KN, Wang H, Bartlett BR, Aulakh LK, Lu S, Kemberling H, Wilt C, Luber BS, et al. Mismatch-repair deficiency predicts response of solid tumors to PD-1 blockade. Science. 2017;357:409–13. doi:10.1126/science.aan6733.
3. Woerner SM, Tosti E, Yuan YP, Kloor M, Bork P, Edelmann W, Gebert J. Detection of coding microsatellite frameshift mutations in DNA mismatch repair-deficient mouse intestinal tumors. Mol Carcinog. 2015;54(11):1376–86. doi:10.1002/mc.22213. PMID:25213383.
4. Speetjens FM, Lauwen MM, Franken KL, Janssen-van Rhijn CM, van Duikeren S, Bres SA, van de Velde CJ, Melief CJ, Kuppen PJ, van der Burg SH, et al. Prediction of the immunogenic potential of frameshift-mutated antigens in microsatellite instable cancer. Int J Cancer. 2008;123(4):838–45. doi:10.1002/ijc.23570. PMID:18506693.
5. Westdorp H, Kolders S, Hoogerbrugge N, de Vries IJM, Jongmans MCJ, Schreibelt G. Immunotherapy holds the key to cancer treatment and prevention in constitutional mismatch repair deficiency (CMMRD) syndrome. Cancer Lett. 2017;403:159–64. doi:10.1016/j.canlet.2017.06.018. PMID:28645564.
6. Lynch HT, Drescher K, Knezetic J, Lanspa S. Genetics, biomarkers, hereditary cancer syndrome diagnosis, heterogeneity and treatment: a review. Curr Treat Options Oncol. 2014;15(3):429–42. doi:10.1007/s11864-014-0293-5. PMID:24827900.
7. Vasen HF, Ghorbanoghli Z, Bourdeaut F, Cabaret O, Caron O, Duval A, Entz-Werle N, Goldberg Y, Ilencikova D, Kratz CP, et al. EU-Consortium Care for CMMR-D (C4CMMR-D). Guidelines for surveillance of individuals with constitutional mismatch repair-deficiency proposed by the European Consortium "Care for CMMR-D" (C4CMMR-D). J Med Genet. 2014;51(5):283–93. doi:10.1136/jmedgenet-2013-102238. PMID:24556086.
8. Maletzki C, Huehns M, Bauer I, Ripperger T, Mork MM, Vilar E, Klöcking S, Zettl H, Prall F, Linnebacher M. Frameshift mutational target gene analysis identifies similarities and differences in constitutional mismatch repair-deficiency and Lynch syndrome. Mol Carcinog. 2017;56(7):1753–64. doi:10.1002/mc.22632. PMID:28218421.
9. Maletzki C, Beyrich F, Hühns M, Klar E, Linnebacher M. The mutational profile and infiltration pattern of murine MLH1−/− tumors: concurrences, disparities and cell line establishment for functional analysis. Oncotarget. 2016;7(33):53583–98. doi:10.18632/oncotarget.10677. PMID:27447752.
10. Bodo S, Colas C, Buhard O, Collura A, Tinat J, Lavoine N, Guilloux A, Chalastanis A, Lafitte P, Coulet F, et al. European Consortium "Care for CMMRD". Diagnosis of Constitutional Mismatch Repair-Deficiency Syndrome Based on Microsatellite Instability and Lymphocyte Tolerance to Methylating Agents. Gastroenterology. 2015;149(4):1017–29.e3. doi:10.1053/j.gastro.2015.06.013. PMID:26116798.
11. Ryan E, Sheahan K, Creavin B, Mohan HM, Winter DC. The current value of determining the mismatch repair status of colorectal cancer: A rationale for routine testing. Crit Rev Oncol Hematol. 2017;116:38–57. doi:10.1016/j.critrevonc.2017.05.006. PMID:28693799.
12. Czink E, Kloor M, Goeppert B, Froehling S, Uhrig S, Weber TF, Meinel J, Sutter C, Weiss KH, Schirmacher P, et al. Successful immune checkpoint blockade in a patient with advanced stage microsatellite unstable biliary tract cancer. Cold Spring Harb Mol Case Stud. 2017;3:a001974. doi:10.1101/mcs.a001974.
13. Bauer K, Nelius N, Reuschenbach M, Koch M, Weitz J, Steinert G, Kopitz J, Beckhove P, Tariverdian M, von Knebel Doeberitz M, et al. T cell responses against microsatellite instability-induced frameshift peptides and influence of regulatory T cells in colorectal cancer. Cancer Immunol Immunother. 2013;62(1):27–37. doi:10.1007/s00262-012-1303-8. PMID:22729559.
14. Reuschenbach M, Kloor M, Morak M, Wentzensen N, Germann A, Garbe Y, Tariverdian M, Findeisen P, Neumaier M, Holinski-Feder E, et al. Serum antibodies against frameshift peptides in microsatellite unstable colorectal cancer patients with Lynch syndrome. Fam Cancer. 2010;9(2):173–9. doi:10.1007/s10689-009-9307-z. PMID:19957108.
15. Schwitalle Y, Kloor M, Eiermann S, Linnebacher M, Kienle P, Knaebel HP, Tariverdian M, Benner A, von Knebel Doeberitz M. Immune response against frameshift-induced neopeptides in HNPCC patients and healthy HNPCC mutation carriers. Gastroenterology. 2008;134(4):988–97. doi:10.1053/j.gastro.2008.01.015. PMID:18395080.
16. Reeves E, James E. Antigen processing and immune regulation in the response to tumours. Immunology. 2017;150(1):16–24. doi:10.1111/imm.12675. Epub 2016 Oct 12.
17. Bernal M, Ruiz-Cabello F, Concha A, Paschen A, Garrido F. Implication of the β2-microglobulin gene in the generation of tumor escape phenotypes. Cancer Immunol Immunother. 2012;61(9):1359–71. doi:10.1007/s00262-012-1321-6.
18. Hirata T, Yamamoto H, Taniguchi H, Horiuchi S, Oki M, Adachi Y, Imai K, Shinomura Y. Characterization of the immune escape phenotype of human gastric cancers with and without high-frequency microsatellite instability. J Pathol. 2007;211(5):516–23. doi:10.1002/path.2142.
19. Chiang CL, Coukos G, Kandalaft LE. Whole Tumor Antigen Vaccines: Where Are We? Vaccines (Basel). 2015;3(2):344–72. doi:10.3390/vaccines3020344. PMID:26343191.
20. Bourdais R, Rousseau B, Pujals A, Boussion H, Joly C, Guillemin A, Baumgaertner I, Neuzillet C, Tournigand C. Polymerase proofreading domain mutations: New opportunities for immunotherapy in hypermutated colorectal cancer beyond MMR deficiency. Crit Rev Oncol Hematol. 2017 May;113:242–8. doi:10.1016/j.critrevonc.2017.03.027.
21. Shlien A, Campbell BB, de Borja R, Alexandrov LB, Merico D, Wedge D, Van Loo P, Tarpey PS, Coupland P, Behjati S, et al. Combined hereditary and somatic mutations of replication error repair genes result in rapid onset of ultra-hypermutated cancers. Nat Genet. 2015;47(3):257–62. doi:10.1038/ng.3202. PMID:25642631.
22. Linnebacher M, Maletzki C, Emmrich J, Kreikemeyer B. Lysates of S. pyogenes serotype M49 induce pancreatic tumor growth delay by specific and unspecific antitumor immune responses. J Immunother. 2008;31(8):704–13. doi:10.1097/CJI.0b013e3181829f62. PMID:18779749.
23. Antonios JP, Soto H, Everson RG, Moughon D, Orpilla JR, Shin NP, Sedighim S, Treger J, Odesa S, Tucker A, et al. Immunosuppressive tumor-infiltrating myeloid cells mediate adaptive immune resistance

via a PD-1/PD-L1 mechanism in glioblastoma. Neuro Oncol. 2017;19(6):796–807. doi:10.1093/neuonc/now287. PMID:28115578.

24. Wimmer K, Rosenbaum T, Messiaen L. Connections between constitutional mismatch repair deficiency syndrome and neurofibromatosis type 1. Clin Genet. 2017;91(4):507–19. doi:10.1111/cge.12904. PMID:27779754.
25. Maletzki C, Schmidt F, Dirks WG, Schmitt M, Linnebacher M. Frameshift-derived neoantigens constitute immunotherapeutic targets for patients with microsatellite-instable haematological malignancies: frameshift peptides for treating MSI+ blood cancers. Eur J Cancer. 2013 Jul;49(11):2587–95. doi:10.1016/j.ejca.2013.02.035.
26. Thomas S, Prendergast GC. Cancer Vaccines: A Brief Overview. Methods Mol Biol. 2016;1403:755–61. doi:10.1007/978-1-4939-3387-7_43. PMID:27076165.
27. Inderberg EM, Wälchli S, Myhre MR, Trachsel S, Almåsbak H, Kvalheim G, Gaudernack G. T cell therapy targeting a public neoantigen in microsatellite instable colon cancer reduces in vivo tumor growth. Oncoimmunology. 2017;6(4):e1302631. doi:10.1080/2162402X.2017.1302631. PMID:28507809.
28. Bouffet E, Larouche V, Campbell BB, Merico D, de Borja R, Aronson M, Durno C, Krueger J, Cabric V, Ramaswamy V, et al. Immune Checkpoint Inhibition for Hypermutant Glioblastoma Multiforme Resulting From Germline Biallelic Mismatch Repair Deficiency. J Clin Oncol. 2016;34(19):2206–11. doi:10.1200/JCO.2016.66.6552. PMID:27001570.
29. Rohde S, Lindner T, Polei S, Stenzel J, Borufka L, Achilles S, Hartmann E, Lange F, Maletzki C, Linnebacher M, et al. Application of in vivo imaging techniques to monitor therapeutic efficiency of vemurafenib in an experimental model of microsatellite instable colorectal cancer. Oncotarget. 2017;8:69756–67. doi:10.18632/oncotarget.19263.
30. Ishikawa E, Yamamoto T, Matsumura A. Prospect of Immunotherapy for Glioblastoma: Tumor Vaccine, Immune Checkpoint Inhibitors and Combination Therapy. Neurol Med Chir (Tokyo). 2017;57(7):321–30. doi:10.2176/nmc.nmc.ra.2016-0334.
31. Borie C, Colas C, Dartigues P, Lazure T, Rince P, Buhard O, Folliot P, Chalastanis A, Muleris M, Hamelin R, et al. The mechanisms underlying MMR deficiency in immunodeficiency-related non-Hodgkin lymphomas are different from those in other sporadic microsatellite instable neoplasms. Int J Cancer. 2009;125(10):2360–6. doi:10.1002/ijc.24681. PMID:19551857.
32. Tian Y, Li M, Yu C, Zhang R, Zhang X, Huang R, Lu L, Yuan F, Fan Y, Zhou B, et al. The novel complex combination of alum, CpG ODN and HH2 as adjuvant in cancer vaccine effectively suppresses tumor growth in vivo. Oncotarget. 2017;8(28):45951–64. doi:10.18632/oncotarget.17504.
33. Talmadge JE, Adams J, Phillips H, Collins M, Lenz B, Schneider M, Schlick E, Ruffmann R, Wiltrout RH, Chirigos MA. Immunomodulatory effects in mice of polyinosinic-polycytidylic acid complexed with poly-L-lysine and carboxymethylcellulose. Cancer Res. 1985;45(3):1058–65.
34. Wada S, Jackson CM, Yoshimura K, Yen HR, Getnet D, Harris TJ, Goldberg MV, Bruno TC, Grosso JF, Durham N, et al. Sequencing CTLA-4 blockade with cell-based immunotherapy for prostate cancer. J Transl Med. 2013;11:89. doi:10.1186/1479-5876-11-89. PMID:23557194.
35. Péron S, Metin A, Gardès P, Alyanakian MA, Sheridan E, Kratz CP, Fischer A, Durandy A. Human PMS2 deficiency is associated with impaired immunoglobulin class switch recombination. J Exp Med. 2008;205(11):2465–72. doi:10.1084/jem.20080789. PMID:18824584.
36. Li H, Durbin R. Fast and accurate short read alignment with Burrows-Wheeler transform. Bioinformatics. 2009;25(14):1754–60. doi:10.1093/bioinformatics/btp324. PMID:19451168.
37. McKenna A, Hanna M, Banks E, Sivachenko A, Cibulskis K, Kernytsky A, Garimella K, Altshuler D, Gabriel S, Daly M, et al. The Genome Analysis Toolkit: a MapReduce framework for analyzing next-generation DNA sequencing data. Genome Res. 2010;20(9):1297–303. doi:10.1101/gr.107524.110. PMID:20644199.
38. DePristo MA, Banks E, Poplin R, Garimella KV, Maguire JR, Hartl C, Philippakis AA, del Angel G, Rivas MA, Hanna M, et al. A framework for variation discovery and genotyping using next-generation DNA sequencing data. Nat Genet. 2011;43(5):491–8. doi:10.1038/ng.806. PMID:21478889.
39. Cingolani P. snpEff: Variant effect prediction". http://snpeff.sourceforge.net; 2012.
40. Wickham H. ggplot2. Elegant Graphics for Data Analysis Book Use R; 2009.
41. Gu Z, Gu L, Eils R, Schlesner M, Brors B. circlize implements and enhances circular visualization in R. Bioinformatics. 2014;30:2811–2. doi:10.1093/bioinformatics/btu393. PMID:24930139.
42. Chen H, Boutros PC. VennDiagram: a package for the generation of highly-customizable Venn and Euler diagrams in R. BMC Bioinformatics. 2011;12:35. doi:10.1186/1471-2105-12-35. PMID:21269502.
43. Gao J, Aksoy BA, Dogrusoz U, Dresdner G, Gross B, Sumer SO, Sun Y, Jacobsen A, Sinha R, Larsson E, et al. Integrative analysis of complex cancer genomics and clinical profiles using the cBioPortal. Sci Signal. 2013;6(269):pl1. doi:10.1126/scisignal.2004088. PMID:23550210.
44. Cerami E, Gao J, Dogrusoz U, Gross BE, Sumer SO, Aksoy BA, Jacobsen A, Byrne CJ, Heuer ML, Larsson E, et al. The cBio cancer genomics portal: an open platform for exploring multidimensional cancer genomics data. Cancer Discov. 2012;2(5):401–4. doi:10.1158/2159-8290.CD-12-0095. PMID:22588877.
45. Edelmann W, Yang K, Kuraguchi M, Heyer J, Lia M, Kneitz B, Fan K, Brown AM, Lipkin M, Kucherlapati R. Tumorigenesis in Mlh1 and Mlh1/Apc1638N mutant mice. Cancer Res. 1999;59(6):1301–7. PMID:10096563.
46. Vandenberk L, Belmans J, Van Woensel M, Riva M, Van Gool SW. Exploiting the Immunogenic Potential of Cancer Cells for Improved Dendritic Cell Vaccines. Front Immunol. 2016;6:663. doi:10.3389/fimmu.2015.00663. PMID:26834740.

5.2 Wissenschaftlicher Lebenslauf

Studium

1999 – 2004	**Diplomstudium Biologie, Dipl.-Biol.**, Universität Rostock, Diplomarbeit: „Charakterisierung der chronischen DBTC-Pankreatitis der Ratte: Eine intravitalfluoreszenzmikroskopische, histologische und immunhistochemische Analyse“, Studienabschlussnote: 1,1.
2005 – 2008	**Promotion, Dr. rer. nat.**, Universität Rostock, Dissertation: „Evaluierung und Etablierung eines aktiven, immuntherapeutischen Ansatzes mit *S. pyogenes* im experimentellen Pankreaskarzinommodell der Maus“, Promotionsgebiet: Zellbiologie, Prädikat: *magna cum laude*.

Beruflicher Werdegang

2001 – 2003	**Studentische Hilfskraft**, Universität Rostock, Fachbereich Biowissenschaften/Immunbiologie, Abteilung Genetik/Immunbiologie.
2004 – 2010	**Wissenschaftliche Mitarbeiterin**, Universitätsmedizin Rostock, Abteilung für Gastroenterologie.
2010 – 08/2012	**Postdoktorand**, Universitätsmedizin Rostock, Arbeitsbereich Molekulare Onkologie und Immuntherapie, Abteilung für Allgemeine, Thorax-, Gefäß- und Transplantationschirurgie.
09/2012 – 08/2013	Elternzeit
09/2013 – 12/2014	**Postdoktorand**, Universitätsmedizin Rostock, Arbeitsbereich Molekulare Onkologie und Immuntherapie, Abteilung für Allgemeine, Thorax-, Gefäß- und Transplantationschirurgie.
01/2015 – 12/2015	Elternzeit
01/2016 – 12/2017	**Postdoktorand**, Universitätsmedizin Rostock, Arbeitsbereich Molekulare Onkologie und Immuntherapie, Abteilung für Allgemeine, Thorax-, Gefäß- und Transplantationschirurgie.
Seit 01/2018	**Arbeitsgruppenleiterin**, Universitätsmedizin Rostock, Abteilung für Hämatologie, Onkologie und Palliativmedizin.

Hochschuldidaktische Fortbildungen

06/2017	Stimmbildung – Eine starke Stimme für die Lehre I (Kompetenzentwicklung Lehre und Lernen, Universität Rostock)
02/2018	Prüfen und Bewerten (Kompetenzentwicklung Lehre und Lernen, Universität Rostock)

Stipendien und eingeworbene Drittmittel

2005 - 2008	**Promotionsstipendium**, Universitätsmedizin Rostock, Landesgraduiertenförderung und Förderungen durch das FORUN Programm der Medizinischen Fakultät.
01/2011 - 09/2011	**Forschungsprojekt**, Hermes-Junior-Programm der Universität Rostock, Thema: Steigerung zellulärer Immunantworten gegen Tumorinitiierende Zellen durch PAMP Substanzen.
01/2016 - 12/2016	**Forschungsprojekt**, Lieselotte Beutel Stiftung, Thema: *S. pyogenes A*DI induzierter Argininentzug zur Therapie des Glioblastoma multiforme.
06/2016 - 06/2019	**Sachbeihilfe**, Deutsche Forschungsgemeinschaft (Einzelantrag, Modul: „eigene Stelle“), Thema: Charakterisierung eines murinen Lynch Syndrom-Modells zur präklinischen Entwicklung einer zellulären Vakzine.
01/2018 - 06/2019	**Forschungsstipendium**, Stiftung Betroffen, Thema: Immunstatusbestimmung bei Patienten mit Lynch-Syndrom und Anlage-trägern zur Verbesserung von Diagnostik, Therapie und Nachsorge.

5.3. Vollständiges Publikationsverzeichnis

Originalarbeiten: 40

Übersichtsartikel: 2

Begutachtete Originalarbeiten

1. Bock S, Mullins CS, Klar E, Pérot P, Maletzki C, Linnebacher M. Murine Endogenous Retroviruses Are Detectable in Patient-Derived Xenografts but Not in Patient-Individual Cell Lines of Human Colorectal Cancer. *Front Microbiol*. 2018 Apr 24;9:789. IF: 4.07

2. Maletzki C, Gladbach YS, Hamed M, Fuellen G, Semmler ML, Stenzel J, Linnebacher M. Cellular vaccination of MLH1(-/-) mice - an immunotherapeutic proof of concept study. *Oncoimmunology*. 2017 Dec 14;7(3):e1408748. IF: 7.71

3. Rohde S, Lindner T, Polei S, Stenzel J, Borufka L, Achilles S, Hartmann E, Lange F, Maletzki C, Linnebacher M, Glass Ä, Schwarzenböck SM, Kurth J, Hohn A, Vollmar B, Krause BJ, Jaster R. Application of in vivo imaging techniques to monitor therapeutic efficiency of PLX4720 in an experimental model of microsatellite instable colorectal cancer. *Oncotarget*. 2017 Jul15;8(41):69756-69767. IF: 5.16

4. Prall F, Maletzki C, Hühns M, Krohn M, Linnebacher M. Colorectal carcinoma tumour budding and podia formation in the xenograft microenvironment. *PLoS One*. 2017 Oct 17;12(10):e0186271. IF: 2.80

5. Maletzki C, Rosche Y, Riess C, Scholz A, William D, Classen CF, Kreikemeyer B, Linnebacher M, Fiedler T. Deciphering molecular mechanisms of arginine deiminase-based therapy - Comparative response analysis in paired human primary and recurrent glioblastomas. *Chem Biol Interact*. 2017 Dec 25;278:179-188. IF: 3.14

6. Maletzki C*, Huehns M*, Bauer I, Ripperger T, Mork MM, Vilar E, Klöcking S, Zettl H, Prall F, Linnebacher M. Frameshift mutational target gene analysis identifies similarities and differences in constitutional mismatch repair-deficiency and Lynch syndrome. *Mol Carcinog*. 2017 Jul;56(7):1753-1764. IF: 4.18

7. Maletzki C*, Beyrich F*, Hühns M, Klar E, Linnebacher M. The mutational profile and infiltration pattern of murine MLH1-/- tumors: concurrences, disparities and cell line establishment for functional analysis. *Oncotarget*. 2016 Aug 16;7(33):53583-53598. IF: 5.16

8. Maletzki C, Huehns M, Knapp P, Waukosin N, Klar E, Prall F, Linnebacher M. Functional Characterization and Drug Response of Freshly Established Patient-Derived Tumor Models with CpG Island Methylator Phenotype. *PLoS One*. 2015 Nov 30;10(11):e0143194. IF: 2.80

9. Fiedler T, Strauss M, Hering S, Redanz U, William D, Rosche Y, Classen CF, Kreikemeyer B, Linnebacher M, Maletzki C. Arginine deprivation by arginine deiminase of Streptococcus pyogenes controls primary glioblastoma growth in vitro and in vivo. *Cancer Biol Ther*. 2015;16(7):1047-55. IF: 3.29

10. Maletzki C*, Gock M*, Randow M, Klar E, Huehns M, Prall F, Linnebacher M. Establishment and characterization of cell lines from chromosomal instable colorectal cancer. *World J Gastroenterol*. 2015 Jan 7;21(1):164-76. IF: 3.36

11. Lange F, Franz B, Maletzki C, Linnebacher M, Hühns M, Jaster R. Biological and molecular effects of small molecule kinase inhibitors on low-passage human colorectal cancer cell lines. *Biomed Res Int*. 2014;2014:568693. IF: 2.47

12. Maletzki C, Klier U, Marinkovic S, Klar E, Andrä J, Linnebacher M. Host defense peptides for treatment of colorectal carcinoma - a comparative in vitro and in vivo analysis. *Oncotarget*. 2014 Jun 30;5(12):4467-79. IF: 5.16

13. Stier S, Maletzki C, Klier U, Linnebacher M. Combinations of TLR ligands: a promising approach in cancer immunotherapy. *Clin Dev Immunol*. 2013;2013:271246. IF: 3.60

14. Maletzki C, Stier S, Linnebacher M. Microsatellite instability in hematological malignancies: Hypermutation vs. immune control-who is challenging who? *Oncoimmunology*. 2013 Aug 1;2(8):e25419. IF: 7.71

15. Maletzki C, Linnebacher M, Savai R, Hobohm U. Mistletoe lectin has a shigatoxin-like structure and should be combined with other Toll-like receptor ligands in cancer therapy. *Cancer Immunol Immunother*. 2013 Aug;62(8):1283-92. IF: 4.71

16. Bodammer P, Kerkhoff C, Maletzki C, Lamprecht G. Bovine colostrum increases pore-forming claudin-2 protein expression but paradoxically not ion permeability possibly by a change of the intestinal cytokine milieu. *PLoS One*. 2013 May 23;8(5):e64210. IF: 2.80

17. Maletzki C*, Schmidt F*, Dirks WG, Schmitt M, Linnebacher M. Frameshift-derived neoantigens constitute immunotherapeutic targets for patients with microsatellite-instable haematological malignancies: frameshift peptides for treating MSI+ blood cancers. *Eur J Cancer*. 2013 Jul;49(11):2587-95. IF: 6.02

18. Bodammer P, Zirzow E, Klammt S, Maletzki C, Kerkhoff C. Alteration of DSS-mediated immune cell redistribution in murine colitis by oral colostral immunoglobulin. *BMC Immunol*. 2013 Feb 20;14:10. IF: 2.48

19. Maletzki C, Stier S, Gruenert U, Gock M, Ostwald C, Prall F, Linnebacher M. Establishment, characterization and chemosensitivity of three mismatch repair deficient cell lines from sporadic and inherited colorectal carcinomas. *PLoS One*. 2012;7(12):e52485. IF: 2.80

20. Maletzki C, Klier U, Obst W, Kreikemeyer B, Linnebacher M. Reevaluating the concept of treating experimental tumors with a mixed bacterial vaccine: Coley's Toxin. *Clin Dev Immunol*. 2012;2012:230625. IF: 3.60

21. Linnebacher M, Maletzki C. Tumor-infiltrating B cells: The ignored players in tumor immunology. *Oncoimmunology*. 2012 Oct 1;1(7):1186-1188. IF: 7.71

22. Prall F, Maletzki C, Linnebacher M. Microdensitometry of osteopontin as an immunohistochemical prognostic biomarker in colorectal carcinoma tissue microarrays: potential and limitations of the method in 'biomarker pathology'. *Histopathology*. 2012 Nov;61(5):823-32. IF: 3.52

23. Maletzki C*, Jahnke A*, Ostwald C, Klar E, Prall F, Linnebacher M. Ex-vivo clonally expanded B lymphocytes infiltrating colorectal carcinoma are of mature immunophenotype and produce functional IgG. *PLoS One*. 2012;7(2):e32639. IF: 2.80

24. Klier U*, Maletzki C*, Kreikemeyer B, Klar E, Linnebacher M. Combining bacterial-immunotherapy with therapeutic antibodies: a novel therapeutic concept. *Vaccine*. 2012 Apr 5;30(17):2786-94. IF: 3.23

25. Linnebacher M*, Maletzki C*, Klier U, Klar E. Bacterial immunotherapy of gastrointestinal tumors. *Langenbecks Arch Surg*. 2012 Apr;397(4):557-68. IF: 2.20

26. Garbe Y, Maletzki C, Linnebacher M. An MSI tumor specific frameshift mutation in a coding microsatellite of MSH3 encodes for HLA-A0201-restricted CD8+cytotoxic T cell epitopes. *PLoS One*. 2011;6(11):e26517. IF: 2.80

27. Bodammer P, Maletzki C, Waitz G, Emmrich J. Prophylactic application of bovine colostrum ameliorates murine colitis via induction of immunoregulatory cells. *J Nutr*. 2011 Jun;141(6):1056-61. IF: 4.14

28. Klier U*, Maletzki C*, Göttmann N, Kreikemeyer B, Linnebacher M. Avitalized bacteria mediate tumor growth control via activation of innate immunity. *Cell Immunol*. 2011;269(2):120-7. IF: 3.17

29. Maletzki C, Emmrich J. Inflammation and immunity in the tumor environment. *Dig Dis*. 2010;28(4-5):574-8. IF: 1.77

30. Linnebacher M, Maletzki C, Ostwald C, Klier U, Krohn M, Klar E, Prall F. Cryopreservation of human colorectal carcinomas prior to xenografting. *BMC Cancer*. 2010 Jul 8;10:362. IF: 3.28

31. Prall F, Maletzki C, Linnebacher M. The EpCAM high/CD44 high colorectal carcinoma stem cell phenotype is not preferentially expressed in tumour buds. *Histopathology*. 2010 Mar;56(4):553-5. IF: 3.52

32. Bodammer P, Waitz G, Loebermann M, Holtfreter MC, Maletzki C, Krueger MR, Nizze H, Emmrich J, Reisinger EC. Schistosoma mansoni infection but not egg antigen promotes recovery from colitis in outbred NMRI mice. *Dig Dis Sci*. 2011 Jan;56(1):70-8. IF: 2.87

33. Sturm D*, Maletzki C*, Braun D, Emmrich J. cis-Hydroxyproline-mediated pancreatic carcinoma growth inhibition in mice. *Int J Colorectal Dis*. 2010 Aug;25(8):921-9. IF: 2.42

34. Klier U, Maletzki C, Klar E, Linnebacher M. Generation of highly pure fusions of colorectal carcinoma and antigen-presenting cells. *Langenbecks Arch Surg*. 2010 Apr;395(4):365-71. IF: 2.20

35. Zautner AE, Krause M, Stropahl G, Holtfreter S, Frickmann H, Maletzki C, Kreikemeyer B, Pau HW, Podbielski A. Intracellular persisting Staphylococcus aureus is the major pathogen in recurrent tonsillitis. *PLoS One*. 2010 Mar 1;5(3):e9452. IF: 2.80

36. Linnebacher M*, Maletzki C*, Emmrich J, Kreikemeyer B. Lysates of S. pyogenes serotype M49 induce pancreatic tumor growth delay by specific and unspecific antitumor immune responses. *J Immunother*. 2008 Oct;31(8):704-13. IF: 3.91

37. Maletzki C, Linnebacher M, Kreikemeyer B, Emmrich J. Pancreatic cancer regression by intratumoural injection of live Streptococcus pyogenes in a syngeneic mouse model. *Gut*. 2008 Apr;57(4):483-91. IF: 16.65

38. Schuett H, Eipel C, Maletzki C, Menger MD, Vollmar B. NO counterbalances HO-1 overexpression-induced acceleration of hepatocyte proliferation in mice. *Lab Invest*. 2007 Jun;87(6):602-12. IF: 4.85

39. Eipel C, Schuett H, Glawe C, Bordel R, Menger MD, Vollmar B. Pifithrin-alpha induced p53 inhibition does not affect liver regeneration after partial hepatectomy in mice. *J Hepatol*. 2005 Nov;43(5):829-35. IF: 12.48

40. Glawe C, Emmrich J, Sparmann G, Vollmar B. In vivo characterization of developing chronic pancreatitis in rats. *Lab Invest*. 2005 Feb;85(2):193-204. IF: 4.85
* Autoren haben in gleichem Maße beigetragen

Übersichtsartikel

1. Maletzki C*, Gock M*, Klier U, Klar E, Linnebacher M. Bacteriolytic therapy of experimental pancreatic carcinoma. *World J Gastroenterol*. 2010 Jul 28;16(28):3546-52. IF: 3.36

2. Maletzki C, Bodammer P, Breitrück A, Kerkhoff C. S100 proteins as diagnostic and prognostic markers in colorectal and hepatocellular carcinoma. *Hepat Mon*. 2012 Oct;12(10 HCC):e7240. IF: 1.67

Kongressbeiträge

Vorträge

1. Maletzki C, Gladbach YS, Hamed M, Stenzel J, Klar E, Linnebacher M. Cellular vaccination of MLH1-/- mice – an immunotherapeutic proof of concept study. *135. Kongress Deutsche Gesellschaft für Chirurgie*, Berlin, 17. - 20. April 2018

2. Maletzki C, Scheinpflug P, Witt A, Klar E, Linnebacher M. IDO as target structure for cancer therapy – a comprehensive in vitro analysis on patient-derived tumor models. *135. Kongress Deutsche Gesellschaft für Chirurgie,* Berlin, 17. - 20. April 2018

3. Maletzki C, Stenzel J, Lindner T, Polei S, Vollmar B, Krause B, Klar E, Linnebacher M. Therapeutic cellular vaccination prolongs survival of MLH1-/- mice by re-activating spe

4. cific antitumoral immune responses. *7th BIENNIAL Insight Meeting*, Florenz, Italien 5. – 8. Juli 2017

5. Maletzki C, Beyrich F, Hühns M, Klar E, Linnebacher M. The mutational profile and infiltration pattern of murine MLH1-/- tumors – concurrences, disparities and cell line establishment for functional analysis. *20. Chirurgische Forschungstage*, Magdeburg, 08. – 10. September 2016.

6. Maletzki C, Knapp P, Klar E, Linnebacher M. Establishment, genetic & functional characterization of patient-derived colorectal carcinoma cell lines showing CpG-island methylator phenotype *18. Chirurgische Forschungstage* Hannover, 09.–11. Oktober 2014
7. Maletzki C, Strauß M, Kreikemeyer B, Klar E, Linnebacher M, Fiedler T. Improving arginine deiminase-based therapy against glioblastoma by combination with cytostatic drug. *131. Kongress der Deutschen Gesellschaft für Chirurgie*, Berlin, 25. – 28. März 2014

8. Maletzki C, Knapp P, Klar E, Linnebacher M. Establishment, genetic & functional characterization of patient-derived colorectal carcinoma cell lines showing CpG-island methylator phenotype. *131. Kongress der Deutschen Gesellschaft für Chirurgie*, Berlin, 25. – 28. März 2014

9. Maletzki C, Jahnke A, Ostwald C, Prall F, Klar E, Linnebacher M. Ex-vivo clonally expanded B lymphocytes infiltrating colorectal carcinoma are of mature immunophenotype and produce functional IgG. *15. Chirurgische Forschungstage*, Dresden, 22. – 24. September 2011.

10. Maletzki C, Garbe Y, Linnebacher M. An MSI tumor specific frameshift mutation in a coding microsatellite of MSH3 encodes for HLA-A0201-restricted CD8+ cytotoxic T cell epitopes. *Annual Joint Meeting of the German Society for Immunology (DGfI) and the Italian Society for Immunology, Clinical Immunology and Allergology (SIICA)*, Riccione, Italien, 28. September – 01. Oktober, 2011.

11. Maletzki C, Kreikemeyer B, Emmrich J, Klar E, Linnebacher M. Antitumoral potential of the streptococcal toxin Streptolysin S. *14. Chirurgische Forschungstage*, Rostock, 23. – 25. September, 2010.

12. Maletzki C, Schmidt F, Schmitt M, Linnebacher M. Cellular immune responses towards MSI-induced frameshift mutations in leukaemia cells. *40. Jahrestagung der Deutschen Gesellschaft für Immunologie (DGfI)*, Leipzig, 22. – 25. September 2010.

13. Schuschan S, Gock M, Maletzki C, Eisold S, Klar E, Linnebacher M. Bakteriolytische Tumortherapie mit attenuierten Clostridium novyi Sporen beim experimentellen Pankreaskarzinom. *126. Kongress der Deutschen Gesellschaft für Chirurgie*, München, 28. April – 1. Mai, 2009.

6 Danksagung

Mein erster Dank gilt Herrn Prof. Dr. Junghanß für die Unterstützung und insbesondere dafür, dass er mir die Möglichkeit gegeben hat, die Arbeit an seiner Abteilung abschließen zu dürfen.

Ein besonderer Dank gebührt meinem ehemaligen wissenschaftlichen Mentor Herrn PD Dr. Linnebacher, der mich insbesondere in meiner früher Postdoktorandenphase unterstützt und in mir die Leidenschaft für die Immunologie geweckt hat. Die jahrelange Zusammenarbeit hat mir die Möglichkeit eröffnet, eigenständig zu forschen und mich ständig weiterzuentwickeln.

Unseren Kollegen im Institut für Pathologie, vor allem Herrn Prof. Dr. Prall, Dr. Hühns und Dr. Schneider, danke ich für die angenehm freundschaftliche und erfolgreiche Zusammenarbeit in den zurückliegenden Jahren.

Danken möchte ich auch meinen Kooperationspartnern aus dem Institut für Medizinische Mikrobiologie, Virologie und Hygiene. Ganz besonders erwähnen möchte ich hierbei Herrn Prof. Dr. Kreikemeyer, der mich seit Beginn meiner ersten wissenschaftlichen Arbeiten unterstützt, mich stets in seinem Team willkommen heißt und damit eine sehr freundschaftliche Arbeitsatmosphäre schafft. Danke auch Tomas und Sonja für die überaus angenehme Zusammenarbeit in jüngster Zeit.

Ganz herzlich bedanken möchte ich mich auch bei meinen Studenten, die durch ihren Fleiß und ihr Engagement im Labor zur Entstehung der hier dargestellten Publikationen beigetragen haben, insbesondere Tilly Ritz, Willy Obst, Franziska Beyrich, Samuel Marinkovic, Patrick Knapp, Philipp Kleinschmidt und Luise Semmler.

Frau Prof. Dr. Vollmar, Direktorin des Instituts für experimentelle Chirurgie mit zentraler Versuchstierhaltung danke ich für die Möglichkeit, alle tierexperimentellen Untersuchungen in ihrem Haus durchzuführen. Ein ganz persönlicher Dank gilt Ilona Klamfuss für den Aufbau und die Erhaltung der MLH1-Zucht – danke für die Unterstützung und die Möglichkeit, ein genetisches Tiermodell in „meinen Händen“ zu haben.

Catrin Roolf danke ich für die freundschaftliche Bürogemeinschaft.

Natürlich sei auch allen aktuellen und ehemaligen Kolleginnen und Kollegen gedankt, die hier nicht namentlich erwähnt sind.

Schließlich gilt mein herzlichster Dank meiner Familie, meinen Eltern und Schwiegereltern für die liebevolle Betreuung unser beiden Kinder, Lara und Hanna und natürlich meinem Mann Gunnar. Danke, dass Ihr immer für mich da seid und jeden Tag lebenswert macht!

7 Eidesstattliche Erklärung

Hiermit erkläre ich die vorliegende Habilitationsschrift selbständig und ohne unerlaubte fremde Hilfe angefertigt zu haben. Ich habe keine anderen als die im Literaturverzeichnis angeführten Quellen benutzt und sämtliche Textstellen die wörtlich oder sinngemäß aus veröffentlichten oder unveröffentlichten Schriften entnommen wurden, sowie alle Angaben, die auf mündlichen Auskünften beruhen, als solche kenntlich gemacht. Ich versichere weiterhin, dass diese Arbeit nicht vorher und auch nicht gleichzeitig bei einer anderen als der Medizinischen Fakultät der Universität Rostock zur Eröffnung eines Habilitationsverfahrens eingereicht worden ist.

Rostock, den 12.07.2018 Dr. rer. nat. Claudia Maletzki